frontiers | Research Topics

Novel biomarkers for clinical and molecular stratification of organ involvement in rheumatic diseases

Edited by
Xiaolin Sun, Yudong Liu, Jing He, Jill M. Kramer and Miao Pan

Published in
Frontiers in Medicine
Frontiers in Immunology

ISSN 1664-8714
ISBN 978-2-8325-3459-5
DOI 10.3389/978-2-8325-3459-5

About Frontiers

Frontiers is more than just an open access publisher of scholarly articles: it is a pioneering approach to the world of academia, radically improving the way scholarly research is managed. The grand vision of Frontiers is a world where all people have an equal opportunity to seek, share and generate knowledge. Frontiers provides immediate and permanent online open access to all its publications, but this alone is not enough to realize our grand goals.

Frontiers journal series

The Frontiers journal series is a multi-tier and interdisciplinary set of open-access, online journals, promising a paradigm shift from the current review, selection and dissemination processes in academic publishing. All Frontiers journals are driven by researchers for researchers; therefore, they constitute a service to the scholarly community. At the same time, the *Frontiers journal series* operates on a revolutionary invention, the tiered publishing system, initially addressing specific communities of scholars, and gradually climbing up to broader public understanding, thus serving the interests of the lay society, too.

Dedication to quality

Each Frontiers article is a landmark of the highest quality, thanks to genuinely collaborative interactions between authors and review editors, who include some of the world's best academicians. Research must be certified by peers before entering a stream of knowledge that may eventually reach the public - and shape society; therefore, Frontiers only applies the most rigorous and unbiased reviews. Frontiers revolutionizes research publishing by freely delivering the most outstanding research, evaluated with no bias from both the academic and social point of view. By applying the most advanced information technologies, Frontiers is catapulting scholarly publishing into a new generation.

What are Frontiers Research Topics?

Frontiers Research Topics are very popular trademarks of the *Frontiers journals series*: they are collections of at least ten articles, all centered on a particular subject. With their unique mix of varied contributions from Original Research to Review Articles, Frontiers Research Topics unify the most influential researchers, the latest key findings and historical advances in a hot research area.

Find out more on how to host your own Frontiers Research Topic or contribute to one as an author by contacting the Frontiers editorial office: frontiersin.org/about/contact

Novel biomarkers for clinical and molecular stratification of organ involvement in rheumatic diseases

Topic editors

Xiaolin Sun — Peking University People's Hospital, China

Yudong Liu — The Key Laboratory of Geriatrics, Beijing Institute of Geriatrics, Beijing Hospital, National Center of Gerontology, Institute of Geriatric Medicine, Chinese Academy of Medical Sciences, China

Jing He — Peking University People's Hospital, China

Jill M. Kramer — University at Buffalo, United States

Miao Pan — Children's National Hospital, United States

Citation

Sun, X., Liu, Y., He, J., Kramer, J. M., Pan, M., eds. (2023). *Novel biomarkers for clinical and molecular stratification of organ involvement in rheumatic diseases*. Lausanne: Frontiers Media SA. doi: 10.3389/978-2-8325-3459-5

Table of contents

frontiers | Frontiers in Medicine

TYPE Editorial
PUBLISHED 28 August 2023
DOI 10.3389/fmed.2023.1274950

OPEN ACCESS

EDITED AND REVIEWED BY
Jiuliang Zhao,
Peking Union Medical College Hospital (CAMS), China

*CORRESPONDENCE
Xiaolin Sun
✉ sunxiaolin_sxl@126.com
Miao Pan
✉ mpan@childrensnational.org

RECEIVED 09 August 2023
ACCEPTED 16 August 2023
PUBLISHED 28 August 2023

CITATION
Sun X and Pan M (2023) Editorial: Novel biomarkers for clinical and molecular stratification of organ involvement in rheumatic diseases. *Front. Med.* 10:1274950. doi: 10.3389/fmed.2023.1274950

Editorial: Novel biomarkers for clinical and molecular stratification of organ involvement in rheumatic diseases

Xiaolin Sun[1]* and Miao Pan[2,3]*

[1]Department of Rheumatology and Immunology, Peking University People's Hospital, Beijing, China, [2]Division of Pathology and Laboratory Medicine, Children's National Hospital, Washington, DC, United States, [3]Departments of Pathology and Pediatrics, The George Washington University School of Medicine and Health Sciences, Washington, DC, United States

KEYWORDS

rheumatic disease, biomarker, organ involvement, molecular stratification, precision medicine

Editorial on the Research Topic
Novel biomarkers for clinical and molecular stratification of organ involvement in rheumatic diseases

Multiple organ involvements develop in most of the leading rheumatic diseases including rheumatoid arthritis, systemic lupus erythematosus, systemic vasculitis, etc. While progress has been made in advancing diagnosis and treatment strategies, the elusive goal of early prediction, accurate diagnosis, and precise treatment endures. This challenge persists due to the absence of robust biomarkers and practical predictive models that can reliably guide clinicians in navigating the complex and diverse manifestations of these conditions. The integration of genomics, proteomics, and high-throughput screening, holds great potential for unearthing these elusive biomarkers. In this Research Topic of Frontier in Medicine, multiple studies deciphered the intricate molecular signatures associated with rheumatic disease and organ involvement patterns, which pave the way for the development of diagnostic tests that enable early detection and prediction. Additionally, the data generated from these technologies can be harnessed to construct predictive models that account for the complex interplay of variables contributing to disease progression.

Systemic lupus erythematosus (SLE) is a typical systemic rheumatic disease affecting most organs of the body. However, there is still an unmet need of clinically useful biomarkers that can predict organ involvement for personalized treatment. Fenton and Pedersen reviewed current research progress to identify advanced methods and possible biomarkers to be utilized in the diagnosis, disease monitoring, and prediction of treatment response in SLE. The authors proposed to look for biomarkers and methods that have specificity and sensitivity for distinct organ involvement across different diseases. Combined strategies with biomarkers, multi-omics methods and novel clinical measurements such as molecular imaging might be the best strategy to explore the precision medicine of SLE (Fenton and Pedersen). In a mini review, Tsuchida et al. summarized the abnormal expression and pathogenic roles of autotaxin in patients with SLE. Autotaxin is produced by plasmacytoid dendritic cells and is associated with type I interferons, which may become a potential biomarker in SLE (Tsuchida et al.).

Hydroxychloroquine (HCQ) is another immunosuppressant commonly used in treatment of autoimmune disease such as SLE. A small fraction of patients taking HCQ may develop acute generalized exanthematous pustulosis (AGEP) as an adverse response. Luo et al. explored the clinical features and associated gene expression of AGEP induced in HCQ treated patients with rheumatic diseases including SLE, RA, or pSS, and showed that HCQ-induced AGEP might have a longer latency period and regression time than AGEP induced by other drugs. CARD14 gene mutations might contribute to the molecular basis of AGEP (Luo et al.).

Sjögren's syndrome (SS) is a systemic autoimmune disease characterized by the immune system attacking and damaging the exocrine glands, leading to a reduction in their secretory function. The existing diagnostic methodology for SS is both invasive and lacking in efficiency, necessitating the exploration of more advanced and effective approaches. In a systematic investigation by Kamounah et al., the proteomics and miRNA-expression profile were established and analyzed. It is found that upregulation of cystatin A, β2M, α-enolase, actin, E-FABP, N-GAL, Ig-κ light-chain and C3 as well as downregulation of PRPs, CA6, α-amylase, histatins, PIP, cystatin S, and cystatin SN in patients with SS. The discriminatory performance of an anti-SSA/Ro combined with TRIM29 showed a higher sensitivity than anti-SSA/Ro positivity alone.

Rheumatoid arthritis (RA) is a chronic joint destructive autoimmune disease leading to systemic involvement and disabling. First-line treatment for RA is methotrexate (MTX), but 20–40% of RA patients do not respond to MTX (Brynedal et al.). It is therefore important to identify the variable biological effect of MTX between responders and non-responders. By employing a multi-omics approach that combines the strengths of flow cytometry, RNA sequencing, and multiplex protein quantification, Brynedal et al. performed a deep molecular and cellular phenotyping of peripheral blood cells in RA patients treated with MTX. This integrated strategy enabled them to elucidate the differences between responders and non-responders and the results might be helpful to explore the mechanism of non-responsiveness to MTX in RA treatment.

With bioinformatical analysis, Sun et al. established a lncRNA–miRNA–mRNA network in circulating exosomes (cirexos) to identify potential biomarkers for systemic sclerosis (SSc). Differentially expressed mRNAs (DEmRNAs) and lncRNAs (DElncRNAs) in SSc cirexos were screened and the ENST00000313807-hsa-miR-29a-3p-COL1A1 network in plasma cirexos could perform as a combined biomarker for the clinical diagnosis and treatment of SSc.

Systemic vasculitis are composed of a series of heterogeneous autoimmune diseases characterized by blood vessel inflammation potentially involving multiple organs and systems. Umezawa et al. reported that leucine-richα-2 glycoprotein (LRG), could be a novel biomarker for CRP-negative patients to indicate disease activity.

Liu et al. investigated the correlation between *FGA* gene polymorphisms and coronary artery lesion in Kawasaki disease (KD). Their study showed that *FGA* gene polymorphisms affected coronary artery lesion in children with KD (Liu et al.). Lung involvement is one of the most severe organ damages in patients with myeloperoxidase (MPO)-anti-neutrophil cytoplasmic antibody (ANCA)-associated vasculitis (MPO-AAV). Chen et al. exploited the image features of lung involvement to predict the therapeutic response and facilitate decision making in MPO-AAV treatment. They developed and validated a radiomics nomogram model to predict treatment resistance of Chinese MPO-AAV patients based on low-dose multiple slices computed tomography (MSCT) of the involved lung with cohorts from two centers, and this model might work as a non-invasive tool for predicting treatment response and improve individualizing treatment decisions (Chen et al.).

Overall, this Research Topic focus on *Novel biomarkers for clinical and molecular stratification of organ involvement in rheumatic diseases*. Over the past decades, numerous advances have been made in multiple omic approaches, which enable us to screen clinical samples and combine multi-layer data to exploit useful biomarkers. Some of the innovations might become part of the routine clinical practice in the future.

Author contributions

XS: Writing—original draft, Writing—review and editing. MP: Writing—original draft, Writing—review and editing.

Funding

XS was supported by National Natural Science Foundation of China (81971520 and 82171775) and Peking University People's Hospital Research and Development Funds (RDGS2022-05). MP was supported by a grant from National Institutes of Health (1U01HG011745 and 1UG3TR004033).

Acknowledgments

We thank all the topic editors and reviewers for their contributions to this Research Topic.

Conflict of interest

The authors declare that the research was conducted in the absence of any commercial or financial relationships that could be construed as a potential conflict of interest.

Publisher's note

frontiers | Frontiers in Medicine

TYPE Original Research
PUBLISHED 16 February 2023
DOI 10.3389/fmed.2023.1111812

OPEN ACCESS

EDITED BY
Xiaolin Sun,
Peking University People's Hospital, China

REVIEWED BY
Jianping Guo,
Peking University People's Hospital, China
Fanlei Hu,
Peking University People's Hospital, China
Yanying Liu,
Capital Medical University, China
Ângelo Calado,
Universidade de Lisboa, Portugal

*CORRESPONDENCE
Yongfu Wang
✉ wyf18686198868@163.com

†These authors have contributed equally to this work and share first authorship

SPECIALTY SECTION
This article was submitted to Rheumatology, a section of the journal Frontiers in Medicine

RECEIVED 30 November 2022
ACCEPTED 18 January 2023
PUBLISHED 16 February 2023

CITATION
Sun X, Ding T, Wang B, Chang Z, Fei H, Geng L and Wang Y (2023) Identification of lncRNA–miRNA–mRNA networks in circulating exosomes as potential biomarkers for systemic sclerosis. *Front. Med.* 10:1111812. doi: 10.3389/fmed.2023.1111812

Identification of lncRNA–miRNA–mRNA networks in circulating exosomes as potential biomarkers for systemic sclerosis

Xiaolin Sun†, Tiantian Ding†, Baoyue Wang, Zhifang Chang, Hongchang Fei, Lixia Geng and Yongfu Wang*

The First Affiliated Hospital of Baotou Medical College, Inner Mongolia University of Science and Technology, Baotou, Inner Mongolia, China

Objective: This study aimed to analyze potential biomarkers for systemic sclerosis (SSc) by constructing lncRNA–miRNA–mRNA networks in circulating exosomes (cirexos).

Materials and methods: Differentially expressed mRNAs (DEmRNAs) and lncRNAs (DElncRNAs) in SSc cirexos were screened using high-throughput sequencing and detected with real-time quantitative PCR (RT-qPCR). Differentially expressed genes (DEGs) were analyzed using the DisGeNET, GeneCards, GSEA4.2.3, Gene Ontology (GO), and Kyoto Encyclopedia of Genes and Genomes (KEGG) databases. Receiver operating characteristic (ROC) curves, correlation analyses, and a double-luciferase reporter gene detection assay were used to analyze competing endogenous RNA (ceRNA) networks and clinical data.

Results: In this study, 286 DEmRNAs and 192 DElncRNAs were screened, of which 18 DEGs were the same as the SSc-related genes. The main SSc-related pathways included extracellular matrix (ECM) receptor interaction, local adhesion, platelet activation, and IgA production by the intestinal immune network. A hub gene, *COL1A1*, was obtained by a protein–protein interaction (PPI) network. Four ceRNA networks were predicted through Cytoscape. The relative expression levels of *COL1A1*, ENST0000313807, and NON-HSAT194388.1 were significantly higher in SSc, while the relative expression levels of hsa-miR-29a-3p, hsa-miR-29b-3p, and hsa-miR-29c-3p were significantly lower in SSc ($P < 0.05$). The ROC curve showed that the ENST00000313807-hsa-miR-29a-3p-*COL1A1* network as a combined biomarker of SSc is more valuable than independent diagnosis, and that it is correlated with high-resolution CT (HRCT), Scl-70, C-reactive protein (CRP), Ro-52, IL-10, IgM, lymphocyte percentage, neutrophil percentage, albumin divided by globulin, urea, and RDW-SD ($P < 0.05$). Double-luciferase reporter gene detection showed that ENST00000313807 interacts with hsa-miR-29a-3p, which interacts with *COL1A1*.

Conclusion: The ENST00000313807-hsa-miR-29a-3p-*COL1A1* network in plasma cirexos represents a potential combined biomarker for the clinical diagnosis and treatment of SSc.

KEYWORDS

systemic sclerosis, circulating exosomes, lncRNA, bioinformatics analysis, biomarkers

1. Introduction

Systemic sclerosis (SSc) is an autoimmune disease that includes diffuse systemic sclerosis (dSSc) and localized systemic sclerosis (lSSc) (1). The clinical manifestations of SSc include skin, lung, gastrointestinal, and cardiovascular damage (1). Lung damage includes pulmonary fibrosis and pulmonary vascular disease, which are characterized by a non-expectorant cough and dyspnea (1). SSc is a rare disease that mainly occurs in women, with an annual incidence rate of 10–20 per million people and a prevalence rate of 30–300 per million people (1). Traditional therapy is a combination of immunosuppressants, such as mycophenolate mofetil or cyclophosphamide, while hematopoietic stem cell transplantation is also used to treat refractory SSc (2). In view of the limited treatment methods at present, the quality of life and prognosis of patients with SSc are poor, and the early diagnosis of SSc without skin lesions is difficult. Therefore, it is particularly important to find appropriate biomarkers to assist in diagnosis or use in targeted therapy.

At present, the pathogenesis of SSc is incompletely understood. In addition to possible genetic and environmental factors, three other major factors play a critical role in the pathogenesis of SSc: endothelial injury and fibroproliferative vasculopathy, immune system abnormalities, and fibroblast dysfunction (3). Wasson et al. (4) showed that overexpression of lncRNA HOTAIR in the dermal fibroblasts of SSc induced the expression of collagen and α-smooth muscle actin, activated the NOTCH pathway, and inhibited the expression of miRNA-34a. They also found that HOTAIR was upregulated in *in vitro* cultured myofibroblasts from patients with SSc and in skin biopsies from SSc patients, while miRNA-34a was downregulated in the dermal fibroblasts of SSc *in vitro*. Mounting evidence has suggested that exosomes (EXOs) are closely related to vascular injury, immune abnormalities, and fibrosis in SSc (3). Circulating exosomes (circexos) are membrane-bound vesicles with a diameter of 30–120 nm that are secreted from tissue cells into blood (5). Cirexos can fuse with the cell membrane and transport proteins, lipids, and nucleic acids of the recipient cell for communication between cells or between cells and the environment, thus affecting the physiological and pathological functions of both the recipient cell and parent cell (6, 7). Thus, cirexos may be a novel and disease-specific biomarker for the diagnosis of SSc (8). Several miRNAs associated with profibrosis have been found to be significantly increased in cirexos isolated from the serum of patients with SSc, and serum cirexos isolated from patients with SSc stimulated the expression of genes encoding extracellular matrix components, such as collagen type I alpha 1 (*COL1A1*), collagen type III alpha 1 (*COL3A1*), and fibronectin 1 (9). Serum exosomes from patients with dSSc and lSSc also induced dose-dependent increases in the expression of genes related to myofibroblast activation (9). Therefore, cirexos may be involved in fibrosis in SSc.

Recently, researchers have paid increasing attention to competing endogenous RNAs (ceRNAs). ceRNAs do not specifically refer to one type of RNA, but rather a novel mechanism for RNAs interacting with each other. ceRNAs are involved in various diseases, such as cancer, immune-related diseases, cardiovascular diseases, and neurological diseases (10). Wang et al. (11) identified the regulatory role of lncRNA SNHG16 in myasthenia gravis (MG), an autoimmune disease, by constructing the ceRNA network. They found that SNHG16 was upregulated in patients with MG and was involved in its pathogenesis by competitively binding let-7c-5p to increase the expression of IL-10. Based on ceRNA, Fan et al. (12) found that lncRNA LOC100912373 could upregulate the expression of pyruvate dehydrogenase kinase 1 (*PDK1*), accelerate the phosphorylation of protein kinase B (AKT), induce the proliferation of fibroblast-like synoviocytes by competitively binding to miR-17-5p, and promote the occurrence and development of rheumatoid arthritis (RA). Extracellular lncRNAs are mainly enriched in exosomes, and cirexos can act as a protective barrier shielding lncRNAs from extracellular degradation, thus making lncRNAs stably expressed and easily detected as a biomarker of disease (13). LncRNAs, miRNAs, and mRNAs carried by cirexos have the potential to become new biomarkers and therapeutic targets of SSc (8, 14). However, there are limited studies on lncRNAs in cirexos in SSc and other autoimmune diseases, and many lncRNAs in plasma cirexos have not been fully studied.

In this study, cirexos were extracted and identified from the plasma of healthy controls (HCs) and patients with SSc. High-throughput sequencing and bioinformatics analysis were used to screen ceRNA networks in the SSc plasma cirexos. The ceRNA networks that were correlated with the clinical data of patients with SSc were verified with real-time quantitative PCR (RT-qPCR) and a double-luciferase reporter gene test (**Figure 1**). The results from this study provide potential biomarkers for the diagnosis and treatment of SSc.

2. Materials and methods

2.1. Patients and samples

Whole blood samples were collected from 20 patients with SSc and 20 age- and sex-matched HCs in the Department of Rheumatology and Physical Examination at the First Affiliated Hospital of Baotou Medical College, Inner Mongolia University of Science and Technology. The inclusion criteria of patients with SSc were in accordance with the 2013 American College of Rheumatology (ACR)/European League Against Rheumatism (EULAR) classification criteria. This study protocol was approved by the Ethics Committee of the First Affiliated Hospital of

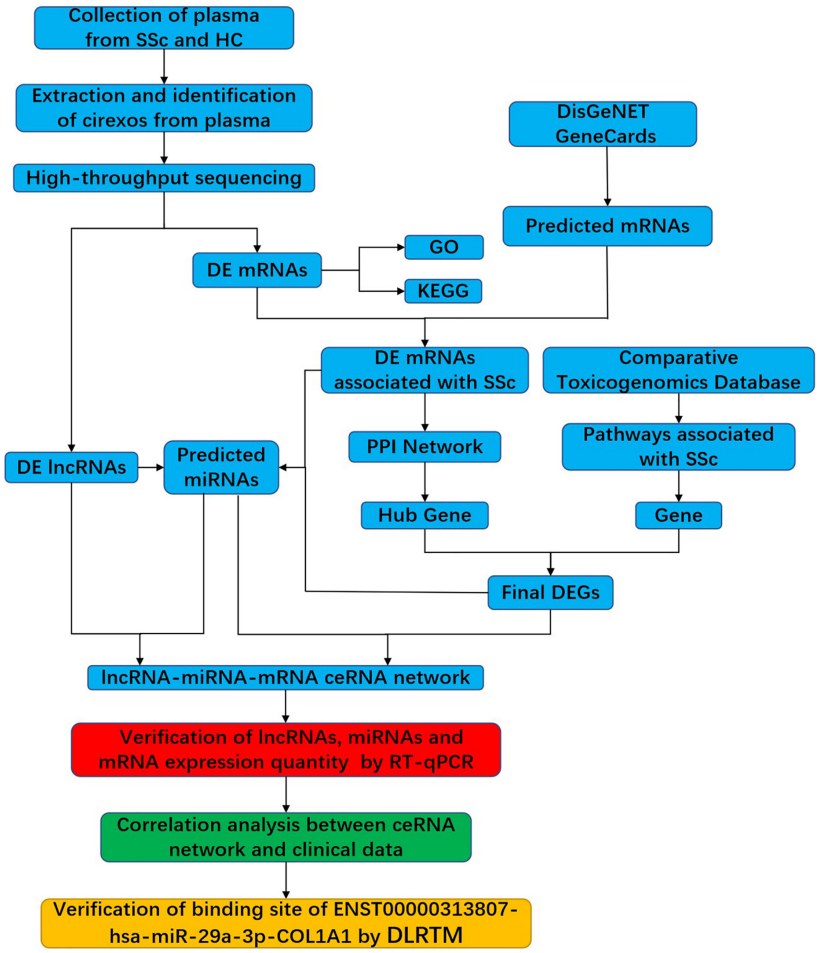

FIGURE 1
Flowchart of the experimental design. SSc, systemic sclerosis; HC, healthy control; cirexos, circulating exosomes; DEmRNAs, differentially expressed mRNAs; DElncRNAs, differentially expressed lncRNAs; DEGs, differentially expressed genes; GO, gene ontology; KEGG, Kyoto Encyclopedia of Genes and Genomes; PPI, protein–protein interaction; RT-qPCR, real-time quantitative PCR; DLRTM, dual-luciferase reporter.

Baotou Medical College, Inner Mongolia University of Science and Technology [Approval No. 2018 (017)].

2.2. Extraction and identification of cirexos

Peripheral whole blood samples (8 mL) were collected with EDTA anticoagulant-coated tubes and then centrifuged at 3,000 rpm for 10 min at 25°C. The supernatant was divided into centrifuge tubes (Eppendorf, Hamburg, Germany) and stored at −80°C. The process was completed within 2 h. Cirexos were extracted with the miRNeasy serum/plasma kit (Qiagen, Hilden, Germany) according to the manufacturer's instructions.

Precipitated cirexos were resuspended in radioimmunoprecipitation assay (RIPA) buffer (Solarbio, Beijing, China) to extract proteins. The protein concentration was determined using a BCA kit (Thermo Fisher Scientific, Waltham, MA, USA), and the cirexo protein markers were detected by western blot (WB). The protein was transferred to a polyvinylidene fluoride (PVDF) membrane following sodium dodecyl sulfate-polyacrylamide gel electrophoresis (SDS-PAGE). After blocking with 5% skimmed milk powder at 25°C for 2 h, specific primary antibodies against CD9 (1:5000), HRS (1:500) (Invitrogen, Camarillo, CA, USA), TSG101 (1:200), and calnexin (1:500) (Santa Cruz Biotechnology, San Diego, CA, USA) were incubated at 4°C for 8 h. The primary antibody was discarded the next day, and the secondary antibody (goat anti-rabbit HRP, 1:20,000) (Santa Cruz Biotechnology, CA, USA) was added and incubated at 37°C for 1 h. After incubating with a chemiluminescent substrate, the blot was photographed with an E-Gel imager (Thermo Fisher Scientific, Waltham, MA, USA). The particle size and distribution of cirexos were determined by a nanoparticle tracking analyzer (NTA) (ZetaView, Particle Matrix, Meersbusch, Germany). Analysis was performed using ZetaView 8.04.02 and Izon Control Suite 3.3.2 (IZON Science Ltd., Oxford, UK). In addition, transmission electron microscopy (TEM) (JEOL Ltd., Tokyo, Japan) was used to observe the isolated cirexos, and 10 mL of cirexos was used for electron microscopy detection and imaging at 100 kV.

2.3. RNA isolation and sequencing of cirexos

Prefiltered plasma was mixed with 2x binding buffer (XBP) at a ratio of 1:1 and then added to the exoEasy membrane affinity

TABLE 1 Sequences of the primers used in this study.

Name	Sequence of primers (5′-3′)
ENST00000313807	Forward: GTGCTGGGTCGGGCTTCC
	Reverse: GTCGGGCGGCGGTCTTC
NONHSAT194388.1	Forward: TTAGCCAACATCACACTACTCCAAG
	Reverse: CCCACCTCAACCTCTCAAATAGC
COL1A1	Forward: AGGGCTGGGCGGGAGAG
	Reverse: ACACATCAAGACAAGAACGAGGTAG
hsa-miR-29a-3p	Stem-loop RT-primer: CTCAACTGGTGTCGTGGAGTCGGCAATTCAGTTGAGTAACCGAT
	Forward: ACACTCCAGCTGGGTAGCACCATCTGAAAT
hsa-miR-29b-3p	Stem-loop RT-primer: CTCAACTGGTGTCGTGGAGTCGGCAATTCAGTTGAGAACACTGA
	Forward: ACACTCCAGCTGGGTAGCACCATTTGAAATC
hsa-miR-29c-3p	Stem-loop RT-primer: CTCAACTGGTGTCGTGGAGTCGGCAATTCAGTTGAGTAACCGAT
	Forward: ACACTCCAGCTGGGTAGCACCATTTGAAAT

column. After centrifugation, the effluent was discarded, and washing buffer (XWP) was added to the column. After centrifugation, the flow through was discarded. QIAzol kit (QIAGEN, Hilden, Germany) was used to lyse the vesicles. Following centrifugation, the lysate was collected and chloroform was added and then thoroughly mixed. After centrifugation, ethanol was added to the aqueous phase. The sample–ethanol mixture was added onto RNeasy MinElute spin columns. After centrifugation, columns were washed once with buffer RWT, then twice with RPE buffer, before eluting RNA in water (15). The total RNA extracted from cirexos was subjected to high-throughput sequencing.

2.4. High-throughput screening of DEmRNAs and DElncRNAs

According to the P-value < 0.05 and $|\log2$ (a Fold–change)$| \geq 1$ standard, the differentially expressed mRNAs (DEmRNAs) and differentially expressed lncRNAs (DElncRNAs) in cirexos were obtained by high-throughput sequencing. The expression and clustering of DEmRNAs and DElncRNAs are presented by heatmaps and volcano maps. The mRNAs associated with SSc were predicted with the GeneCards database[1] and DisGeNET database,[2] and then the overlapping SSc-related genes and DEmRNAs were screened out and visualized by the online website Venn2.1.[3]

2.5. Analysis of gene ontology (GO) and Kyoto Encyclopedia of Genes and Genomes (KEGG) pathways

Gene ontology (GO) analysis of DEmRNAs was conducted by a Fisher's exact test. The GO items with $P < 0.05$ were considered significantly enriched. Gene set enrichment analysis (GSEA, version 4.2.3)[4] was used to perform GO analysis on all DEmRNAs obtained by sequencing. The random combination was set as 1,000 times. The gene matrix was set as c5.all.v7.5.1 symbols.gmt (GO), and GO items with a normalized enrichment score (NES) absolute value > 1 and $P < 0.05$ were screened. DEmRNAs were analyzed using the KEGG database with Fisher's exact test. Pathways with a $P < 0.05$ were considered significantly enriched. The network of KEGG pathways was reconstructed by the ClueGO plug-in of Cytoscape3.9.1.[5]

2.6. Prediction of miRNAs targeted by DElncRNAs and DEmRNAs

lncRNASNP2[6] was used to predict the miRNAs bound to DElncRNAs. Mature miRNA sequences from miRBase (21st edition) were collected in lncRNASNP2. To reduce false positives, the same miRNAs in MiRanda, TargetScan, and Pita were selected as the final target in lncRNASNP2 (16). miRNAs that interacted with SSc-associated DEmRNAs were predicted using Starbase v2.0.[7] Data in lncRNASNP2 and Starbase v2.0 were supported by purple diplomatic immunoprecipitation and high-throughput sequencing experiments (17).

2.7. Prediction of lncRNA–miRNA–mRNA ceRNA networks

lncRNA–miRNA–mRNA networks were established according to the upregulated or downregulated mRNAs and lncRNAs in SSc, as well as the miRNAs that interacted with them. The STRING online tool[8] was used to construct the protein–protein interaction (PPI) network of DEmRNAs. The minimum interaction score was set to be > 0.15. The data from the STING database were visualized and analyzed *via* Cytoscape 3.9.1 software. Hub genes in networks were identified with the cytoHubba plugin in Cytoscape 3.9.1 (18).

1 https://www.genecards.org/
2 https://www.disgenet.org/home/
3 https://bioinfogp.cnb.csic.es/tools/venny/index.html
4 https://www.gsea-msigdb.org/gsea/index.jsp
5 https://cytoscape.org/
6 http://bioinfo.life.hust.edu.cn/lncRNASNP
7 https://starbase.sysu.edu.cn/
8 https://string-db.org/

Hub genes were calculated with three algorithms, including Maximal Clique Centrality (MCC), Degree, and Maximum Neighborhood Component (MNC), and then presented using the Venn diagram online tool (19, 20). The pathways related to SSc were predicted by the Comparative Toxicogenomics Database.[9] The corresponding genes of the pathways were found, and the same DEmRNAs were used as the hub genes of the PPI networks. The lncRNA–miRNA–mRNA networks were drawn with Cytoscape3.9.1 software.

2.8. Prediction of mRNA and lncRNA localization

LncLocator[10] is the prediction database of lncRNA subcellular localization, including localization of 15 cell lines (21, 22). The mRNALocator[11] is a database for predicting mRNA subcellular localization (23). In this study, lncLocator and mRNALocator were used to predict the subcellular localization of lncRNA and mRNA, respectively.

2.9. Prediction of upstream transcription factors (TFs) and downstream binding proteins of lncRNAs

The binding sites of TFs for lncRNA were predicted by the ConSite database. The CatRAPID database[12] was used to predict proteins that bind with lncRNA. PubMed[13] was used to search for TFs and binding proteins related to SSc (24, 25).

2.10. ceRNA networks were verified by RT-qPCR

The relative expression levels of lncRNAs, miRNAs, and mRNAs involved in ceRNA networks from the plasma cirexo samples of 20 patients with SSc and 20 HCs were verified by RT-qPCR. The PCR cycling conditions were as follows: 95°C for 1 min; 40 cycles of 95°C for 15 s and 60°C for 30 s; and dissociation at 72 and 99°C. Data were analyzed by the 2-ΔΔCt method. Three technical replicates were used for each sample. The sequences of primers used in this study are listed in **Table 1**.

2.11. Correlation analysis between ceRNA networks and clinical data and receiver operating characteristic (ROC) curve drawing

The correlation between ceRNA networks was analyzed by IBM SPSS software Version 26.0 (SPSS Inc., Chicago, IL, USA) and GraphPad Prism 9.0.0 (GraphPad, La Jolla, CA, USA). Correlations between ceRNA networks and clinical data, such as high-resolution CT (HRCT), antinuclear antibody profile (Scl-70, CENP-B, Ro-52), C-reactive protein (CRP), IL-10, lymphocyte percentage, and neutrophil percentage, were analyzed, and then the receiver operating characteristic curve (ROC) for SSc diagnosis was drawn.

2.12. Verification of ceRNA interactions by a double-luciferase reporter gene assay

We synthesized the wild-type (WT) sequences of ENST00000313807 and *COL1A1* and cloned them into the pGL3 basic vector. According to the predicted interaction sites, the plasmid was used as a point-mutation template to construct a pGL3 basic vector. The pGL3 basic vector contains Firefly luciferase, and the pRL-TK plasmid contains Renilla luciferase, which was used as the control. The WT or mutation reporter plasmid was co-transfected with the hsa-miR-29a-3p mimic or negative control (NC) mimic into 293T cells. After 48 h, the luciferase activity of different groups was detected with the double-luciferase report gene detection kit (Beyotime, Shanghai, China). The relative light unit (RLU) values determined by firefly luciferase were divided by those determined by sea kidney luciferase. According to the ratio obtained, the activation degree of the target reporter gene was detected in different groups. The plasmids were divided into the following groups: NC mimics + ENST-WT; hsa-miR-29a-3p-mimics + ENST-WT; NC-mimics + ENST-mutant (MT); hsa-miR-29a-3p-mimics + ENST-MT; NC-mimics + *COL1A1*-WT; hsa-miR-29a-3p-mimics + *COL1A1*-WT; NC-mimics + *COL1A1*-MT; and hsa-miR-29a-3p-mimics + *COL1A1*-MT.

2.13. Statistical analysis

The data were analyzed by IBM SPSS software Version 26.0 (SPSS Inc., Chicago, IL, USA), GraphPad Prism 9.0.0 (GraphPad, La Jolla, CA, USA) and R Studio 4.1.0 (Boston, MA, USA). When the data of the correlation analysis were linear and conformed to normal distribution, Pearson correlation analysis was used for correlation analysis between ceRNA networks and clinical data; otherwise, Spearman's correlation was used. When the data conformed to a normal distribution and the variance was homogeneous, an independe nt-sample t test was used; when the data conformed to a normal distribution and the variance was inhomogeneous, Welch's t test was used; otherwise, a non-parametric test was used. Data are presented as the mean ± SEM, and tests were repeated three or five independent times. P-values < 0.05 were considered statistically significant. Binary logistic regression was also used for ROC curve analysis.

3. Results

3.1. Identification of plasma cirexos

In this study, TEM, WB, and NTA were used to identify the extracted cirexos. The results are shown in **Figure 2**. Clear vesicle structures were observed in plasma cirexos of SSc and HC by TEM,

9 http://ctdbase.org/
10 http://www.csbio.sjtu.edu.cn/bioinf/lncLocator/
11 http://bio-bigdata.cn/mRNALocater/
12 http://s.tartaglialab.com/page/catrapid_group
13 https://pubmed.ncbi.nlm.nih.gov/

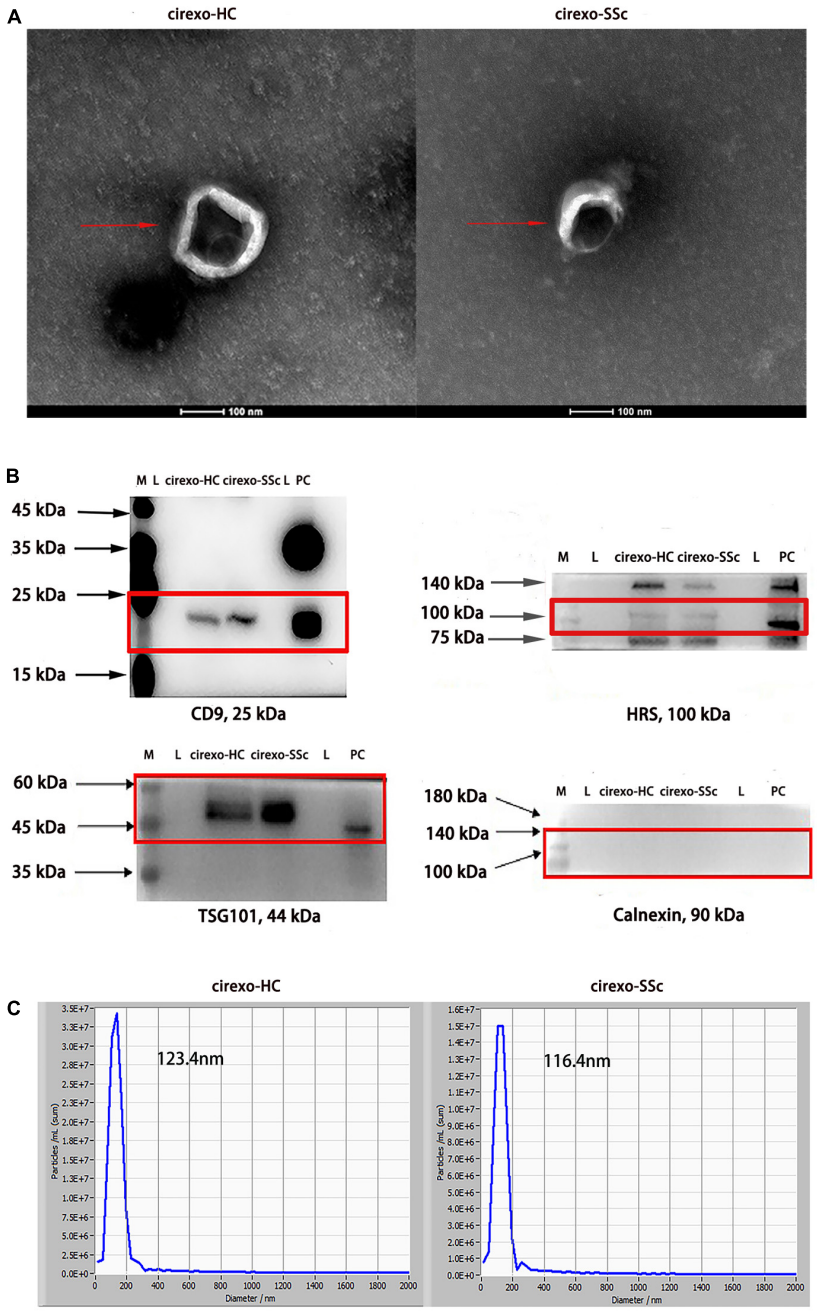

FIGURE 2
Identification of circulating exosomes (cirexos). **(A)** The morphology of cirexos was detected by transmission electron microscopy (TEM) (magnification: 300,000×). **(B)** Identification of cirexo surface markers by western blot (WB). M, marker; L, loading buffer; PC, exosomes (EXOs) derived from mouse macrophage supernatant, which was used as the positive control. **(C)** Determination of cirexo concentration and particle size by nanoparticle tracking analyzer (NTA). Cirexos, circulating exosomes; EXOs, exosomes.

and the vesicle size was consistent with the detection standard of EXOs (Figure 2A). WB analysis showed the presence of the exosome markers hepatocyte growth factor-regulated tyrosine kinase substrate (HRS), CD9, and tumor susceptibility gene 101 (TSG101), but the absence of Calnexin (Figure 2B). The particle size of samples detected by NTA was consistent with the standard. The cirexo diameter of the HC sample was 123.4 nm, and the concentration was 1.2×10^{11} particles/mL. The cirexo diameter of the SSc sample was 116.4 nm, and the concentration of the sample was 9.5×10^{10} particles/mL (Figure 2C). The data indicated that cirexos were successfully extracted.

3.2. Analysis of DEmRNAs and DElncRNAs in plasma cirexos by high-throughput sequencing

High-throughput sequencing was used to screen DEmRNAs and DElncRNAs in the plasma cirexos of SSc. The volcano map showed the overall distribution of differentially expressed genes (DEGs). The horizontal coordinate of the volcano map was the multiple of the difference, and a fold change greater than 2 was set to identify the differential genes. The ordinate was set as the minus

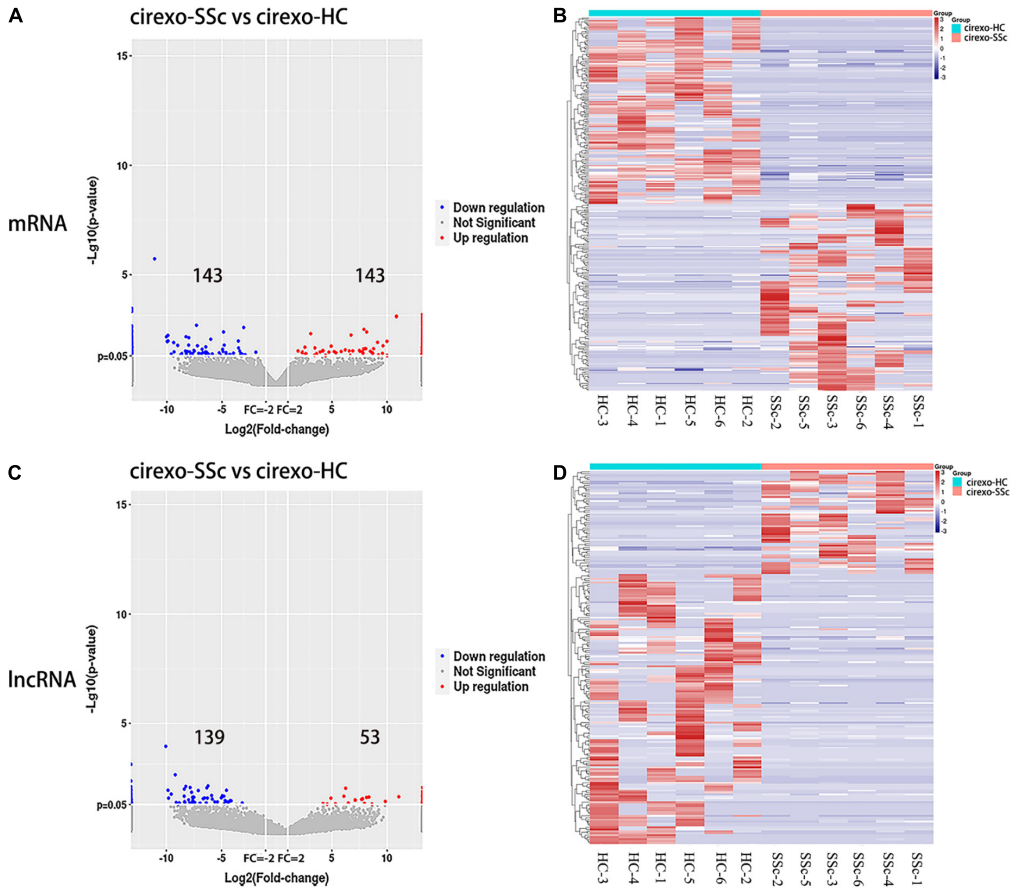

FIGURE 3
Expression profiles of mRNA and lncRNA in cirexos in the circulating exosomes–systemic sclerosis (cirexo-SSc) and circulating exosomes–healthy control (cirexo-HC) groups (n = 6). **(A,C)** Volcano plots show upregulated (red) and downregulated (blue) mRNA and lncRNA. The abscissa represents the fold change of gene expression in the different samples [log2 (fold-change)], and the ordinate represents the significance level of the differential gene expression [−log10 (p-value)]. **(B,D)** Heatmaps showing the hierarchical clustering analysis of differentially expressed mRNAs (DEmRNAs) and differentially expressed lncRNAs (DElncRNAs). The rows represent genes, and the columns represent the expression of the same sample. Red indicates high expression, and blue indicates low expression.

base-10 logarithm of the P-value, which is -log 10 (P-value). The log10 (FPKM + 1) values were normalized and then clustered. The volcano map showed 286 DEmRNAs, including 143 upregulated genes and 143 downregulated genes (Figure 3A) ($P < 0.05$). The volcano map showed 192 DElncRNAs, including 53 upregulated lncRNAs and 139 downregulated lncRNAs (Figure 3C) ($P < 0.05$). The heatmap showed the expression levels of DEmRNAs (Figure 3B) and DElncRNAs (Figure 3D) in cirexos from the SSc and HC groups. The selected 286 DEmRNAs were used for further GO and KEGG enrichment analysis to explore the potential biological functions of DEmRNAs and the corresponding enrichment pathways.

3.3. GO enrichment analysis of DEmRNAs in cirexo

The number of DEmRNAs corresponding to the cell component (CC), molecular function (MF), and biological process (BP) of GO was counted and graphically displayed. In biological processes, DEmRNA mainly focuses on cellular process, metabolic process, single biological process, biological regulation, regulation of biological process, response to stimulus, cellular component organization and biogenesis, multicellular biological process, signal, and localization. In cellular components, DEmRNAs were mainly concentrated in the cell, cell part, organelle, membrane, organelle part, membrane part, extracellular region, membrane closed cavity, polymer complex, and extracellular region part. Among the molecular functions, binding and catalytic activities were mainly enriched (Figure 4A). There were 67 GO biological pathways with a P-value < 0.05, including 47 biological process pathways, 11 cellular-component pathways, and 9 molecular-function pathways. Pathways related to SSc were screened through the Comparative Toxicogenomics Database. Among the top 30 enriched pathways, the pathways related to SSc mainly included matrix adhesion-dependent cell spreading, post-Golgi vesicle-mediated transport, epithelial–mesenchymal transition (EMT), endonuclease activity, intracellular transport, cell-matrix adhesion, and other processes (Figure 4B).

3.4. Analysis of pathway enrichment of DEmRNAs in cirexos

Pathway analysis of DEmRNAs was performed on the KEGG database using Fisher's exact test. DEmRNAs in cirexos of patients

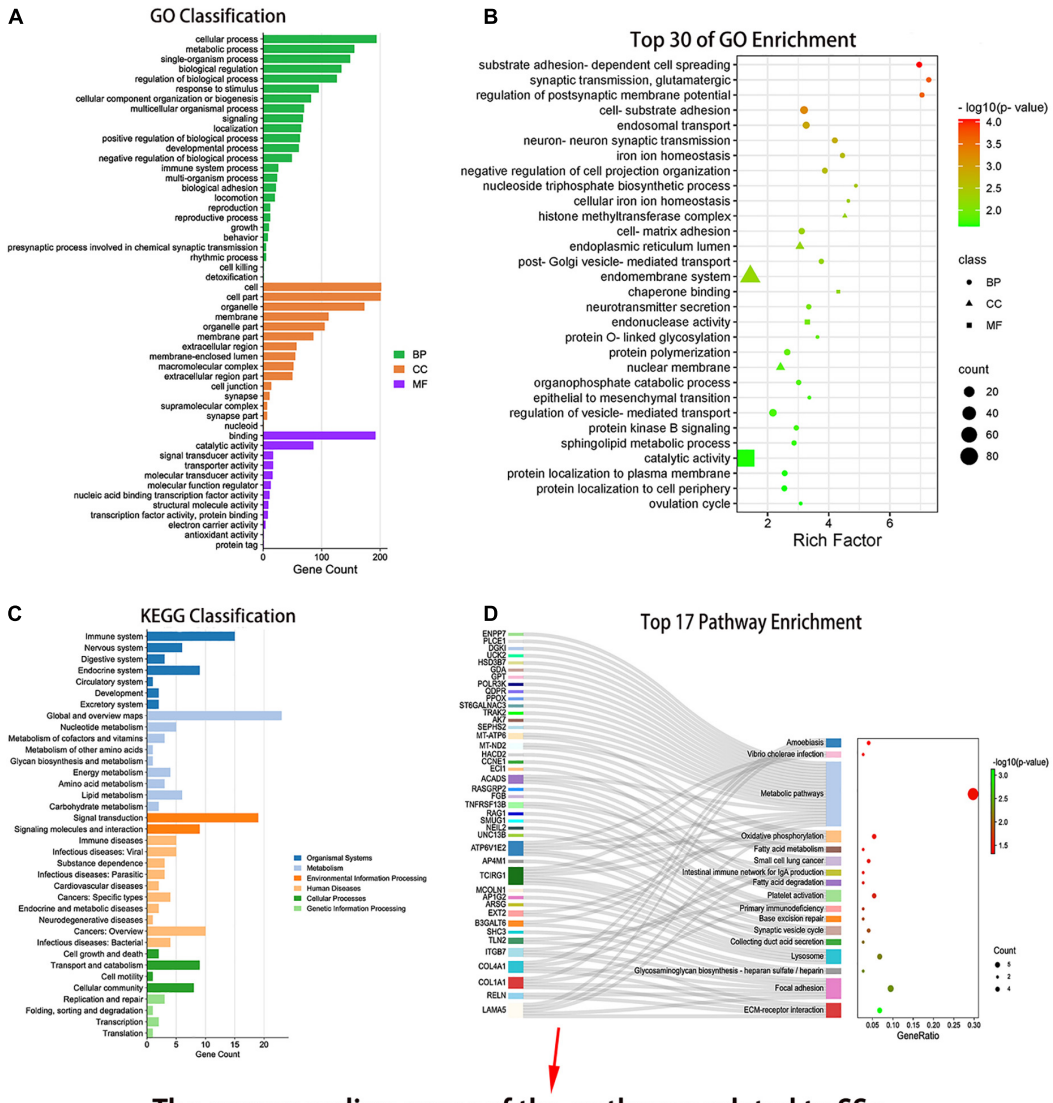

E

The corresponding genes of the pathways related to SSc

Passway	DEmRNAs	*P*-value
ECM-receptor interaction	COL1A1, COL4A1, ITGB7, LAMA5, RELN	0.000743
Focal adhesion	TLN2, SHC3, RELN, LAMA5, ITGB7, COL4A1, COL1A1	0.00465
Platelet activation	COL1A1, FGB, RASGRP2, TLN2	0.024495
Intestinal immune network for IgA production	ITGB7, TNFRSF13B	0.031078

FIGURE 4
Gene ontology (GO) and Kyoto Encyclopedia of Genes and Genomes (KEGG) enrichment analysis of the DEmRNAs. **(A)** The number of differentially expressed genes (DEGs) corresponding to the three GO levels, including biological process (BP), cellular component (CC), and molecular function (MF), was counted. **(B)** Top 30 GO entries with enrichment degree. The ordinate is the specific GO entry name. **(C)** KEGG classification. The abscissa is the number of genes mapped to a pathway class by DEGs, and the ordinate is the KEGG entries enriched by DEGs. **(D)** Pathway enrichment of the differential mRNAs. The abscissa is the proportion of genes corresponding to a certain pathway from the corresponding genes of all pathways. The ordinate is the KEGG entry name with $P < 0.05$ and the DEGs corresponding to the enrichment pathway. **(E)** Pathways related to SSc and corresponding genes with $P < 0.05$. GO, gene ontology; KEGG, Kyoto Encyclopedia of Genes and Genomes; BP, biological process; CC, cellular component; MF, molecular function.

with SSc were mainly enriched in immune system, immune diseases, signal transduction, lipid metabolism, cell growth and apoptosis, and cell movement (Figure 4C). Seventeen pathways had a *P*-value < 0.05 (Figure 4D). The pathways related to SSc were screened through the Comparative Toxicogenomics Database. The pathways related to SSc and corresponding DEmRNAs are shown in Figure 4E, including extracellular matrix (ECM) receptor interaction, focal adhesion, platelet activation, and intestinal immune network for IgA production (Figure 4E).

The Cytoscape plug-in ClueGO was used to analyze pathway enrichment of the DEmRNAs, and a total of 11 significantly enriched pathways were obtained. Pathways related to SSc were screened using the Comparative Toxicogenomics Database. ECM receptor interaction, focal adhesion, and platelet activation were associated with SSc. *TCIRG1*, *ITGB7*, *RELN*, *COL4A1*, *LAMA5*, and *COL1A1* were enriched in more than three pathway terms (Figure 5A). GSEA was used to analyze the pathway enrichment of DEmRNAs. The ECM-receptor interaction gene set showed the leading subset in the

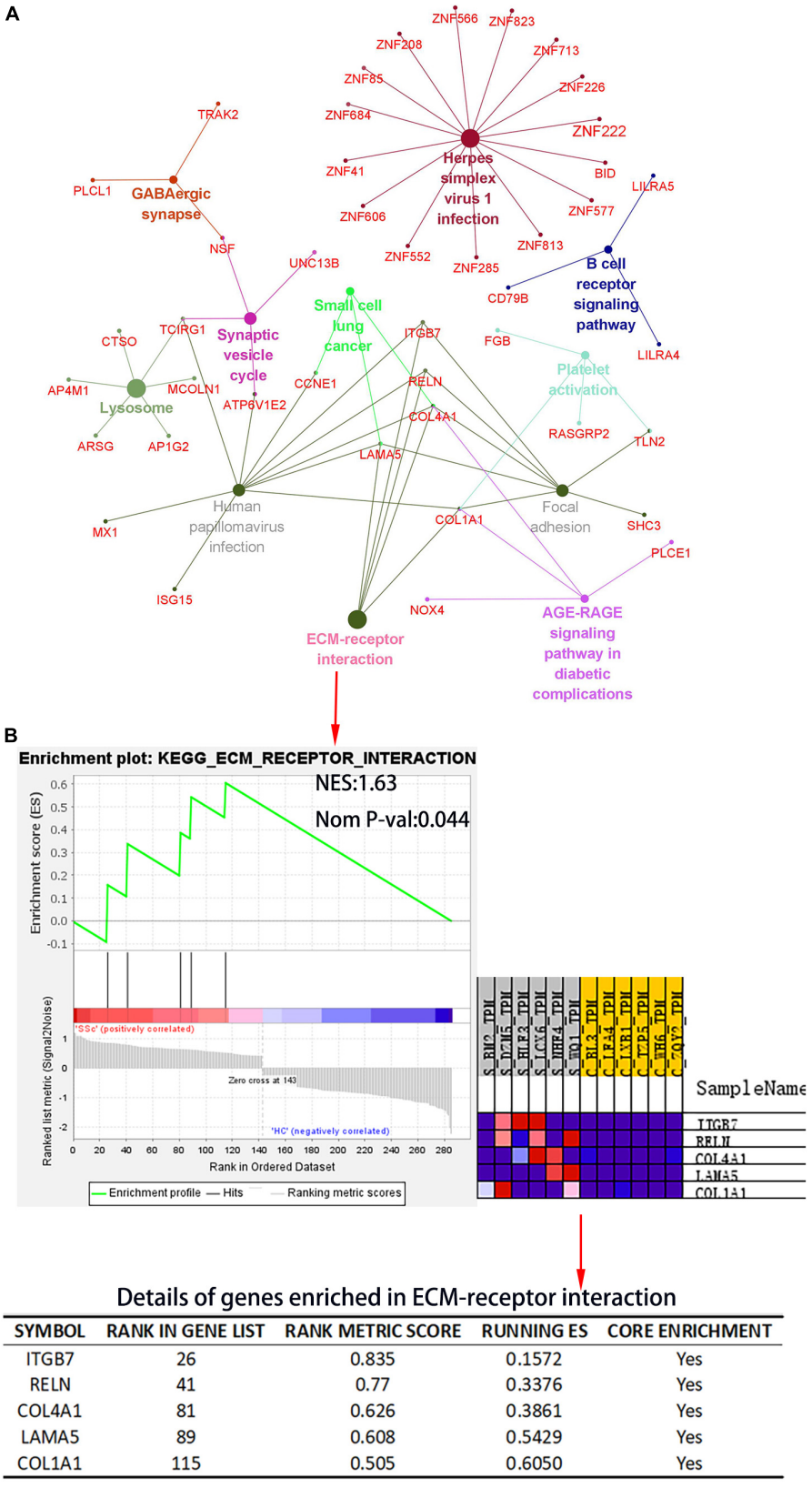

Details of genes enriched in ECM-receptor interaction

SYMBOL	RANK IN GENE LIST	RANK METRIC SCORE	RUNNING ES	CORE ENRICHMENT
ITGB7	26	0.835	0.1572	Yes
RELN	41	0.77	0.3376	Yes
COL4A1	81	0.626	0.3861	Yes
LAMA5	89	0.608	0.5429	Yes
COL1A1	115	0.505	0.6050	Yes

FIGURE 5
Kyoto Encyclopedia of Genes and Genomes (KEGG) pathway analysis of the DEmRNA and gene set enrichment analysis (GSEA) of differential gene expression profiles by c2, curated gene sets. **(A)** KEGG pathway analysis of DEmRNAs. The plug-in ClueGO of Cytoscape was used to map KEGG pathway interactions. Different colors represent different pathways. **(B)** The c2: KEGG gene set was used to conduct pathway enrichment analysis of DEmRNA profiles. In the table, "RANK IN GENE LIST" represents the position of a gene in the sorted gene set, "RANK METRIC SCORE" is the ranking score of genes, "RUNNING ES" is the dynamic enrichment score (ES) value in the analysis process, and "CORE ENRICHMENT" is the gene that mainly contributes to the ES value. NES, normalized enrichment score; Nom *P*-val, nominal *P*-value.

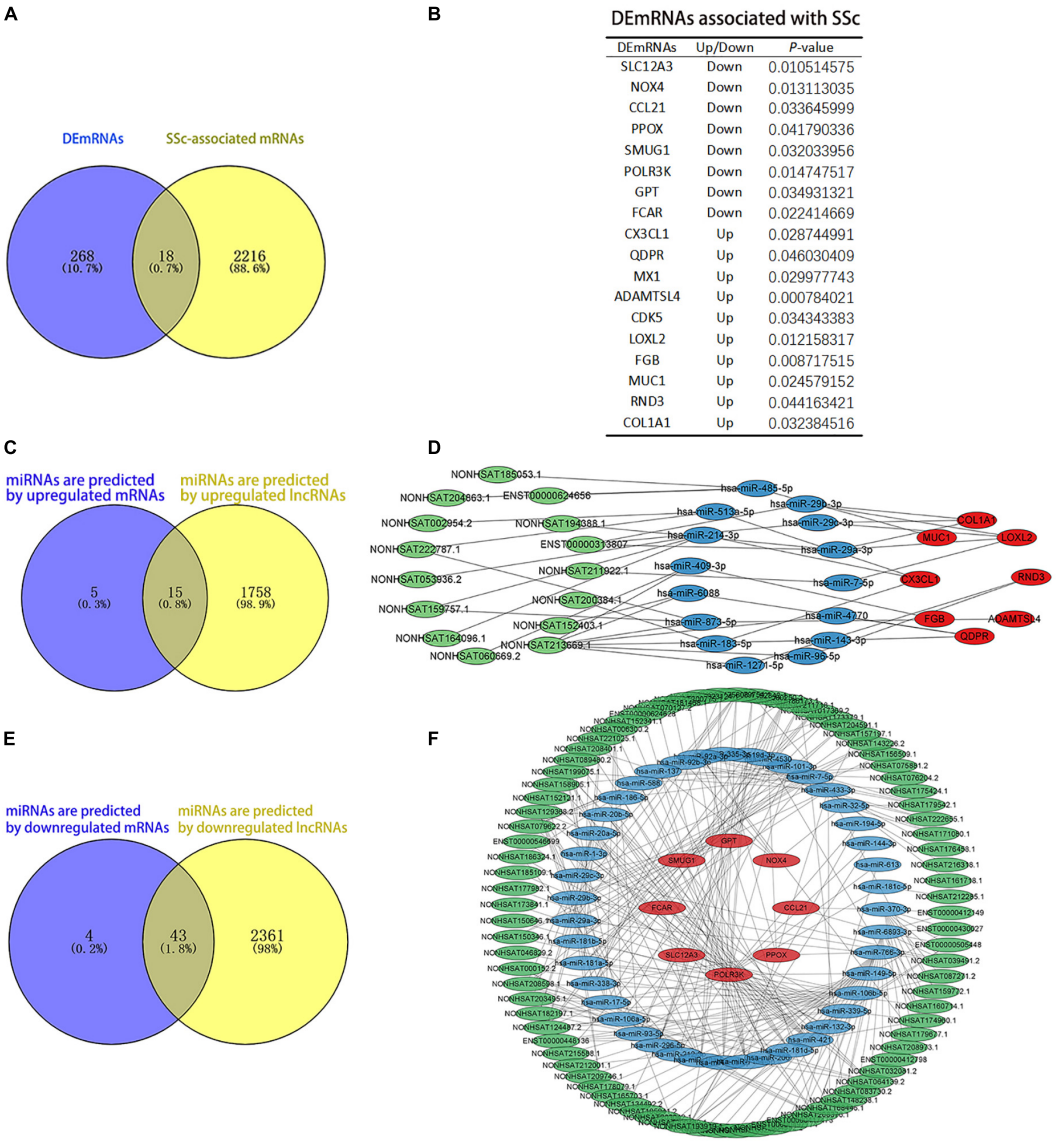

FIGURE 6
Analysis of competing endogenous RNAs (ceRNAs) networks. **(A)** The blue and yellow parts are Venn diagrams. The blue part shows the DEmRNAs obtained by sequencing. The yellow part is the mRNAs predicted by the DisGeNET and GeneCards databases, and the middle part represents the overlapping DEmRNAs of the two groups. **(B)** The table of DEmRNAs related to SSc. **(C,D)** Upregulated ceRNA network. Panel **(C)** the blue and yellow parts are Venn diagrams. The blue part shows the miRNAs that are predicted by upregulated mRNAs. The yellow part shows the miRNAs that are predicted by upregulated lncRNAs. Panel **(D)** green parts are upregulated lncRNA, blue parts are miRNAs that interact with lncRNA and mRNA, and red parts are upregulated mRNA. **(E,F)** Downregulated ceRNA network. Panel **(E)** the blue and yellow parts are Venn diagrams. The blue part shows the miRNAs predicted by downregulated mRNAs. The yellow part shows the miRNAs predicted by downregulated lncRNAs. Panel **(F)** the green parts are downregulated lncRNA, blue parts are miRNAs that interact with lncRNA and mRNA, and red parts are downregulated mRNA.

enrichment score (ES) diagram, with the absolute value of NES > 1, $P < 0.05$, indicating that this functional gene set had significant biological significance. *ITGB7*, *RELN*, *COL4A1*, *LAMA*, and *COL1A1* played core roles in the curated gene sets. The heatmap shows that the expression of these genes was upregulated in SSc ($P < 0.05$) (Figure 5B).

3.5. Prediction of miRNAs targeted by DElncRNAs and DEmRNAs

The results showed that 2,234 mRNAs were associated with SSc, as predicted by the Genecards and DisGeNET databases. We found 18 DEmRNAs that overlapped with mRNAs associated with SSc as predicted by the databases (Figure 6A). Among them, 10 were upregulated and 8 were downregulated (Figure 6B). ENCORI was used to predict the miRNAs bound to upregulated and downregulated DEmRNAs. LncRNASNP2 was used to predict the miRNAs bound to upregulated and downregulated DElncRNAs. The results showed that there were 20 miRNAs that interacted with the upregulated DEmRNAs, and 1,773 miRNAs that interacted with upregulated DElncRNAs, 15 of which were the same miRNAs (Figure 6C). Moreover, there were 47 miRNAs that interacted with downregulated DEmRNAs, and 2,404 miRNAs that interacted with downregulated DElncRNAs, 43 of which were the same miRNAs (Figure 6E). In addition, 15 upregulated lncRNAs, 15 miRNAs, and

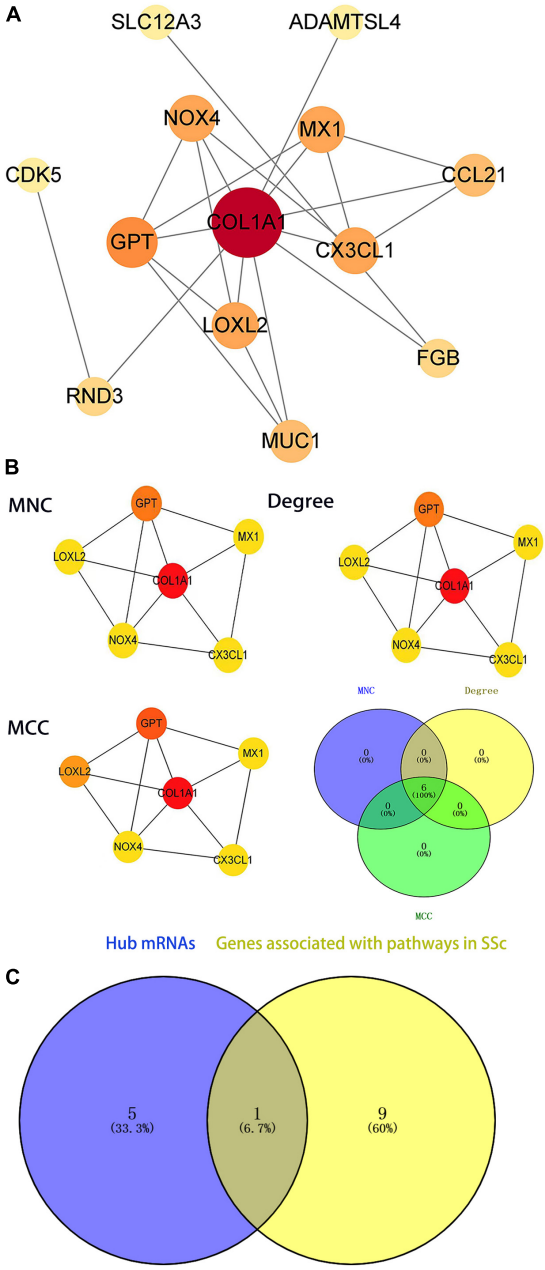

FIGURE 7
Identification of the hub genes in the protein–protein interaction (PPI) network. **(A)** PPI network of differentially expressed genes (DEGs) related to systemic sclerosis (SSc). The ceRNA networks of DEG encoded proteins are composed of 18 nodes and 19 edges. Each node represents a protein, and each edge represents a protein-protein association. **(B)** Identification of the hub genes of DEGs associated with SSc in the PPI network. The hub genes are identified by three algorithms: Maximal Clique Centrality (MCC), Degree, and Maximum Neighborhood Component (MNC). The color density represents the score of the algorithm. **(C)** The blue part presents the hub genes of the PPI network. The yellow part shows the genes associated with SSc-related pathways ($P < 0.05$ in KEGG). The middle part represents the overlapping hub genes of the two groups. MCC, maximal clique centrality; MNC, maximum neighborhood component.

8 upregulated mRNAs were obtained to construct ceRNA networks (Figure 6D), and 85 downregulated lncRNAs, 43 miRNAs, and 8 downregulated mRNAs were obtained to construct the ceRNA networks (Figure 6F).

3.6. Hub genes were screened by PPI networks

To further illustrate the interactions between selected DEGs, the STRING online tool was used to form a PPI network. Protein interaction analysis of DEmRNAs was performed with the STRING online tool. PPI networks were constructed with the lowest interaction score > 0.15 and visualized in Cytoscape (Figure 7A). The top six hub genes were calculated according to MCC, Degree, and MNC algorithms (Figure 7B), and included *COL1A1*, *CX3CL1*, *LOXL2*, *GPT*, *NOX4*, and *MX1*. These genes were the most important genes in the PPI network and may contribute to the pathogenesis of SSc. *COL1A1* was a hub gene in the PPI network and also in the SSc-related pathway *via* KEGG analysis, with a *P*-value < 0.05 (Figure 7C). Therefore, in the follow-up study, we will focus on the screened hub gene, namely *COL1A1*.

3.7. GO enrichment analysis of DEG expression profiles by the GSEA c5 gene set

Next, GO enrichment analysis of the DEG expression profile was performed by GSEA to further explore the biological function of DEGs. The DEmRNAs obtained by high-throughput sequencing were uploaded to GSEA, and the expression profiles were analyzed with c5 (GO gene sets). GO items with a NES absolute value > 1 and $P < 0.05$ were screened. The significantly upregulated gene sets in the BP include peptidyl amino acid modification, transmembrane transport, cell morphogenesis, regulation of cell differentiation, and ion transmembrane transport. The significantly downregulated gene sets include regulation of cellular component biogenesis. In MF, the gene sets with significantly enriched upregulated genes were transporter activity and identical protein binding. In CC, the gene sets of significantly enriched downregulated genes were catalytic complex mitochondrion and mitochondrion. Genes that played a central role in the above sets, including *COL1A1*, *NOX4*, and *CX3CL1*, were the same as the hub genes in the PPI network. According to our results, *NOX4*, which interacts with *COL1A1*, plays a central role in the cellular complex mitochondrion. *CX3CL1*, which interacts with *COL1A1*, plays a central role in transport, regulation of cell differentiation, and ion transport. *COL1A1* is involved in the regulation of cell differentiation in BP and is associated with conspecific protein binding in MF. *NOX4* is involved in protein modification and cell morphology in BP and is related to catalysis and mitochondria in CC. *CX3CL1* is involved in the regulation of cell differentiation, ion transmembrane transport, and biogenesis of cellular components in BP (Figure 8). The results showed that *COL1A1* plays a key role in GO enrichment. Therefore, in this study, ceRNA networks were established for further analysis of *COL1A1*.

3.8. Prediction of CeRNA networks and the lncRNA–miRNA–mRNA interaction sites

Salmena et al. (26) proposed a ceRNA hypothesis suggesting that, due to the existence of miRNA response elements (MREs) on mRNA and lncRNA, miRNAs can bind to target mRNA

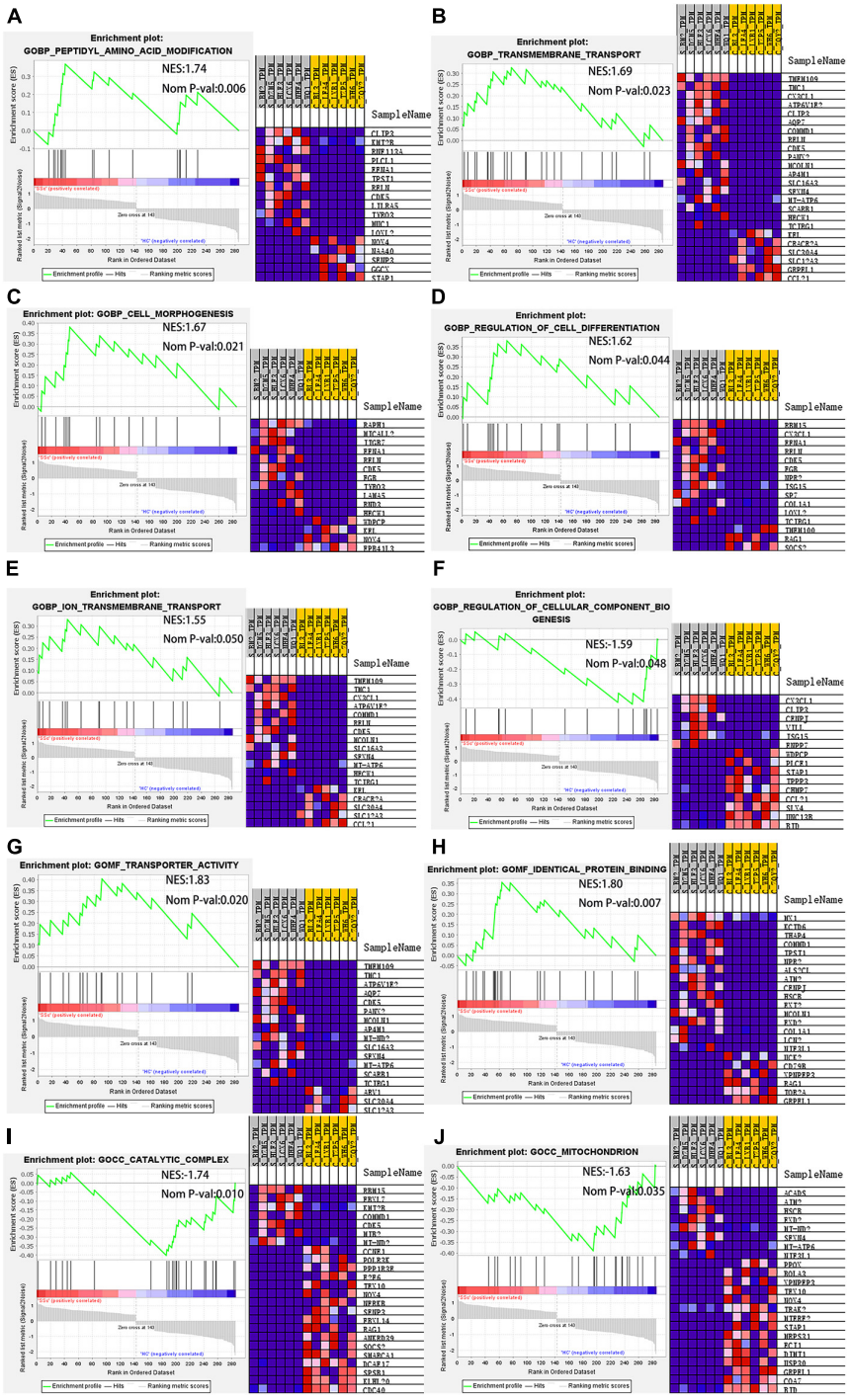

FIGURE 8
GSEA. In BP, the gene sets with significantly enriched upregulated genes include **(A)** peptidyl amino acid modification, **(B)** transmembrane transport, **(C)** cell morphogenesis, **(D)** regulation of cell differentiation, and **(E)** ion transmembrane transport. The gene set with significantly enriched downregulated genes includes **(F)** regulation of cellular component biogenesis. In MF, the gene sets with significantly enriched upregulated genes include **(G)** transporter activity and **(H)** identical protein binding. In CC, the gene sets with significant enrichment of downregulated genes include **(I)** catalytic complex mitochondrion and **(J)** mitochondrion. GSEA, gene set enrichment analysis; BP, biological process; MF, molecular function; CC, cell component.

and lncRNA to post-transcriptionally regulate gene expression. As complementary sequences of miRNAs, mRNA and lncRNA form a large-scale regulatory network in various parts of the transcriptome (26). Based on this hypothesis, mRNA or lncRNA binds to miRNA, forming a competitive relationship. In this study, the hub gene *COL1A1* was upregulated in SSc ($P < 0.05$). According to the ENCORI database, the predicted miRNAs that interacted with *COL1A1* included hsa-miR-29a-3p, hsa-miR-29b-3p, and hsa-miR-29c-3p. The predicted lncRNAs that interacted with hsa-miR-29a-3p, hsa-miR-29b-3p, and hsa-miR-29c-3p included ENST00000313807 and NON-HSAT194388.1. Therefore, four ceRNA networks were constructed (Figure 9A), and the lncRNA–miRNA–mRNA interaction sites were predicted (Figures 9B–E).

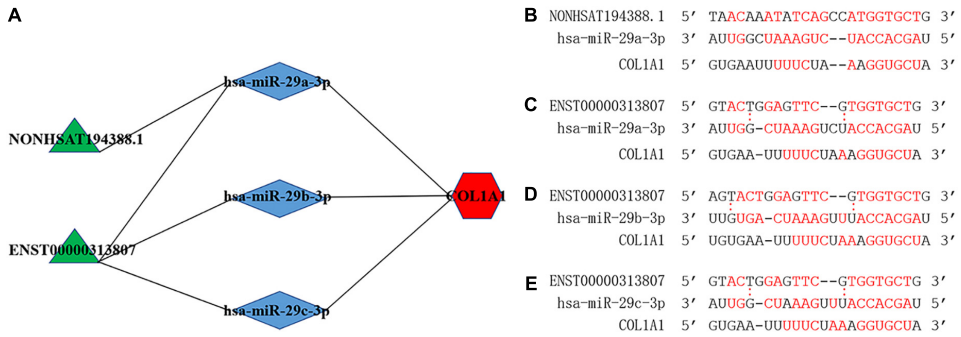

F

Prediction of mRNAs and lncRNAs location

RNA Locator	Gene Type		
	COL1A1 (mRNA)	ENST00000313807 (lncRNA)	NONHSAT194388.1 (lncRNA)
Cytoplasm	0.5678*	0.0123350291164	0.910248439134*
Endoplasmic reticulum	0.2892	/	/
Extracellular region	0.0508	/	/
Mitochondria	0.0159	/	/
Nucleus	0.0764	0.00799019307016	0.0280167008948
Ribosome	/	0.432523961377	0.0140893938309
Cytosol	/	0.528091899256*	0.045957640087
Exosome	/	0.0190589171804	0.00168782605333

FIGURE 9
Prediction of the binding sites and location of the ceRNA networks. **(A)** Prediction of ceRNA networks. Green parts are lncRNA, blue parts are miRNAs that interact with lncRNA and mRNA, and red parts are mRNA. **(B)** The red text represents binding sites of the NON-HSAT194388.1-hsa-miR-29a-3p-*COL1A1* interaction network. **(C)** The red text represents binding sites of the ENST00000313807-hsa-miR-29a-3p-*COL1A1* interaction network. **(D)** The red text represents binding sites of the ENST00000313807-hsa-miR-29b-3p-*COL1A1* interaction network. **(E)** The red text represents binding sites of the ENST00000313807-hsa-miR-29c-3p-*COL1A1* interaction network. ":" Means that the bond is not firm, and the red font means that the bond is stable. **(F)** Prediction of miRNA and lncRNA localization. The "∗" indicates the final predicted position on the website.

3.9. Prediction of mRNA and lncRNA localization

The subcellular localization of lncRNAs involved in ceRNA is crucial for the study of ceRNAs. As the main location of ceRNAs is the cytoplasm, lncRNAs involved in ceRNAs need to be expressed in the cytoplasm to regulate the expression of targeted mRNAs (27, 28). Cytoplasmic lncRNAs play key roles in the cell through various molecular mechanisms, including regulating the transport of cytoplasmic proteins from the cytosol to nucleus to regulate transcription (28–30). Based on the prediction score in the mRNALocater online database, *COL1A1* was predicted to be located in the cytoplasm. Based on the prediction score, ENST00000313807 and NON-HSAT194388.1 were predicted to be located in the cytoplasm by the lncLocater online database (**Figure 9F**). The results suggested that *COL1A1*, ENST00000313807, and NON-HSAT194388.1 were consistent with the mechanism of ceRNA in the cytoplasm.

3.10. Prediction of upstream TFs and downstream binding proteins of lncRNAs

Transcription factors (TFs) can regulate the expression of lncRNA by binding to its promoter region (31). The upstream TFs of ENST00000313807 and NON-HSAT194388.1 were predicted by the database ConSite. The TFs that overlapped between both groups included E74A, c-FOS, Hunchback, Sox-5, FREAC-4, Snail, HFH-2, HNF-3beta, HFH-1, SOX17, and HFH-3. Among them, the TFs related to SSc were c-FOS, Snail, and SOX17, as identified from the PubMed database (32–35; **Figures 10A, B**). Interaction with binding proteins is an important function of lncRNAs. We predicted the downstream binding proteins of ENST00000313807 and NON-HSAT194388.1 through the online website catrapid, and selected the top 10 scores of predicted binding ability. The following five binding proteins were obtained: SLC4A1AP, L1TD1, WDR43, HTATSF1, and BAZ2B (**Figures 10C, D**). However, an extensive literature search involving these proteins in the PubMed database did not reveal any studies related to SSc.

3.11. Validation of RNA-Seq data by RT-qPCR and ROC curve

To detect the expression of RNA in the ceRNA networks predicted above, plasma cirexos in 20 SSc and 20 HC cases were detected by RT-qPCR. Compared to the cirexo-HC group, the expression levels of ENST00000313807 ($P < 0.05$), NON-HSAT194388.1 ($P < 0.05$), and *COL1A1* ($P < 0.01$) in the SSc-cirexo group were significantly increased, while the expression levels of

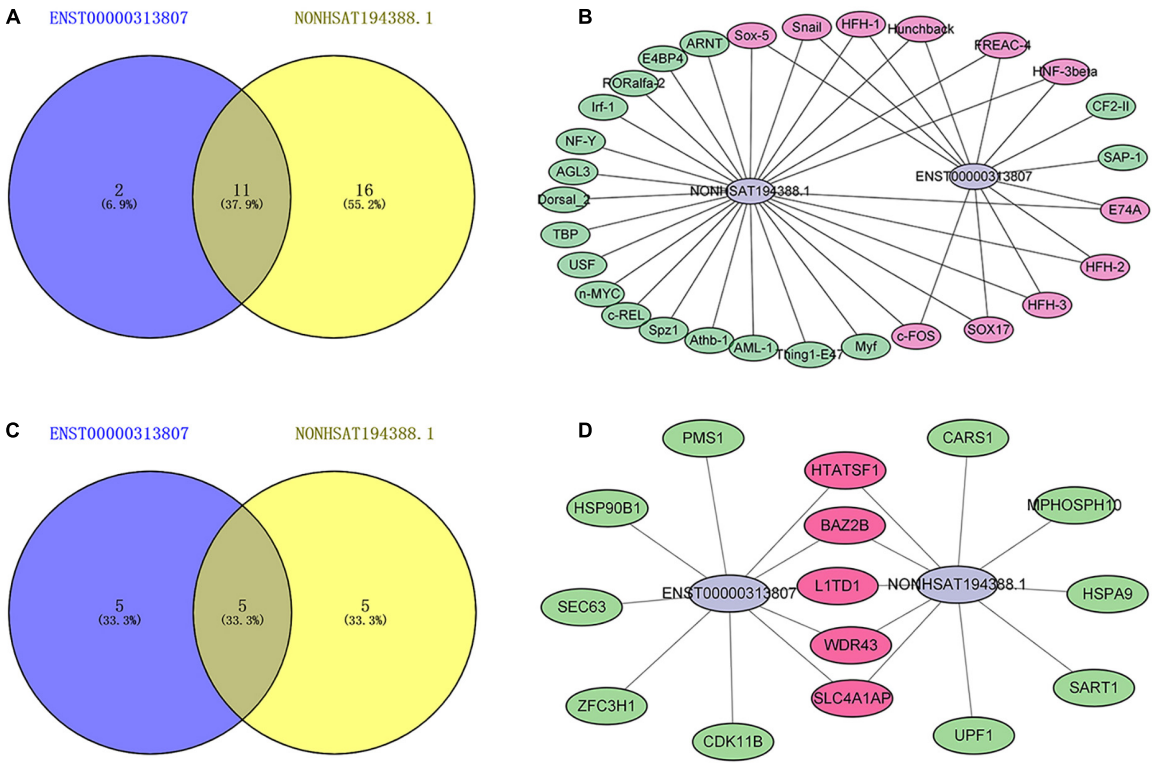

FIGURE 10
Maps of lncRNAs binding to upstream transcription factors (TFs) and downstream binding proteins. **(A)** A Venn diagram of TFs binding to ENST00000313807 and NON-HSAT194388.1. The blue part shows the TFs binding to ENST00000313807. The yellow part shows the TFs binding to NON-HSAT194388.1, and the middle part represents the overlapping TFs of the two groups. **(B)** Binding map of lncRNAs and upstream TFs. The green part shows the TFs binding to ENST00000313807 or NON-HSAT194388.1. The purple part represents the overlapping TFs of the two groups. **(C)** A Venn diagram of proteins binding to ENST00000313807 and NON-HSAT194388.1. The blue part shows the proteins binding to ENST00000313807. The yellow part shows the proteins binding to NON-HSAT194388.1, and the middle part represents the overlapping proteins of the two groups. **(D)** Binding map of lncRNAs and downstream proteins. The green part shows the proteins binding to ENST00000313807 or NON-HSAT194388.1. The purple part represents the overlapping proteins of the two groups.

hsa-miR-29a-3p ($P < 0.0001$), hsa-miR-29b-3p ($P < 0.01$), and hsa-miR-29c-3p ($P < 0.01$) were significantly decreased (Figure 11A). ENST00000313807, NON-HSAT194388.1, and *COL1A1* were upregulated in cirexos isolated from the plasma of patients with SSc. These results were consistent with the high-throughput sequencing data.

The correlation analysis of the lncRNA–miRNA–mRNA networks was analyzed. The results showed that ENST00000313807 and NON-HSAT194388.1 were negatively correlated with hsa-miR-29a-3p ($P < 0.01$). ENST00000313807 ($P < 0.0001$), and NON-HSAT194388.1 ($P = 0.0001$) were positively correlated with *COL1A1*, and hsa-miR-29a-3p was negatively correlated with *COL1A1* ($P < 0.01$). lncRNAs involved in the ceRNA mechanism are positively correlated with mRNAs, while lncRNAs and mRNAs are negatively correlated with miRNAs (10, 36). The relationships of ENST00000313807-hsa-miR-29a-3p-*COL1A1* and NON-HSAT194388.1-hsa-miR-29a-3p-*COL1A1* conformed to the ceRNA mechanism. ENST00000313807 was negatively correlated with hsa-miR-29b-3p ($P < 0.05$), while *COL1A1* was not significantly correlated with hsa-miR-29b-3p ($P > 0.05$). There was no significant correlation between ENST00000313807 and hsa-miR-29c-3p ($P > 0.05$), while *COL1A1* was negatively correlated with hsa-miR-29c-3p ($P < 0.05$) (Figure 11B). Therefore, the relationships of ENST00000313807-hsa-miR-29b-3p-*COL1A1* and ENST00000313807-hsa-miR-29c-3p-*COL1A1* did not conform to the ceRNA mechanism.

The ROC curve was used for independent or combined diagnosis of SSC. The results showed that the independent diagnostic value of hsa-miR-29a-3p was higher than that of the others [area under curve (AUC): 0.8725, cutoff: 0.9115]. The top combined diagnosis ceRNA networks were as follows: ENST00000313807-hsa-miR-29a-3p-*COL1A1* (AUC: 0.94, $P < 0.0001$), NON-HSAT194388.1-hsa-miR-29a- 3p-*COL1A1* (AUC: 0.935, $P < 0.0001$), hsa-miR-29a-3p-*COL1A1* (AUC: 0.935, $P < 0.0001$), ENST00000313807-hsa-miR-29b-3p-*COL1A1* (AUC: 0.89, $P < 0.0001$), and ENST00000313807-hsa-miR-29a-3p (AUC: 0.89, $P < 0.0001$) (Figure 11C). Therefore, ENST00000313807, NON-HSAT194388.1, *COL1A1*, hsa-miR-29a-3p, hsa-miR-29b-3p, and hsa-miR-29c-3p may be used as biomarkers for the diagnosis of SSc. The combined diagnosis is more valuable than independent diagnosis.

3.12. Correlation analysis between ceRNA networks and clinical data

We further evaluated the relationship between ceRNA networks in the plasma cirexos and the clinical features of 20 patients with SSc. The results showed that ENST00000313807 was positively correlated with HRCT score ($r = 0.5101$, $P = 0.0109$), Scl-70 ($r = 0.398$,

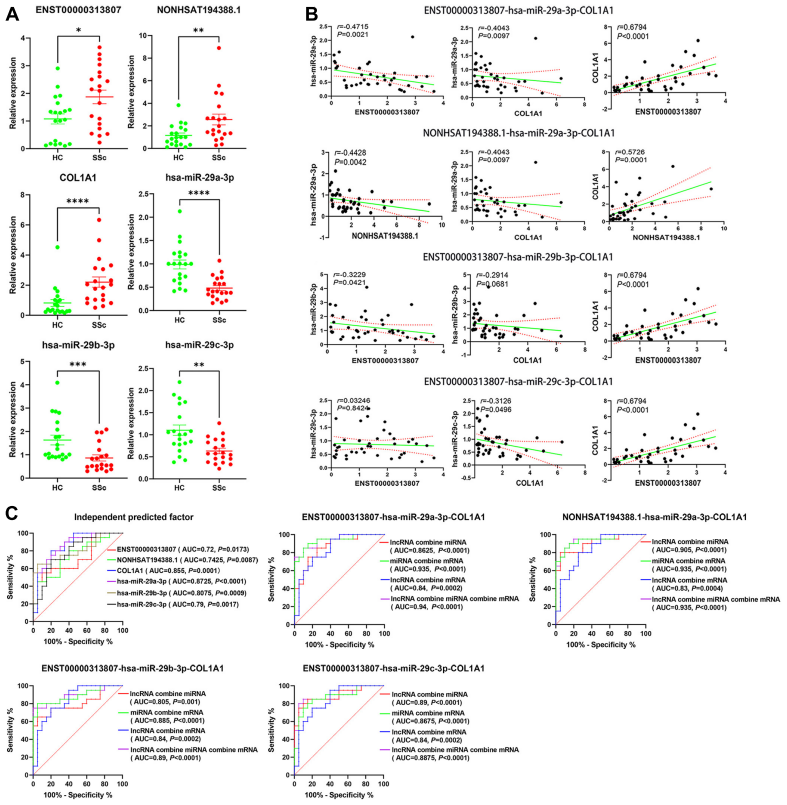

FIGURE 11
(A) The relative expression of ENST00000313807, NON-HSAT194388.1, *COL1A1*, hsa-miR-29a-3p, hsa-miR-29b-3p, and hsa-miR-29c-3p in plasma cirexos was verified by Real-time Quantitative PCR (RT-qPCR) (n = 20). The green part shows the relative expression of RNA in healthy control; (HCs). The red part shows the relative expression of RNA in patients with SSc. $^{*}P < 0.05$, $^{**}P < 0.01$, $^{***}P < 0.001$, and $^{****}P < 0.0001$. **(B)** Correlation analysis of the ENST00000313807-hsa-miR-29a-3p-*COL1A1* networks, NON-HSAT194388.1-hsa-miR-29a-3p-*COL1A1* networks, ENST00000313807-hsa-miR-29b-3p-*COL1A1* networks, and ENST00000313807-hsa-miR-29c-3p-*COL1A1* networks found in plasma cirexos (n = 20). The solid green line is a regression straight line, which is used to describe the relationship curve between the dependent variable y and the independent variable x with a linear relationship. The area formed by the red dotted line represents the 95% confidence interval. **(C)** Receiver operating characteristic (ROC) curve analysis of the independent diagnosis of ceRNA networks, ENST00000313807-hsa-miR-29a-3p-*COL1A1* combined diagnosis, NON-HSAT194388.1-hsa-miR-29a-3p-*COL1A1* combined diagnosis, ENST00000313807-hsa-miR-29b-3p-*COL1A1* combined diagnosis, and ENST00000313807-hsa-miR-29c-3p-*COL1A1* combined diagnosis in plasma cirexos (n = 20). AUC, area under curve.

P = 0.0441), Ro-52 (r = 0.4229, P = 0.0314), CRP (r = 0.4205, P = 0.4205), IgM (r = 0.622, P = 0.0034), neutrophil count (NEUT) (r = 0.3819, P = 0.034), neutrophil percentage (NEUT%) (r = 0.4589, P = 0.0094), and urea (r = 0.3606, P = 0.0393). ENST00000313807 was negatively correlated with lymphocyte percentage (LYM%) (r = −0.4927, P = 0.0049), albumin (ALB) (r = −0.4168, P = 0.0197), and white sphere ratio (ALB/GLB) (r = −0.3803, P = 0.0348). The results showed that NON-HSAT194388.1 was positively correlated with NEUT% (r = 0.3666, P = 0.0425), and NON-HSAT194388.1 was negatively correlated with LYM (r = −0.3569, P = 0.0488), LYM% (r = −0.4173, P = 0.0195), ALB (r = −0.4031, P = 0.0245), and ALB/GLB (r = −0.3773, P = 0.0364). Furthermore, *COL1A1* was positively correlated with HRCT score (r = 0.4129, P = 0.0449), Ro-52 (r = 0.4749, P = 0.0142), and CENP-B (r = 0.501, P = 0.0091), and *COL1A1* was negatively correlated with IL-10 (r = −0.4872, P = 0.0116), ALB (r = −0.4803, P = 0.0062), and LYM (r = −0.3714, P = 0.0397). The results showed that hsa-miR-29a-3p was positively correlated with LYM% (r = 0.4044, P = 0.024), ALB (r = 0.46, P = 0.0092), and ALB/GLB (r = 0.5194, P = 0.0028), and hsa-miR-29a-3p was negatively correlated with CENP-B (r = −0.4359, P = 0.026), NEUT% (r = −0.3954, P = 0.0277), and the standard deviation of red blood cell distribution width (RDW-SD) (r = −0.3912, P = 0.0295). Moreover, hsa-miR-29b-3p was positively correlated with ALB/GLB (r = 0.4194, P = 0.0188), and hsa-miR-29b-3p was negatively correlated with IgM (r = −0.4581, P = 0.0422). The results showed that hsa-miR-29c-3p was negatively correlated with CENP-B (r = 0.4229, P = 0.0314) (Figures 12, 13). Therefore, ENST00000313807, NON-HSAT194388.1, *COL1A1*, hsa-miR-29a-3p, hsa-miR-29b-3p, and hsa-miR-29c-3p in ceRNA networks may be used as a diagnostic biomarker or therapeutic target for SSc in the future. It is worth noting that the greatest correlation was observed between the clinical data and the ENST00000313807-hsa-miR-29a-3p-*COL1A1* network. Thus, the ENST00000313807-hsa-miR-29a-3p-*COL1A1* network could have the most potential as a combined biomarker to diagnose SSc.

3.13. Verification of the ENST00000313807-hsa-miR-29a-3p-*COL1A1* interaction by a double-luciferase reporter gene assay

The interaction of ENST00000313807-miR-29a-3p-*COL1A1* in plasma cirexos was detected by a double-luciferase reporter gene

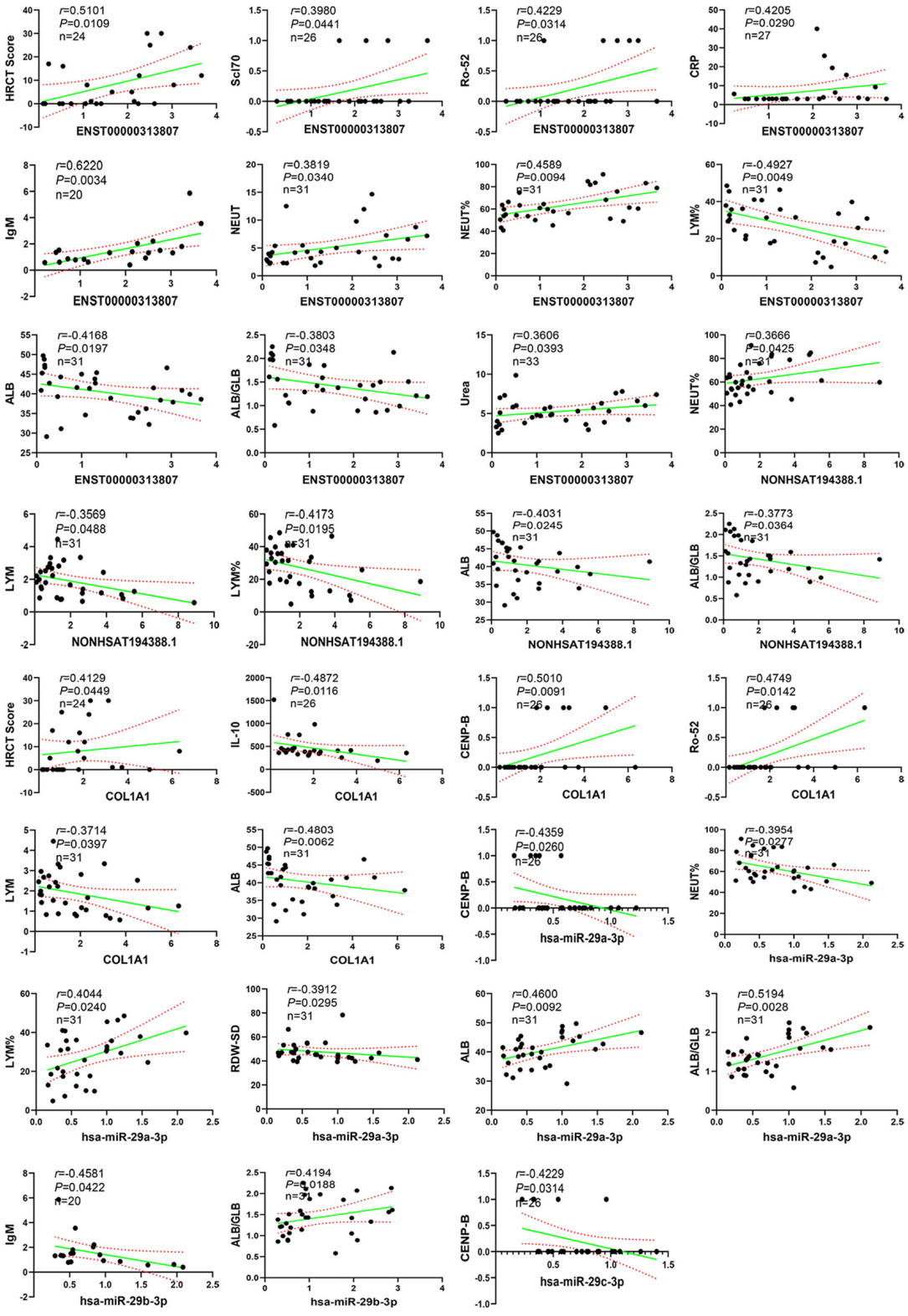

FIGURE 12
Correlation analysis between RNA expression and clinical data. The solid green line is a regression straight line, which is used to describe the relationship curve between the dependent variable y and the independent variable x with a linear relationship. The area formed by the red dotted line represents the 95% confidence interval. NEUT, neutrophil; NEUT%, neutrophil percentage; LYM, lymphocytes; LYM%, lymphocytes percentage; ALB, albumin; ALB/GLB, albumin divided by globulin; RDW-SD, red cell distribution width-standard deviation; HRCT, high-resolution CT; CRP, C-reactive protein.

test. The results showed that the fluorescence value of the hsa-miR-29a-3p-mimics + ENST-WT group was significantly lower than that of the NC mimics + ENST-WT group ($P < 0.0001$). There was no significant difference in the fluorescence value between the hsa-miR-29a-3p-mimics + ENST-MT group and the NC mimics + ENST-MT group ($P > 0.05$). Compared to the NC

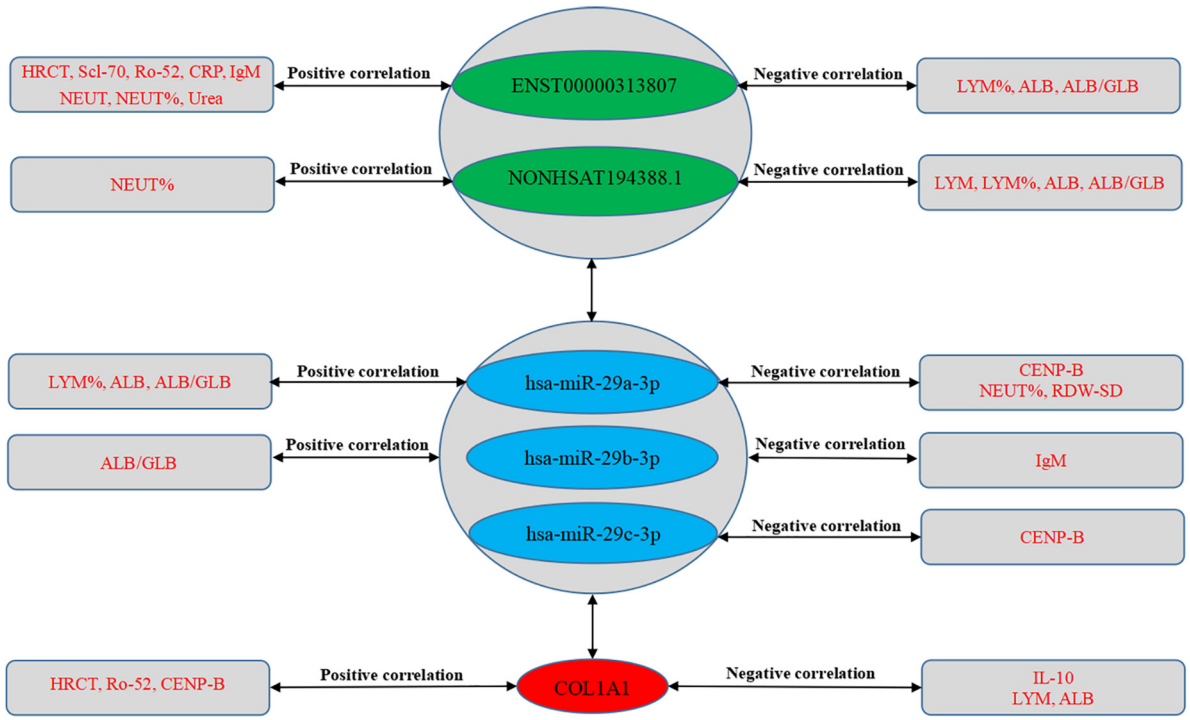

FIGURE 13
Correlation between RNA expression and clinical data. The green part shows lncRNAs, the blue part shows miRNAs, and the red part shows mRNAs in the middle of the figure. The text in the rectangles on both sides of the figure is clinical data.

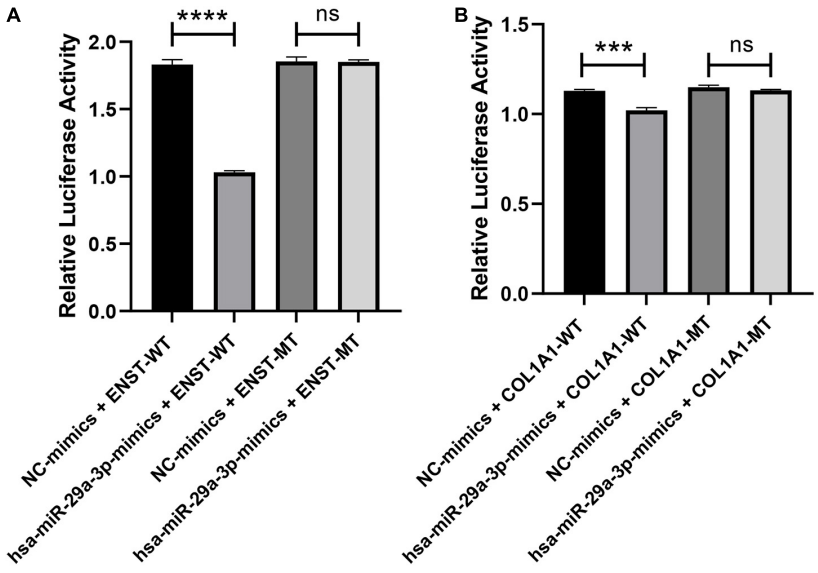

FIGURE 14
Verification of the ENST00000313807-hsa-miR-29a-3p-*COL1A1* interaction by a double-luciferase reporter gene assay. **(A)** The WT or mutation reporter plasmid of ENST00000313807 was co-transfected with the hsa-miR-29a-3p mimic or negative control (NC) mimic into 293T cells. **(B)** The WT or mutation reporter plasmid of *COL1A1* was co-transfected with the hsa-miR-29a-3p mimic or negative control (NC) mimic into 293T cells. ****$P < 0.0001$, ***$P < 0.001$. NC, negative control; WT, wild type; MT, mutant; ns, no significance.

mimics + *COL1A1*-WT group, the fluorescence value of the hsa-miR-29a-3p-mimics + *COL1A1*-WT group decreased significantly ($P < 0.0001$). There was no significant difference in the fluorescence value between the hsa-miR-29a-3p-mimics + *COL1A1*-MT group and the NC mimics + *COL1A1*-MT group ($P > 0.05$) (Figure 14). The results showed an interaction between ENST00000313807 and hsa-miR-29a-3p, and *COL1A1* and hsa-miR-29a-3p in plasma cirexos. Therefore, the ENST00000313807-hsa-miR-29a-3p-*COL1A1* network can not only be used as a combined biomarker to diagnose SSc, but ENST00000313807 also interacts with hsa-miR-29a-3p, which interacts with *COL1A1*. However, whether the ENST00000313807-hsa-miR-29a-3p-*COL1A1* network participates

in the biological process of SSc pathogenesis through interaction, as well as the underlying mechanism, requires further study.

4. Discussion

At present, there are few specific markers for SSc, and their sensitivity is low. Most patients with SSc can be diagnosed only after they have had organ damage in the middle and late stages of disease. Biomarkers with high specificity and sensitivity are needed for the diagnosis of SSc in the early stage of disease development (37). Wu et al. (38) analyzed the differentially expressed miRNAs (DEmiRNAs) and DEmRNAs in the lung tissues of patients with SSc-ILD and HCs. The core mRNAs in the ceRNA networks included *COL1A1*, endothelin (*EDN1*) and fos proto-oncogene (*FOS*). The expression of *COL1A1* had a negative relationship with central granulocyte. The expression of *FOS* was associated with increased mast cells. The expression of *EDN1* had a positive relationship with the number of mast cells and natural killer cells. Yan et al. (39) analyzed the DEmRNAs and DEmiRNAs between lung tissues in SSc-ILD and HCs, and predicted lncRNAs and mRNAs binding to miRNAs using online databases. They found that ceRNA networks, such as LINC01128/has miR-21-5p/PTX3, SNHG16, LIN01128, RP11-834C11.4 (LINC02381)/hsa-let-7f-5p/IL6, and LINC00665/hsa-miR-155-5p/PLS1, could be used as potential targets and biomarkers of SSc-ILD. In this study, the role of ceRNA networks in plasma cirexos in SSc was analyzed. The lipid membrane structure of cirexos can prevent degradation of the contents. In cirexos, miRNA, mRNA, and lncRNA have higher concentrations than inside the cells, which is advantageous for diagnosing diseases (13). The main role of lipid molecules in EXOs is to maintain their external morphology, and they can also participate in the biological process of disease development as signal molecules. Several studies have demonstrated the importance of EXOs for the onset or development of SSc. Nakamura et al. (40) found that EXOs were increased in the skin fibroblasts of SSc compared with normal fibroblasts, which may induce the increased expression of type I collagen in the fibroblasts of patients with SSc. In addition, they found that EXOs isolated from the culture medium of fibroblasts from patients with SSc were able to stimulate the expression of type I collagen in normal fibroblasts. Neutrophil-derived EXOs contain many miRNAs and lncRNAs involved in the pathogenesis of SSc. Li et al. (41) found that miRNAs, lncRNAs, and mRNAs in neutrophil-derived EXOs associated with diffuse cutaneous systemic sclerosis (dcSSc) could promote fibrosis by activating the Wnt, AMPK, IL23, and NOTCH signaling pathways. This study not only provides effective biomarkers for the diagnosis of SSc, but also provides potential targets for the mechanism research and clinical treatment of SSc.

Previous studies have found that abnormal accumulation of ECM components can destroy physiological structures leading to organ fibrosis (42, 43). An important process in the development of fibrosis is the transformation of fibroblasts into myofibroblasts, which is driven by many pro-fibrotic factors (44). The activated myofibroblasts can synthesize collagen, resulting in the deposition of ECM collagen and leading to fibrosis (34). Studies have shown that the expression of focal adhesion molecules in the dermis may be important players in SSc pathophysiology (45). Cell adhesion molecules mainly mediate the bidirectional signal transduction between cells and the ECM (45, 46). The key role of cirexos in cell-to-cell communication is mainly related to their cargo, including proteins; these have the ability to activate signaling pathways, which in turn regulate host cell activity and behavior (47). In this study, we found that DEmRNAs in plasma cirexos were mainly enriched in ECM receptor interaction, focal adhesion, and platelet activation pathways. RT-qPCR showed that the hub gene *COL1A1* was upregulated in SSc plasma cirexos. Increased collagen deposition in the alveolar wall leads to progressive destruction of the normal alveolar structure, resulting in increased strength of the ECM (48). In addition, *COL1A1* can induce the differentiation of mesenchymal cells into myofibroblasts through different pathways, which is characterized by the increased expression of α-smooth muscle actin (49). Therefore, *COL1A1* plays an important role in pulmonary fibrosis, and interstitial lung disease (ILD) is an important complication of SSc. Indeed, Velazquez-Enriquez et al. (47) showed that the expression of *COL1A1* in fibroblast-derived exosomes was upregulated in idiopathic pulmonary fibrosis and correlated with the progression of idiopathic pulmonary fibrosis. However, there is a lack of relevant studies on the role of *COL1A1* carried by cirexos in the development of SSc. Based on bioinformatics analysis, we further explored the significance of cirexos in clinical diagnosis. We speculated that the upregulation of *COL1A1* in SSc plasma cirexos may be related to the expression of *COL1A1* in SSc fibroblast-derived exosomes or in the airway ECM of SSc. The expression of *COL1A1* in SSc plasma cirexos may not only be used to diagnose SSc, but may also participate in the biological process of SSc pathogenesis.

Pulmonary complications of SSc, including ILD and pulmonary hypertension (PAH), are the main causes of morbidity and mortality of SSc (50). In this case, there is a great need for biomarkers for diagnosis and prognosis to help clinicians predict the development of SSc and SSc-ILD and provide appropriate treatment for patients. Distler et al. (51) confirmed that high-resolution computed tomography (HRCT) is helpful for predicting the disease progression of SSc-ILD. Therefore, the assessment of the HRCT score is crucial for the diagnosis of fibrosis in SSc. The higher the HRCT score, the more severe the fibrosis. This study found that ENST00000313807 and *COL1A1* in plasma cirexos were positively correlated with the HRCT score, while other RNAs were not statistically correlated with the HRCT score. The expression of HRCT-related genes may represent the degree of lung injury. Christmann et al. (52) confirmed *via* immunohistochemical tests of lung tissue that the expression of *COL1A1* is increased in patients with SSc-ILD, and the high level of type I collagen is positively correlated with the deterioration of the HRCT score. In addition, studies have confirmed that cirexos in patients with SSc can stimulate the expression of genes encoding extracellular matrix components, such as *COL1A1*, *COL3A1*, and fibronectin-1 (9). Therefore, the expression of ENST00000313807 and *COL1A1* in plasma cirexos may become an important indicator for the evaluation of pulmonary fibrosis, as well as a biomarker for the diagnosis of SSc-ILD.

Activated B cells in SSc promote endothelial cells and fibroblasts to secrete proinflammatory and fibrogenic factors, leading to vascular injury and fibrosis (53). Serum IgM is a soluble marker of B cell activation and one of the diagnostic markers of SSc (53). In this study, we found that ENST00000313807 and hsa-miR-29b-3p in the plasma cirexos of patients with SSc were positively correlated with IgM. Based on our results, we speculated that ENST00000313807 and hsa-miR-29b-3p may be diagnosis markers for the expression of serum IgM in SSc. To date, the most commonly used diagnostic biomarker for SSc is serum autoantibodies. More than 90% of patients with SSc have anti-nuclear antibodies (ANA) in their serum

(50). Anti-topoisomerase I (anti-SCL-70) and anti-centromere (anti-CENP-B) antibodies are also highly specific for SSc and SSC-ILD (50). In addition, anti-RO-52 and anti-CENP-A have potential value in the diagnosis of SSc-ILD (54). We found that in plasma cirexos, the expression of ENST00000313807 was positively correlated with Scl-70 and Ro-52, the expression of hsa-miR-29a-3p and hsa-miR-29c-3p was negatively correlated with CENP-B, and *COL1A1* was positively correlated with Ro-52 and CENP-B. Corallo et al. (55) showed that SSc-specific autoantibodies, including anti-Scl-70 and anti-CENP-B, directly induced the increased expression of *COL1A1* in human dermal fibroblasts to promote fibrosis. In addition, our results showed that there is an interaction between ENST00000313807 and hsa-miR-29a-3p, and *COL1A1* and hsa-miR-29a-3p in plasma cirexos. According to our study, we speculated that the ENST00000313807-hsa-miR-29a-3p-*COL1A1* network in SSc plasma cirexos may interact with the high expression of Scl-70, Ro-52, CENP-B, and other specific markers in the serum of patients with SSc, thus affecting the development of SSc fibrosis. The expression of ENST00000313807-hsa-miR-29a-3p- *COL1A1* in SSc plasma cirexos can also be used as a diagnosis marker for the expression of Scl-70, Ro-52, CENP-B, and other specific markers in the serum of patients with SSc. However, few studies have investigated the effect of autoantibodies on pulmonary fibrosis, and further in-depth studies are needed.

Several studies have highlighted that CRP is significantly increased in patients with SSc-ILD. Thus, CRP could be used as an independent biomarker associated with SSc and the presence and severity of ILD (56–58). In this study, we found that the expression of ENST00000313807 was upregulated in SSc plasma cirexos. In SSc plasma cirexos, ENST00000313807 was positively correlated with CRP in SSc serum. Therefore, we speculated that ENST00000313807 in SSc plasma cirexos may be a marker of high CRP expression in SSc serum. Scleroderma renal crisis is a serious and potentially life-threatening complication of scleroderma (1). Urea is an indicator used to evaluate renal function (56). We found that ENST00000313807 in SSc plasma cirexos was positively correlated with urea in SSc serum. Based on the above results, we speculated that the expression of ENST00000313807 in SSc plasma cirexos may be a diagnosis marker of renal function in SSc serum. Both T and B cells participate in abnormal activation of the immune system, which are key factors leading to vascular abnormalities and fibrosis in SSc (59, 60). In addition, several studies have highlighted that the number of lymphocytes is decreased in patients with SSc during the early stage; this is mainly due to scleroderma itself rather than immunomodulation therapy (61–63). Therefore, based on our results, the high expression of ENST00000313807, NON-HSAT194388.1, and *COL1A1,* as well as the low expression of hsa-miR-29a-3p, in SSc plasma cirexos may lead to a lower lymphocyte count in SSc serum and further promote the vascular abnormalities and fibrosis in SSc. The ENST00000313807-hsa-miR-29a-3p-*COL1A1* network in plasma cirexos can also be used as a monitoring index for the expression of peripheral blood lymphocyte subsets in patients with SSc.

Neutrophil infiltration in diseased tissues is an important factor in fibrosis. In chronic inflammatory or autoimmune diseases, the high expression of inflammatory cytokines drives neutrophils to form neutrophil extracellular traps (NETs). The number of neutrophils in peripheral blood may reflect the infiltration of neutrophils into tissues (64). Our results showed that ENST00000313807 and NON-HSAT194388.1 in plasma cirexos were positively correlated with the absolute value and percentage of neutrophils in serum. However, hsa-miR-29a-3p in the plasma cirexos was negatively correlated with the percentage of neutrophils in serum. Tu et al. (64) found that the number of neutrophils in peripheral blood of patients with SSc increased significantly. Wareing et al. (65) observed that higher neutrophil counts predicted a worse ILD course and higher long-term mortality in patients with SSc-ILD. In addition, Chikhoune et al. (56) showed that the absolute neutrophil count was significantly increased in patients with dcSSc or ILD. Kase et al. (66) used fractional analysis of bronchoalveolar lavage (FBAL) to analyze the bronchoalveolar lavage fluid of patients with SSc-ILD. The results showed that there were more neutrophils in the FBAL-3 of SSc-ILD patients with anti-SCL-70 autoantibodies than those without anti-SCL-70 autoantibodies. A higher percentage of neutrophils in FBAL-3 is associated with the development of end-stage SSc-ILD. Cakmak et al. (67) performed FBAL, HRCT, pulmonary function tests, and dyspnea measurements in 65 patients with progressive SSc. The results suggest a correlation between NEUT% and honeycombing of the lung. Therefore, NEUT% is associated with fibrosis in SSc. In this study, ENST00000313807 and NON-SAT194388.1 were found to be positively correlated with NEUT%, and hsa-miR-29a-3p was found to be negatively correlated with NEUT%. Therefore, the results of the present study indicate that ENST00000313807, NON-HSAT194388.1, and hsa-miR-29a-3p in plasma cirexos could also be used as monitoring indicators of serum neutrophil content in regard to the occurrence and development of SSc.

The red cell distribution width (RDW) is a biomarker to quantify the abnormal size of red blood cells in peripheral blood and has value as a biomarker to assess the severity of vascular damage (68). We found that the expression of hsa-miR-29a-3p in plasma cirexos was negatively correlated with the standard deviation of RDW in serum. Farkas et al. (68) found that increased RDW was associated with dcSSc. Therefore, hsa-miR-29a-3p may have an influence on RDW in SSc, which is an indicator of the vascular damage in SSc. In this study, hsa-miR-29a-3p was found to be negatively correlated with RDW-SD, while there was a lack of references regarding RDW-SD expression in patients with SSc. Patients with SSc often suffers from gastrointestinal tract damage, characterized by atrophy of smooth muscle and decreased intestinal motility, which is mainly caused by autonomic nervous dysfunction. These changes significantly affect intestinal transport and nutrient absorption, resulting in malnutrition caused by malabsorption (69). Serum albumin, hemoglobin, and body mass index reflect nutritional status. Paolino et al. (69) found that the expression of serum hemoglobin and albumin was significantly reduced in malnourished patients with SSc. In addition, Chikhoune et al. (56) found that hypoalbuminemia was related to the skin and lung severity of SSc. However, few studies have investigated the expression of the albumin/globulin ratio in patients with SSc. Therefore, according to the results of this study, we speculated that the high expression of ENST00000313807, NON-HSAT194388.1, and *COL1A1* in plasma cirexos of patients with SSc, and the low expression of I-miR-29a-3p and has-miR-29b-3p may be indices for the expression of serum albumin and albumin/white in patients with SSc.

In fibroblasts derived from scar skin and skin fibroblasts induced by lipopolysaccharides, IL-10 downregulated the expression of toll-like receptor 4 [TLR4hosphorpho-NF-κB p65 (pp65) collagen type I, collagen type III, and α-smooth muscle actin (70)]. Therefore, IL-10 can regulate the TLR4/NF-κB pathway in dermal fibroblasts through the IL-10 receptor (IL-10R)/STAT3 axis to reduce both ECM protein

deposition and fibroblast transformation to myofibroblasts, thereby inhibiting the formation of skin scar induced by lipopolysaccharide. In addition, Thoreau et al. (71) found that the expression of IL-10 was reduced in mouse models and patients with SSc and was associated with ILD formation. We found that the expression of *COL1A1* in SSc plasma cirexos was negatively correlated with IL-10 in the SSc serum, which is consistent with the abovementioned studies. However, the mechanism needs to be further verified.

miR-29a inhibits the expression of collagen in human fetal scleral fibroblasts by regulating the Hsp47/Smad3 signaling pathway (72). Jafarinejad-Farsangi et al. (73) found that the expression of has-miR-29a was downregulated in dermal fibroblasts of dcSSc patients and dermal fibroblasts treated with transforming growth factor (TGF)-β *in vitro*. In addition, hsa-miR-29a was able to effectively reduce TGF-β-induced collagen production in dermal fibroblasts. Therefore, hsa-miR-29a may serve as a therapeutic target for SSc and other fibrotic diseases with abnormal collagen expression. In this study, hsa-miR-29a-3p was downregulated and COL1A1 was upregulated in patients with SSc. hsa-miR-29a-3p-COL1A1 can be used as a therapeutic target for SSc.

Increasing studies have investigated non-invasive biomarkers to diagnose, evaluate, and treat SSc; however, few of these biomarkers are used clinically (8). Compared to circulating non-coding RNAs in the serum or plasma, the abnormal expression of non-coding RNAs carried by cirexos in SSc have the advantages of stability and practicability as novel biomarkers and therapeutic targets for the diagnosis and treatment of SSc (13, 74, 75).

5. Conclusion

In this study, the ROC curve results suggested that the combined diagnosis of the four lncRNA–miRNA–mRNA networks of plasma cirexos had more advantages than the independent diagnosis of SSc. The ENST00000313807-hsa-miR-29a-3p-*COL1A1* network was correlated with the clinical data of patients with SSc. These indicators play an important role as biomarkers in the diagnosis of SSc. The ENST00000313807-hsa-miR-29a-3p-*COL1A1* network exhibited the most potential as a combined diagnosis biomarker for the clinical diagnosis and treatment of SSc. It is worth noting that our results showed that ENST00000313807 interacts with hsa-miR-29a-3p, which interacts with *COL1A1*, although the mechanism still needs to be uncovered.

Data availability statement

The data presented in the study are deposited in the Gene Expression Omnibus (GEO) repository, accession number GSE224884.

Ethics statement

The studies involving human participants were reviewed and approved by the Ethics Committee of the First Affiliated Hospital of Baotou Medical College, Inner Mongolia University of Science and Technology [Approval No. 2018 (017)]. The patients/participants provided their written informed consent to participate in this study.

Author contributions

XS and TD designed and performed the experiments. XS, TD, BW, and HF analyzed the data. XS, TD, ZC, LG, and YW reviewed and edited the manuscript. All authors have contributed to read and approved the submitted version.

Funding

This work was supported by the National Natural Science Foundation (grant number: 81860294), the Inner Mongolia Autonomous Region University Scientific Research Project (grant numbers: 2021MS08045 and 2019MS08055), and the Science and Technology Planning Project of Inner Mongolia Autonomous Region (grant numbers: 2019GG052 and 201802089).

Conflict of interest

The authors declare that the research was conducted in the absence of any commercial or financial relationships that could be construed as a potential conflict of interest.

Publisher's note

References

1. Maritati F, Provenzano M, Lerario S, Corradetti V, Bini C, Busutti M, et al. Kidney transplantation in systemic sclerosis: advances in graft, disease, and patient outcome. *Front Immunol.* (2022) 13:878736. doi: 10.3389/fimmu.2022.878736

2. Nie M, Kong B, Chen G, Xie Y, Zhao Y, Sun L. MSCs-laden injectable self-healing hydrogel for systemic sclerosis treatment. *Bioact Mater.* (2022) 17:369–78. doi: 10.1016/j.bioactmat.2022.01.006

3. Colletti M, Galardi A, De Santis M, Guidelli GM, Di Giannatale A, Di Luigi L, et al. Exosomes in systemic sclerosis: messengers between immune, vascular and fibrotic components? *Int J Mol Sci.* (2019) 20:4337. doi: 10.3390/ijms20184337

4. Wasson C, Abignano G, Hermes H, Malaab M, Ross R, Jimenez S, et al. Long non-coding RNA HOTAIR drives EZH2-dependent myofibroblast activation in systemic sclerosis through miRNA 34a-dependent activation of NOTCH. *Ann Rheum Dis.* (2020) 79:507–17. doi: 10.1136/annrheumdis-2019-216542

5. Luo Y, Huang L, Luo W, Ye S, Hu Q. Genomic analysis of lncRNA and mRNA profiles in circulating exosomes of patients with rheumatic heart disease. *Biol Open.* (2019) 8:bio045633. doi: 10.1242/bio.045633

6. Zhang C, Yang J, Chen Y, Jiang F, Liao H, Liu X, et al. miRNAs derived from plasma small extracellular vesicles predict organo-tropic metastasis of gastric cancer. *Gastric Cancer.* (2022) 25:360–74. doi: 10.1007/s10120-021-01267-5

7. Nedaeinia R, Manian M, Jazayeri M, Ranjbar M, Salehi R, Sharifi M, et al. Circulating exosomes and exosomal microRNAs as biomarkers in gastrointestinal cancer. *Cancer Gene Ther.* (2017) 24:48–56. doi: 10.1038/cgt.2016.77

8. Wermuth PJ, Piera-Velazquez S, Rosenbloom J, Jimenez SA. Existing and novel biomarkers for precision medicine in systemic sclerosis. *Nat Rev Rheumatol.* (2018) 14:421–32. doi: 10.1038/s41584-018-0021-9

9. Wermuth PJ, Piera-Velazquez S, Jimenez SA. Exosomes isolated from serum of systemic sclerosis patients display alterations in their content of profibrotic and antifibrotic microRNA and induce a profibrotic phenotype in cultured normal dermal fibroblasts. *Clin Exp Rheumatol.* (2017) 35(Suppl. 106):21–30.

10. Wang Y, Tang Y, Yang X, Xu J, Chen Y, Xu J, et al. Immune dysfunction mediated by the ceRNA regulatory network in human placenta tissue of intrahepatic cholestasis pregnancy. *Front Immunol.* (2022) 13:883971. doi: 10.3389/fimmu.2022.883971

11. Wang J, Cao Y, Lu X, Wang X, Kong X, Bo C, et al. Identification of the regulatory role of lncRNA SNHG16 in myasthenia gravis by constructing a competing endogenous RNA network. *Mol Ther Nucleic Acids.* (2020) 19:1123–33. doi: 10.1016/j.omtn.2020.01.005

12. Fan C, Cui X, Chen S, Huang S, Jiang H. LncRNA LOC100912373 modulates PDK1 expression by sponging miR-17-5p to promote the proliferation of fibroblast-like synoviocytes in rheumatoid arthritis. *Am J Transl Res.* (2020) 12:7709–23.

13. Wang M, Wang Y, Ye F, Yu K, Wei W, Liu M, et al. Exosome encapsulated ncRNAs in the development of HCC: potential circulatory biomarkers and clinical therapeutic targets. *Am J Cancer Res.* (2021) 11:3794–812.

14. Abd-Elmawla MA, Hassan M, Elsabagh YA, Alnaggar AR, Senousy MA. Deregulation of long noncoding RNAs ANCR, TINCR, HOTTIP and SPRY4-IT1 in plasma of systemic sclerosis patients: SPRY4-IT1 as a novel biomarker of scleroderma and its subtypes. *Cytokine.* (2020) 133:155124. doi: 10.1016/j.cyto.2020.155124

15. Enderle D, Spiel A, Coticchia C, Berghoff E, Mueller R, Schlumpberger M, et al. Characterization of RNA from exosomes and other extracellular vesicles isolated by a novel spin column-based method. *PLoS One.* (2015) 10:e0136133. doi: 10.1371/journal.pone.0136133

16. Miao YR, Liu W, Zhang Q, Guo AY. lncRNASNP2: an updated database of functional SNPs and mutations in human and mouse lncRNAs. *Nucleic Acids Res.* (2018) 46:D276–80. doi: 10.1093/nar/gkx1004

17. Li JH, Liu S, Zhou H, Qu LH, Yang JH. starBase v2.0: decoding miRNA-ceRNA, miRNA-ncRNA and protein-RNA interaction networks from large-scale CLIP-Seq data. *Nucleic Acids Res.* (2014) 42:D92–7. doi: 10.1093/nar/gkt1248

18. Chin CH, Chen SH, Wu HH, Ho CW, Ko MT, Lin CY. cytoHubba: identifying hub objects and sub-networks from complex interactome. *BMC Syst Biol.* (2014) 8 (Suppl 4):S11. doi: 10.1186/1752-0509-8-s4-s11

19. Li Y, Huang C, Yang Z, Wang L, Luo D, Qi L, et al. Identification of potential biomarkers of gout through competitive endogenous RNA network analysis. *Eur J Pharm Sci.* (2022) 173:106180. doi: 10.1016/j.ejps.2022.106180

20. Luan H, Zhang C, Zhang T, He Y, Su Y, Zhou L. Identification of key prognostic biomarker and its correlation with immune infiltrates in pancreatic ductal adenocarcinoma. *Dis Markers.* (2020) 2020:8825997. doi: 10.1155/2020/8825997

21. Cao Z, Pan X, Yang Y, Huang Y, Shen HB. The lncLocator: a subcellular localization predictor for long non-coding RNAs based on a stacked ensemble classifier. *Bioinformatics.* (2018) 34:2185–94. doi: 10.1093/bioinformatics/bty085

22. Lin, Y, Pan X, Shen HB. lncLocator 2.0: a cell-line-specific subcellular localization predictor for long non-coding RNAs with interpretable deep learning. *Bioinformatics.* (2021) 37:2308–16. doi: 10.1093/bioinformatics/btab127

23. Tang Q, Nie F, Kang J, Chen W. mRNALocater: enhance the prediction accuracy of eukaryotic mRNA subcellular localization by using model fusion strategy. *Mol Ther.* (2021) 29:2617–23. doi: 10.1016/j.ymthe.2021.04.004

24. Fu J, Yu Q, Xiao J, Li S. Long noncoding RNA as a biomarker for the prognosis of ischemic stroke: a protocol for meta-analysis and bioinformatics analysis. *Medicine.* (2021) 100:e25596. doi: 10.1097/md.0000000000025596

25. Han Z, Chen H, Guo Z, Zhu J, Xie X, Li Y, et al. Bioinformatics analysis: the regulatory network of hsa_circ_0007843 and hsa_circ_0007331 in colon cancer. *Biomed Res Int.* (2021) 2021:6662897. doi: 10.1155/2021/6662897

26. Salmena L, Poliseno L, Tay Y, Kats L, Pandolfi PP A ceRNA hypothesis: the rosetta stone of a hidden RNA language? *Cell.* (2011) 146:353–8. doi: 10.1016/j.cell.2011.07.014

27. Bai Y, Long J, Liu Z, Lin J, Huang H, Wang D, et al. Comprehensive analysis of a ceRNA network reveals potential prognostic cytoplasmic lncRNAs involved in HCC progression. *J Cell Physiol.* (2019) 234:18837–48. doi: 10.1002/jcp.28522

28. Jing Z, Guo S, Zhang P, Liang Z. LncRNA-associated ceRNA network reveals novel potential biomarkers of laryngeal squamous cell carcinoma. *Technol Cancer Res Treat.* (2020) 19:1533033820985787. doi: 10.1177/1533033820985787

29. Ma Y, Zhang J, Wen L, Lin A. Membrane-lipid associated lncRNA: a new regulator in cancer signaling. *Cancer Lett.* (2018) 419:27–9. doi: 10.1016/j.canlet.2018.01.008

30. Rashid F, Shah A, Shan G. Long non-coding RNAs in the cytoplasm. *Genomics Proteomics Bioinformatics.* (2016) 14:73–80. doi: 10.1016/j.gpb.2016.03.005

31. Wang J, Gu J, You A, Li J, Zhang Y, Rao G, et al. The transcription factor USF1 promotes glioma cell invasion and migration by activating lncRNA HAS2-AS1. *Biosci Rep.* (2020) 40:BSR20200487. doi: 10.1042/bsr20200487

32. Krezdorn N, Lian CG, Wells M, Wo L, Tasigiorgos S, Xu S, et al. Chronic rejection of human face allografts. *Am J Transplant.* (2019) 19:1168–77. doi: 10.1111/ajt.15143

33. Qi Q, Mao Y, Tian Y, Zhu K, Cha X, Wu M, et al. Geniposide inhibited endothelial-mesenchymal transition via the mTOR signaling pathway in a bleomycin-induced scleroderma mouse model. *Am J Transl Res.* (2017) 9:1025–36.

34. Yu Y, Shen L, Xie X, Zhao J, Jiang M. The therapeutic effects of exosomes derived from human umbilical cord mesenchymal stem cells on scleroderma. *Tissue Eng Regen Med.* (2022) 19:141–50. doi: 10.1007/s13770-021-00405-5

35. Frost J, Estivill X, Ramsay M, Tikly M. Dysregulation of the WNT signaling pathway in South African patients with diffuse systemic sclerosis. *Clin Rheumatol.* (2019) 38:933–8. doi: 10.1007/s10067-018-4298-5

36. Sun T, Dong L, Guo Y, Zhao H, Wang M. Revealing key lncRNAs in cytogenetically normal acute myeloid leukemia by reconstruction of the lncRNA-miRNA-mRNA network. *Sci Rep.* (2022) 12:4973. doi: 10.1038/s41598-022-08930-6

37. Bayati P, Kalantari M, Assarehzadegan M, Poormoghim H, Mojtabavi N. MiR-27a as a diagnostic biomarker and potential therapeutic target in systemic sclerosis. *Sci Rep.* (2022) 12:18932. doi: 10.1038/s41598-022-23723-7

38. Wu Q, Liu Y, Xie Y, Wei S, Liu Y. Identification of potential ceRNA network and patterns of immune cell infiltration in systemic sclerosis-associated interstitial lung disease. *Front Cell Dev Biol.* (2021) 9:622021. doi: 10.3389/fcell.2021.622021

39. Yan Y, Zheng J, Wu L, Rao Q, Yang Q, Gao D, et al. Prediction of a competing endogenous RNA Co-expression network by comprehensive methods in systemic sclerosis-related interstitial lung disease. *Front Genet.* (2021) 12:633059. doi: 10.3389/fgene.2021.633059

40. Nakamura K, Jinnin M, Harada M, Kudo H, Nakayama W, Inoue K, et al. Altered expression of CD63 and exosomes in scleroderma dermal fibroblasts. *J Dermatol Sci.* (2016) 84:30–9. doi: 10.1016/j.jdermsci.2016.06.013

41. Li L, Zuo X, Liu D, Luo H, Zhu H. The profiles of miRNAs and lncRNAs in peripheral blood neutrophils exosomes of diffuse cutaneous systemic sclerosis. *J Dermatol Sci.* (2020) 98:88–97. doi: 10.1016/j.jdermsci.2020.02.009

42. Liakouli V, Cipriani P, Di Benedetto P, Ruscitti P, Carubbi F, Berardicurti O, et al. The role of extracellular matrix components in angiogenesis and fibrosis: possible implication for systemic sclerosis. *Mod Rheumatol.* (2018) 28:922–32. doi: 10.1080/14397595.2018.1431004

43. Xu D, Li T, Wang R, Mu R. Expression and pathogenic analysis of integrin family genes in systemic sclerosis. *Front Med (Lausanne).* (2021) 8:674523. doi: 10.3389/fmed.2021.674523

44. Sapao, P, Roberson E, Shi B, Assassi S, Skaug B, Lee F, et al. Reduced SPAG17 expression in systemic sclerosis triggers myofibroblast transition and drives fibrosis. *J Invest Dermatol.* (2022). 143:284–93. doi: 10.1016/j.jid.2022.08.052

45. Villano M, Borghini A, Manetti M, Gabbrielli E, Rossi A, Sestini P, et al. Systemic sclerosis sera affect fibrillin-1 deposition by dermal blood microvascular endothelial cells: therapeutic implications of cyclophosphamide. *Arthritis Res Ther.* (2013) 15:R90. doi: 10.1186/ar4270

46. Altorok N, Tsou P, Coit P, Khanna D, Sawalha AH. Genome-wide DNA methylation analysis in dermal fibroblasts from patients with diffuse and limited systemic sclerosis reveals common and subset-specific DNA methylation aberrancies. *Ann Rheum Dis.* (2015) 74:1612–20. doi: 10.1136/annrheumdis-2014-205303

47. Velázquez-Enríquez JM, Santos-Álvarez JC, Ramírez-Hernández AA, Reyes-Jiménez E, López-Martínez A, Pina-Canseco S, et al. Proteomic analysis reveals key proteins in extracellular vesicles cargo associated with idiopathic pulmonary fibrosis in vitro. *Biomedicines.* (2021) 9:1058. doi: 10.3390/biomedicines9081058

48. Liu L, Stephens B, Bergman M, May A, Chiang T. Role of collagen in airway mechanics. *Bioengineering.* (2021) 8:13. doi: 10.3390/bioengineering8010013

49. Liu X, Long X, Liu W, Zhao Y, Hayashi T, Yamato M, et al. Type I collagen induces mesenchymal cell differentiation into myofibroblasts through YAP-induced TGF-β1 activation. *Biochimie.* (2018) 150:110–30. doi: 10.1016/j.biochi.2018.05.005

50. Guiot J, Njock MS, André B, Gester F, Henket M, De Seny D, et al. Serum IGFBP-2 in systemic sclerosis as a prognostic factor of lung dysfunction. *Sci Rep.* (2021) 11:10882. doi: 10.1038/s41598-021-90333-0

51. Distler O, Assassi S, Cottin V, Cutolo M, Danoff SK, Denton C, et al. Predictors of progression in systemic sclerosis patients with interstitial lung disease. *Eur Respir J.* (2020) 55:1902026. doi: 10.1183/13993003.02026-2019

52. Christmann RB, Sampaio-Barros P, Stifano G, Borges CL, De Carvalho CR, Kairalla R, et al. Association of Interferon- and transforming growth factor β-regulated genes and macrophage activation with systemic sclerosis-related progressive lung fibrosis. *Arthritis Rheumatol.* (2014) 66:714–25. doi: 10.1002/art.38288

53. Sanges S, Guerrier T, Duhamel A, Guilbert L, Hauspie C, Largy A, et al. Soluble markers of B cell activation suggest a role of B cells in the pathogenesis of systemic sclerosis-associated pulmonary arterial hypertension. *Front Immunol.* (2022) 13:954007. doi: 10.3389/fimmu.2022.954007

54. Liu C, Hou Y, Yang Y, Xu D, Li L, Li J, et al. Evaluation of a commercial immunoassay for autoantibodies in Chinese Han systemic sclerosis population. *Clin Chim Acta.* (2019) 491:121–5. doi: 10.1016/j.cca.2019.01.020

55. Corallo C, Cheleschi S, Cutolo M, Soldano S, Fioravanti A, Volpi N, et al. Antibodies against specific extractable nuclear antigens (ENAs) as diagnostic and prognostic tools and inducers of a profibrotic phenotype in cultured human skin fibroblasts: are they functional? *Arthritis Res Ther.* (2019) 21:152. doi: 10.1186/s13075-019-1931-x

56. Chikhoune L, Brousseau T, Morell-Dubois S, Farhat M, Maillard H, Ledoult E, et al. Association between routine laboratory parameters and the severity and progression of systemic sclerosis. *J Clin Med.* (2022) 11:152. doi: 10.3390/jcm11175087

57. De Almeida Chaves S, Porel T, Mounié M, Alric L, Astudillo L, Huart A, et al. Sine scleroderma, limited cutaneous, and diffused cutaneous systemic sclerosis survival and predictors of mortality. *Arthritis Res Ther.* (2021) 23:295. doi: 10.1186/s13075-021-02672-y

58. Tezcan D, Turan Ç, Yılmaz S, Sivrikaya A, Gülcemal S, Limon M, et al. What do simple hematological parameters tell us in patients with systemic sclerosis? *Acta Dermatovenerol Alp Pannonica Adriat.* (2020) 29:101–7.

59. Gumkowska-Sroka O, Jagoda K, Owczarek A, Helbig G, Giemza-Stokłosa J, Kotyla PJ. Cytometric Characterization of main immunocompetent cells in patients with systemic sclerosis: relationship with disease activity and type of immunosuppressive treatment. *J Clin Med.* (2019) 8:625. doi: 10.3390/jcm8050625

60. Yoshizaki A, Fukasawa T, Ebata S, Yoshizaki-Ogawa A, Sato S. Involvement of B cells in the development of systemic sclerosis. *Front Immunol.* (2022) 13:938785. doi: 10.3389/fimmu.2022.938785

61. Shah A, Storek J, Woolson R, Pinckney A, Keyes-Elstein L, Wallace PK, et al. Lymphocyte subset abnormalities in early severe scleroderma favor a Th2 phenotype and are not altered by prior immunosuppressive therapy. *Rheumatology.* (2022) 61:4155–62. doi: 10.1093/rheumatology/keac015

62. Fox DA, Lundy SK, Whitfield ML, Berrocal V, Campbell P, Rasmussen S, et al. Lymphocyte subset abnormalities in early diffuse cutaneous systemic sclerosis. *Arthritis Res Ther.* (2021) 23:10. doi: 10.1186/s13075-020-02383-w

63. Yayla ME, İlgen U, Okatan İE, Usluyurteri E, Torgutalp M, Keleşoğlu Dinçer AB, et al. Association of simple hematological parameters with disease manifestations, activity, and severity in patients with systemic sclerosis. *Clin Rheumatol.* (2020) 39:77–83. doi: 10.1007/s10067-019-04685-0

64. Tu J, Jin J, Chen X, Sun L, Cai Z. Altered cellular immunity and differentially expressed immune-related genes in patients with systemic sclerosis-associated pulmonary arterial hypertension. *Front Immunol.* (2022) 13:868983. doi: 10.3389/fimmu.2022.868983

65. Wareing N, Mohan V, Taherian R, Volkmann ER, Lyons MA, Wilhalme H, et al. Blood neutrophil count and neutrophil-to-lymphocyte ratio predict disease progression and mortality in two independent systemic sclerosis cohorts. *Arthritis Care Res (Hoboken).* (2022). doi: 10.1002/acr.24880

66. Kase K, Watanabe S, Saeki K, Waseda Y, Takato H, Ichikawa Y, et al. Fractional analysis of bronchoalveolar lavage in systemic sclerosis-associated interstitial lung disease. *J Thorac Dis.* (2021) 13:4146–55. doi: 10.21037/jtd-20-2596

67. Cakmak G, Selcuk Can T, Gundogdu S, Akman C, Ikitimur H, Musellim B, et al. Relationship between abnormalities on high-resolution computerized tomography, pulmonary function, and bronchoalveolar lavage in progressive systemic sclerosis. *Sarcoidosis Vasc Diffuse Lung Dis.* (2016) 33:349–54.

68. Farkas N, Szabó A, Lóránd V, Sarlós DP, Minier T, Prohászka Z, et al. Clinical usefulness of measuring red blood cell distribution width in patients with systemic sclerosis. *Rheumatology.* (2014) 53:1439–45. doi: 10.1093/rheumatology/keu022

69. Paolino S, Pacini G, Schenone C, Patanè M, Sulli A, Sukkar SG, et al. Nutritional status and bone microarchitecture in a cohort of systemic sclerosis patients. *Nutrients.* (2020) 12:1632. doi: 10.3390/nu12061632

70. Shi J, Shi S, Xie W, Zhao M, Li Y, Zhang J, et al. IL-10 alleviates lipopolysaccharide-induced skin scarring via IL-10R/STAT3 axis regulating TLR4/NF-κB pathway in dermal fibroblasts. *J Cell Mol Med.* (2021) 25:1554–67. doi: 10.1111/jcmm.16250

71. Thoreau B, Chaigne B, Mouthon L. Role of B-Cell in the pathogenesis of systemic sclerosis. *Front Immunol.* (2022) 13:933468. doi: 10.3389/fimmu.2022.933468

72. Tang X, Liu L, Liu S, Song S, Li H. MicroRNA-29a inhibits collagen expression and induces apoptosis in human fetal scleral fibroblasts by targeting the Hsp47/Smad3 signaling pathway. *Exp Eye Res.* (2022) 225:109275. doi: 10.1016/j.exer.2022.109275

73. Jafarinejad-Farsangi S, Gharibdoost F, Farazmand A, Kavosi H, Jamshidi A, Karimizadeh E, et al. MicroRNA-21 and microRNA-29a modulate the expression of collagen in dermal fibroblasts of patients with systemic sclerosis. *Autoimmunity.* (2019) 52:108–16. doi: 10.1080/08916934.2019.1621856

74. Guo X, Lv X, Ru Y, Zhou F, Wang N, Xi H, et al. Circulating exosomal gastric cancer-associated long noncoding RNA1 as a biomarker for early detection and monitoring progression of gastric cancer: a multiphase study. *JAMA Surg.* (2020) 155:572–9. doi: 10.1001/jamasurg.2020.1133

75. Liu Y, Cheng L, Zhan H, Li H, Li X, Huang Y, et al. The roles of noncoding RNAs in systemic sclerosis. *Front Immunol.* (2022) 13:856036. doi: 10.3389/fimmu.2022.856036

frontiers | Frontiers in Medicine

TYPE Original Research
PUBLISHED 27 March 2023
DOI 10.3389/fmed.2023.1146353

OPEN ACCESS

EDITED BY
Xiaolin Sun,
Peking University People's Hospital, China

REVIEWED BY
Jianping Guo,
Peking University People's Hospital, China
Guo-Min Deng,
Huazhong University of Science and Technology, China

*CORRESPONDENCE
Boel Brynedal
✉ boel.brynedal@ki.se
Leonid Padyukov
✉ leonid.padyukov@ki.se

SPECIALTY SECTION
This article was submitted to Rheumatology, a section of the journal Frontiers in Medicine

RECEIVED 17 January 2023
ACCEPTED 22 February 2023
PUBLISHED 27 March 2023

CITATION
Brynedal B, Yoosuf N, Ulfarsdottir TB, Ziemek D, Maciejewski M, Folkersen L, Westerlind H, Müller M, Sahlström P, Jelinsky SA, Hensvold A, Padyukov L, Pomiano NV, Catrina A, Klareskog L and Berg L (2023) Molecular signature of methotrexate response among rheumatoid arthritis patients. *Front. Med.* 10:1146353. doi: 10.3389/fmed.2023.1146353

Molecular signature of methotrexate response among rheumatoid arthritis patients

Boel Brynedal[1,2]*, Niyaz Yoosuf[1,3,4], Tinna Bjorg Ulfarsdottir[1], Daniel Ziemek[5], Mateusz Maciejewski[5], Lasse Folkersen[6], Helga Westerlind[1,7], Malin Müller[3,4], Peter Sahlström[3,4], Scott A. Jelinsky[5], Aase Hensvold[3,4,8], Leonid Padyukov[3,4]*, Nancy Vivar Pomiano[3,4], Anca Catrina[3,4], Lars Klareskog[3,4] and Louise Berg[3,4]

[1]Translational Epidemiology, Institute of Environmental Medicine, Karolinska Institutet, Stockholm, Sweden, [2]Centre for Epidemiology and Community Medicine, Region Stockholm, Stockholm, Sweden, [3]Division of Rheumatology, Department of Medicine Solna, Karolinska Institutet and Karolinska University Hospital, Stockholm, Sweden, [4]Center for Molecular Medicine, Karolinska Institutet, Stockholm, Sweden, [5]Pfizer, Cambridge, MA, United States, [6]Nucleus Genomics, New York, NY, United States, [7]Clinical Epidemiology Division, Department of Medicine Solna, Karolinska Institutet, Stockholm, Sweden, [8]Center for Rheumatology, Academic Specialist Center, Region Stockholm, Stockholm, Sweden

Background: Methotrexate (MTX) is the first line treatment for rheumatoid arthritis (RA), but failure of satisfying treatment response occurs in a significant proportion of patients. Here we present a longitudinal multi-omics study aimed at detecting molecular and cellular processes in peripheral blood associated with a successful methotrexate treatment of rheumatoid arthritis.

Methods: Eighty newly diagnosed patients with RA underwent clinical assessment and donated blood before initiation of MTX, and 3 months into treatment. Flow cytometry was used to describe cell types and presence of activation markers in peripheral blood, the expression of 51 proteins was measured in serum or plasma, and RNA sequencing was performed in peripheral blood mononuclear cells (PBMC). Response to treatment after 3 months was determined using the EULAR response criteria. We assessed the changes in biological phenotypes during treatment, and whether these changes differed between responders and non-responders with regression analysis. By using measurements from baseline, we also tried to find biomarkers of future MTX response or, alternatively, to predict MTX response.

Results: Among the MTX responders, (Good or Moderate according to EULAR treatment response classification, n =60, 75%), we observed changes in 29 partly overlapping cell types proportions, levels of 13 proteins and expression of 38 genes during treatment. These changes were in most cases suppressions that were stronger among responders compared to non-responders. Within responders to treatment, we observed a suppression of FOXP3 gene expression, reduction of immunoglobulin gene expression and suppression of genes involved in cell proliferation. The proportion of many HLA-DR expressing T-cell populations were suppressed in all patients irrespective of clinical response, and the proportion of many IL21R+ T-cells were reduced exclusively in non-responders. Using only the baseline measurements we could not detect any biomarkers or prediction models that could predict response to MTX.

Conclusion: We conclude that a deep molecular and cellular phenotyping of peripheral blood cells in RA patients treated with methotrexate can reveal previously not recognized differences between responders and non-responders during 3 months of treatment with MTX. This may contribute to the understanding of MTX mode of action and explain non-responsiveness to MTX therapy.

KEYWORDS

rheumatoid anhritis, treatment response, methotrexate, gene expression, flow cytometry, plasma proteins, transcriptomics

Introduction

Rheumatoid arthritis (RA) is a chronic inflammatory disease caused by genetic and environmental factors, resulting in symmetric inflammation and destruction of the joints (1). First-line treatment for RA is methotrexate (MTX). Treatment with MTX leads to suppression of immune cells, for example decreased cytokine production by T-cells (2). Tasaki et al. has shown that successful drug treatments (MTX, infliximab or tocilizumab in different individuals) alter the molecular profile closer to that of healthy controls at the transcriptome, serum proteome, and immunophenotype level (3). In their paper the effect of MTX was smaller than the effect of other treatments, but the specific effects of MTX were not elucidated and the number of patients on MTX was small (ten responders and 11 non-responders). It is still unknown which effects of MTX that specifically ameliorates RA symptoms. Between 20 and 40% of RA patients do not respond to MTX, and it is known that response to first-line treatment predicts long-term outcomes in RA patients (4). It would therefore be valuable to understand how the biological effect of MTX differs between responders and non-responders. Such knowledge may provide insights into which mechanisms that can be regulated in order to avoid disease progression.

To investigate the effect of treatment, a good classification of treatment response is needed as well as relevant biological measurements. Patients with RA are routinely examined for their level of inflammation, number of inflamed joints and overall assessment of health. From these measurements the disease activity score DAS28 is calculated (5). In this prospective project, we evaluated the EULAR response criterion after 3 month of MTX in DMARD monotherapy (6). We investigated a wide range of potential biomarkers measured in peripheral blood before treatment initiation and after 3 months of MTX treatment. Gene expression was measured by RNA sequencing; absolute cell counts, cell proportions and phenotypes was measured by flow cytometry; protein levels were measured in serum or plasma. These measurements reflect biological processes within the individual, and we hypothesized that a subset of such measurements may be suitable as biomarkers for the responsiveness to treatment. We also had information regarding several factors known to impact treatment response, such as smoking status, age, sex, and steroid treatment, in the newly diagnosed RA patients before staring MTX treatment.

Our primary aim was to investigate the biological effect of MTX among RA patients, and whether these effects differed between responders and non-responders. Secondarily, we also investigated if we could predict MTX response based on cellular, molecular and clinical features at baseline.

Materials and methods

COMBINE cohort

We utilized the COMBINE cohort, which includes 246 individuals, whereof 92 are treatment naïve early RA patients who started MTX treatment at Karolinska University Hospital with a maximum symptom duration of approximately 14 months before inclusion to the study. Demographics and clinical phenotypes at baseline are shown in Table 1. Patients donated peripheral blood at

TABLE 1 Demographics at inclusion of the 80 patients with newly diagnosed RA during 2011–2013 who consented to participation and contributed blood at both time points.

	RA (*n* =80)
Female (%)	60 (75.0)
Age, median years (range)	62 (22–88)
HLA-DR shared epitope positive (%)	54 (67.5)
Self-reported Swedish ethnicity (%)	66 (82.5)
Current smoker (%)	27 (34.6)
Symptom duration in days, median (range)	168 (46–428)
Erosions/osteopenia (%)	20 (25)
ACPA positive (%)	49 (61.3)
DAS28, median (range)	5.0 (0.84–7.6)
Patient global health assessment, median (range)	47 (1–100)
Health professional global health assessment, median (range)	45 (2–84)
Physical function (HAQ), median (range)	1.06 (0–2.5)
CRP, median (range)	6 (0.5–146)
Prednisolone treatment (%)	44 (55.0)

Abbreviations: ACPA, Anti-citrullinated protein antibodies; MTX, Methotrexate; RA, Rheumatoid arthritis; PCA, Principal components analysis; PBMC, Peripheral blood mononuclear cells; EULAR, The European Alliance of Associations for Rheumatology; HLA-DR, Human leukocyte antigen – DR isotype; CRP, C-reactive protein; DAS28, Disease activity score 28 joints; CCP2, Second generation anti-cyclic citrullinated peptide; RNA, Ribonucleic acid; UPPMAX, Uppsala Multidisciplinary Center for Advanced Computational Science; LOO, Leave one out; AUC, Are under curve; ROC, Receiver operator characteristic.

the appointment prior to MTX initiation. All patients returned for a follow up visit after approximately 3 months (full range 67–126 days, median 93 days) where they again underwent a clinical examination and donated peripheral blood (stored in −80°C). Out of the 92 patients who started MTX therapy 12 dropped out during the follow-up period, leaving a total of 80 patients for which we have biological measurements and clinical follow up data (Table 1). The majority of patients in our cohort were prescribed Prednisolone treatment (Table 1), a glucocorticoid with immune suppressive effects. Prednisolone was prescribed either before initiating MTX treatment (N:19) or along with MTX prescription (N:25).

Patients were asked about their ethnicity as well as past and current smoking behavior. We detected anti-citrullinated protein autoantibodies (ACPA) using the multiplex anti-CCP2 assay (Eurodiagnostica) at Karolinska University Hospital. The presence of joint erosions or bone decalcifications was detected using X-ray and assessed by radiologists at Karolinska University Hospital.

Response outcome

The primary outcome was determined using the EULAR response criteria (7). We dichotomized response, so that those who achieved Good or Moderate EULAR response at 3 months of treatment were considered "responders" and the rest being "non-responders."

Flow cytometry

The Clinical Chemistry laboratory of Karolinska University hospital measured the concentration of leukocytes, neutrophils, eosinophils, basophils and monocytes per liter of peripheral blood using XE Sysmex flow cytometry-based analysis.

Additionally, several immune cell phenotypes were measured by flow cytometry at the Rheumatology Laboratory at the Center for Molecular Medicine, Karolinska Institutet (for an overview of the gating strategy see Supplementary Figure S1). Peripheral blood mononuclear cells (PBMC) were isolated and whole blood lysed using Serotec Erythrolyse buffer (Bio-Rad AbD Serotec Ltd). Cells were stained freshly using the following antibodies (clones): CD45RA (B56), TcRgd (B1), HLA-DR (L43), CD4 (OKT4), CD138 (ID4 or DL-101), CD19 (HIB19), NKp44 (P44-8), CD16 (3G8), CD69 (FN50), CD28 (CD28.2), CD45 (HI30), IL21R (2G1-K12), TREM-1 (TREM-26) all from Biolegend, CD3 (UCHT1) and NGG2A (Z199.1) from Beckman Coulter, IgD (IA6-2), CD14 (Mphi 9), CD27 (M-T271), CD56 (BI59) from Beckton Dickinson, NKG2D (1D11) from eBioscience. Only the HLA-DR staining was controlled using an isotype control antibody from Biolegend, while the staining of NKG2A, NKG2D, IL21R and TREM-1 were controlled by absence of added antibody (FMO, fluorescence minus one). The stainings were performed using different antibody panels. One panel focusing on T-cell stainings of PBMC, another on B-cell stainings, a third on NK cells and monocytes, and a fourth staining performed on whole lysed blood where granulocytes were identified by size and granularity (forward and side scattering properties). All measurements were performed on Gallios flow cytometer (Beckman Coulter) and data analyzed using FlowJo (TreeStar Inc., Ashland, OR, United States). In the statistical analyses we utilized a total of 427 flow cytometry variables.

Protein measurements

We collected information of plasma protein concentrations using different multiplex platforms as described previously (8). Protein levels below detection level were re-coded as 0.001. Within the cohort the distributions of plasma protein concentrations were highly skewed with long tails, and a log transformation was therefore applied prior to association analysis. Only when at least 8 different protein levels above detection threshold within each test was available the proteins were considered for further analyses, resulting in 51 analyzed proteins, including 16 proteins measured using multiple methods.

RNA sequencing

RNA was purified from PBMCs and sequenced as previously described (8). After removing samples with insufficient quality, we obtained 60 high quality RNA seq samples from the baseline visit, and 60 RNA samples from the follow up visit. From 52 patients we obtained a high-quality RNA seq data set from both baseline and follow up. For 30 of the samples in the MTX cohort the initial sequencing produced very few reads and was therefore repeated. The read files from the two sequencing rounds were merged. We employed Trimgalore (v. 0.4.1) to remove adapter sequence and low-quality bases from reads (−-paired --phred33 --length 25), and reads were aligned to the human genome using STAR (v. 2.5.3a) and summarized across genes using the *gencode* (v.27) annotation. The alignments were performed on resources provided by the SNIC informatics network through Uppsala Multidisciplinary Center for Advanced Computational Science (UPPMAX).

Statistical analysis

We performed both longitudinal and cross-sectional analyses for each biological measurement. The aim of the longitudinal analyses was to identify changes between baseline and the 3 months visit for responders and non-responders separately, and to analyze whether there were any differences in changes between these two groups. The measurements at baseline were also used to investigate whether any features seen at baseline could predict response after 3 months. All analyses were performed in R (v.3.5.1), and gene expression analyses using DESeq2 (v. 1.20.0).

When analyzing the change in protein and flow cytometry measures during treatment we used a mixed linear model (lme from nlme v. 3.1–137) and assessed the different contrasts using *emmeans* (*lsmeans* v. 2.30–0). We modelled each measurement as dependent on time point (baseline or follow-up), response, an interaction between time point and response, prednisolone, and a random effect of each individual.

When modelling gene expression changes during treatment we wanted to model changes both within (treatment effect) and between (responders vs. non-responders) samples obtained at baseline and at 3 months, respectively. We used the approach outlined in *edgeR* user guide regarding comparisons both between and within subjects (9). Further, gene expression is known to vary greatly between and within individuals, and a major part of this variation is due to differences in proportion of different cell populations in peripheral blood. In our gene expression analyses we therefore aimed to describe changes that are not due to changes in major cell type proportions, but due to changes in gene expression within cells. Changes in cell composition, on the other hand, are better detected using flow cytometry data. We therefore chose to adjust our analysis of gene expression levels based on the proportion of major immune cell types in PBMCs: B-cells, T-cells, NK-cells, or monocytes out of total PBMC. Gene expression was thereby modelled as dependent on response, the interaction between response and patient ID, the interaction between visit and response, prednisolone, the proportion of B, T, NK-cells, and the proportion of monocytes.

In all the prospective analyses using baseline data (gene expression, protein levels, or cell type proportions) to detect biomarkers of response to MTX after 3 months, we adjusted our analyses for factors that might be associated to both response status and biomarker levels (i.e., likely confounders). All baseline analyses were accordingly adjusted for age, sex, whether the individual was of self-reported Swedish ethnicity, had erosions at baseline, was a current smoker when treatment was initiated, presence of ACPA, and treatment with Prednisolone at the time of blood donation. For flow cytometry and measurement of plasma protein concentrations, we analyzed the association between response status and cellular or protein phenotypes using logistic regression.

A few additional covariates were included in the cross-sectional analysis of gene expression data at baseline. We used principal component analysis (PCA) of variance stabilized gene expression data (*rlog* in DESeq2) to look for outlier RNA seq samples. PCA revealed no outlier samples, nor any separation between baseline visit and follow up visit or responders and non-responders (data not shown). PCA analysis revealed a major axis of variation that was strongly, but not completely, associated to measured RNA quality scores (r^2: 0.60). We estimated a surrogate variable (using *svaseq* v. 3.28.0) in the baseline sample set to account for this major axis of variation, which was included as a covariate in cross-sectional gene expression modelling. Since the major cell type proportions of PBMCs are likely confounders, they were again included as covariates in the DESeq2 analysis.

We experienced that DESeq2 was sensitive to single high-count outliers in the cross-sectional analyses, and we therefore implemented a leave-one-out (LOO) approach to assess the stability of the detected gene expression biomarkers. In each iteration, one sample was excluded, and the cross-sectional analyses repeated.

In all gene expression association analyses, we chose to analyze genes where at least 20% of the samples has a normalized count of one or higher, and we did not shrink the log2 (fold changes). Significance was assessed using a Wald test.

Gene set enrichment was investigated using a non-parametric test on gene ranks (tmodCERNOtest function in *tmod* (v. 0.36)), using 1329 canonical pathways (8904 genes) from KEGG,[1] BioCarta,[2] Signal Transduction KE,[3] SigmaAldrich,[4] Signalling Gateway,[5] SuperArray SABiosciences,[6] Pathway Interaction Database,[7] reactome[8] and Matrisome Project,[9] collected by MSigDB. We tested whether gene sets were enriched for having smaller probability values, higher fold change and lower fold change. To avoid enrichments due to lowly expressed genes with inflated fold changes we only report those gene sets that showed significant enrichment both in probability values and fold change ranking.

For all tests we defined a false discovery rate (FDR) (10) of <10% as significant. Each analysis type and biological data type was evaluated separately.

Prediction

Prediction models were built based on measurements in treatment naïve individuals and based on the difference between post-treatment and pre-treatment measurement.

Three methods were used to classify the response data: a linear method (regression with L1 and L2 regularization *via* the *glmnet* R library), a non-linear method (*via* the *randomForest* library in R), and a kernel-based method (SVM with an RBF kernel, *via* the *smvRadial* library in R). Each learning task was performed in ten repeats, with five-fold cross-validation and with 100 randomly sampled steps of hyperparameter estimation. Covariates outlined above were included as features in each run, and we built predictive models based on gene expression, flow cytometry, protein levels and clinical data, separately and in an integrated fashion. We removed all zero count genes from the expression data, and filtered ncRNAs (miRNA, piRNA, rRNA, siRNA, snoRNA, and tRNAs). In addition, pseudogenes that are lowly expressed and showed high variance were not used in the model. We used protein-coding genes and long non-coding genes in the expression matrix, which resulted in a total of 22,628 genes. The filtered gene expression matrix was normalized using transcript-per-million (TPM).

The performance of resulting models was reported using balanced accuracy and receiver operating characteristic (ROC) curves. Balanced accuracy and area under the ROC curves (AUCs) are calculated as the mean and 95% confidence intervals for each of the repeats in each task. For each ML task, we report the results from the repeat displaying the median of the mean ROC AUCs.

1 http://www.pathway.jp
2 http://cgap.nci.nih.gov/Pathways/BioCarta_Pathways
3 http://stke.sciencemag.org/about/help/cm
4 http://www.sigmaaldrich.com/life-science.html
5 http://www.signaling-gateway.org
6 http://www.sabiosciences.com/ArrayList.php
7 http://pid.nci.nih.gov
8 http://www.reactome.org
9 http://matrisomeproject.mit.edu

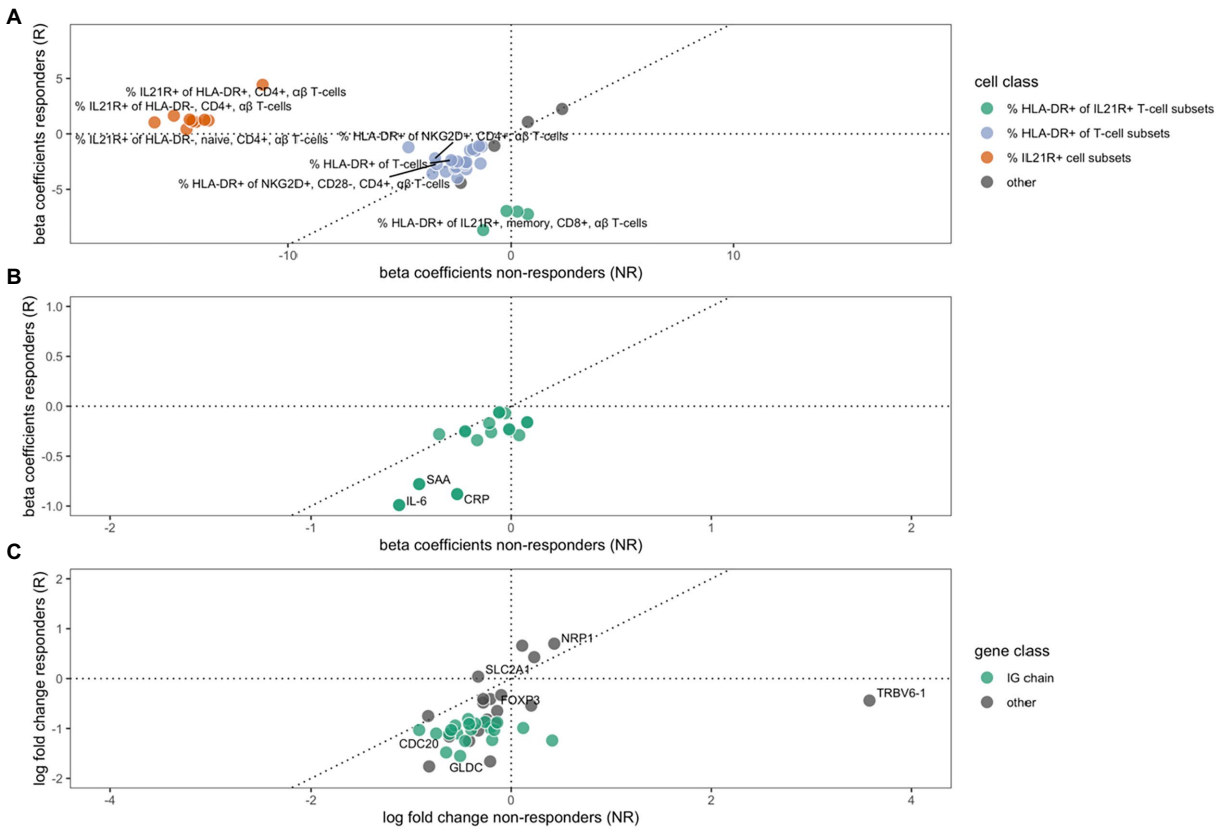

FIGURE 1
The effect of MTX treatment in non-responders (x-axes) or responders (y-axes) on cell type phenotypes **(A)**, protein expression **(B)** and gene expression **(C)**. Beta coefficients in **A** and **B**, and $\log_2$ (fold changes) in **C**, of variables that are significantly regulated (FDR ≤ 10%) during MTX treatment in either non-responders, responders, or both. A dotted 45° inclined line indicates the expected parity for individual effects for groups of non-responders and responders to MTX. **(A)** The changes in cell type phenotypes as measured by flow cytometry. Three different groups of cell phenotypes are indicated by colors: The proportions of HLA-DR+ out of different IL21R+ CD4- T-cell subsets (green), the proportion of HLA-DR+ out of different T-cell subsets (purple), and the proportion of IL21R+ out of several T-cell subsets (red). **(B)** The changes in protein expression. **(C)** The change in gene expression, where a group of immunoglobulin genes are indicated by green color.

Results

Effects of MTX treatment

Clinical effects of MTX treatment

Out of the 80 patients, 32 experienced a good EULAR response, 28 a moderate response and 20 were non-responders according to EULAR response criteria. As expected, MTX treatment had a significant ameliorating effect across clinical parameters for responders, while the effect was lower among the non-responders (see Supplementary Table S1).

Changes in cell concentrations and phenotypes during MTX treatment

We analyzed cell concentrations and proportions of cellular phenotypes among responders and non-responders to MTX. A total of 29 flow cytometry measurements were altered during treatment in responders, and 15 in non-responders (Figure 1A), of which only three were shared in both groups (Table 2). These three all mark a similar decrease of the proportion of HLA-DR-expressing T-cells (HLA-DR+ T-cells, HLA-DR + NKG2D + CD4 + gd- T-cells, and HLA-DR+ CD28 + CD4 + gd- T-cells) among responders and non-responders. Overall, the changes in cell proportions within responders during treatment are dominated by a reduction of the proportions of different HLA-DR+ T-cell subsets. We note that the proportion of several HLA-DR+ subsets of IL21R + CD4- T-cells were strongly suppressed among the MTX-responders, while not affected among non-responders (marked by green in Figure 1A). Among the non-responders, we instead noticed a very strong reduction in the proportion of IL21R+ T-cell subsets (Figure 1A).

We furthered investigated whether the effect that MTX had on cell concentrations and proportions of cellular phenotypes differed significantly between responders and non-responders. Here we observed a significant difference in the changes that occurred between responders and non-responders for eleven cell phenotypes. These eleven subsets all include changes in the proportions of IL21R+ cells, usually CD4+ T-cells. Notably, this change was significant in non-responders, while unaltered in responders (Table 2, marked by red in Figure 1).

Changes in protein levels during MTX treatment

Treatment with MTX significantly decreased the concentration of 17 proteins in serum of responders, while no significant changes were

10.3389/fmed.2023.1146353

TABLE 2 The regulation of cell proportions and within patients during MTX follow up.

	Change in non-responders		Change in responders		Difference	
Flow cytometry measure	Beta	FDR	Beta	FDR	Beta	FDR
% HLA-DR+ cells of IL21R+ CD45RA− CD4-gd- T-cells	−1.26	0.88	−8.67	4.2E-03	−7.41	0.37
% HLA-DR+ cells of IL21R+ CD28− CD4-gd- T-cells	0.75	0.94	−7.24	0.023	−7.99	0.35
% HLA-DR+ cells of IL21R+ CD4-gd- T-cells	0.28	0.99	−7.00	0.013	−7.28	0.33
% HLA-DR+ cells of IL21R+ CD28+ CD4-gd- T-cells	−0.21	0.99	−6.95	0.020	−6.74	0.42
MFI NKG2A of NKp44+ CD16- NK cells	−2.27	0.60	−4.41	0.020	−2.15	0.88
% HLA-DR+ cells of NKG2D+ CD45RA− CD4-gd- T-cells	−2.42	0.33	−3.96	3.9E-03	−1.54	0.88
% HLA-DR+ cells of NKG2D+ CD45RA− CD4+ gd- T-cells	−3.54	0.12	−3.58	3.9E-03	−0.04	0.99
% HLA-DR+ cells of CD45RA− CD4− gd- T-cells	−2.94	0.27	−3.40	0.010	−0.47	0.99
% HLA-DR+ cells of NKG2D+ CD28+ CD4-gd- T-cells	−2.02	0.33	−3.18	3.9E-03	−1.16	0.88
% HLA-DR+ cells of CD28+ CD4- gd- T-cells	−2.52	0.27	−3.08	7.5E-03	−0.56	0.98
% HLA-DR+ cells of NKG2D+ CD28− CD4-gd- T-cells	−2.48	0.20	−2.97	4.5E-03	−0.49	0.98
% HLA-DR+ cells of NKG2D+ CD4-gd- T-cells	−2.08	0.27	−2.76	4.5E-03	−0.67	0.95
% HLA-DR+ cells of NKG2D+ CD28+ CD4+ gd- T-cells	−3.35	0.034	−2.72	3.9E-03	0.63	0.95
% HLA-DR+ cells of gd+ T-cells	−1.38	0.76	−2.67	0.094	−1.28	0.91
% HLA-DR+ cells of NKG2D+ gd- T-cells	−2.08	0.26	−2.60	5.7E-03	−0.51	0.97
% HLA-DR+ cells of NKG2D+ gd + T-cells	−2.02	0.38	−2.55	0.046	−0.53	0.98
% HLA-DR+ cells of CD28− CD4− gd- T-cells	−2.60	0.20	−2.52	0.021	0.09	0.99
% HLA-DR+ cells of CD4− gd- T-cells	−2.42	0.20	−2.49	0.013	−0.07	0.99
% HLA-DR+ cells of T-cells	−2.70	0.079	−2.37	3.9E-03	0.33	0.98
% HLA-DR+ cells of NKG2D+ CD4 + gd- T-cells	−3.42	0.025	−2.20	0.016	1.23	0.85
% HLA-DR+ cells of NKG2D+ CD45RA+ CD4-gd- T-cells	−1.59	0.13	−1.49	0.013	0.10	0.99
% HLA-DR+ cells of CD45RA-CD4+ gd- T-cells	−1.61	0.13	−1.49	7.5E-03	0.12	0.99
% HLA-DR+ cells of gd- T-cells	−1.85	0.13	−1.47	0.020	0.38	0.97
% HLA-DR+ cells of CD45RA + CD4- gd- T-cells	−1.72	0.13	−1.38	0.032	0.34	0.97
% HLA-DR+ cells of NKG2D+ CD28- CD4 + gd- T-cells	−4.62	0.082	−1.20	0.59	3.42	0.39
% HLA-DR+ cells of CD28 + CD4+ gd- T-cells	−1.32	0.12	−1.14	7.5E-03	0.18	0.98
% HLA-DR+ cells of CD4+ gd- T-cells	−1.44	0.12	−1.09	0.020	0.35	0.93
% CD16+ of NK cells	−0.76	0.49	−1.07	0.068	−0.30	0.97
% IL21R+ cells of DR- CD4+ gd- T-cells	−14.56	0.018	0.43	0.97	14.99	0.050
% IL21R+ cells of CD28-CD4+ gd- T-cells	−16.00	0.025	1.04	0.90	17.03	0.050
% IL21R+ cells of CD4+ T-cells	−14.15	0.018	1.08	0.84	15.23	0.046
% CD16- cells of NK cells	0.75	0.50	1.08	0.062	0.33	0.97
% IL21R+ cells of CD45RA− CD4+ gd- T-cells	−14.14	0.018	1.09	0.84	15.22	0.046
% IL21R+ cells of CD4+ gd- T-cells	−14.33	0.018	1.14	0.84	15.46	0.046
% IL21R+ cells of CD28+ CD4+ gd- T-cells	−14.28	0.018	1.15	0.84	15.43	0.046
% IL21R+ cells of total T-cells	−13.57	0.026	1.21	0.84	14.78	0.050
% IL21R+ cells of gd- T-cells	−13.75	0.025	1.27	0.84	15.02	0.050
% IL21R+ cells of Lymphocyte	−14.42	0.019	1.29	0.84	15.71	0.046
% IL21R+ cells of CD45RA+ CD4+ gd- T-cells	−15.13	0.018	1.64	0.81	16.77	0.046
% HLA-DR- cells of CD4− gd- T-cells	2.29	0.23	2.25	0.024	−0.04	0.99
% IL21R+ cells of HLA-DR+ CD4+ gd- T-cells	−11.14	0.12	4.43	0.40	15.57	0.050

TABLE 3 Protein levels significantly altered during MTX treatment. Some proteins were measured using multiple separate methods.

	Change in non-responders		Change in responders	
	Beta	FDR	Beta	FDR
IL-6	−0.56	0.38	−0.99	$1.7*10^{-6}$
CRP	−0.27	0.75	−0.88	$7.6*10^{-4}$
CRP	−0.27	0.75	−0.88	$7.6*10^{-4}$
SAA	−0.46	0.53	−0.78	$7.6*10^{-4}$
CXCL10	−0.23	0.38	−0.26	$7.5*10^{-3}$
CXCL9	−0.17	0.70	−0.34	$8.6*10^{-3}$
CCL23 (MPIF-1)	−0.23	0.38	−0.25	$8.7*10^{-3}$
MMP-9	−0.10	0.82	−0.26	0.012
E-Selectin	−0.11	0.55	−0.17	0.012
MCP-2	−0.36	0.36	−0.28	0.012
VEGF	0.08	0.71	−0.16	0.016
VEGF	0.08	0.71	−0.16	0.016
MMP-3	−0.01	0.93	−0.24	0.018
MMP-3	0.04	0.92	−0.29	0.018
MMP-3	−0.01	0.93	−0.23	0.019
ICAM-1	−0.03	0.87	−0.07	0.033
VCAM-1	−0.06	0.54	−0.06	0.068

observed in non-responders (Table 3). The regulation in the two subsets of RA patients is highly correlated (correlation between vectors of beta coefficients; r^2: 0.83, p: $5.6*10^{-6}$, Figure 1B). Our data demonstrates that MTX strongly decreases the levels of IL-6, CRP, and SAA in plasma.

Gene expression changes during MTX treatment

We detected significant changes of gene expression in PBMCs during treatment within the group of responders, where three genes were upregulated and 35 suppressed by MTX (Table 4; Figure 1C). These changes include the suppression of the master regulator of regulatory T-cells, FOXP3, along with several immunoglobulin genes. Gene set enrichment analysis indicated a suppression of cell cycle among RA patients responding to MTX (Table 5). Of note, these changes are beyond the changes in major cell type proportions, which we adjusted for in the analysis.

Within non-responders only two genes were significantly altered by MTX treatment, none of which are overlapping with those significantly regulated among responders. We observed a strong increase in the expression of one of the T-cell receptor beta-chain genes, TRBV6-1 and relatively low decrease of expression of one of glucose transporter genes, SLC2A1. Gene set enrichment analysis indicated the suppression of chemokines, and Calcineurin-regulated NFAT-dependent transcription in lymphocytes (Table 6). We found no overlap between the gene set enrichments in responders and non-responders to MTX treatment. Genes regulated in responders or non-responders had slightly correlated log2 (fold changes) (r^2: 0.35, p: 0.025).

There were no genes that differed significantly in regulation among responders compared to non-responders (the two genes that were regulated by MTX in non-responders, TRBV6-1 and SLC2A1, did however have FDR <20% for having a difference in regulation in responders compared to non-responders).

Differences between future MTX-responders and non-responders at baseline

Demographic and clinical factors at baseline associated to MTX response

We evaluated whether the vast set of demographic and clinical variables that were measured at baseline were associated to future MTX response. None of these variables were significantly associated to future treatment response in our cohort.

Cell types, cell phenotypes and protein measurements at baseline associated to later MTX response

We investigated the association between 427 immune phenotypes from flow cytometry and MTX response but did not detect any significant differences between future responders and non-responders at baseline.

We investigated the association of 51 proteins measured in MTX naïve samples (whereof 16 were investigated using multiple assays) and MTX response. No association reached an FDR below 10%.

Gene expression levels at baseline associated to future MTX response

There were 88 genes for which expression levels at baseline were significantly different between patients who would later respond to MTX, compared to those who would not (Supplementary Table S2).

10.3389/fmed.2023.1146353

TABLE 4 Genes significantly regulated during MTX treatment among those who responded or did not respond.

		Regulation among non-responders		Regulation among responders	
Ensembl ID	HGNC	log2FC	FDR	log2FC	FDR
ENSG00000211896	IGHG1	−0.51	1.00	−1.55	$4.5*10^{-6}$
ENSG00000211895	IGHA1	−0.65	1.00	−1.48	$6.6*10^{-5}$
ENSG00000010319	SEMA3G	−0.83	0.74	−0.75	$1.4*10^{-3}$
ENSG00000178445	GLDC	−0.21	1.00	−1.66	$1.4*10^{-3}$
ENSG00000049768	FOXP3	−0.21	1.00	−0.41	$1.7*10^{-3}$
ENSG00000211893	IGHG2	−0.54	1.00	−1.10	$2.9*10^{-3}$
ENSG00000099250	NRP1	0.43	1.00	0.70	$4.8*10^{-3}$
ENSG00000132465	JCHAIN	−0.42	1.00	−1.25	$5.9*10^{-3}$
ENSG00000117399	CDC20	−0.62	1.00	−1.16	$1.1*10^{-2}$
ENSG00000157168	NRG1	0.20	1.00	−0.54	$1.3*10^{-2}$
ENSG00000155962	CLIC2	0.23	1.00	0.43	$1.7*10^{-2}$
ENSG00000211679	IGLC3	0.12	1.00	−0.99	0.017
ENSG00000088325	TPX2	−0.24	1.00	−0.82	0.021
ENSG00000136235	GPNMB	0.11	1.00	0.66	0.024
ENSG00000148773	MKI67	−0.16	1.00	−0.89	0.024
ENSG00000211662	IGLV3-21	−0.75	1.00	−1.10	0.024
ENSG00000211669	IGLV3-10	−0.46	1.00	−1.25	0.024
ENSG00000211941	IGHV3-11	−0.92	1.00	−1.03	0.024
ENSG00000211663	IGLV3-19	−0.62	1.00	−1.11	0.028
ENSG00000011590	ZBTB32	−0.28	1.00	−0.48	0.028
ENSG00000211592	IGKC	−0.21	1.00	−0.99	0.030
ENSG00000115884	SDC1	−0.82	1.00	−1.76	0.036
ENSG00000126787	DLGAP5	−0.33	1.00	−1.04	0.038
ENSG00000211648	IGLV1-47	−0.40	1.00	−1.02	0.047
ENSG00000266088		−0.28	1.00	−0.41	0.060
ENSG00000211673	IGLV3-1	−0.56	1.00	−0.94	0.060
ENSG00000170476	MZB1	−0.14	1.00	−0.65	0.060
ENSG00000163599	CTLA4	−0.10	1.00	−0.33	0.061
ENSG00000211892	IGHG4	0.41	1.00	−1.24	0.062
ENSG00000239951	IGKV3-20	−0.26	1.00	−0.87	0.064
ENSG00000282122	IGHV7-4-1	−0.19	1.00	−1.23	0.064
ENSG00000211677	IGLC2	−0.36	1.00	−0.90	0.076
ENSG00000211934	IGHV1-2	−0.17	1.00	−1.03	0.082
ENSG00000211966	IGHV5-51	−0.42	1.00	−0.91	0.082
ENSG00000211644	IGLV1-51	−0.43	1.00	−0.81	0.082
ENSG00000211653	IGLV1-40	−0.60	1.00	−1.03	0.083
ENSG00000211955	IGHV3-33	−0.14	1.00	−0.88	0.096
ENSG00000211660	IGLV2-23	−0.43	1.00	−0.96	0.10
ENSG00000211706	TRBV6-1	3.58	0.07	−0.44	0.99
ENSG00000117394	SLC2A1	−0.33	0.08	0.04	0.99

However, none of these 88 genes remained significant in every of the 60 LOO iteration. The maximum number of leave-one-out iterations when a gene was significant was 58 (for 8 genes). The number of significant genes across the 60 leave-one-out iterations fluctuated between zero and 1,066. We therefore concluded that no single gene expression level at baseline was consistently associated to future

TABLE 5 Gene sets suppressed during MTX treatment among RA patients who had responded to MTX treatment (EULAR classification "Moderate" or "Good").

			By fold change		By value of *p*	
Gene set	Source	N1	AUC	FDR	AUC	FDR
PLK1 pathway	PID	43	0.62	$5.5*10^{-3}$	0.68	$8.9*10^{-6}$
Cyclin A B1 associated events during G2 M transition	Reactome	15	0.75	0.012	0.74	0.028
Kinesins	Reactome	21	0.71	0.012	0.71	0.028
Cell cycle mitotic	Reactome	297	0.57	0.017	0.55	0.035
Foxm1 pathway	PID	36	0.65	0.017	0.63	0.040
G1 S specific transcription	Reactome	17	0.70	0.017	0.67	0.061
Aurora B Pathway	PID	38	0.61	0.045	0.61	0.061
Aurora A Pathway	PID	29	0.62	0.072	0.62	0.028

TABLE 6 Gene sets suppressed during MTX treatment among RA patients who did not respond to MTX treatment (EULAR classification "No").

			By fold change		By value of p	
Gene set	Source	N	AUC	FDR	AUC	FDR
Chemokine receptors bind chemokines	Reactome	40	0.71	$1.0*10^{-3}$	0.61	0.085
NFAT TF pathway	PID	41	0.76	$3.7*10^{-3}$	0.68	$2.4*10^{-3}$
CD8 TCR downstream pathway	PID	52	0.75	$3.7*10^{-3}$	0.66	$6.6*10^{-4}$
IL12 pathway	PID	62	0.66	0.039	0.63	$4.4*10^{-4}$

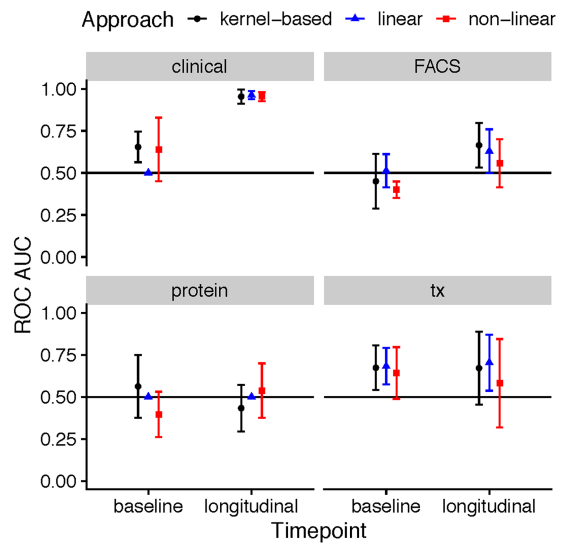

FIGURE 2
ROC AUC performance of ML models predicting response based on clinical, flow cytometry, protein, and RNA-seq data in MTX therapies recorded during the baseline patient visit, and a longitudinal difference between the three-month follow-up and baseline. The points in the plots showcase the mean ROC AUC values of the median repeat in each of the ML tasks, along with the corresponding 95% confidence interval of the standard error of the mean (SEM).

clinical response. Further, given the large fluctuation in analysis results depending on the exclusion of single samples in these cross-sectional analyses, we also refrained from performing gene set enrichment analysis.

Predicting MTX response

The predictive ability varied across the four data types (clinical, flow cytometry, transcriptomics, and protein), time point, and employed method. At baseline, a total of three combinations achieved ROC AUCs with a confidence interval which did not include the 0.5 level: the kernel-based prediction model utilizing clinical variables (mean AUC: 0.65, 95% CI: 0.56–0.75), the kernel-based and linear models of gene expression data (mean AUC: 0.67, 95% CI: 0.54–0.81 and mean AUC: 0.68, 95% CI: 0.57–0.79, respectively) (Figure 2). As expected, the longitudinal changes in clinical variables resulted in a very accurate prediction of response. Further, changes in measurements of gene expression, protein or flow cytometry phenotypes did not achieve successful prediction models. Further, although baseline FACS models yielded no successful predictions, the longitudinal kernel-based model resulted in more predictive models with mean AUC of 0.66, 95% CI: 0.53–0.80; in transcriptomics, the linear longitudinal model displayed a positive predictivity with a mean ROC AUC of 0.70, with a 95% CI of 0.54–0.87.

Discussion

Here we report insights from a clinically and biologically well-characterized cohort of newly diagnosed RA patients starting MTX treatment and followed during 3 months of treatment. The availability of information regarding important demographic, clinical and immunological confounders enabled us to conduct a thorough and robust analysis, less sensitive to bias. We detect strong effects of MTX across clinical measurements, protein expression in peripheral blood, gene expression in PBMCs and cell phenotype proportions, mainly a suppression across all tissue types. The biological effects in immune

cell proportions and gene expression differed between responders and non-responders, indicating that there are indeed different biological processes occurring in those who respond clinically compared to those who do not.

At the rheumatology clinics the rheumatologist evaluates the treatment response of each patient according to their specific disease phenotype and progression, and one treatment response definition might not fit all patients. This can also be seen in the literature where different investigators use a diverse set of treatment outcomes. We chose to analyze EULAR treatment response that takes both the resulting DAS28 and the change induced by treatment into account, which is often employed in clinical trials. In this study we chose to analyze whether patients had any convincing effect of treatment, where a moderate and good EULAR treatment response were merged. We focused on the statistically most powerful analyses: the effect of treatment within individuals. In this analysis, we were particularly interested in whether different mechanisms are active in the patients that respond to MTX, compared to those who do not respond. Secondly, we also attempted to detect biomarkers that can predict whether a patient will respond to MTX treatment by using measurements from the baseline visit only.

In our flow cytometry data of PBMC we observed significant changes in many immune cell proportions during MTX treatment. MTX strongly diminished the proportion of HLA-DR+ T-cells in relation to other T cells in responders and non-responders, but more notably so within responders. As HLA-DR expression is considered a sign of activated T-cells, this indicates that across all patients MTX was able to specifically suppress the activation of T-cells, alternatively affect their abundance in peripheral blood. Additionally, the proportion of T-cells expressing IL21R were suppressed exclusively in non-responders. IL21 is a pleiotropic cytokine with context-dependent mainly pro-inflammatory effects on T cell differentiation (11), and thus a potential treatment target in RA (12). The receptor for IL21 is expressed upon cellular activation on T cells as well as on many other leukocytes. We analyzed IL21R expression on T cells as well as on NK cells, B cells and monocytes, and found suppressed proportions of only T cells expressing IL21R. The decreased proportion of IL-21-expressing T-cells in non-responding patients could indicate an altered tissue distribution of these cells, or a reduced overall expression of IL21R in T cells specifically.

The effect of MTX on protein levels in serum was similar across responders and non-responders. However, the coefficients of change were always larger for responders, indicating that the detected regulation tended to be stronger among responders. As expected we saw a drop in CRP levels. Blockage of IL-6 has been shown to be clinically beneficial in RA (reviewed in (13)), and here we observed a significant decrease in IL-6 among patients who responded to treatment. We did not observe a significant regulation of IL-6 gene expression, which might be due to limitations in power or a decreasing of IL-6 gene expression by cells other than PBMC. In addition, VEGF was significantly decreased by MTX within responders, whereas levels in non-responders increased slightly (not significant). Here the difference in regulation among responders and non-responders was nominally significant (p: 0.011). VEGF has previously been suggested to be positively correlated with disease severity (DAS28) and CRP levels (14). In our material there was a positive correlation between CRP and VEGF among treatment naïve patients (r^2: 0.44, p: $2.4*10^{-5}$), but no correlation was seen after MTX treatment (r^2: 0.01, p: 0.92). CCL23 has been suggested as a severity marker for RA (15), and we observed that it decreased significantly during treatment in responders. We saw a significant correlation between CCL23 and DAS28 in MTX-naïve patients (r^2: 0.27, p: 0.0086), but this correlation disappeared in MTX-treated patients (r^2: 0.02, p: 0.85). We also found a suppression of CXCL10 and E-selectin, in line with data in a previous reports (16, 17). Additionally, we detected the suppression of pro-inflammatory proteins Serum Amyloid A and CXCL9, and the metalloproteinase MMP-9 in responders.

MTX treatment had a large effect on gene expression levels, with some similarities between responders and non-responder, i.e., no single genes had a significantly differential regulation in responders as compared to non-responders. Among the patients that responded to MTX there was a clear suppression of the expression of cell cycle genes, indicating that MTX decreased the proliferation of the PBMC alternatively that MTX caused sequestration of proliferating cells in tissues. Also, the expression of several immunoglobulin genes were significantly suppressed by MTX among the responders. In our flow cytometry panel we measured the proportion of IgD-CD138+ CD27+ of all B cells, a staining that is considered to identify antibody-secreting plasma cells. The proportion of plasma cells measured this way was indeed suppressed by MTX, but had a FDR > 10% (beta: −033, p: 0.015). These findings could be a result of an altered distribution of immunoglobulin-expressing cells in the body induced by MTX, or a direct effect of MTX on antibody-production and B cell maturation processes. The gene expression level for the master regulator of regulatory T-cells, FOXP3, was also suppressed by treatment in those who responded to MTX. This was surprising given several earlier reports indicating that successful MTX treatment increases the proportion of regulatory T-cells in the peripheral blood of individuals with RA (18). Notably, transcripts of FOXP3 is expressed not only by regulatory T-cells, but also transiently by activated T-cells (19) and other cell lineages (20).

Among non-responders the effect of MTX on gene expression was generally weaker than in responders. The two genes that were significantly regulated among non-responders only, TRBV6-1 (log2FC:3.58) and SLC2A1 (log2FC: −0.33), were the genes with the strongest evidence for differential regulation by MTX treatment in responders compared to non-responders (FDR < 20%). Comparing the log2 (fold changes) in responders and non-responders showed only weak correlation (r^2: 0.35, p: 0.025). Notably, gene set enrichment analysis indicated the suppression of inflammatory gene sets such as chemokines and chemokine receptors, IL12, NFAT and the pathway downstream the TCR of CD8+ T-cells also within clinical non-responders, gene sets which were not enriched in responders. Non-responders also experienced a decrease in the proportion of IL21R+ T-cell subsets during treatment, and an increased expression of the T-cell receptor gene TRBV6-1.

Prednisolone has a large effect on immune cells (21). In exploratory analysis, we accordingly observed that the effect of MTX and prednisolone jointly was larger than the effect of MTX alone on gene expression (results not shown). This exemplifies why adjusting for prednisolone in our analyses was essential.

We did not detect any biomarkers or prediction models with sufficient predictive value to aid in MTX therapy at baseline. Although the transcriptome models displayed positive predictivity, the ROC AUCs were relatively low which indicates that these results are fit as

supplementary evidence, rather than serve as a basis of treatment choice. The set of proteins we investigated was, however, rather limited (n:51). We assayed a broad range of immune phenotypes, but the focus was to look at all major cell types and not the more functional ones. Previous reports have indicated that non-responders of MTX had a higher concentration of monocytes, and a proportion of CD14brightCD16−, CD14brightCD16+ and CD14dimCD16+ monocyte subsets before treatment initiation (22). Here neither of those signals was replicated, although we do detect a trend for higher proportion of CD14brightCD16+ among non-responders (OR: 0.86, *p*: 0.096). The level of IL1beta produced by PBMC has previously been suggested as a biomarker of response to MTX (23) but we detect no such pattern in serum, and when looking at gene expression by PBMC the level was slightly lower in future responders but far from significant [log2 (fold change): −0.34, *p*: 0.22]. Our results indicate that no major immune cell phenotypes in peripheral blood was able to predict who will later respond to MTX. Plant et al. (24) has previously demonstrated similar predictive ability of whole blood gene expression at baseline as we observe here. They additionally show that the difference in gene expression at baseline and 4 weeks into treatment is valuable to predict long-term MTX response. We are unable to interrogate this in our sample set as patients did not donate blood until their follow up clinical appointment at 3 months. Overall, we demonstrate some prediction models that are significantly better than random, yet not strong enough to warrant clinical implementation. This might be due to the heterogeneity, and limited size, of the included sample set.

In this study we are focusing on measurements done in peripheral blood due to the accessibility and low discomfort for the donors. This might however limit our possibility of detecting biomarkers or understanding the mechanisms associated to a good response to MTX. The important processes might in fact happen elsewhere in the body, as in the synovial or lymphoid tissue. Another limitation of this project is that gene expression alterations in specific cell types might be diluted and missed when total RNA is sequenced. We only investigated a subset of all cell type proportions and proteins, so important biomarkers might have been missed.

Conclusion

In summary, we herein show that MTX treatment leads to significantly different biological effects among those who respond clinically to treatment and those who do not. Within those who responded to MTX we observed a suppression of the proportions of HLA-DR+ T-cell subsets, a suppression of cell cycle genes, and a downregulation of IL-6. In non-responders we instead observed the suppression of IL21R+ T-cell subsets. These findings might represent biological processes that are involved in the clinical response, or lack of response, to MTX among RA patients.

Data availability statement

The datasets generated and analysed in the current study is not available in a public repository since this is restricted by GDPR and the ethical permissions for COMBINE. We encourage researchers with an interested in the material to arrange an ethical approval and contact author LB with data requests for applicable studies.

Ethics statement

The studies involving human participants were reviewed and approved by the Stockholm (number 2010-351-31-2) and Uppsala (2009-013) Regional Ethics Committees. The patients/participants provided their written informed consent to participate in this study. Written informed consent was obtained from the individual(s) for the publication of any potentially identifiable images or data included in this article.

Funding

The vast majority of expenses related to this study including laboratory measurements and study costs were funded by the pharmaceutical company Novo Nordisk A/S. Novo Nordisk was involved in the design and collection of data. Pfizer Inc. contributed funds for conducting the included analyzes. Pfizer Inc was involved in analysis design, decision to publish and preparation of the manuscript. LP was supported by NORA consortium.

Author contributions

BB formulated the research question, derived a subset of the included variables, designed and performed the statistical analysis, interpreted the results and wrote the manuscript. NY trimmed and aligned RNA seq data, participated in analysis design and manuscript reviewing. TU reviewed and cleaned the flow cytometry data, and performed statistical analysis of the flow cytometry data. DZ participated in analysis design and interpretation, as well as illustrations and paper manuscript review. MMa designed, performed and interpreted the machine learning analysis. LF cleaned and integrated all the different data sets. HW, LP, and SJ participated in results interpretation and manuscript review. NP, MMü, and PS built the biobank, ran the flow cytometry and analysed the flow cytometry raw data. AH and AC selected the patient and performed the clinical evaluation. LK and AC initiated the COMBINE study. LB designed the patient sample laboratory analyses, supervised the laboratory work, coordinated data collection and interpreted flow cytometry and plasma protein findings. All authors contributed to the article and approved the submitted version.

Acknowledgments

We wish to thank all the participating patients and healthy individuals and the research nurse Karin Lundvall.

Conflict of interest

SJ, MMa, and DZ were employed by Pfizer. LF was employed by Novo Nordisk A/S during data generation for this study and currently is employed by Nucleus Genomics.

The remaining authors declare that the research was conducted in the absence of any commercial or financial relationships that could be construed as a potential conflict of interest.

Publisher's note

All claims expressed in this article are solely those of the authors and do not necessarily represent those of their affiliated organizations, or those of the publisher, the editors and the reviewers. Any product that may be evaluated in this article, or claim that may be made by its manufacturer, is not guaranteed or endorsed by the publisher.

Supplementary material

The Supplementary material for this article can be found online at: https://www.frontiersin.org/articles/10.3389/fmed.2023.1146353/full#supplementary-material

References

1. Klareskog L, Catrina AI, Paget S. Rheumatoid arthritis. *Lancet*. (2009) 373:659–72. doi: 10.1016/S0140-6736(09)60008-8

2. Gerards AH, de Lathouder S, de Groot ER, Dijkmans BA, Aarden LA. Inhibition of cytokine production by methotrexate. Studies in healthy volunteers and patients with rheumatoid arthritis. *Rheumatology (Oxford)*. (2003) 42:1189–96. doi: 10.1093/rheumatology/keg323

3. Tasaki S, Suzuki K, Kassai Y, Takeshita M, Murota A, Kondo Y, et al. Multi-omics monitoring of drug response in rheumatoid arthritis in pursuit of molecular remission. *Nat Commun*. (2018) 9:2755. doi: 10.1038/s41467-018-05044-4

4. Farragher TM, Lunt M, Fu B, Bunn D, Symmons DP. Early treatment with, and time receiving, first disease-modifying antirheumatic drug predicts long-term function in patients with inflammatory polyarthritis. *Ann Rheum Dis*. (2010) 69:689–95. doi: 10.1136/ard.2009.108639

5. van Riel PL. The development of the disease activity score (DAS) and the disease activity score using 28 joint counts (DAS28). *Clin Exp Rheumatol*. (2014) 32:S65–74.

6. van Gestel AM, Prevoo ML, Vant Hof MA, Van Rijswijk MH, Van De Putte LB, Van Riel PL. Development and validation of the European league against rheumatism response criteria for rheumatoid arthritis. Comparison with the preliminary American College of Rheumatology and the World Health Organization/international league against rheumatism criteria. *Arthritis Rheum*. (1996) 39:34–40. doi: 10.1002/art.1780390105

7. Fransen J, van Riel PL. The disease activity score and the EULAR response criteria. *Rheum Dis Clin N Am*. (2009) 35:745–57. doi: 10.1016/j.rdc.2009.10.001

8. Folkersen L, Brynedal B, Diaz-Gallo LM, Ramskold D, Shchetynsky K, Westerlind H, et al. Integration of known DNA, RNA and protein biomarkers provides prediction of anti-TNF response in rheumatoid arthritis: results from the COMBINE study. *Mol Med*. (2016) 22:322–8. doi: 10.2119/molmed.2016.00078

9. Chen Y, Ritchie M., Robinson M., Smyth G. *edgeR: Differential Analysis of Sequence Read Count Data: User's Guide*. (2021).

10. Benjamini Y, Hochberg Y. Controlling the false discovery rate: a practical and powerful approach to multiple testing. *J. R. Stat. Soc. B*. (1995) 57:289–300.

11. Tian Y, Zajac AJ. IL-21 and T cell differentiation: consider the context. *Trends Immunol*. (2016) 37:557–68. doi: 10.1016/j.it.2016.06.001

12. Young DA, Hegen M, Ma HL, Whitters MJ, Albert LM, Lowe L, et al. Blockade of the interleukin-21/interleukin-21 receptor pathway ameliorates disease in animal models of rheumatoid arthritis. *Arthritis Rheum*. (2007) 56:1152–63. doi: 10.1002/art.22452

13. Davies R, Choy E. Clinical experience of IL-6 blockade in rheumatic diseases - implications on IL-6 biology and disease pathogenesis. *Semin Immunol*. (2014) 26:97–104. doi: 10.1016/j.smim.2013.12.002

14. Roeder DJ, Lei MG, Morrison DC. Endotoxic-lipopolysaccharide-specific binding proteins on lymphoid cells of various animal species: association with endotoxin susceptibility. *Infect Immun*. (1989) 57:1054–8. doi: 10.1128/iai.57.4.1054-1058.1989

15. Rioja I, Hughes FJ, Sharp CH, Warnock LC, Montgomery DS, Akil M, et al. Potential novel biomarkers of disease activity in rheumatoid arthritis patients: CXCL13, CCL23, transforming growth factor alpha, tumor necrosis factor receptor superfamily member 9, and macrophage colony-stimulating factor. *Arthritis Rheum*. (2008) 58:2257–67. doi: 10.1002/art.23667

16. Dhir V, Sandhu A, Gupta N, Sharma A, Sharma S. Change in CXCL10 on treatment with methotrexate similar to that reported with infliximab: comments on the article by Eriksson et al. *Scand J Rheumatol*. (2014) 43:83–4. doi: 10.3109/03009742.2013.813961

17. Hjeltnes G, Hollan I, Forre O, Wiik A, Lyberg T, Mikkelsen K, et al. Serum levels of lipoprotein(a) and E-selectin are reduced in rheumatoid arthritis patients treated with methotrexate or methotrexate in combination with TNF-alpha-inhibitor. *Clin Exp Rheumatol*. (2013) 31:415–21.

18. Avdeeva A, Rubtsov Y, Dyikanov D, Popkova T, Nasonov E. Regulatory T cells in patients with early untreated rheumatoid arthritis: phenotypic changes in the course of methotrexate treatment. *Biochimie*. (2020) 174:9–17. doi: 10.1016/j.biochi.2020.03.014

19. Wang J, Ioan-Facsinay A, van der Voort EIH, Huizinga TWJ, Toes REM. Transient expression of FOXP3 in human activated nonregulatory CD4+ T cells. *Eur J Immunol*. (2007) 37:129–38. doi: 10.1002/eji.200636435

20. Yamamoto M, Tsuji-Takayama K, Suzuki M, Harashima A, Sugimoto A, Motoda R, et al. Comprehensive analysis of FOXP3 mRNA expression in leukemia and transformed cell lines. *Leuk Res*. (2008) 32:651–8. doi: 10.1016/j.leukres.2007.08.020

21. Hu Y, Carman JA, Holloway D, Kansal S, Fan L, Goldstine C, et al. Development of a molecular signature to monitor Pharmacodynamic responses mediated by in vivo Administration of Glucocorticoids. *Arthritis Rheumatol*. (2018) 70:1331–42. doi: 10.1002/art.40476

22. Chara L, Sanchez-Atrio A, Perez A, Cuende E, Albarran F, Turrion A, et al. The number of circulating monocytes as biomarkers of the clinical response to methotrexate in untreated patients with rheumatoid arthritis. *J Transl Med*. (2015) 13:2. doi: 10.1186/s12967-014-0375-y

23. Seitz M, Zwicker M, Villiger PM. Pretreatment cytokine profiles of peripheral blood mononuclear cells and serum from patients with rheumatoid arthritis in different American College of Rheumatology Response Groups to Methotrexate. *J Rheumatol*. (2003) 30:28–35.

24. Plant D, Maciejewski M, Smith S, Nair N. Maximising therapeutic utility in rheumatoid arthritis consortium tRSG, Hyrich K, et al. profiling of gene expression biomarkers as a classifier of methotrexate nonresponse in patients with rheumatoid arthritis. *Arthritis Rheumatol*. (2019) 71:678–84. doi: 10.1002/art.40810

frontiers | Frontiers in Medicine

TYPE Mini Review
PUBLISHED 04 April 2023
DOI 10.3389/fmed.2023.1166343

OPEN ACCESS

EDITED BY
Jill M. Kramer,
University at Buffalo,
United States

REVIEWED BY
Satoshi Kubo,
University of Occupational and Environmental Health Japan,
Japan

*CORRESPONDENCE
Yumi Tsuchida
✉ yumitsuchida@g.ecc.u-tokyo.ac.jp

SPECIALTY SECTION
This article was submitted to Rheumatology, a section of the journal Frontiers in Medicine

RECEIVED 15 February 2023
ACCEPTED 15 March 2023
PUBLISHED 04 April 2023

CITATION
Tsuchida Y, Shoda H, Sawada T and Fujio K (2023) Role of autotaxin in systemic lupus erythematosus.
Front. Med. 10:1166343.
doi: 10.3389/fmed.2023.1166343

Role of autotaxin in systemic lupus erythematosus

Yumi Tsuchida[1]*, Hirofumi Shoda[1], Tetsuji Sawada[2] and Keishi Fujio[1]

[1]Department of Allergy and Rheumatology, Graduate School of Medicine, The University of Tokyo, Tokyo, Japan, [2]Department of Rheumatology, Tokyo Medical University Hospital, Tokyo, Japan

Systemic lupus erythematosus (SLE) is a prototypic systemic autoimmune disease characterized by the production of various autoantibodies and deposition of immune complexes. SLE is a heterogenous disease, and the pattern of organ involvement and response to treatment differs significantly among patients. Novel biological markers are necessary to assess the extent of organ involvement and predict treatment response in SLE. Lysophosphatidic acid is a lysophospholipid involved in various biological processes, and autotaxin (ATX), which catalyzes the production of lysophosphatidic acid in the extracellular space, has gained attention in various diseases as a potential biomarker. The concentration of ATX is increased in the serum and urine of patients with SLE and lupus nephritis. Recent evidence suggests that ATX produced by plasmacytoid dendritic cells may play an important role in the immune system and pathogenesis of SLE. Furthermore, the production of ATX is associated with type I interferons, a key cytokine in SLE pathogenesis, and ATX may be a potential biomarker and key molecule in SLE.

KEYWORDS

autotaxin (ATX), SLE, lysophosphatidic acid, lysophospholipids, type I interferons

1. Introduction

Systemic lupus erythematosus (SLE) is a systemic autoimmune disease, common in young women. SLE is characterized by the production of various autoantibodies, such as anti-nuclear and anti-dsDNA antibodies, and deposition of immune complexes. SLE can affect various organs including the skin, heart, kidneys, and central nervous system. Current treatment for SLE includes antimalarials, corticosteroids, immunosuppressants, and biologics; however, it is far from perfect, and many patients do not achieve an adequate response or experience side effects.

SLE is a heterogenous disease and the pattern of organ involvement and response to treatment differs significantly among patients. Various biological markers, such as complement levels, anti-dsDNA antibody titers, and urine tests, are used in clinical settings to assess disease activity of SLE (1). Different autoantibodies have been reported to be associated with certain clinical features of SLE, for example, the association of anti-ribosomal P antibodies with neuropsychiatric lupus and lupus hepatitis (2). Other novel markers are also being investigated (3), for example, monocyte chemoattractant protein-1 levels in urine have been reported to correlate with the activity and prognosis of lupus nephritis (4–6). Serum interferon levels have been associated with disease activity (7, 8). However, these biomarkers are not sufficient to assess the extent of disease and predict treatment response, and it is pertinent to find markers that can stratify patients to provide treatment most effective for each individual.

Recently, lysophosphatidic acid (LPA) and autotaxin (ATX), an enzyme that catalyzes the production of LPA, have recently gained attention in many fields. Many ATX inhibitors are being

developed as potential therapeutic agents for cancer and idiopathic pulmonary fibrosis, and there are currently several clinical trials underway (9–11). Recently, a role for the ATX-LPA axis in SLE has also been reported. In this review, we will discuss the roles of LPA and ATX and whether they are their possible biological markers in SLE.

2. Lysophospholipids and the autotaxin–lysophosphatidic acid axis

Lysophospholipids are lipids with one carbon chain and a polar head group. They are classified into two groups, lysoglycerophospholipids and lysosphingolipids. *Via* signaling through G protein-coupled receptors, lysophospholipids play an important role in regulating cell function. LPA and sphingosine-1-phosphate are among the most well-studied lysophospholipids involved in cell signaling.

LPA transduces signals through LPA receptors (LPAR1–6) and is involved in various biological processes, including cell migration, proliferation, and aggregation of platelets (12). Under physiological conditions, ATX is the lysophospholipase mainly responsible for the production of LPA in blood and catalyzes the production of LPA from lysoglycerophospholipids, such as lysophosphatidylcholine (12) (Figure 1A). Five ATX isoforms have been reported, all of which exhibit lysophospholipase D activity. ATXβ and ATXγ are the isoforms mainly expressed in peripheral tissue and the central nervous system, respectively (13). ATX is abundantly expressed in adipose tissue. In mice, adipose tissue-specific knockout of ATX significantly decreased the concentration of LPA in plasma, suggesting that adipose tissue is an important source of ATX in blood (14). ATX is also highly expressed in the central nervous and reproductive systems, as well as in lymphoid tissues (13, 15). In the extracellular space, ATX binds to integrins, preventing its clearance and allowing for localized LPA production (16, 17). Tumor necrosis factor (TNF), interleukin-6 (IL-6), and lipopolysaccharide, as well as type I interferons, have been reported to induce the expression of ATX, while the expression of ATX is inhibited by LPA in a negative feedback loop (15, 18) (Figure 1B).

3. Measuring lysophosphatidic acid and autotaxin concentrations

Many studies have investigated the concentrations of LPA and ATX in clinical specimens. Both LPA and ATX are abundant in the blood. Concentrations of LPA in the plasma of healthy individuals vary significantly among reports, ranging from 40–60 nM (19) to 120 nM (20). Concentrations as high as 0.1–6.3 μM have also been reported (21). Significant differences among these reports are thought to reflect the difficulty of accurately measuring LPA concentrations. That is, the concentration of LPA increases rapidly after blood collection due to its production *in vitro*. Therefore, to accurately measure the concentration of LPA in clinical specimens, samples must be handled carefully to avoid the production and degradation of LPA (19, 20). Further, its concentration is slightly higher in females (22).

The concentration of ATX in serum has been reported to be closely correlated with that of LPA and is more stable (22–24); thus, the measurement of ATX may serve as a more practical marker. The serum concentration of ATX is also higher in females than in males: 0.625–1.323 mg/L and 0.438–0.914 mg/L, respectively (9). The serum level of ATX increases during pregnancy (25) and various diseases, which will be discussed in section 4. Serum concentration of ATX may be affected by treatment with steroids (26, 27).

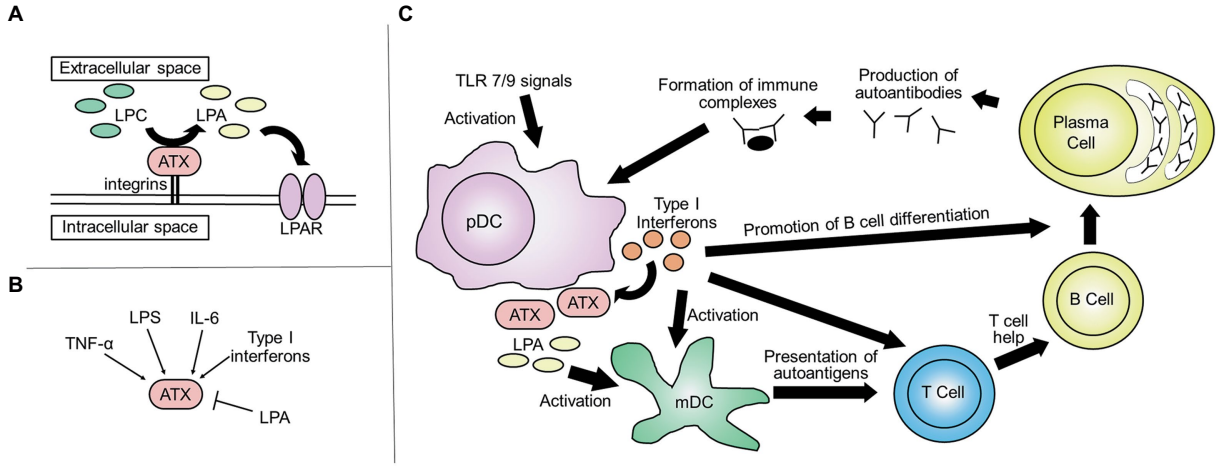

FIGURE 1
An Overview of ATX. **(A)** The ATX-LPA axis: ATX is a lysophospholipase that mainly catalyzes the production of LPA from lysoglycerophospholipids, such as lysophosphatidylcholine. (LPC, lysophosphatidylcholine; ATX, autotaxin; LPA, lysophosphatidic acid; LPAR, LPA receptor). **(B)** Regulation of ATX expression: the expression of ATX is induced by TNF, IL-6, LPS, and type I interferons and inhibited by LPA. (TNF, tumor necrosis factor; IL-6, interleukin-6; LPS, lipopolysaccharide). **(C)** ATX and the pathogenesis of SLE: pDCs are activated by TLR7 and TLR9 signals, resulting in the production of type I interferons. Type I interferons induce the production of ATX and thus the production of LPA. This results in the activation of mDCs, which present autoantigens to T cells and activate them. Together, this leads to the maturation of B cells and the production of autoantibodies. Immune complexes further enhance the activation of pDCs, resulting in a positive feedback loop, contributing to the organ damage in SLE (pDC, plasmacytoid dendritic cell; TLR, toll-like receptors; mDC, myeloid dendritic cell).

4. Autotaxin and human diseases

Reflecting the importance of ATX in the function of various systems, it has been implicated in many human diseases, some of which will be discussed here.

4.1. Autotaxin and malignancies

Before being identified as a phospholipase that catalyzes the production of LPA, ATX was originally reported as a substance present in the supernatant of melanoma cells that induces their migration (28). Serum ATX levels have been reported to be elevated in patients with various malignancies, including hepatocellular carcinoma (29) and follicular lymphoma (25). Serum ATX levels may also be useful in assessing disease progression. For example, in patients with hematological malignancies, ATX levels in cerebrospinal fluid is increased in patients who have malignant cells within the central nervous system (30).

4.2. Autotaxin and liver diseases

Serum ATX levels increases in various liver diseases, such as chronic hepatitis C (31) and non-alcoholic fatty liver disease (32). Serum ATX correlates with the histological staging of liver fibrosis and is approved as a marker for liver fibrosis in Japan (33, 34).

4.3. Autotaxin and cardiovascular diseases

By producing LPA and mediating platelet activation, ATX also plays an important role in atherosclerosis and cardiovascular diseases. For example, ATX is overexpressed in the cardiac tissue of patients with acute myocardial infarction (AMI) and is involved in the induction of inflammation after AMI (35). LPA is also involved in cardiac remodeling following AMI.

4.4. Autotaxin, idiopathic pulmonary fibrosis, and systemic sclerosis

ATX is also implicated in fibrosis, and ATX levels are increased in lungs of patients with idiopathic pulmonary fibrosis (IPF). The ATX-LPA axis may be a potential therapeutic target in IPF, and clinical trials of ziritaxestat, an ATX inhibitor, are being conducted (9, 36). The ATX-LPA axis is also involved in skin fibrosis in systemic sclerosis (37), and a recent clinical trial of ziritaxestat for patients with early diffuse cutaneous systemic sclerosis indicated that inhibition of ATX may improve skin symptoms (38).

4.5. Autotaxin and rheumatoid arthritis

The ATX-LPA axis is also involved in pathogenesis of autoimmune diseases, including rheumatoid arthritis (RA) (15). TNF-α, a key cytokine in the pathogenesis of RA, induces expression of ATX in synovial fibroblasts (39), and LPAR1 and ATX are highly expressed in the synovium of patients with RA (39, 40). The ATX-LPA axis has been reported to contribute to the pathogenesis of RA by inducing infiltration of immune cells to joints and may promote differentiation of Th17 cells in the synovium (15, 40).

5. Autotaxin and systemic lupus erythematosus

ATX is also expressed by cells of the immune system. In the immune system, ATX and LPA exert various effects––regulating the development, function, and migration of various immune cells––and there is growing evidence that ATX may also play a role in the pathogenesis of SLE. In the following section we will discuss the role of ATX in the immune system and in SLE.

5.1. Autotaxin, type I interferons, and plasmacytoid dendritic cells

Production of type I interferons by plasmacytoid dendritic cells (pDCs) plays a central role in the pathogenesis of SLE (41–44). Type I interferons produced by pDCs induce the differentiation of dendritic cells (DCs). It also enhances the ability of DCs to present autoantigens to T cells (44, 45). Type I interferons also promote the maturation of B cells and production of autoantibodies (46–48), and immune complexes further induce the activation of pDCs and production of type I interferons (Figure 1C). Among peripheral blood immune cells, the expression of *ENPP2*, which encodes ATX, is highest in pDCs (49, 50), and several lines of evidence suggest that there is an association between the ATX-LPA axis and production of type I interferons by pDCs in SLE.

First, type I interferons are involved in the production of ATX. The induction of ATX by interferons has been reported in various cell types, including THP-1 cells, human monocyte-derived DCs, and human monocytes. The production of type I interferons upon TLR stimulation plays a critical role in the induction of ATX, and blocking interferons inhibits this process (18).

In addition, the expression of *ENPP2* is increased in pDCs of patients with SLE, especially those with high disease activity (49). However, this is not specific to SLE and is seen in other inflammatory diseases, including COVID-19 infection (50). In single-cell RNA-seq analysis of pDCs, clusters enriched in type I IFN transcripts expressed *ENPP2*, as well as *SLC7A11* and *MYO1E*. *ENPP2* and *SLC7A11* were also expressed in pDCs obtained from kidney biopsies of patients with lupus nephritis. *In vitro* studies suggest that *SLC7A11* induces the expression of *MYO1E* and *ENPP2* during pDC activation and that ATX is necessary for production of IFN-α and TNF. Therefore, ATX may play a critical role in activated pDCs that are directly involved in SLE pathogenesis at the site of inflammation (51). LPA has been reported to modulate the activity of TCF4, a transcription factor essential for pDC development (16).

Other studies have suggested an interaction between the ATX-LPA axis and pDCs in SLE. In our recent weighted gene co-expression network analysis (52) of transcriptome data of pDCs from patients with SLE, *ENPP2* belonged to a module (a group of genes with high correlation in expression patterns) enriched in genes involved with interferon signaling (49). Furthermore, this module included genes whose expression are influenced by single-nucleotide

polymorphisms (SNP) associated with SLE in genome-wide association studies. For example, this module included *RASGRP3*, whose expression is increased in pDCs of patients with the SLE risk allele at rs13425999. Although it is not clear whether there is a direct causal relationship between the expression of those genes with ATX, it suggests that ATX may be involved in the connection between genetic risk factors of SLE and disease pathogenesis (49).

Furthermore, among patients with SLE, rs10980684, an intron SNP located in the *LPAR1* gene, is associated with anti-Ro and anti-Sm antibody positivity, which are known to be associated with high serum levels of interferon α. Among patients with anti-Ro and anti-Sm antibody positivity, the T allele at rs10980684 was associated with high serum levels of interferon α (53).

Together, these studies suggest that there is an association of the ATX-LPA axis in pDCs with type I interferons and that genetic factors of SLE play a possible role in this process.

5.2. Autotaxin and other myeloid cells

Other DC subsets and macrophages are also involved in the pathogenesis of SLE (44, 54), and the ATX-LPA axis is also critical in the regulation of those cells. For example, expression of ATX in macrophages increases upon activation in both humans and mice. LPA has been reported to increase the production of proinflammatory cytokines, such as TNF. LPA enhances the ability of human macrophages to stimulate T cells (55), and knockdown of ATX expression in mouse macrophages impairs their migratory capacity and ability to activate T cells (56). It has also been reported that LPA modulates the differentiation of monocyte-derived DCs (57). The altered expression of ATX, and thus LPA, in SLE may contribute to the altered function of macrophages and DCs.

5.3. Autotaxin and lymphocytes

In lymph nodes, high endothelial venules express ATX at high levels (58). Activated T cells express receptors for ATX, and transendothelial migration of T cells is enhanced by the LPA produced by ATX on high endothelial venules (58, 59). Consistent with this, LPAR2-deficient CD4+ cells exhibit a defect in early intranodal migration (60). In lymph nodes, ATX is also expressed by stromal cells, and the ATX-LPA axis, along with other chemokines, is also involved in the regulation of T cell migration in the paracortex (61). In addition to its role in the migration of lymphocytes, the ATX-LPA axis has been reported to play a role in the formation of immune synapses in CD8+ cells (62).

The ATX-LPA axis is also important for B cells. Some *in vivo* studies suggest that B cells may also be involved in production of ATX during inflammation (63). Furthermore, *via* signaling through LPAR5, LPA has been reported to inhibit B cell receptor signaling (64).

Various abnormalities involving the ATX-LPA axis have been reported in lymphocytes of patients with SLE (65). *LPAR3* has been reported to be upregulated in CD4+ and CD8+ T cells of patients with SLE (66). In addition, in a transcriptome analysis of B cells from patients with SLE and healthy controls, differentially expressed genes were enriched in "chemotaxis and lysophosphatidic acid signaling *via* GPCRs" (67).

5.4. Autotaxin–lysophosphatidic acid axis in other organ systems

Cardiovascular diseases are a major cause of mortality among patients with SLE in many cohorts (68, 69). Steroids used for the treatment of SLE promotes progression of atherosclerosis. SLE is often associated with anti-phospholipid syndrome that is characterized by the presence of anti-phospholipid antibodies and thrombosis (70). Consistent with the role of ATX in the activation of platelets, the proportion of ATX+ platelets were reported to be higher in patients with SLE, especially those with a history of thrombosis, compared with that in healthy controls (71). Thus, ATX might be useful as a marker for thrombosis in SLE.

The ATX-LPA axis is also involved in neuropathic pain (72, 73). Among patients with SLE, pain is often a significant burden, even among those whose disease activity is not high (74, 75). It may be possible that ATX is involved in pain in SLE.

6. Autotaxin as a biomarker for systemic lupus erythematosus

Reflecting the potential role of the ATX-LPA axis in SLE pathogenesis, various studies have addressed the potential role of ATX as a biological marker in SLE (Table 1).

6.1. Autotaxin in serum of patients with systemic lupus erythematosus

Consistent with the increase in *ENPP2* mRNA expression levels observed in patients with SLE, the concentration of ATX in the serum is increased in patients with active, untreated SLE compared with that in healthy controls (49). It has also been reported that ATX levels are increased in the serum of patients with lupus nephritis compared with those in patients with other glomerulonephritis, such as diabetic nephropathy and membranous nephropathy (27). The level of ATX in the serum inversely correlates with the dosage of steroids in patients with lupus nephritis (27), and ATX serum levels may decrease upon treatment with steroids (26). Therefore, the effect of treatment must be considered based on ATX serum levels.

6.2. Autotaxin in urine of patients with systemic lupus erythematosus

The concentration of ATX in urine shows correlation with various parameters associated with kidney injury, such as the concentration of proteins, N-acetyl-β-D-glucosaminidase, and α1-microglobulin in the urine (76). Urinary ATX/Cre concentrations were higher in patients with lupus nephritis compared to those in controls (76). The concentration of urinary ATX is also increased in patients with membranous nephropathy (76) and active sarcoidosis (77). Therefore, although it may not be disease specific, urinary ATX levels may serve as a potential marker for lupus nephritis.

TABLE 1 Studies assessing autotaxin or *ENPP2* in clinical samples from patients with systemic lupus erythematosus.

	Sample	Results	References
1	Serum ATX concentrations	The concentration of ATX was higher in patients with untreated SLE compared to that of HC in both females and males.	(49)
2	mRNA expression level of *ENPP2* in immune cells	*ENPP2* expression was higher in pDCs of patients with SLE compared to that in HC.	(49)
3	Serum ATX concentrations	ATX levels were higher in patients with lupus nephritis compared to those with other glomerulonephritis, such as diabetic nephropathy.	(27)
4	Urinary ATX/Cre concentrations	Urinary ATX/Cre concentrations were higher in patients with lupus nephritis compared to those with HC.	(76)

ATX, autotaxin; HC, healthy controls; pDCs, plasmacytoid dendritic cells; SLE, systemic lupus erythematosus.

7. Discussion

SLE is a heterogenous disease, and to provide better care for patients with SLE, there is an eminent for biological markers to assess the pattern and extent of organ involvement and to predict treatment response. The ATX-LPA axis is involved in various biological processes, including immune responses. Recent evidence suggests that the ATX-LPA axis is associated with the abnormal production of type I interferons in pDCs that characterizes SLE (49, 51); thus, the ATX-LPA axis may play a critical role in SLE pathogenesis, and ATX may serve as a potential biomarker.

In the immune system, expression of ATX is high in pDCs and induced by type I interferons (18). ATX may be a marker of activated pDCs that are involved in the pathology of SLE, and in addition to acting as a marker for activated pDCs, ATX may directly be involved in the activation of pDCs (51). Reflecting this, expression of *ENPP2* is high in pDCs of patients with SLE, especially those with high disease activity (49), and ATX concentrations increase in the serum of patients with untreated SLE (49) and lupus nephritis (27). The concentration of ATX is also increased in the urine of patients with lupus nephritis (76). Although the ATX concentration increases observed in serum and urine are not specific to SLE, it may be possible that ATX serves as a useful marker for assessing disease activity and the pattern of organ involvement. Furthermore, biologic therapies that directly inhibit type I interferon signaling, such as anifrolumab, have recently become available for the treatment of SLE (78), and novel markers to identify patients who could benefit the most from those therapies need to be identified (79). ATX may serve as a useful marker in this aspect, as it can be measured with a commercial automated immunoassay analyzer (80), which may be more convenient than measuring the expression of interferon-associated genes with quantitative polymerase chain reaction as performed in some clinical studies (78). More studies are needed to assess the potential role of ATX in predicting treatment response.

In conclusion, the ATX-LPA axis plays a critical role in the pathogenesis of SLE and is associated with the production of interferons by pDCs. ATX may serve as a potential marker for assessing disease activity, the pattern of organ involvement, and predicting treatment responses. Thus, further investigation of the role of ATX in these aspects are warranted.

Author contributions

YT, HS, TS, and KF contributed to the literature review and drafting of the manuscript. All authors contributed to the article and approved the submitted version.

Conflict of interest

The authors declare that the research was conducted in the absence of any commercial or financial relationships that could be construed as a potential conflict of interest.

Publisher's note

References

1. Gladman DD, Ibañez D, Urowitz MB. Systemic lupus erythematosus disease activity index 2000. *J Rheumatol.* (2002) 29:288–91.

2. Choi MY, FitzPatrick RD, Buhler K, Mahler M, Fritzler MJ. A review and meta-analysis of anti-ribosomal P autoantibodies in systemic lupus erythematosus. *Autoimmun Rev.* (2020) 19:102463. doi: 10.1016/j.autrev.2020.102463

3. Arriens C, Wren JD, Munroe ME, Mohan C. Systemic lupus erythematosus biomarkers: the challenging quest. *Rheumatology.* (2017) 56:i32–45. doi: 10.1093/rheumatology/kew407

4. Gupta R, Yadav A, Aggarwal A. Longitudinal assessment of monocyte chemoattractant protein-1 in lupus nephritis as a biomarker of disease activity. *Clin Rheumatol.* (2016) 35:2707–14. doi: 10.1007/s10067-016-3404-9

5. Lan L, Han F, Lang X, Chen J. Monocyte chemotactic Protein-1, Fractalkine, and receptor for advanced glycation end products in different pathological types of lupus nephritis and their value in different treatment prognoses. *PLoS One.* (2016) 11:e0159964. doi: 10.1371/journal.pone.0159964

6. Brunner HI, Bennett MR, Mina R, Suzuki M, Petri M, Kiani AN, et al. Association of noninvasively measured renal protein biomarkers with histologic features of lupus nephritis. *Arthritis Rheum.* (2012) 64:2687–97. doi: 10.1002/art.34426

7. Ytterberg SR, Schnitzer TJ. Serum interferon levels in patients with systemic lupus erythematosus. *Arthritis Rheum.* (1982) 25:401–6. doi: 10.1002/art.1780250407

8. Hooks JJ, Moutsopoulos HM, Geis SA, Stahl NI, Decker JL, Notkins AL. Immune interferon in the circulation of patients with autoimmune disease. *N Engl J Med.* (1979) 301:5–8. doi: 10.1056/NEJM197907053010102

9. Maher TM, Kreuter M, Lederer DJ, Brown KK, Wuyts W, Verbruggen N, et al. Rationale, design and objectives of two phase III, randomised, placebo-controlled studies of GLPG1690, a novel autotaxin inhibitor, in idiopathic pulmonary fibrosis

(ISABELA 1 and 2). *BMJ Open Respir Res*. (2019) 6:e000422. doi: 10.1136/bmjresp-2019-000422

10. Tang X, Wuest M, Benesch MGK, Dufour J, Zhao Y, Curtis JM, et al. Inhibition of Autotaxin with GLPG1690 increases the efficacy of radiotherapy and chemotherapy in a mouse model of breast cancer. *Mol Cancer Ther*. (2020) 19:63–74. doi: 10.1158/1535-7163.MCT-19-0386

11. Iwaki Y, Ohhata A, Nakatani S, Hisaichi K, Okabe Y, Hiramatsu A, et al. ONO-8430506: a novel Autotaxin inhibitor that enhances the antitumor effect of paclitaxel in a breast cancer model. *ACS Med Chem Lett*. (2020) 11:1335–41. doi: 10.1021/acsmedchemlett.0c00200

12. Tan ST, Ramesh T, Toh XR, Nguyen LN. Emerging roles of lysophospholipids in health and disease. *Prog Lipid Res*. (2020) 80:101068. doi: 10.1016/j.plipres.2020.101068

13. Zhang X, Li M, Yin N, Zhang J. The expression regulation and biological function of Autotaxin. *Cells*. (2021) 10:939. doi: 10.3390/cells10040939

14. Dusaulcy R, Rancoule C, Grès S, Wanecq E, Colom A, Guigné C, et al. Adipose-specific disruption of autotaxin enhances nutritional fattening and reduces plasma lysophosphatidic acid. *J Lipid Res*. (2011) 52:1247–55. doi: 10.1194/jlr.M014985

15. Magkrioti C, Galaris A, Kanellopoulou P, Stylianaki EA, Kaffe E, Aidinis V. Autotaxin and chronic inflammatory diseases. *J Autoimmun*. (2019) 104:102327. doi: 10.1016/j.jaut.2019.102327

16. Ntatsoulis K, Karampitsakos T, Tsitoura E, Stylianaki EA, Matralis AN, Tzouvelekis A, et al. Commonalities between ARDS, pulmonary fibrosis and COVID-19: the potential of Autotaxin as a therapeutic target. *Front Immunol*. (2021) 12:687397. doi: 10.3389/fimmu.2021.687397

17. Fulkerson Z, Wu T, Sunkara M, Kooi CV, Morris AJ, Smyth SS. Binding of autotaxin to integrins localizes lysophosphatidic acid production to platelets and mammalian cells. *J Biol Chem*. (2011) 286:34654–63. doi: 10.1074/jbc.M111.276725

18. Song J, Guan M, Zhao Z, Zhang J. Type I interferons function as autocrine and paracrine factors to induce Autotaxin in response to TLR activation. *PLoS One*. (2015) 10:e0136629. doi: 10.1371/journal.pone.0136629

19. Kano K, Matsumoto H, Kono N, Kurano M, Yatomi Y, Aoki J. Suppressing postcollection lysophosphatidic acid metabolism improves the precision of plasma LPA quantification. *J Lipid Res*. (2021) 62:100029. doi: 10.1016/j.jlr.2021.100029

20. Nakamura K, Kishimoto T, Ohkawa R, Okubo S, Tozuka M, Yokota H, et al. Suppression of lysophosphatidic acid and lysophosphatidylcholine formation in the plasma in vitro: proposal of a plasma sample preparation method for laboratory testing of these lipids. *Anal Biochem*. (2007) 367:20–7. doi: 10.1016/j.ab.2007.05.004

21. Xu Y, Shen Z, Wiper DW, Wu M, Morton RE, Elson P, et al. Lysophosphatidic acid as a potential biomarker for ovarian and other gynecologic cancers. *JAMA*. (1998) 280:719–23. doi: 10.1001/jama.280.8.719

22. Hosogaya S, Yatomi Y, Nakamura K, Ohkawa R, Okubo S, Yokota H, et al. Measurement of plasma lysophosphatidic acid concentration in healthy subjects: strong correlation with lysophospholipase D activity. *Ann Clin Biochem*. (2008) 45:364–8. doi: 10.1258/acb.2008.007242

23. Watanabe N, Ikeda H, Nakamura K, Ohkawa R, Kume Y, Aoki J, et al. Both plasma lysophosphatidic acid and serum autotaxin levels are increased in chronic hepatitis C. *J Clin Gastroenterol*. (2007) 41:616–23. doi: 10.1097/01.mcg.0000225642.90898.0e

24. Masuda A, Nakamura K, Izutsu K, Igarashi K, Ohkawa R, Jona M, et al. Serum autotaxin measurement in haematological malignancies: a promising marker for follicular lymphoma. *Br J Haematol*. (2008) 143:60–70. doi: 10.1111/j.1365-2141.2008.07325.x

25. Masuda A, Fujii T, Iwasawa Y, Nakamura K, Ohkawa R, Igarashi K, et al. Serum autotaxin measurements in pregnant women: application for the differentiation of normal pregnancy and pregnancy-induced hypertension. *Clin Chim Acta*. (2011) 412:1944–50. doi: 10.1016/j.cca.2011.06.039

26. Sumida H, Nakamura K, Yanagida K, Ohkawa R, Asano Y, Kadono T, et al. Decrease in circulating autotaxin by oral administration of prednisolone. *Clin Chim Acta*. (2013) 415:74–80. doi: 10.1016/j.cca.2012.10.003

27. Iwata Y, Kitajima S, Yamahana J, Shimomura S, Yoneda-Nakagawa S, Sakai N, et al. Higher serum levels of autotaxin and phosphatidylserine-specific phospholipase a (1) in patients with lupus nephritis. *Int J Rheum Dis*. (2021) 24:231–9. doi: 10.1111/1756-185X.14031

28. Stracke ML, Krutzsch HC, Unsworth EJ, Arestad A, Cioce V, Schiffmann E, et al. Identification, purification, and partial sequence analysis of autotaxin, a novel motility-stimulating protein. *J Biol Chem*. (1992) 267:2524–9. doi: 10.1016/S0021-9258(18)45911-X

29. She S, Zhang Q, Shi J, Yang F, Dai K. Roles of Autotaxin/Autotaxin-lysophosphatidic acid Axis in the initiation and progression of liver cancer. *Front Oncol*. (2022) 12:922945. doi: 10.3389/fonc.2022.922945

30. Shimura T, Kurano M, Morita Y, Yoshikawa N, Nishikawa M, Igarashi K, et al. Autotaxin and soluble IL-2 receptor concentrations in cerebrospinal fluids are useful for the diagnosis of central nervous system invasion caused by haematological malignancies. *Ann Clin Biochem*. (2019) 56:240–6. doi: 10.1177/0004563218818197

31. Takemura K, Takizawa E, Tamori A, Nakamae M, Kubota H, Uchida-Kobayashi S, et al. Association of serum autotaxin levels with liver fibrosis in patients pretreatment and posttreatment with chronic hepatitis C. *J Gastroenterol Hepatol*. (2021) 36:217–24. doi: 10.1111/jgh.15114

32. Fujimori N, Umemura T, Kimura T, Tanaka N, Sugiura A, Yamazaki T, et al. Serum autotaxin levels are correlated with hepatic fibrosis and ballooning in patients with non-alcoholic fatty liver disease. *World J Gastroenterol*. (2018) 24:1239–49. doi: 10.3748/wjg.v24.i11.1239

33. Ikeda H, Kobayashi M, Kumada H, Enooku K, Koike K, Kurano M, et al. Performance of autotaxin as a serum marker for liver fibrosis. *Ann Clin Biochem*. (2018) 55:469–77. doi: 10.1177/0004563217741509

34. Ikeda H, Yatomi Y. Autotaxin in liver fibrosis. *Clin Chim Acta*. (2012) 413:1817–21. doi: 10.1016/j.cca.2012.07.014

35. Tripathi H, Al-Darraji A, Abo-Aly M, Peng H, Shokri E, Chelvarajan L, et al. Autotaxin inhibition reduces cardiac inflammation and mitigates adverse cardiac remodeling after myocardial infarction. *J Mol Cell Cardiol*. (2020) 149:95–114. doi: 10.1016/j.yjmcc.2020.09.011

36. Maher TM, van der Aar EM, Van de Steen O, Allamassey L, Desrivot J, Dupont S, et al. Safety, tolerability, pharmacokinetics, and pharmacodynamics of GLPG1690, a novel autotaxin inhibitor, to treat idiopathic pulmonary fibrosis (FLORA): a phase 2a randomised placebo-controlled trial. *Lancet Respir Med*. (2018) 6:627–35. doi: 10.1016/S2213-2600(18)30181-4

37. Castelino FV, Bain G, Pace VA, Black KE, George L, Probst CK, et al. An Autotaxin/lysophosphatidic acid/Interleukin-6 amplification loop drives scleroderma fibrosis. *Arthritis Rheumatol*. (2016) 68:2964–74. doi: 10.1002/art.39797

38. Khanna D, Denton CP, Furst DE, Mayes MD, Matucci-Cerinic M, Smith V, et al. A 24-week, phase IIa, randomized, double-blind, placebo-controlled study of Ziritaxestat in early diffuse cutaneous systemic sclerosis (NOVESA). *Arthritis Rheumatol*. (2023) inpress. doi: 10.1002/art.42477

39. Nikitopoulou I, Oikonomou N, Karouzakis E, Sevastou I, Nikolaidou-Katsaridou N, Zhao Z, et al. Autotaxin expression from synovial fibroblasts is essential for the pathogenesis of modeled arthritis. *J Exp Med*. (2012) 209:925–33. doi: 10.1084/jem.20112012

40. Miyabe Y, Miyabe C, Iwai Y, Takayasu A, Fukuda S, Yokoyama W, et al. Necessity of lysophosphatidic acid receptor 1 for development of arthritis. *Arthritis Rheum*. (2013) 65:2037–47. doi: 10.1002/art.37991

41. Huang X, Dorta-Estremera S, Yao Y, Shen N, Cao W. Predominant role of Plasmacytoid dendritic cells in stimulating systemic autoimmunity. *Front Immunol*. (2015) 6:526. doi: 10.3389/fimmu.2015.00526

42. Lövgren T, Eloranta ML, Båve U, Alm GV, Rönnblom L. Induction of interferon-alpha production in plasmacytoid dendritic cells by immune complexes containing nucleic acid released by necrotic or late apoptotic cells and lupus IgG. *Arthritis Rheum*. (2004) 50:1861–72. doi: 10.1002/art.20254

43. Psarras A, Wittmann M, Vital EM. Emerging concepts of type I interferons in SLE pathogenesis and therapy. *Nat Rev Rheumatol*. (2022) 18:575–90. doi: 10.1038/s41584-022-00826-z

44. Liu J, Zhang X, Cao X. Dendritic cells in systemic lupus erythematosus: from pathogenesis to therapeutic applications. *J Autoimmun*. (2022) 132:102856. doi: 10.1016/j.jaut.2022.102856

45. Blanco P, Palucka AK, Gill M, Pascual V, Banchereau J. Induction of dendritic cell differentiation by IFN-alpha in systemic lupus erythematosus. *Science*. (2001) 294:1540–3. doi: 10.1126/science.1064890

46. Jego G, Palucka AK, Blanck JP, Chalouni C, Pascual V, Banchereau J. Plasmacytoid dendritic cells induce plasma cell differentiation through type I interferon and interleukin 6. *Immunity*. (2003) 19:225–34. doi: 10.1016/S1074-7613(03)00208-5

47. Poeck H, Wagner M, Battiany J, Rothenfusser S, Wellisch D, Hornung V, et al. Plasmacytoid dendritic cells, antigen, and CpG-C license human B cells for plasma cell differentiation and immunoglobulin production in the absence of T-cell help. *Blood*. (2004) 103:3058–64. doi: 10.1182/blood-2003-08-2972

48. Soni C, Perez OA, Voss WN, Pucella JN, Serpas L, Mehl J, et al. Plasmacytoid dendritic cells and type I interferon promote Extrafollicular B cell responses to extracellular self-DNA. *Immunity*. (2020) 52:1022–38.e7. doi: 10.1016/j.immuni.2020.04.015

49. Tsuchida Y, Shoda H, Nakano M, Ota M, Okamura T, Yamamoto K, et al. Autotaxin is a potential link between genetic risk factors and immunological disturbances of plasmacytoid dendritic cells in systematic lupus erythematosus. *Lupus*. (2022) 31:1578–85. doi: 10.1177/09612033221128494

50. Nikitopoulou I, Fanidis D, Ntatsoulis K, Moulos P, Mpekoulis G, Evangelidou M, et al. Increased Autotaxin levels in severe COVID-19, correlating with IL-6 levels, endothelial dysfunction biomarkers, and impaired functions of dendritic cells. *Int J Mol Sci*. (2021) 22:10006. doi: 10.3390/ijms221810006

51. Grzes KM, Sanin DE, Kabat AM, Stanczak MA, Edwards-Hicks J, Matsushita M, et al. Plasmacytoid dendritic cell activation is dependent on coordinated expression of distinct amino acid transporters. *Immunity*. (2021) 54:2514–30.e7. doi: 10.1016/j.immuni.2021.10.009

52. Langfelder P, Horvath S. WGCNA: an R package for weighted correlation network analysis. *BMC Bioinformatics*. (2008) 9:559. doi: 10.1186/1471-2105-9-559

53. Kariuki SN, Franek BS, Kumar AA, Arrington J, Mikolaitis RA, Utset TO, et al. Trait-stratified genome-wide association study identifies novel and diverse genetic associations with serologic and cytokine phenotypes in systemic lupus erythematosus. *Arthritis Res Ther*. (2010) 12:R151. doi: 10.1186/ar3101

54. Kwant LE, Vegting Y, Tsang ASMWP, Kwakernaak AJ, Vogt L, Voskuyl AE, et al. Macrophages in lupus nephritis: exploring a potential new therapeutic avenue. *Autoimmun Rev*. (2022) 21:103211. doi: 10.1016/j.autrev.2022.103211

55. Panther E, Idzko M, Corinti S, Ferrari D, Herouy Y, Mockenhaupt M, et al. The influence of lysophosphatidic acid on the functions of human dendritic cells. *J Immunol*. (2002) 169:4129–35. doi: 10.4049/jimmunol.169.8.4129

56. Lee JH, Choi SY, Park SY, Jung NC, Noh KE, Nam JH, et al. Enpp2 expression by dendritic cells is a key regulator in migration. *Biomedicine*. (2021) 9:1727 doi: 10.3390/biomedicines9111727

57. Chen R, Roman J, Guo J, West E, McDyer J, Williams MA, et al. Lysophosphatidic acid modulates the activation of human monocyte-derived dendritic cells. *Stem Cells Dev*. (2006) 15:797–804. doi: 10.1089/scd.2006.15.797

58. Kanda H, Newton R, Klein R, Morita Y, Gunn MD, Rosen SD. Autotaxin, an ectoenzyme that produces lysophosphatidic acid, promotes the entry of lymphocytes into secondary lymphoid organs. *Nat Immunol*. (2008) 9:415–23. doi: 10.1038/ni1573

59. Zhang Y, Chen YC, Krummel MF, Rosen SD. Autotaxin through lysophosphatidic acid stimulates polarization, motility, and transendothelial migration of naive T cells. *J Immunol*. (2012) 189:3914–24. doi: 10.4049/jimmunol.1201604

60. Knowlden SA, Capece T, Popovic M, Chapman TJ, Rezaee F, Kim M, et al. Regulation of T cell motility in vitro and in vivo by LPA and LPA2. *PLoS One*. (2014) 9:e101655. doi: 10.1371/journal.pone.0101655

61. Katakai T, Kondo N, Ueda Y, Kinashi T. Autotaxin produced by stromal cells promotes LFA-1-independent and rho-dependent interstitial T cell motility in the lymph node paracortex. *J Immunol*. (2014) 193:617–26. doi: 10.4049/jimmunol.1400565

62. Kremer KN, Buser A, Thumkeo D, Narumiya S, Jacobelli J, Pelanda R, et al. LPA suppresses T cell function by altering the cytoskeleton and disrupting immune synapse formation. *Proc Natl Acad Sci U S A*. (2022) 119:e2118816119. doi: 10.1073/pnas.2118816119

63. Lin S, Haque A, Raeman R, Guo L, He P, Denning TL, et al. Autotaxin determines colitis severity in mice and is secreted by B cells in the colon. *FASEB J*. (2019) 33:3623–35. doi: 10.1096/fj.201801415RR

64. Hu J, Oda SK, Shotts K, Donovan EE, Strauch P, Pujanauski LM, et al. Lysophosphatidic acid receptor 5 inhibits B cell antigen receptor signaling and antibody response. *J Immunol*. (2014) 193:85–95. doi: 10.4049/jimmunol.1300429

65. Li H, Boulougoura A, Endo Y, Tsokos GC. Abnormalities of T cells in systemic lupus erythematosus: new insights in pathogenesis and therapeutic strategies. *J Autoimmun*. (2022) 132:102870. doi: 10.1016/j.jaut.2022.102870

66. Olferiev M, Jacek E, Kirou KA, Crow MK. Novel molecular signatures in mononuclear cell populations from patients with systemic lupus erythematosus. *Clin Immunol*. (2016) 172:34–43. doi: 10.1016/j.clim.2016.08.018

67. Udhaya Kumar S, Thirumal Kumar D, Siva R, George Priya Doss C, Younes S, Younes N, et al. Dysregulation of signaling pathways due to differentially expressed genes from the B-cell transcriptomes of systemic lupus erythematosus patients—a bioinformatics approach. *Front Bioeng Biotechnol*. (2020) 8:276. doi: 10.3389/fbioe.2020.00276

68. Yurkovich M, Vostretsova K, Chen W, Aviña-Zubieta JA. Overall and cause-specific mortality in patients with systemic lupus erythematosus: a meta-analysis of observational studies. *Arthritis Care Res*. (2014) 66:608–16. doi: 10.1002/acr.22173

69. Lee YH, Choi SJ, Ji JD, Song GG. Overall and cause-specific mortality in systemic lupus erythematosus: an updated meta-analysis. *Lupus*. (2016) 25:727–34. doi: 10.1177/0961203315627202

70. Tektonidou MG, Andreoli L, Limper M, Amoura Z, Cervera R, Costedoat-Chalumeau N, et al. EULAR recommendations for the management of antiphospholipid syndrome in adults. *Ann Rheum Dis*. (2019) 78:1296–304. doi: 10.1136/annrheumdis-2019-215213

71. Hasse S, Julien AS, Duchez AC, Zhao C, Boilard E, Fortin PR, et al. Red blood cell-derived phosphatidylserine positive extracellular vesicles are associated with past thrombotic events in patients with systemic erythematous lupus. *Lupus Sci Med*. (2022) 9:e000605. doi: 10.1136/lupus-2021-000605

72. Kuwajima K, Sumitani M, Kurano M, Kano K, Nishikawa M, Uranbileg B, et al. Lysophosphatidic acid is associated with neuropathic pain intensity in humans: an exploratory study. *PLoS One*. (2018) 13:e0207310. doi: 10.1371/journal.pone.0207310

73. Uranbileg B, Ito N, Kurano M, Kano K, Uchida K, Sumitani M, et al. Inhibition of autotaxin activity ameliorates neuropathic pain derived from lumbar spinal canal stenosis. *Sci Rep*. (2021) 11:3984. doi: 10.1038/s41598-021-83569-3

74. Nichilatti LP, Fernandes JM, Marques CP. Physiopathology of pain in systemic erythematosus lupus. *Lupus*. (2020) 29:721–6. doi: 10.1177/0961203320919872

75. Cornet A, Andersen J, Myllys K, Edwards A, Arnaud L. Living with systemic lupus erythematosus in 2020: a European patient survey. *Lupus Sci Med*. (2021) 8:e000469. doi: 10.1136/lupus-2020-000469

76. Morita Y, Kurano M, Morita E, Shimamoto S, Igarashi K, Sawabe M, et al. Urinary autotaxin concentrations are associated with kidney injury. *Clin Chim Acta*. (2020) 509:156–65. doi: 10.1016/j.cca.2020.06.019

77. Murakami K, Tamada T, Saigusa D, Miyauchi E, Nara M, Ichinose M, et al. Urine autotaxin levels reflect the disease activity of sarcoidosis. *Sci Rep*. (2022) 12:4372. doi: 10.1038/s41598-022-08388-6

78. Morand EF, Furie R, Tanaka Y, Bruce IN, Askanase AD, Richez C, et al. Trial of Anifrolumab in active systemic lupus erythematosus. *N Engl J Med*. (2020) 382:211–21. doi: 10.1056/NEJMoa1912196

79. Vital EM, Merrill JT, Morand EF, Furie RA, Bruce IN, Tanaka Y, et al. Anifrolumab efficacy and safety by type I interferon gene signature and clinical subgroups in patients with SLE: post hoc analysis of pooled data from two phase III trials. *Ann Rheum Dis*. (2022) 81:951–61. doi: 10.1136/annrheumdis-2021-221425

80. Nakamura K, Igarashi K, Ide K, Ohkawa R, Okubo S, Yokota H, et al. Validation of an autotaxin enzyme immunoassay in human serum samples and its application to hypoalbuminemia differentiation. *Clin Chim Acta*. (2008) 388:51–8. doi: 10.1016/j.cca.2007.10.005

frontiers | Frontiers in Medicine

TYPE Original Research
PUBLISHED 06 April 2023
DOI 10.3389/fmed.2023.1161837

OPEN ACCESS

EDITED BY
Miao Pan,
Children's National Hospital,
United States

REVIEWED BY
Xiang Dong Jian,
Qilu Hospital,
Shandong University,
China
Savas Yayli,
Koç University,
Türkiye
Giovanni Damiani,
University of Milan,
Italy

*CORRESPONDENCE
Xue-ming Yao
✉ yxming19@foxmail.com

SPECIALTY SECTION
This article was submitted to Rheumatology, a section of the journal Frontiers in Medicine

RECEIVED 08 February 2023
ACCEPTED 20 March 2023
PUBLISHED 06 April 2023

CITATION
Luo F, Yuan X-M, Xiong H, Yang Y-Z, Chen C-M, Ma W-K and Yao X-M (2023) Clinical features of acute generalized exanthematous pustulosis caused by hydroxychloroquine in rheumatology patients and exploration of *CARD14* gene mutations. *Front. Med.* 10:1161837. doi: 10.3389/fmed.2023.1161837

Clinical features of acute generalized exanthematous pustulosis caused by hydroxychloroquine in rheumatology patients and exploration of *CARD14* gene mutations

Feng Luo[1], Xue-mei Yuan[1], Hong Xiong[1], Yu-zheng Yang[1], Chang-ming Chen[2], Wu-kai Ma[1,2] and Xue-ming Yao[1,2]*

[1]Graduate School, Guizhou University of Traditional Chinese Medicine, Guiyang, China, [2]Department of Rheumatology and Immunology, Second Affiliated Hospital of Guizhou University of Chinese Medicine, Guiyang, China

Introduction: Acute generalized exanthematous pustulosis (AGEP) is a rare condition characterized by superficial pustules following drug ingestion or infection. Currently, there is no clear link between rheumatism and AGEP. It has been described that hydroxychloroquine (HCQ) is a rare cause of acute generalized epidermal necrolysis (AGEP). Presently, there are limited studies on HCQ-induced AGEP. We aimed to explore the clinical features and associated gene expression of AGEP induced after HCQ treatment exposure in rheumatology patients.

Methods: We assessed patients with HCQ-induced AGEP diagnosed at the Second Affiliated Hospital of Guizhou University of Chinese Medicine between January 1, 2017, and May 1, 2022. We also reviewed similar cases reported in specific databases.

Results: The study included five females (mean age, 40.2years), and the mean time from initiation of HCQ treatment to symptom onset was 12.2 d. All patients received steroids and allergy medications after HCQ discontinuation, and the rash completely resolved within an average of 25.2 d. We performed whole exome sequencing and Sanger validation in our patient sample. *CARD14* gene mutations were detected in three patients. Additionally, seven mutation sites were detected.

Discussion: HCQ-induced AGEP may have a longer latency period and regression time than AGEP induced by other drugs. Our patients all experienced *CARD14* gene mutations. AGEP often resolves with topical therapy and drug discontinuation, although some cases require systemic steroid therapy. In the future, patients with rheumatism should pay attention to the effectiveness of HCQ during treatment and be aware of the associated skin toxicity.

KEYWORDS

acute generalized exanthematous pustulosis, hydroxychloroquine, *CARD14*, gene mutation, gene sequencing

1. Introduction

A rheumatic disease is an inflammatory disorder that affects the skin, mucous membranes, bone, joints, and surrounding soft tissues including muscles, synovium, bursa, and tendons (1). The most common symptom of acute generalized exanthematous pustulosis is the presence of numerous non-follicular, sterile pustules on top of an edematous background (2). It is usually accompanied by fever and peripheral blood leukocytosis (3). About 90% of AGEP cases are caused by drugs such as antibiotics, antifungals, diltiazem, and antimalarial agents (4, 5). Approximately 20% of patients with AGEP develop systemic involvement; mostly impaired liver, kidney, lung function and, in severe cases, multiple organ failure, diffuse intravascular coagulation, and death (6, 7). Hydroxychloroquine (HCQ) sulfate regulates immune function and can be used clinically as initial treatment for malaria, rheumatoid arthritis (RA), and systemic lupus erythematosus (SLE) (8, 9). With the widespread use of HCQ, an increasing number of adverse events are being reported in clinical practice, among which AGEP is rare. Owing to its low incidence, we have limited information on AGEP. Previous research has demonstrated that some patients with AGEP carry mutations in the *IL36RN* and *CARD14* genes, suggesting that AGEP may have a genetic basis (10). In addition, there is evidence that AGEP is linked to mutations in the *CARD14* gene, and the predicted p. (Arg430Trp) variant of heterozygous c.1288C c.1288C > T transition (11). We conducted a literature search and found only a few reported cases of Chinese clusters (12, 13). Therefore, the study aimed to describe the clinical and genetic characteristics of Chinese patients with HCQ-induced AGEP.

2. Materials and methods

We observed five patients of HCQ-induced AGEP at the Second Affiliated Hospital of Guizhou University of Chinese Medicine between January 1, 2017, and May 1, 2022. The patients were diagnosed with HCQ-induced AGEP based on EuroSCAR scores validated by (5); five patients scored 5–12 points, indicating a definite or probable diagnosis of AGEP (5). We collected the following information from the medical records of these patients: demographic characteristics, clinical features, onset date, time of symptom resolution, and laboratory test results. In addition, we used next-generation whole exome sequencing to evaluate the mutated gene, and performed Sanger verification on the mutant gene; *IL36RN* and *CARD14* mutation sites were reported. Our gene sequencing experiments were all entrusted to the Beijing Luhe Huada Gene Technology Co., Ltd., Wuhan, China, and the specific process can be found on the company's website.[1] Furthermore, we reviewed similar cases reported in the Wanfang Data, PubMed, Embase, China National Knowledge Infrastructure (CNKI), Web of Science, and other databases from their inception to May 2022. Search terms included "acute generalized exanthematous pustulosis," "AGEP," "HCQ," "hydroxychloroquine," and "side effects." The present study was approved by the Institutional Review Committee of the Second Affiliated Hospital of Guizhou University of Chinese Medicine and conducted in accordance with the Declaration of Helsinki. Throughout the study, all participants provided their informed consent.

3. Results

The average age at diagnosis was 40.2 years (range, 28–63 years) for all five participants. Patient history included two cases of RA, one case of RA with Sjogren's syndrome, and two cases of SLE. None of the five patients had any skin reactions or a personal or family history of psoriasis. The details of each case are presented in Table 1.

Our five cases were accustomed to hospital treatment because of a poor response to the long-term use of disease-modifying antirheumatic drugs (DMARDs), such as methotrexate for rheumatism, and skin allergic reactions caused by adjusting to the use of HCQ. The dosage of HCQ among the five patients was the same: two tablets, administered twice daily at the same time. The average delay in the appearance of a rash in all five cases was 12.2 d after admission (range: 7–25 d). In all patients, the skin eruptions were non-follicular and pinhead-sized, resulting from sudden, acute onset. The rash was initially seen on the cheeks and face in two patients, on a limb joint in one patient, on the scalp in one patient, and on the hands in one patient. In all cases, a rapid spread of the rash throughout the body was observed, with facial involvement (Figures 1A–F). After the rash appeared, all patients immediately stopped HCQ treatment. No patients developed mucosal involvement or lymphatic system disease. Over the course of symptom duration, four patients developed fever and all patients had pruritis.

Laboratory results showed that the percentage of neutrophils increased to 81.3% (normal, 40–75%) in three patients, and the percentage of eosinophils decreased to 0.3% (normal, 0.4–8.0%) in two patients. C-reactive protein levels increased to 11.21 mg/L (the norm, 0–10 mg/L) in one patient, and the erythrocyte sedimentation rate increased to 59 mm/L (normal, 0–20 mm/L) in one patient. Several routine laboratory tests were also performed, including renal and hepatic function and serologic tests to determine influenza, hepatitis B, enteroviruses, and mycoplasmas, which were unremarkable. The bacteriological and mycological findings of pustules were negative.

Skin tissue biopsy showed histopathological changes in the skin, where the epidermis showed mild vacuolar degeneration and varying numbers of neutrophil infiltrates just beneath the surface of the deep dermis—primarily the superficial dermis—as well as cavernous pustules under the epidermis; an example of these changes is presented in Figure 2. We performed whole exome sequencing and Sanger validation on all five patients and identified *CARD14* gene mutations in three patients. Seven mutation sites were detected: c.1641G > C (p.Arg547Ser) heterozygous mutation, c.2422A > G (p.Thr808Ala) heterozygous/homozygous mutation, c.2458C > T (p.Arg820Trp) heterozygous mutation, c.1323C > T (p.Asp441Asp) heterozygous mutation, c.633G > A (p.Glu211Glu) heterozygous mutation, c.1753G > A (p.Val585Ile) heterozygous mutation, and c.2481C > T (p.Pro827Pro) heterozygous mutation (Figure 3). No mutations were identified in the *IL-36RN* gene.

One patient was treated with topical steroids plus antihistamines, three patients received systemic steroids plus antihistamines, and one patient was treated with steroids plus antihistamines, mycophenolate

1 http://www.bgi-write.com

TABLE 1 Clinical characteristics, laboratory abnormalities, and allergological findings.

Age/ sex	Primary disease	Delay to onset of symptoms	Co-medication	Fever	Cutaneous involvement	Neutrophilia	Eosinophilia	Treatment	Resolution	Specific mutation
32/F	SLE	15 d	Low dose steroid/ calcium carbonate and vitamin D3/ pantoprazole sodium enteric-coated (long-term use)	Yes	Initially affecting the limbs, an itching pustular rash with an erythematous base that spread to other parts	No	No	Systemic steroids/ antihistamine/ mycophenolate mofetil/ thalidomide	41 d	No
33/F	RA	7 d	Methotrexate/folic acid (long-term use)	No	Pustules with an erythematous base that started on the scalp and spread throughout the body	No	No	Topical steroid/ antihistamine	15 d	No
63/F	SLE	9 d	Low dose steroid/ calcium carbonate/ pantoprazole sodium enteric-coated	Yes	Itchy pustular rash with an erythematous base, beginning on the face and spreading to the body	Yes	No	Systemic steroids/ antihistamine	19 d	NM_001366385.1(CARD14):c.1641G > C (p.Arg547Ser); NM_001366385.1(CARD14):c.2458C > T (p.Arg820Trp); NM_001366385.1(CARD14):c.2422A > G (p.Thr808Ala); NM_001366385.1(CARD14):c.1323C > T (p.Asp441Asp).
28/F	RA	20 d	Leflunomide (long-term use)	Yes	Itching pustular rash with an erythematous base that started on the hand and spread to other parts	Yes	No	Systemic steroids/ antihistamine	24 d	NM_001366385.1(CARD14):c.2458C > T (p.Arg820Trp); NM_001366385.1(CARD14):c.2422A > G (p.Thr808Ala).
45/F	RA/pSS	25 d	Low dose steroid/ pantoprazole sodium enteric-coated/iguratimod	Yes	Itchy pustular rash with an erythematous base, beginning on the face and spreading to the body	Yes	No	Systemic steroids/ antihistamine	36 d	NM_001366385.1(CARD14):c.1753G > A (p.Val585Ile); NM_001366385.1(CARD14):c.633G > A(p. Glu211Glu); NM_001366385.1(CARD14):c.2481C > T (p.Pro827Pro)

F, female; pSS, primary dryness syndrome; RA, rheumatoid arthritis; SLE, systemic lupus erythematosus.

10.3389/fmed.2023.1161837

FIGURE 1
Rash before and after treatment. **(A)** Rash on the face; **(B)** rash on the hands; **(C)** rash on the legs; **(D)** rash on the back; **(E)** rash on the abdomen; **(F)** rash on the chest; **(G)** improvement in the rash on the legs; and **(H)** improvement in the rash on the back.

mofetil, and thalidomide. All patients achieved good results after treatment, the rash completely resolved within 15–45 d after HCQ discontinuation, and diffuse superficial desquamation was observed during treatment. All patients were followed-up for 6 months to 1 year, without rash recurrence (Figures 1G,H).

From our literature search strategy, 221 relevant articles were retrieved. After screening, 33 valid articles were obtained, including 46 similar cases. Table 2 shows the clinical features of these cases. The cases we reported were similar to those reported in the literature. These similarities concerned the greater proportion of females, average age of onset and mean delay to diagnosis, treatment with topical or systemic steroids, and complete rash resolution within 7–119 d.

4. Discussion

AGEP is an acute-onset non-follicular aseptic impetigo that typically presents with sudden high fever and a rash characterized by a dense distribution of needle tip to soybean-sized pustules based on diffuse flushing, usually without mucosal and general organ damage (29). The incidence of AGEP is approximately 1–5/1,000,000/year. Approximately 90% of patients are on medication prior to disease onset, mainly in the form of antibiotics, with β-lactam medications being the most common (45). In a small number of patients, AGEP is caused by an infection or other factors (46) including other drugs that rheumatological patients may take to fight biologics-related infections, e.g., doxycycline or new anticoagulants (dabigatran) (47, 48). The specific pathogenesis of AGEP remains incompletely understood (49). HCQ has immunosuppressive, anti-inflammatory, and possibly antiviral properties, and common adverse effects include headache, various types of rashes, pruritus, and gastrointestinal dysfunctions, such as nausea, vomiting, and diarrhea (50). Several dermatological side-effects have been associated with the use of HCQ, including dryness, pigmentation, itching, alopecia, urticaria, measles, contact dermatitis, and worsening psoriasis, of which AGEP is one of the more serious but rare types (51). With the wide application of HCQ in clinical practice, HCQ-induced AGEP should be seriously considered.

The incubation time of AGEP is generally 3–30 d, and the median time of occurrence is 15 d after starting drug treatment. The time from

FIGURE 2
Histopathological examination of a skin biopsy from the left chest showed mild vacuolar degeneration of epidermal basal cells, varying numbers of neutrophil infiltrates in the superficial-deep dermis (mainly in the superficial dermis), and epidermal cavernous pustule formation (hematoxylin and eosin staining; original magnification, ×400).

drug exposure to the appearance of a rash depends on the causative drug; primitive mycin and amoxicillin can cause AGEP rash onset 1 d after the first dose, whereas other drugs trigger a reaction only after 1–2 weeks (52). For instance, carbamazepine-induced AGEP may take 5–35 d to manifest symptoms (53); when diltiazem induces AGEP, symptom onset occurs within 1–3 weeks (54). Previous cases of HCQ-induced AGEP ranged from 2 to 30 d between the initiation of HCQ treatment and rash onset (15, 52). Rash onset in the cases we reported ranged from 7 to 25 d, which is similar to results reported in the literature. In addition, studies have found that blood drug levels peak after 5–6 weeks of HCQ trial treatment, which may be the reason for the slow appearance of AGEP symptoms (55). This indicates that HCQ-related AGEP may be associated with its metabolic properties.

In the cases we studied, there were no mutations in the *IL-36RN* gene; however, we identified novel mutations in the *CARD14* gene in three cases at seven mutation sites. Of the three patients, one had SLE, one had RA, and one had RA with Sjogren's syndrome. None of the three patients was in an active disease state, and there were no obvious symptoms of joint pain, swelling, skin allergies, or mouth ulcers. To date, *CARD14* gene mutations have been associated with various diseases that produce widespread pustular rashes, such as generalized pustular psoriasis (GPP), psoriatic arthritis, and pityriasis rosea (10, 56). In addition, mutations in other *CARD* genes are known to cause pustular skin disorders, similar to Burau syndrome (*CARD15*/*NOD2* mutations) (57). Owing to the limited number of reported cases, further research is

TABLE 2 Previous reports on cases of acute generalized exanthematous pustulosis induced by HCQ.

Study	Number of cases	Age/Sex	Primary disease	Delay to onset of symptoms	Treatment	Resolution after HCQ-withdrawal
Di Lernia et al. (14)	1	63/F	RA	30 d	Systemic steroids/ cyclosporine	55 d
Liccioli et al. (15)	1	9/F	Juvenile Sjogren's syndrome	30 d	No treatment	7 d
Di Maso et al. (16)	1	34/F	Undifferentiated connective tissue disease	2 d	Systemic steroids/CPFA	Not reported
Soria et al. (17)	6	48/23/45/F 9/52/M	Erythematous facialdermatitis/ Photosensitivity/SLE/ RA/Cutaneous lupus erythematosus	3–18 d	Not reported	7–18 d
Pearson et al. (18)	1	50/F	RA	14 d	Topical steroid	81 d
İslamoğlu et al. (19)	1	64/F	pSS	20 d	Systemic steroids/ cyclosporine	37 d
Matsuda-Hirose et al. (20)	1	31/F	SLE	15 d	Systemic steroids	119 d
Bailey et al. (21)	1	48/F	SLE	14 d	Systemic steroids	18 d
Assier-Bonnet et al. (22)	1	36/F	Seronegative polyarthritis	12 d	No treatment	13 d
Evans et al. (23)	1	28/F	SLE	15 d	No treatment	21 d
Martins et al. (24)	1	51/F	RA	14 d	Systemic steroids	21 d
Paradisi et al. (25)	3	36/F 70/79 M	RA and pSS/RA/ polymyalgia rheumatica	21/20/20 d	Systemic steroids	8 d/12 d/15 d
Avram et al. (26)	1	79/F	RA	14 d	No treatment	14 d
Park et al. (27)	1	38/F	Dermatomyositis	20 d	Systemic steroids	Not reported
Charfi et al. (28)	1	33/F	SLE	17 d	No treatment	7 d
Zhang et al. (29)	1	60/F	pSS	25 d	Systemic steroids	14 d
Yalcin et al. (30)	1	67/F	Seronegative polyarthritis	15 d	Systemic steroids/ cyclosporine	21 d
Castner et al. (31)	1	56/F	pSS	21 d	Systemic steroids/ cyclosporine	17 d
Duman et al. (32)	1	42/F	RA	20 d	Systemic steroids	35 d
Mohaghegh et al. (33)	1	44/F	Distal joint pain	5 d	Topical steroids	68 d
Chaabouni et al. (34)	7	47 (range: 35–64)/7F	pSS (three cases)/lichen planus (one case)/ recurrent aphthous stomatitis (one case)/ systemic scleroderma (one case)/Melkersson–Rosenthal syndrome (one case)	40 d (range: 15–122 d)	Topical steroids (seven cases)	39 d (range: 15–91 d)
Mofarrah et al. (35)	1	49F	RA	17 d	Topical steroids	7 d
Munshi et al. (36)	1	76 M	Calcium pyrophosphate dihydrate crystal deposition disease	18 d	Ixekizumab	11 d
Otake-Irie et al. (37)	1	61 M	SLE	7 d	Systemic steroids	70 d

(Continued)

TABLE 2 (Continued)

Study	Number of cases	Age/Sex	Primary disease	Delay to onset of symptoms	Treatment	Resolution after HCQ-withdrawal
Enos et al. (38)	1	29F	Stevens-Johnson syndrome	4 d	Systemic steroids	38 d
Mercogliano et al. (39)	1	71/F	RA	14 d	No treatment	13 d
Robustelli et al. (40)	1	70/F	SARS-CoV-2 pneumonia	10 d	Topical steroids	30 d
Litaiem et al. (41)	1	39/F	SARS-CoV-2 pneumonia	18 d	Died of pulmonary embolism	-
Sánchez-Velázquez et al. (42)	1	31/F	COVID-19	9 d	Cyclosporine	40 d
Lateef et al. (43)	1	67/F	SLE	21 d	Systemic steroids	14 d
Coleman et al. (44)	1	68/F	Stevens-Johnson syndrome	20 d	Systemic steroids/ intravenous immunoglobulin	10 d
Liu et al. (13)	1	69/F	pSS/hypertension/ pulmonary fibrosis	20 d	Systemic steroids	16 d
Tian et al. (12)	1	35/F	Undifferentiated connective tissue diseases	10 d	Systemic steroids/ cyclosporine	29 d

COVID-19, coronavirus disease 2019; CPFA, coupled plasma filtration adsorption; F, female; HCQ, hydroxychloroquine; M, male; pSS, primary dryness syndrome; RA, rheumatoid arthritis; SLE, systemic lupus erythematosus.

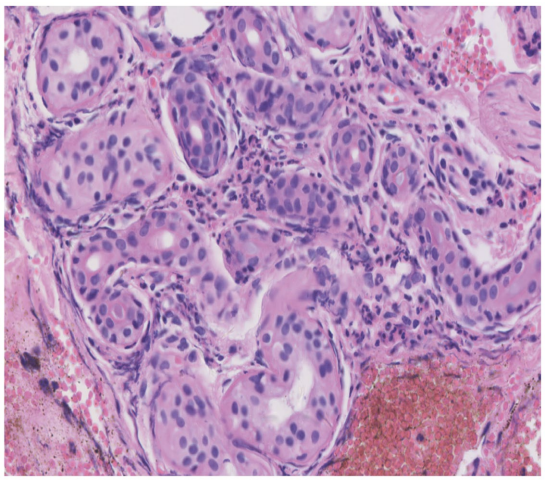

FIGURE 3
Mutation sites detected in the samples.

needed to determine whether *CARD14* mutations form the molecular basis of AGEP.

The typical manifestations of AGEP include tens to hundreds of non-follicular pinhead-sized sterile pustules that appear rapidly as edematous erythema, generally originating on the face or intertriginous areas of the body, and rapidly spreading to the trunk and limbs. Histopathology on sub-corneal pustules located in the superficial layer of the epidermis reveals the presence of immune cells—mainly neutrophils and occasionally eosinophils—and an almost unchanged epidermis below the pustules, showing only infiltrated neutrophils and mild intercellular edema (2). In the five patients we reported, the rash initially appeared on the cheeks and facial area, joints of the extremities, scalp, and hands. Afterward, the rash spread rapidly to other parts of the body. All cases had facial involvement, which is consistent with the clinical presentation of AGEP. HCQ-related AGEP can be clearly distinguished from GPP—which recurs often—and there may be typical psoriasis lesions before the appearance of pustules; these appear on the original plaque or rash and can expand and fuse to form "pus lakes." In addition, some patients with GPP have a family history, and the histopathological manifestations are psoriasis-like hyperplasia of the epidermis with keratosis, Kogoj micro-abscesses in the upper part of the spinous layer, and superficial dermal telangiectasia and tortuous vessels (58). In this sample, there was no family history of psoriasis, the rash appeared after HCQ treatment, and pustule formation was observed on histopathology, which is not the case in patients with GPP. Therefore, patients with suspected HCQ-induced AGEP may benefit from histopathology and skin biopsy.

AGEP is self-limiting and has a short disease course, and lesions generally disappear within 15 d of stopping the causative drug. However, HCQ-induced AGEP is prolonged and recurrent, ranging from 7–81 d (18, 37). As HCQ has a longer half-life, HCQ-associated AGEP lesions may last for longer, i.e., 1–2 months (19). All five patients in our sample were discharged within 15–45 d, similar to the results reported in the literature. The first principles and priorities of AGEP treatment are cessation of exposure to suspected triggers and symptomatic supportive care, avoiding antibiotics as much as possible, except in cases where co-infection is suspected; in such

cases, antibiotics should be cautiously used (59). The use of topical emollients may aid the treatment of mild symptoms, whereas patients with severe symptoms require systemic steroids to relieve itching, inhibit telangiectasia and inflammation, and shorten the course of the disease; for recalcitrant disease, systemic therapy is recommended with dapsone and cyclosporine (60). Our patients received topical or systemic steroids and antihistamines, and the most severely ill patient also received mycophenolate and thalidomide, which rarely present with serious complications and sequelae. The mortality rate of AGEP is less than 5% and is often due to multi-organ dysfunction. Patients at high mortality risk typically have comorbidities or extensive skin lesions with mucosal involvement (4). The condition rarely recurs after treatment, but exposure to the same trigger may lead to recurrence. None of the patients we reported on had any recurrence after a 1–2 year-follow-up period.

Herein, we reported five cases of HCQ-induced AGEP. The need to distinguish HCQ-induced AGEP from GPP is of clinical concern. Compared to AGEP induced by other drugs, the latency and regression time of AGEP caused by HCQ are longer. AGEP often resolves with topical therapy and with drug discontinuation, although systemic steroid therapy may be necessary in some cases. In addition, a new *CARD14* mutation was identified in our study and was validated using Sanger sequencing.

Data availability statement

The original contributions presented in the study are included in the article/supplementary material, further inquiries can be directed to the corresponding author.

Ethics statement

The studies involving human participants were reviewed and approved by Medical Ethics Committee of the Second Affiliated Hospital of Guizhou University of Chinese Medicine. The patients/participants provided their written informed consent to participate in this study.

Author contributions

W-kM and X-mYa: conceptualization. C-mC: methodology. Y-zY: software. W-kM, X-mYa, and FL: validation. HX: formal analysis. X-mYu: investigation. FL: data curation. FL: writing—first draft preparation. W-kM and X-mYa: writing—review and editing. All authors contributed to the article and approved the submitted version.

Funding

The study was funded by the Guizhou Province Science and Technology Plan Project, Grant/Award Number: Oiankehe Platform Talent [2020] 2202, [2016] 5650; Guizhou Province Science and Technology Plan Project, Grant/Award Number: Guizhou Qiankehe Support [2021] General 006.

Acknowledgments

We thank all the researchers and participants who contributed to this study.

Conflict of interest

The authors declare that the research was conducted in the absence of any commercial or financial relationships that could be construed as a potential conflict of interest.

Publisher's note

References

1. Wesemael TV, Huizinga T, Toes R. From Phenotypeto pathophysiology—placing rheumatic diseases in an immunological perspective. *Rheumatol DJTL*. (2022) 4:e166–7. doi: 10.1016/S2665-9913(21)00369-6

2. Hadavand MA, Kaffenberger B, Cartron AM, Trinidad JCL. Clinical presentation and Management of Atypical and Recalcitrant Acute Generalized Exanthematous Pustulosis. *J Am Acad Dermatol*. (2022) 87:632–9. doi: 10.1016/j.jaad.2020.09.024

3. Duong TA, Valeyrie-Allanore L, Wolkenstein P, Chosidow O. Severe cutaneous adverse reactions to drugs. *Lancet (London, England)*. (2017) 390:1996–2011. doi: 10.1016/s0140-6736(16)30378-6

4. Szatkowski J, Schwartz RA. Acute generalized Exanthematous Pustulosis (Agep): a review and update. *J Am Acad Dermatol*. (2015) 73:843–8. doi: 10.1016/j.jaad.2015.07.017

5. Sidoroff A, Dunant A, Viboud C, Halevy S, Bavinck JN, Naldi L, et al. Risk factors for acute generalized Exanthematous Pustulosis (Agep)-results of a multinational case-control study (Euroscar). *Br J Dermatol*. (2007) 157:989–96. doi: 10.1111/j.1365-2133.2007.08156.x

6. Creadore A, Desai S, Alloo A, Dewan AK, Bakhtiar M, Cruz-Diaz C, et al. Clinical characteristics, disease course, and outcomes of patients with acute generalized Exanthematous Pustulosis in the us. *JAMA Dermatol*. (2022) 158:176–83. doi: 10.1001/jamadermatol.2021.5390

7. Hotz C, Valeyrie-Allanore L, Haddad C, Bouvresse S, Ortonne N, Duong TA, et al. Systemic involvement of acute generalized Exanthematous Pustulosis: a retrospective study on 58 patients. *Br J Dermatol*. (2013) 169:1223–32. doi: 10.1111/bjd.12502

8. Schrezenmeier E, Dörner T. Mechanisms of action of Hydroxychloroquine and Chloroquine: implications for rheumatology. *Nat Rev Rheumatol*. (2020) 16:155–66. doi: 10.1038/s41584-020-0372-x

9. Wang M, Cao R, Zhang L, Yang X, Liu J, Xu M, et al. Remdesivir and Chloroquine effectively inhibit the recently emerged novel coronavirus (2019-Ncov) in vitro. *Cell Res*. (2020) 30:269–71. doi: 10.1038/s41422-020-0282-0

10. Podlipnik S, Castellanos-Moreira R, Florez-Enrich H, Arostegui JI, Mascaró JM Jr. Acute generalized Exanthematous Pustulosis and polyarthritis associated with a novel Card14 mutation. *Australas J Dermatol*. (2018) 59:e70–3. doi: 10.1111/ajd.12669

11. Navarini AA, Simpson MA, Borradori L, Yawalkar N, Schlapbach C. Homozygous missense mutation in Il36rn in generalized Pustular Dermatosis with intraoral involvement compatible with both Agep and generalized Pustular psoriasis. *JAMA Dermatol*. (2015) 151:452–3. doi: 10.1001/jamadermatol.2014.3848

12. Tian Q, Xu B, Zhou X. A case of hydroxychloroquine causing refractory acute generalized exanthematous impetigo. Chinese. *J Dermatol*. (2018) 51:64–5. doi: 10.3760/cma.j.issn.0412-4030.2018.01.021

13. Liu JJ, Yang JJ, Li H, Huang S. Pharmacological analysis of acute generalized exanthematous impetigo caused by hydroxychloroquine sulfate in patients with Sjogren's syndrome. *Primary Med Forum*. (2019) 23:5140–1. doi: 10.19435/j.1672-1721.2019.35.083

14. Di Lernia V, Grenzi L, Guareschi E, Ricci C. Rapid clearing of acute generalized Exanthematous Pustulosis after Administration of Ciclosporin. *Clin Exp Dermatol*. (2009) 34:e757–9. doi: 10.1111/j.1365-2230.2009.03480.x

15. Liccioli G, Marrani E, Giani T, Simonini G, Barni S, Mori F. The first pediatric case of acute generalized Exanthematous Pustulosis caused by Hydroxychloroquine. *Pharmacology*. (2019) 104:57–9. doi: 10.1159/000500406

16. Di Maso V, Cozzi M, Gerini U, Bedina E, Olivo E, Bianco F, et al. Coupled plasma filtration adsorption for treatment of capillary leak syndrome superimposed to acute generalized Exanthematous Pustolosis: a case report. *Blood Purif*. (2020) 49:372–8. doi: 10.1159/000503770

17. Soria A, Barbaud A, Assier H, Avenel-Audran M, Tétart F, Raison-Peyron N, et al. Cutaneous adverse drug reactions with Antimalarials and Allergological skin tests. *Dermatol (Basel, Switzerland)*. (2015) 231:353–9. doi: 10.1159/000438787

18. Pearson KC, Morrell DS, Runge SR, Jolly P. Prolonged Pustular eruption from Hydroxychloroquine: an unusual case of acute generalized Exanthematous Pustulosis. *Cutis*. (2016) 97:212–6.

19. İslamoğlu ZGK, Karabağli P. A case of recalcitrant acute generalized Exanthematous Pustulosis with Sjogren's syndrome: successfully treated with low-dose cyclosporine. *Clin Case Rep*. (2019) 7:1721–4. doi: 10.1002/ccr3.2352

20. Matsuda-Hirose H, Sho Y, Yamate T, Nakamura Y, Saito K, Takeo N, et al. Acute generalized Exanthematous Pustulosis induced by Hydroxychloroquine successfully treated with Etretinate. *J Dermatol*. (2020) 47:e53–4. doi: 10.1111/1346-8138.15185

21. Bailey K, McKee D, Wismer J, Shear N. Acute generalized Exanthematous Pustulosis induced by Hydroxychloroquine: first case report in Canada and review of the literature. *J Cutan Med Surg*. (2013) 17:414–8. doi: 10.2310/7750.2013.12105

22. Assier-Bonnet H, Saada V, Bernier M, Clerici T, Saïag P. Acute generalized Exanthematous Pustulosis induced by Hydroxychloroquine. *Dermatol (Basel, Switzerland)*. (1996) 193:70–1. doi: 10.1159/000246211

23. Evans CC, Bergstresser PR. Acute generalized Exanthematous Pustulosis precipitated by Hydroxychloroquine. *J Am Acad Dermatol*. (2004) 50:650–1. doi: 10.1016/s0190-9622(03)02733-6

24. Martins A, Lopes LC, Paiva Lopes MJ, Rodrigues JC. Acute generalized Exanthematous Pustulosis induced by Hydroxychloroquine. *Eur J Dermatol: EJD*. (2006) 16:317–8.

25. Paradisi A, Bugatti L, Sisto T, Filosa G, Amerio PL, Capizzi R. Acute generalized Exanthematous Pustulosis induced by Hydroxychloroquine: three cases and a review of the literature. *Clin Ther*. (2008) 30:930–40. doi: 10.1016/j.clinthera.2008.05.014

26. Avram MM, Hoang M. Case Records of the Massachusetts General Hospital. Case 20-2009. A 79-year-old woman with a blistering cutaneous eruption. *N Engl J Med*. (2009) 360:2771–7. doi: 10.1056/NEJMcpc0900639

27. Park JJ, Yun SJ, Lee JB, Kim SJ, Won YH, Lee SC. A case of Hydroxychloroquine induced acute generalized Exanthematous Pustulosis confirmed by accidental Oral provocation. *Ann Dermatol*. (2010) 22:102–5. doi: 10.5021/ad.2010.22.1.102

28. Charfi O, Kastalli S, Sahnoun R, Lakhoua G. Hydroxychloroquine-induced acute generalized Exanthematous Pustulosis with positive patch-testing. *Indian J Pharm*. (2015) 47:693–4. doi: 10.4103/0253-7613.169589

29. Zhang Z, Liu X. Images in clinical medicine. Acute generalized Exanthematous Pustulosis. *N Engl J Med*. (2015) 372:161. doi: 10.1056/NEJMicm1401196

30. Yalçın B, Çakmak S, Yıldırım B. Successful treatment of Hydroxychloroquine-induced recalcitrant acute generalized Exanthematous Pustulosis with cyclosporine: case report and literature review. *Ann Dermatol*. (2015) 27:431–4. doi: 10.5021/ad.2015.27.4.431

31. Castner NB, Harris JC, Motaparthi K. Cyclosporine for corticosteroid-refractory acute generalized Exanthematous Pustulosis due to Hydroxychloroquine. *Dermatol Ther*. (2018) 31:e12660. doi: 10.1111/dth.12660

32. Duman H, Topal IO, Kocaturk E, Cure K, Mansuroglu I. Acute generalized Exanthematous Pustulosis induced by Hydroxychloroquine: a case with atypical clinical presentation. *An Bras Dermatol*. (2017) 92:404–6. doi: 10.1590/abd1806-4841.20175561

33. Mohaghegh F, Jelvan M, Rajabi P. A case of prolonged generalized Exanthematous Pustulosis caused by Hydroxychloroquine-literature review. *Clin Case Rep*. (2018) 6:2391–5. doi: 10.1002/ccr3.1811

34. Chaabouni R, Bahloul E, Ennouri M, Atheymen R, Sellami K, Marrakchi S, et al. Hydroxychloroquine-induced acute generalized Exanthematous Pustulosis: a series of seven patients and review of the literature. *Int J Dermatol*. (2021) 60:742–8. doi: 10.1111/ijd.15419

35. Mofarrah R, Mofarrah R, Oshriehye M, Ghobadi Aski S, Nazemi N, Nooshiravanpoor P. The necessity of patch testing in determining the causative drug of Agep. *J Cosmet Dermatol*. (2021) 20:2156–9. doi: 10.1111/jocd.13841

36. Munshi M, Junge A, Gadaldi K, Yawalkar N, Heidemeyer K. Ixekizumab for treatment of refractory acute generalized Exanthematous Pustulosis caused by Hydroxychloroquine. *JAAD Case Rep*. (2020) 6:634–6. doi: 10.1016/j.jdcr.2020.05.014

37. Otake-Irie H, Nakajima S, Okamoto N, Toichi E, Nomura T, Kabashima K. Prolonged acute generalized Exanthematous Pustulosis and atypical target-like lesions induced by Hydroxychloroquine. *J Dermatol*. (2020) 47:e387–8. doi: 10.1111/1346-8138.15537

38. Enos T, Jeong HS, Vandergriff T, Jacobe HT, Chong BF. Acute generalized Exanthematous Pustulosis induced by empiric Hydroxychloroquine for presumed Covid-19. *Dermatol Ther*. (2020) 33:e13834. doi: 10.1111/dth.13834

39. Mercogliano C, Khan M, Lin C, Mohanty E, Zimmerman R. Agep overlap induced by Hydroxychloroquine: a case report and literature review. *J Commun Hosp Int Med Perspect*. (2018) 8:360–2. doi: 10.1080/20009666.2018.1547089

40. Robustelli Test E, Vezzoli P, Carugno A, Raponi F, Gianatti A, Rongioletti F, et al. Acute generalized Exanthematous Pustulosis with erythema Multiforme-like lesions induced by Hydroxychloroquine in a woman with coronavirus disease 2019 (Covid-19). *J Eur Acad Dermatol Venereol: JEADV*. (2020) 34:e457–9. doi: 10.1111/jdv.16613

41. Litaiem N, Hajlaoui K, Karray M, Slouma M, Zeglaoui F. Acute generalized Exanthematous Pustulosis after Covid-19 treatment with Hydroxychloroquine. *Dermatol Ther*. (2020) 33:e13565. doi: 10.1111/dth.13565

42. Sánchez-Velázquez A, Arroyo-Andrés J, Falkenhain-López D, Peralto JLR, Romero PLO, Díaz RR, et al. Hydroxychloroquine-induced acute generalized Exanthematous Pustulosis: an adverse reaction to keep in mind during Covid-19 pandemic. *J der Deutschen Dermatologischen Gesellschaft = J German Soc Dermatol: JDDG*. (2021) 19:896–8. doi: 10.1111/ddg.14354

43. Lateef A, Tan KB, Lau TC. Acute generalized Exanthematous Pustulosis and toxic epidermal Necrolysis induced by Hydroxychloroquine. *Clin Rheumatol*. (2009) 28:1449–52. doi: 10.1007/s10067-009-1262-4

44. Coleman I, Ruiz G, Brahmbhatt S, Ackerman L. Acute generalized Exanthematous Pustulosis and Stevens-Johnson syndrome overlap due to Hydroxychloroquine: a case report. *J Med Case Rep*. (2020) 14:210. doi: 10.1186/s13256-020-02504-8

45. Mashiah J, Brenner S. A systemic reaction to patch testing for the evaluation of acute generalized Exanthematous Pustulosis. *Arch Dermatol*. (2003) 139:1181–3. doi: 10.1001/archderm.139.9.1181

46. Davidovici BB, Pavel D, Cagnano E, Rozenman D, Halevy S. Acute generalized Exanthematous Pustulosis following a spider bite: report of 3 cases. *J Am Acad Dermatol*. (2006) 55:525–9. doi: 10.1016/j.jaad.2006.05.010

47. Trüeb RM, Burg G. Acute generalized Exanthematous Pustulosis due to doxycycline. *Dermatol (Basel, Switzerland)*. (1993) 186:75–8. doi: 10.1159/000247308

48. Schrom K, Pacifico A, Conic RRZ, Pigatto PDM, Malagoli P, Morrone A, et al. Dabigatran-associated acute generalized Exanthematous Pustulosis (Agep) in a psoriatic patient undergoing Ixekizumab and its Pathogenetic mechanism. *Dermatol Ther*. (2019) 32:e13018. doi: 10.1111/dth.13018

49. Nakamizo S, Kobayashi S, Usui T, Miyachi Y, Kabashima K. Clopidogrel-induced acute generalized Exanthematous Pustulosis with elevated Th17 cytokine levels as determined by a drug lymphocyte stimulation Test. *Br J Dermatol*. (2010) 162:1402–3. doi: 10.1111/j.1365-2133.2010.09705.x

50. Aviña-Zubieta JA, Galindo-Rodriguez G, Newman S, Suarez-Almazor ME, Russell AS. Long-term effectiveness of antimalarial drugs in rheumatic diseases. *Ann Rheum Dis*. (1998) 57:582–7. doi: 10.1136/ard.57.10.582

51. Nirk EL, Reggiori F, Mauthe M. Hydroxychloroquine in rheumatic autoimmune disorders and beyond. *EMBO Mol Med*. (2020) 12:e12476. doi: 10.15252/emmm.202012476

52. Bahloul E, Jallouli M, Garbaa S, Marzouk S, Masmoudi A, Turki H, et al. Hydroxychloroquine-induced hyperpigmentation in systemic diseases: prevalence, clinical features and risk factors: a cross-sectional study of 41 cases. *Lupus*. (2017) 26:1304–8. doi: 10.1177/0961203317700486

53. Son CH, Lee CU, Roh MS, Lee SK, Kim KH, Yang DK. Acute generalized Exanthematous Pustulosis as a manifestation of carbamazepine hypersensitivity syndrome. *J Investig Allergol Clin Immunol*. (2008) 18:461–4.

54. Fernández-Ruiz M, López-Medrano F, García-Ruiz F, Rodríguez-Peralto JL. Diltiazem-induced acute generalized Exanthemic Pustulosis: a case and review of the literature. *Actas Dermo-Sifiliograficas*. (2009) 100:725–7. doi: 10.1016/S0001-7310(09)72291-4

55. Munster T, Gibbs JP, Shen D, Baethge BA, Botstein GR, Caldwell J, et al. Hydroxychloroquine concentration-response relationships in patients with rheumatoid arthritis. *Arthritis Rheum*. (2002) 46:1460–9. doi: 10.1002/art.10307

56. Armstrong AW, Read C. Pathophysiology, clinical presentation, and treatment of psoriasis: a review. *JAMA*. (2020) 323:1945–60. doi: 10.1001/jama.2020.4006

57. Fuchs-Telem D, Sarig O, van Steensel MA, Isakov O, Israeli S, Nousbeck J, et al. Familial Pityriasis Rubra Pilaris is caused by mutations in Card14. *Am J Hum Genet*. (2012) 91:163–70. doi: 10.1016/j.ajhg.2012.05.010

58. Hoegler KM, John AM, Handler MZ, Schwartz RA. Generalized Pustular psoriasis: a review and update on treatment. *J Eur Acad Dermatol Venereol: JEADV*. (2018) 32:1645–51. doi: 10.1111/jdv.14949

59. Hoetzenecker W, Nägeli M, Mehra ET, Jensen AN, Saulite I, Schmid-Grendelmeier P, et al. Adverse cutaneous drug eruptions: current understanding. *Semin Immunopathol*. (2016) 38:75–86. doi: 10.1007/s00281-015-0540-2

60. Feldmeyer L, Heidemeyer K, Yawalkar N. Acute generalized Exanthematous Pustulosis: pathogenesis, genetic background, clinical variants and therapy. *Int J Mol Sci*. (2016) 17. doi: 10.3390/ijms17081214

frontiers | Frontiers in Medicine

TYPE Brief Research Report
PUBLISHED 05 May 2023
DOI 10.3389/fmed.2023.1153883

OPEN ACCESS

EDITED BY
Xiaolin Sun,
Peking University People's Hospital, China

REVIEWED BY
Lovro Lamot,
University of Zagreb, Croatia
Satoshi Kubo,
University of Occupational and Environmental Health Japan, Japan

*CORRESPONDENCE
Natsuka Umezawa
✉ umezawa.rheu@tmd.ac.jp

RECEIVED 30 January 2023
ACCEPTED 20 April 2023
PUBLISHED 05 May 2023

CITATION
Umezawa N, Mizoguchi F, Maejima Y, Kimura N, Hasegawa H, Hosoya T, Fujimoto M, Kohsaka H, Naka T and Yasuda S (2023) Leucine-rich alpha-2 glycoprotein as a potential biomarker for large vessel vasculitides.
Front. Med. 10:1153883.
doi: 10.3389/fmed.2023.1153883

Leucine-rich alpha-2 glycoprotein as a potential biomarker for large vessel vasculitides

Natsuka Umezawa[1]*, Fumitaka Mizoguchi[1], Yasuhiro Maejima[2], Naoki Kimura[1], Hisanori Hasegawa[1], Tadashi Hosoya[1], Minoru Fujimoto[3,4], Hitoshi Kohsaka[5], Tetsuji Naka[3,4] and Shinsuke Yasuda[1]

[1]Department of Rheumatology, Graduate School of Medical and Dental Sciences, Tokyo Medical and Dental University (TMDU), Tokyo, Japan, [2]Department of Cardiovascular Medicine, Graduate School of Medical and Dental Sciences, Tokyo Medical and Dental University (TMDU), Tokyo, Japan, [3]Department of Clinical Immunology, Kochi Medical School, Kochi University, Kochi, Japan, [4]Division of Allergy and Rheumatology, Department of Internal Medicine, School of Medicine Iwate Medical University, Yahaba, Japan, [5]Rheumatology Center, Chiba-Nishi General Hospital, Matsudo, Japan

Objectives: Serum levels of C-reactive protein (CRP) and erythrocyte sedimentation rate (ESR) have been used as useful biomarkers for reflecting the activity of large vessel vasculitides (LVV). However, a novel biomarker that could have a complementary role to these markers is still required. In this retrospective observational study, we investigated whether leucine-rich α-2 glycoprotein (LRG), a known biomarker in several inflammatory diseases, could be a novel biomarker for LVVs.

Methods: 49 eligible patients with Takayasu arteritis (TAK) or giant cell arteritis (GCA) whose serum was preserved in our laboratory were enrolled. The concentrations of LRG were measured with an enzyme-linked immunosorbent assay. The clinical course was reviewed retrospectively from their medical records. The disease activity was determined according to the current consensus definition.

Results: The serum LRG levels were higher in patients with active disease than those in remission, and decreased after the treatments. While LRG levels were positively correlated with both CRP and erythrocyte sedimentation rate, LRG exhibited inferior performance as an indicator of disease activity compared to CRP and ESR. Of 35 CRP-negative patients, 11 had positive LRG. Among the 11 patients, two had active disease.

Conclusion: This preliminary study indicated that LRG could be a novel biomarker for LVV. Further large studies should be required to promise the significance of LRG in LVV.

KEYWORDS

leucine-rich α-2 glycoprotein, Takayasu arteritis, giant cell arteritis, large vessel vasculitides, biomarkers

1. Introduction

Large vessel vasculitides (LVV) are systemic inflammatory diseases, which mainly affect the aorta and its first branches. The disease activity over time could result in vascular stenosis, occlusion, and dilatation. Serum levels of C-reactive protein (CRP) and erythrocyte sedimentation rate (ESR) are reliable biomarkers for assessing vascular inflammation in large vasculitis and are employed in the current criteria to evaluate disease activity. Meanwhile, they do not necessarily correspond to histopathologically-proved vascular inflammation (1). To predict a possible relapse or progression of the vascular lesions, a novel biomarker is required.

Leucine-rich α-2 glycoprotein (LRG) is a 50-kDa protein, which is produced by hepatocytes, neutrophils, macrophages, and epithelial cells. It promotes angiogenesis, cellular proliferation, and tissue repair through modulating TGF-β signaling (2, 3). As its production is induced by multiple cytokines including interleukin-6 (IL-6), tumor necrosis factor-α (TNF-α), and IL-1α, LRG could be elevated even in patients with active inflammatory diseases with low serum CRP. This is the case with patients suffering from active inflammatory bowel syndrome (IBD) (4) and from active rheumatoid arthritis treated with IL-6 blockade (5).

To investigate whether LRG could be an additional biomarker for LVVs, we evaluated the serum levels of LRG in patients with LVVs.

2. Methods

2.1. Participants and data collection

This study is a retrospective observational study. Patients with Takayasu arteritis (TAK) or giant cell arteritis (GCA) who visited the Tokyo Medical and Dental University (TMDU) hospital between April 2017 and March 2019 were screened. Among them, patients whose serum samples at their visits were preserved with written informed consent for research use were enrolled. The serum samples were collected at any time point regardless of their disease activity. Eligible cases fulfilled the American College of Rheumatology (ACR) criteria 1990 of TAK or GCA (6, 7). Clinical information and laboratory test values including CRP and ESR were obtained from medical records.

Disease activity states, such as active, major/minor relapse, remission, sustained remission, and glucocorticoid-free remission, were defined according to the European Alliance of Associations for Rheumatology (EULAR) consensus definition of disease activity (8). More detailed definitions are as follows; "active disease" was defined as the presence of typical signs or symptoms of active LVV with at least one of the following: current activity on imaging or biopsy/ischemic complications/elevated inflammatory markers, "major relapse" was defined as recurrence of active disease with either of the following: clinical features of ischemia/evidence of active aortic inflammation resulting in progressive aortic or large vessel dilatation, stenosis or dissection, "minor relapse" was defined as recurrence of active disease but not fulfilling the criteria for a major relapse, "remission" was defined as the absence of all clinical signs and symptoms attributable to active LVV and normalization of ESR and CRP, "sustained remission" was defined as remission for at least 6 months with the achievement of the individual target GC dose, and "glucocorticoid-free remission" was defined as sustained remission with discontinued GC therapy.

The baseline characteristics of the participants were evaluated at the time when their serum was obtained initially. Their clinical courses were reviewed retrospectively until October 2022.

2.2. Measurement of LRG

The serum concentrations of LRG were measured with enzyme-linked immunosorbent assay (ELISA) (5) at Kochi University.

2.3. Statistics

For comparisons among the two groups, the values were analyzed by Welch's *t*-test. Correlation between two parameters was assessed by Spearman's correlation analysis. A value of p of 0.05 was employed as a threshold for statistical significance. Receiver operating characteristic (ROC) curves analysis was employed to determine a cut-off value and evaluate the diagnostic performance of a biomarker.

3. Results

3.1. Serum LRG was elevated in active LVVs

Forty patients with TAK and nine with GCA were included in this study (Table 1). All patients had aortic involvement. Treatments with glucocorticoids ($n = 33$) in combination with methotrexate ($n = 3$), azathioprine ($n = 2$), or tocilizumab ($n = 5$) were given to 33 patients when the serum samples were collected. Nineteen patients had active disease and the other 30 were in remission at the baseline evaluation. Eight out of the 19 active patients were active having minor relapses and the rest 11 patients had newly-onset diseases. Sixteen out of the 30 remission patients were in sustained remission, who were in remission for at least 6 months and achieved the target glucocorticoid dose, and eight patients were in glucocorticoid-free remission. The median age of the patients was 55 (range: 16–81) and 60 (range: 21–79) years old, the median disease duration was 0.1 (range: 0.1–47) and 33 (0.1–51) years, and the median dose of glucocorticoids was 25 (range: 0–70) and 2.9 (range: 0–12.5) mg/day in active and remission patients, respectively. Since the elevated inflammatory markers of CRP and ESR are included in the EULAR consensus definition but not indispensable to active diseases, five patients with negative CRP or ESR were categorized into active disease depending on their concurrent ischemic complications or imaging studies. Besides four patients with IBD, neither of them had intestinal symptoms at the evaluation. There was no coexistence of other inflammatory diseases. The rates of complication-associated arteriosclerotic lesions including hypertension, dyslipidemia, and diabetes were comparable between active disease and remission.

Serum LRG levels in the patients with active disease were elevated significantly compared to those in remission [mean values: 30.5 (+ − 17.5) vs. 19.3 (+ − 6.28) μg/mL, $p < 0.05$; Figure 1A]. As

TABLE 1 Baseline characteristics of patients.

	Active disease (n=19)		Remission (n=30)	
Activity state, n	Major relapse[1)]	0	Sustained remission[2)]	16
	Minor relapse[1)]	8	Glucocorticoid-free remission[2)]	8
TAK/GCA, n	11/8		29/1	
Age, years	55 [16–81][3)]		60 [21–79][3)]	
Female, n (%)	13 (68.4)		30 (100)	
Disease duration, years	0.1 [0.1–47][3)]		33 [0.1–51][3)]	
Onset within 1 year, n	11		0	
Current treatments				
Glucocorticoids use, n	15		18	
dose of prednisolone, mg/day	25 [0–70][3)]		2.9 [0–12.5][3)]	
Immunosuppressants, n	4		5	
MTX	2		1	
AZA	0		2	
TCZ, n	2		3	
Complications				
IBD, n (%)	2 (10.5)		2 (6.6)	
HTN, n (%)	6 (31.5)		11 (36.6)	
DLP, n (%)	8 (42.1)		10 (33.3)	
Diabetes, n (%)	2 (10.5)		1 (3.3)	

[1)]Active cases other than major or minor relapses were newly-diagnosed ones. [2)]Remission cases other than sustained or glucocorticoid-free remission were simply in remission since the dose of glucocorticoid did not achieved the target. Two cases with elevated ESR (>30 mm/h) due to renal anemia, who had negative CRP, no signs or symptoms of active vasculitis, and no relapses over 10 years, were categorized into sustained remission. [3)]median [range], AZA, azathioprine; DLP, dyslipidemia; GCA, giant cell arteritis; HTN, hypertension; IBD, inflammatory bowel disease; MTX, methotrexate; TAK, Takayasu arteritis; and TCZ, tocilizumab.

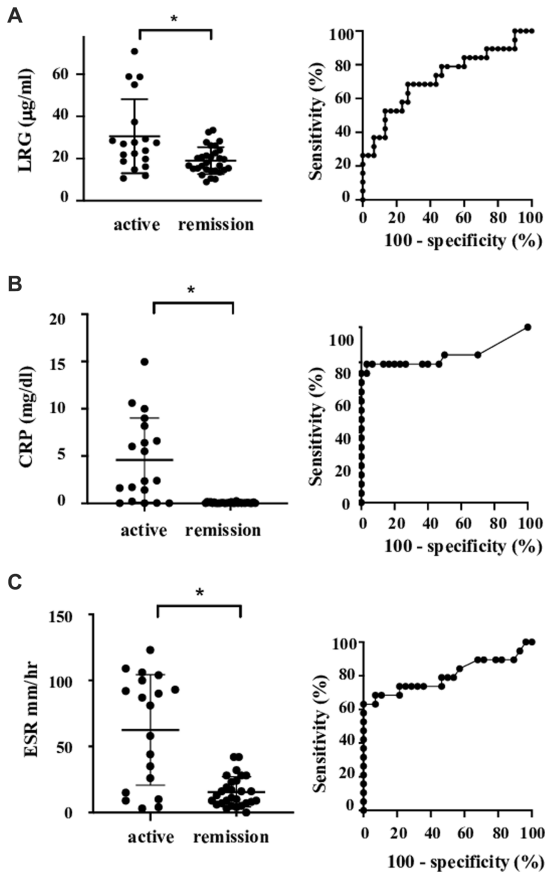

FIGURE 1
Serum levels and ROC curve of the markers in patients with LVV. Serum levels and ROC curve of LRG **(A)**, CRP **(B)**, and ESR **(C)**. Bars show mean and 2SD values. Asterisks represent statistically significant differences (p<0.05). LRG, leucine-rich α-2 glycoprotein; LVV, large vessel vasculitides; and ROC, receiver operating characteristic.

alternative reference variables, the levels of CRP [mean values: 4.58(+−4.44) vs. 0.067 (+−0.058) mg/mL, $p<0.05$; Figure 1B], and ESR [mean values: 62.58 (+−41.92) vs. 15.6 (+−11.4) mm/h, $p<0.05$; Figure 1C] were also elevated significantly in the active disease as well. ROC curve analysis revealed that a cut-off value of LRG to distinguish the active disease from remission was 21.5 μg/mL (sensitivity 66%, specificity 73%, AUC 0.71, Figure 1A). ROC curve with CRP and ESR (Figures 1B,C) showed higher AUC (0.83 and 0.80, respectively) than that with LRG. The sensitivity and specificity were 73 and 96% with CRP (cut-off value 0.3 mg/dL) and 84 and 42% with ESR (cut-off value 10 mm/h). LRG levels were correlated positively with CRP ($p<0.0001$, $r=0.61$) and ESR ($p<0.0001$, $r=0.55$; Figure 2).

3.2. LRG was a complementary maker to CRP for active LVVs except for patients treated with IL-6 inhibitors

Using the calculated cut-off value of LRG, we divided the patients into four groups according to their serum LRG and CRP levels (Table 2). Eleven out of 35 CRP-negative patients had positive LRG. Among them, two had active disease depending on their ischemic complications. In both of the two CRP-negative/LRG-positive cases with disease activity, ESR was increased to 26 and 58 mm/h, respectively. Radiological studies were not performed at that time.

On the other hand, three LRG-negative patients among 14 CRP-positive ones had active disease. They were all newly diagnosed with GCA.

All five patients under the treatments with anti-IL-6 receptor antibodies, tocilizumab (TCZ), had neither positive value of CRP, LRG, nor ESR, regardless of their disease activities.

3.3. LRG decreased after achieving remission

Clinical courses of the patients were observed up to 4 years after the baseline evaluation. Among nine patients whose serum samples were obtained repeatedly at some points apart, five patients who had formerly active disease turned out to be in remission at a subsequent

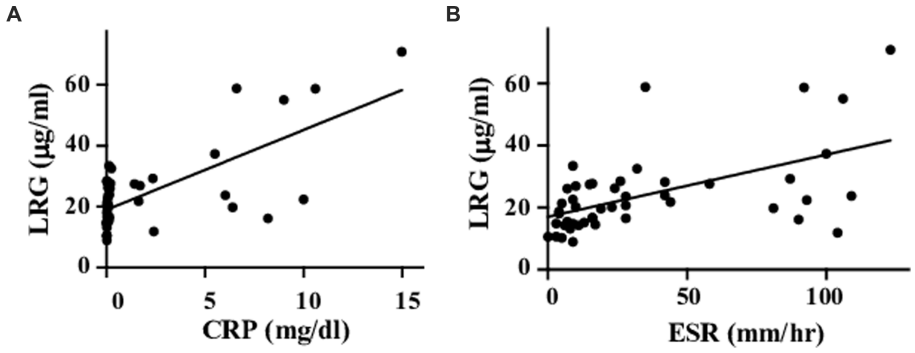

FIGURE 2
Correlations between LRG and inflammatory markers. Serum LRG levels were positively correlated with CRP **(A)** and ESR **(B)**.

TABLE 2 Number of the patients grouped according to the levels of CRP/LRG.

	LRG (+)	LRG (−)
CRP (+)	11	3
Active/remission	11/0	3/0
CRP (−)	11	24
Active/remission	02-Sep	Mar-21

CRP (+): ≥0.3 mg/dL, CRP (−): <0.3 mg/dL, LRG (+): ≥21.5 μg/mL, and LRG (−): <21.5 μg/mL.

point. They achieved remission after the treatments with prednisolone (PSL; $n = 5$) in combination with methotrexate ($n = 2$), TCZ ($n = 2$), or infliximab ($n = 1$). The median interval time between baseline and subsequent evaluations was 24 months. The levels of LRG in all of the five patients dropped below the cut-off value after the treatment as well as CRP and ESR (Supplementary Figure 1).

4. Discussion

In this study, we reported for the first time that the LRG levels were elevated in patients with active LVV. LRG levels in LVV patients were higher than those in healthy subjects reported previously (5, 9). In addition, LRG levels decreased after achieving remission by treatment with immune-suppressive agents including biologics. These findings suggested that LRG could be a novel biomarker for evaluating the activity of LVVs.

Meanwhile, the value of AUC in ROC analysis with LRG was lower than that with CRP or ESR. As it would be attributed partially to the current definition of active disease which includes CRP and ESR themselves, LRG might not be as responsive as CRP or ESR. It is noteworthy, however, that some cases had discrepant results between LRG and CRP levels despite the positive correlation between the two biomarkers. Since two active cases with elevated LRG were identified among the CRP-negative cases, the measurement of LRG would be beneficial to evaluate the disease activity in some CRP-negative cases. Unlike CRP, LRG is induced not only in the liver but also in the peripheral tissues (10) in response to local cytokines other than circulating IL-6. Comprehensive assessments of multiple biomarkers would reinforce the evaluation.

In cases under treatment with TCZ, special consideration should be required in evaluating disease activity of LVVs. All biomarkers of CRP, ESR, and LRG could turn out to be negative with TCZ treatments.

There are some limitations in our study. First, the number of patients is too small to evaluate the covariates including treatments or comorbidities which might affect the LRG levels. We could not analyze patients with TAK and GCA separately due to the small sample size. Second, imaging studies which evaluate the vascular lesions concurrently with the evaluation of the serum markers could not be available in most cases.

With those limitations above, an additional benefit of measuring LRG, such as detecting latent activity or predicting the prognosis of LVVs, would remain to be evaluated. To address this point, a larger study with sequential measurements of biomarkers with radiological studies should be required to promise the significance of LRG in LVVs.

Data availability statement

The original contributions presented in the study are included in the article/Supplementary material, further inquiries can be directed to the corresponding author.

Ethics statement

The studies involving human participants were reviewed and approved by Tokyo Medical and Dental University and Kochi University. The patients/participants provided their written informed consent to participate in this study.

Author contributions

NU, FM, NK, HK, TN, and SY contributed to the conception and design. NU, FM, YM, NK, HH, TH, and MF analyzed the data. NU, FM, YM, NK, HH, TH, MF, HK, TN, and SY contributed to interpretation of data and drafting of the manuscript. All authors contributed to the article and approved the submitted version.

Conflict of interest

The authors declare that the research was conducted in the absence of any commercial or financial relationships that could be construed as a potential conflict of interest.

Publisher's note

All claims expressed in this article are solely those of the authors and do not necessarily represent those of their affiliated organizations, or those of the publisher, the editors and the reviewers. Any product that may be evaluated in this article, or claim that may be made by its manufacturer, is not guaranteed or endorsed by the publisher.

Supplementary material

The Supplementary material for this article can be found online at: https://www.frontiersin.org/articles/10.3389/fmed.2023.1153883/full#supplementary-material

References

1. Salvarani C, Cantini F, Boiardi L, Hunder GG. Laboratory investigations useful in giant cell arteritis and Takayasu's arteritis. *Clin Exp Rheumatol*. (2003) 21:S23–8.

2. Wang X, Abraham S, McKenzie JAG, Jeffs N, Swire M, Tripathi VB, et al. LRG1 promotes angiogenesis by modulating endothelial TGF-β signaling. *Nature*. (2013) 18:6–11. doi: 10.1038/nature12345

3. Naka T, Fujimoto M. LRG is a novel inflammatory marker clinically useful for the evaluation of disease activity in rheumatoid arthritis and inflammatory bowel disease. *Immunol Med*. (2018) 41:62–7. doi: 10.1080/13497413.2018.1481582

4. Shinzaki S, Matsuoka K, Iijima H, Mizuno S, Serada S, Fujimoto M, et al. Leucine-rich alpha-2 glycoprotein is a serum biomarker of mucosal healing in ulcerative colitis. *J Crohns Colitis*. (2017) 11:84–91. doi: 10.1093/ecco-jcc/jjw132

5. Fujimoto M, Serada S, Suzuki K, Nishikawa A, Ogata A, Nanki T, et al. Leucine-rich α2-glycoprotein as a potential biomarker for joint inflammation during anti–interleukin-6 biologic therapy in rheumatoid arthritis. *Arthritis Rheum*. (2015) 67:2056–60. doi: 10.1002/art.39164

6. Arend WP, Michel BA, Bloch DA, Hunder GG, Calabrese LH, Edworthy SM, et al. The American College of Rheumatology 1990 criteria for the classification of Takayasu arteritis. *Arthritis Rheum*. (1990) 33:1129–34.

7. Hunder GG, Blich DA, Michel BA, Stevens MB, Arend WP, Calabrese LH, et al. The American College of Rheumatology 1990 criteria for the classification of giant cell arthritis. *Arthritis Rheum*. (1990) 33:1122–8.

8. Hellmich B, Agueda A, Monti S, Buttgereit F, de Boysson H, Brouwer E, et al. 2018 update of the EULAR recommendations for the management of large vessel vasculitis. *Ann Rheum Dis*. (2020) 79:19–30. doi: 10.1136/annrheumdis-2019-215672

9. Ishida T, Kotani T, Serada S, Fujimoto M, Takeuchi T, Makino S, et al. Correlation of increased serum leucine-rich α2-glycoprotein levels with disease prognosis, progression, and activity of interstitial pneumonia in patients with dermatomyositis: a retrospective study. *PLoS One*. (2020) 15:e0234090. doi: 10.1371/journal.pone.0234090

10. Serada S, Fujimoto M, Terabe F, Iijima H, Shinzaki S, Matsuzaki S, et al. Serum leucine-rich alpha-2 glycoprotein is a disease activity biomarker in ulcerative colitis. *Inflamm Bowel Dis*. (2012) 18:2169–79. doi: 10.1002/ibd.22936

frontiers | Frontiers in Immunology

TYPE Systematic Review
PUBLISHED 18 May 2023
DOI 10.3389/fimmu.2023.1183195

OPEN ACCESS

EDITED BY
Alexandre Wagner Silva De Souza,
Federal University of São Paulo, Brazil

REVIEWED BY
Liting Jiang,
Shanghai Jiao Tong University, China
Jason Dale Turner,
University of Birmingham, United Kingdom

*CORRESPONDENCE
Anne Marie Lynge Pedersen
amlp@sund.ku.dk

RECEIVED 09 March 2023
ACCEPTED 09 May 2023
PUBLISHED 18 May 2023

CITATION
Kamounah S, Sembler-Møller ML, Nielsen CH and Pedersen AML (2023) Sjögren's syndrome: novel insights from proteomics and miRNA expression analysis. *Front. Immunol.* 14:1183195. doi: 10.3389/fimmu.2023.1183195

Sjögren's syndrome: novel insights from proteomics and miRNA expression analysis

Sarah Kamounah[1], Maria Lynn Sembler-Møller[1], Claus Henrik Nielsen[1,2] and Anne Marie Lynge Pedersen[1*]

[1]Section for Oral Biology and Immunopathology/Oral Medicine, Department of Odontology, Faculty of Health and Medical Sciences, University of Copenhagen, Copenhagen, Denmark, [2]Center for Rheumatology and Spine Diseases, University Hospital Rigshospitalet, Copenhagen, Denmark

Introduction: Sjögren's syndrome (SS) is a systemic autoimmune disease, which affects the exocrine glands leading to glandular dysfunction and, particularly, symptoms of oral and ocular dryness. The aetiology of SS remains unclear, and the disease lacks distinctive clinical features. The current diagnostic work-up is complex, invasive and often time-consuming. Thus, there is an emerging need for identifying disease-specific and, ideally, non-invasive immunological and molecular biomarkers that can simplify the diagnostic process, allow stratification of patients, and assist in monitoring the disease course and outcome of therapeutic intervention in SS.

Methods: This systematic review addresses the use of proteomics and miRNA-expression profile analyses in this regard.

Results and discussion: Out of 272 papers that were identified and 108 reviewed, a total of 42 papers on proteomics and 23 papers on miRNA analyses in saliva, blood and salivary gland tissue were included in this review. Overall, the proteomic and miRNA studies revealed considerable variations with regard to candidate biomarker proteins and miRNAs, most likely due to variation in sample size, processing and analytical methods, but also reflecting the complexity of SS and patient heterogeneity. However, interesting novel knowledge has emerged and further validation is needed to confirm their potential role as biomarkers in SS.

KEYWORDS

Sjögren's syndrome, proteomics, miRNA - microRNA, salivary glands, saliva

1 Introduction

Sjögren's syndrome (SS) is an autoimmune disease characterised by chronic lymphocytic infiltration of exocrine glands, particularly the salivary and lacrimal glands, leading to tissue destruction and, subsequently, glandular dysfunction. The predominant symptoms are oral and ocular dryness occurring due to hyposalivation and

keratoconjunctivitis sicca, respectively, accompanied by arthralgia and fatigue (1, 2). The disease may occur alone and is then designated primary SS (pSS), or together with another autoimmune connective tissue disease, most often rheumatoid arthritis (RA), systemic lupus erythematosus (SLE) or systemic sclerosis (SSc), in which case it is designated secondary SS (sSS) (1, 2). SS can affect people of any age, but symptoms usually appear between the ages of 45 and 55. It affects ten times as many women as men (3).

The aetiology and pathogenesis of SS are not fully understood. It has been suggested that exposure to specific environmental factors (e.g. virus) in susceptible individuals results in dysregulation of the innate immune system involving the interferon (IFN) pathway (2, 4). Current evidence suggest that activated T cells are involved in the pathogenesis of SS by producing pro-inflammatory cytokines and by mediating B-cell-hyperactivity (5). The lymphocytic infiltrates observed in the salivary gland tissue mainly comprise CD4+ effector T cells, including IFN-γ-producing Th1 cells, IL-17-producing Th17 cells and IL-21-producing T follicular helper cells. Furthermore, CD4+ T-cell lymphopenia and increased number of circulating follicular helper T cells are often observed in the blood from patients with pSS (6). B-cell hyperactivity leads to autoantibody production, and in some cases, development of lymphoproliferative malignancy (2, 7). Anti-SSA/Ro and/or anti-SSB/La are found in about 70% of patients with pSS, often together with ANA (anti-nuclear antibodies) positivity. Hypergammaglobulinaemia is also prevalent as well as a positive rheumatoid factor (RF) (8). There is evidence to suggest that the salivary gland epithelial cells play a central role in regulation of the local autoimmune responses by inducing B-cell activation and survival of B cells within the target tissue (9, 10).

SS is associated with the human leukocyte antigen (HLA) class II types DR3 and DR2, particularly the DRB1*03/DQB1*02 and DRB1*15/DQB1*01 haplotypes, but only in patients having serum autoantibodies against SSA/Ro and SSB/La antigens (11–13). A recent, large study confirmed the absence of HLA association in patients with pSS negative for SSA and/SSB antibodies (14). On the basis of HLA association, presence of SSA and/or SSB autoantibodies, age of onset and clinical manifestations, it has been suggested that patients with pSS may be divided in two distinct subgroups (14).

Classification of pSS is currently based on the American College of Rheumatology-European League Against Rheumatism (ACR-EULAR) classification criteria utilizing the weighted sum of 5 objective aspects of pSS. These include anti-SSA/Ro antibody positivity, presence of focal lymphocytic sialadenitis with a focus score ≥1 in a labial salivary gland biopsy, an abnormal ocular staining score ≥5 (or van Bijsterveld score ≥4), a Schirmer's test ≤5 mm/5 min and/or an unstimulated salivary flow rate ≤0.1 mL/min (15). None of the paraclinical findings, symptoms or disease manifestations are pathognomonic for SS, but may be observed in other autoimmune connective tissue diseases like RA and SLE (16). Furthermore, the highly variable symptomatology, autoantibody reactivity, histological features and gland functionality encompassed by the diagnosis of pSS suggest the existence of several different aetiopathogenic disease subtypes that may benefit from different treatment regimes. In order to characterize such subtypes, reliable biomarkers need to be identified. Moreover, due to the lack of distinctive clinical features and biomarkers, pSS may be diagnosed at a late stage where irreversible tissue damage has occurred. The diagnostic procedures currently in use are complicated, invasive and often time-consuming. This underlines the need for identification of new, ideally non-invasive, immunological and molecular biomarkers that can simplify the diagnostic work-up and stratification of patients and assist in monitoring the disease course and outcome of therapeutic interventions.

Recent and emerging advances within omics technologies offer opportunities to detect novel and reliable molecular diagnostic biomarkers, which can provide a higher sensitivity and specificity than the simple biomarkers and measures used today, and at the same time improve our insight into the aetiopathogenesis of SS and its subtypes. This systematic review provides an overview of current findings on proteomics and miRNA-expression profile analyses in SS, and presents the methods and biological materials used, such as saliva, blood and salivary gland tissue, for characterization of the proteomic and miRNA profiles.

2 Methods

A literature search was conducted through the PubMed, Medline and Embase databases up to January 2021 according to the standards of the *Preferred Reporting Items* for *Systematic Reviews and Meta-Analyses* (PRISMA) guidelines (Figure 1). Human studies that were published in English, without any restriction on publication date, and that examined proteomics and miRNAs in patients with SS (with and without comparison

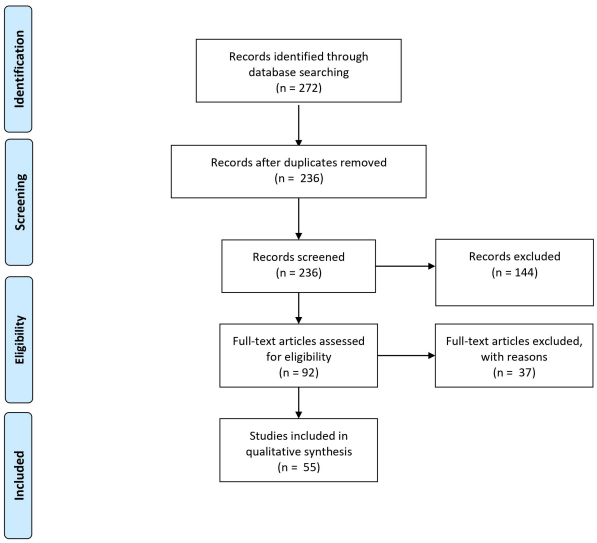

FIGURE 1
PRISMA diagram showing the number of records identified through database search, and the number of records screened and excluded.

to healthy control subjects, or patients with other connective tissue diseases) using various methods and biological material (saliva, salivary gland tissue and blood) were included. Only primary publication types were included. Studies including less than 5 patients with SS were excluded. The following terms were used in combination to identify studies on proteomics in patients with SS: ("Sjögren's syndrome"[MeSH]) AND "Proteomics"[MeSH]) OR Sjögren's* proteomic* OR Sjögren's proteomics OR primary Sjögren's syndrome proteomic* OR primary Sjögren's syndrome proteomics). The following terms were used in combination in the search of studies on miRNA expression-profile in patients with SS: "Sjögren's syndrome"[MeSH]) AND "MicroRNAs" [MeSH]) OR primary Sjögren's syndrome miRNA OR primary Sjögren's syndrome microRNA.

Titles and abstracts were screened by two reviewers (SK and AMLP). If eligible based on the title and abstract, full-text articles were obtained when possible.

2.1 Saliva as a source of biomarkers

Saliva is an attractive source of biomarkers for diagnostic purposes, as salivary glands are the very organs affected by the disease, and saliva may reflect local and, possibly, systemic pathological changes of the disease (17–22). Furthermore, saliva samples can easily be obtained using a non-invasive, simple and safe procedure, and collection of saliva is thus ideal for monitoring of disease progression. Studies on the proteome in SS have mainly been performed on saliva, and stimulated whole saliva has proven more suitable for studying the salivary proteome than gland-specific saliva (23). There is also evidence suggesting that stimulated whole saliva contains a lower proteome variability than unstimulated whole saliva (24). In addition, the unstimulated whole saliva flow rate is often significantly reduced in patients with SS, which makes chewing-stimulated whole saliva more applicable. As the lacrimal glands are major target organs of SS, tear fluid represents another relevant biological material for identification of disease biomarkers. However, it may be challenging to obtain sufficient amount for analysis, and it is more complicated to collect than saliva (25).

2.2 Methods used for proteomic and miRNA profiling

Proteomic analysis provides insight to understand the function of proteins in health and disease. Most studies use mass spectrometry-based proteomics to obtain information on the proteome composition (e.g. shortgun gel-free proteomics) or protein interactions and structure by means of e.g. high-performance liquid chromatography-mass spectrometry (HPLC-MS), tandem mass-spectrometry (MS/MS) and matrix-assisted laser/ionization time-of-flight MS/MS (MALDI-TOF MS/MS). The methods most commonly applied for purification of proteins include absorbance colorimetry, liquid chromatography (LC), native and denaturing one-dimensional and two-dimensional gel-eletrophoresis (2-DGE), and Western blotting. LC separates proteins according to various properties and thus complements subsequent electrophoretic separation.

The method most commonly used for quantification of miRNA is real time (RT)-PCR.

3 Results and discussion

Figure 1 summarizes the number of records identified through database search, and after removal, as well as the number of records screened and excluded. A total of 42 and 23 articles on proteomic profile and miRNA expression profile, respectively, were eligible for inclusion. After screening, a total of 65 full-text articles could be included for further review. These articles were published between 2006 and 2020.

3.1 Proteomic analysis

All studies except 4 used a cross-sectional design, including two experimental studies (26, 27), one case-control study (28) and one longitudinal study (29).

In 22 studies, proteomic analysis was performed on whole saliva (unstimulated or stimulated) or saliva collected from individual glands (19, 21–23, 25, 26, 28, 30–43).

Four studies included proteomic analysis of salivary gland tissue (22, 39, 44, 45) and 19 studies included proteomic analyses of plasma, serum or peripheral mononuclear blood cells (PMBC) (22, 27, 29, 46–63). Two studies included proteomic analysis of both stimulated whole saliva and tear fluid and of extracellular vesicles of both saliva and tear fluid from patients with pSS, healthy controls and non-pSS, sicca controls (21, 25). One study simultaneously characterized the proteome in three different types of biological materials (whole saliva, plasma, and salivary gland tissue) from the same patients and non-pSS, sicca controls (22).

Based on their aim, study design and findings, the papers on proteomics could be divided into the following categories:

1. Comparative proteomic analysis of saliva, salivary gland tissue and/or blood from patients with pSS and healthy control subjects and/or non-pSS, sicca control subjects (21–23, 25, 30, 31, 33–35, 37, 38, 40, 43, 45, 52, 54, 57, 58, 60–62)
2. Comparative proteomic analysis of saliva, salivary gland tissue and/or blood from patients with pSS and patients with RA, SLE, systemic sclerosis (SSc), mixed connective tissue disease (MCTD), polymyositis and dermatomyositis (26, 28, 36, 39, 50, 53, 59, 63).
3. Proteomic analysis of saliva and/or serum specifically related to autoantibodies in patients with SS (pSS or sSS) and control subjects (27, 29, 32, 46–49, 51, 55, 56).
4. Proteomic analysis of saliva in SS patients with and without non-Hodgkin MALT (mucosa-associated lymphoid tissue) lymphoma (41, 42, 44).

3.2 Comparative proteomic analysis of saliva, salivary gland tissue and/or blood from patients with pSS, healthy control subjects and/or non-pSS, sicca control subjects

3.2.1 Proteomic analysis of saliva

Table 1 presents an overview of studies on the salivary proteome of patients with pSS compared to healthy controls and patients with non-pSS sicca. The number and type of differentially expressed salivary proteins identified vary between studies. This most likely reflects the heterogeneity of SS and the underlying complexity of the inflammatory immune responses leading to varying degrees of organ damage. Overall, the studies report upregulation of inflammatory mediators and downregulation of proteins of salivary acinar cell origin in SS patients compared to non-SS patients and healthy controls.

Hu et al. (23) compared different types of saliva from patients with pSS and healthy controls, including whole saliva, parotid saliva and saliva from the sublingual/submandibular glands by means of LC-MS/MS analysis. They found that whole saliva yielded more informative peptides and proteins than specific glandular saliva. On average, 53 MALDI peaks were detected in whole saliva from patients with pSS, in contrast to only 24 peaks and 26 peaks in

TABLE 1 Proteomic analysis of saliva, salivary gland tissue and/or blood from patients with pSS and healthy control (HC) subjects and/or non-pSS, sicca control subjects.

Author (year)	No. of subjects	Materials and methods	Findings
Ryu OH, et al., 2006 (30)	41 pSS 15 non-pSS, sicca 5 HC	PS 2-DGE, SELDI-TOF-MS, ELISA	SELDI-TOF-MS of 10-200 kDa peaks revealed 8 peaks with >2-fold changes in the SS group that differed from non-SS ($p< 0.005$). Peaks of 11.8, 12.0, 14.3, 80.6 and 83.7 kDa were increased, while 17.3, 25.4, and 35.4 kDa peaks were decreased in SS samples. 2D-DIGE identified significant ↑ of β2-microglobulin, lactoferrin, immunoglobulin (Ig) kappa light chain, polymeric Ig receptor, lysozyme C and cystatin C in all stages of SS. Two presumed proline-rich proteins, amylase and carbonic anhydrase VI, were ↓ in the patient group.
Hu S, et al., 2007 (23)	10 pSS 10 HC	WS, PS, sublingual/sub-mandibular saliva MALDI-TOF-MS, 2-DGE, LC-MS/MS, RT-PCR, immunoblotting	Sixteen salivary proteins were ↓ and 25 were ↑ in pSS patients compared with HC. In pSS, the levels of 16 peptides (10 ↑ and 6 ↓) differed significantly from those of HC. WS contained more informative peptides and proteins than gland-specific saliva. Moreover, 27 mRNAs were significantly up-regulated (≥3-fold change) in saliva from pSS. In pSS, 19 of 27 overexpressed genes were interferon-inducible or related to lymphocyte filtration and antigen presentation, known to be involved in the pathogenesis of pSS.
Giusti L, et al., 2007 (31)	12 pSS 12 HC	UWS 2-DGE	The WS protein pattern differed between pSS patients and healthy controls, particularly carbonic anhydrase VI. A comparison of WS protein profile of pSS patients compared with the one obtained from HC revealed a set of differentially expressed proteins. These proteins were related to acute and chronic inflammation while some others were involved in oxidative stress injury.
Hjelmervik T, et al., 2009 (45)	6 pSS 6 non-SS controls	MSG tissue 2-DGE, LC-ESI-MS/MS	A total of 522 proteins were identified in pSS and non-SS controls, out of which 158 in pSS only, 91 in non-SS controls only and 273 in both groups. Heat shock proteins, mucins, carbonic anhydrases, enolase, vimentin and cyclophilin B were among the proteins identified. The differences in the proteomes of MSG tissue from pSS patients and non-SS controls were mainly related to ribosomal proteins, immunity and stress. Alpha-defensin-1 and calmodulin were among six proteins exclusively identified in pSS patients. Overall, proteins related to matrix, metabolism and stress were ↓, while IgG and serum albumin were ↑ in pSS.
Wei P, et al., 2013 (33)	12 pSS 13 HC	UWS MALDI-TOF-MS	The study investigated differences in low molecular weight salivary proteins (1-10 kDa) in pSS patients compared to HC. Seven m/z (mass-to-charge) (m/z 1068.1, 1196.2, 1738.4, 3375.3, 3429.3, 3449.7 and 3490.6 ratio peaks with significant differences between the 2 groups with 5 peptides being up-regulated and 2 down-regulated in the pSS patients compared to HC subjects. In the validation phase, 4 out of 5 pSS patients were diagnosed as pSS, and 4 of the 5 healthy controls were diagnosed as HC.
Gallo A, et al., 2013 (34)	82 pSS 17 non-pSS sicca 29 HC	UWS SELDI-TOF-MS, 2DE, MALDI-TOF-MS, immunohistochemistry	Gross cystic disease fluid protein-15(GCDFP-15)/prolactin-inducible protein (PIP) is a secretory acinar glycoprotein of 14 KDa. Proteomic analysis found that a putative peak of 16547 m/z, identified as the GCDFP-15/PIP protein, was among the best independent biomarkers for pSS to discriminate between patients and HC with a sensitivity of 96% and a specificity of 70%, with a global cross validated error of 29%. The intensity of GCDFP-15/PIP was significantly lower in pSS patients than in non-pSS sicca subjects and HC. GCDFP-15/PIP expression also correlated with salivary flow rate and focus score. Immunohistochemistry confirmed that GCDFP-15/PIP staining was faint in mucus acini, but no obvious difference were in serous acinar cells. RT-PCR showed that GCDFP-15/PIP mRNA was significantly lower in pSS patients than in non-pSS sicca patients and HC, supporting the hypothesis that the reduction of GCDFP-15/PIP is related to a decreased protein synthesis.
Deutsch O, et al., 2015 (35)	18 pSS 18 HC	UWS Affinity and immunodepletion, 2-DGE, LC-MS/MS	The use of depletion strategy before proteomics analysis increased identification ability by 3-fold. Overall, 79 biomarker candidates were identified. Proteins with the most pronounced fold changes were related to SS serum or tissue factors. Bioinformatics analyses of proteins with a >3-fold increase in SS patients showed calcium-binding proteins, defense-response proteins, proteins involved in apoptotic regulation, stress-response proteins and cell motion-related proteins. Preliminary validation by western blotting of profilin and CA-I indicated similar expression profile trends to those identified by quantitative MS.
Nishikawa A, et al., 2016 (52)	82 pSS (30 + 52) 30 HC	Serum High-throughput	82 proteins, identified as pSS-associated, were differentially expressed between 30 pSS patient and 30 HC (57 were ↑, 25 were ↓). Nine were identified as disease activity-associated biomarkers and among these, five proteins (CXCL13, TNF-R2, CD48, BAFF, and PD-L2) were validated as candidate biomarkers by ELISA in a separate

(Continued)

TABLE 1 Continued

Author (year)	No. of subjects	Materials and methods	Findings
		proteomic analysis, ELISA	pSS-validation cohort. CXCL13 exhibited the most significant correlation with the lymphadenopathy, glandular, and pulmonary domains of the ESSDAI. CXCL13, TNF-R2 and CD48 exhibited a positive correlation with the biological domain of the ESSDAI. TNF-R2 exhibited the most negative correlation with uptake in the submandibular gland.
Dalaleu N, et al., 2016 (37)	48 pSS	UWS 187-plex capture antibody-based assay	The study identified disease-phenotype driven biomarker signatures. Hyposalivation was associated with significant alteration in 22 out of 119 reliably detectable biomarkers. Thereof, a 4-plex signature allowed accurate prediction of salivary gland function for >80% of the cases. With respect to histopathological features, the most distinct profiles were identified in conjunction with ectopic germinal centers. Pregnancy-associated plasma protein A, thrombospondin 1 and peptide YY could recapitulate the presence or absence of tertiary lymphoid organization for 93.8% of the patients. Functional annotation of alterations associated with hyposalivation identified the IL1 system as a dominant pro-inflammatory component, while changes observed in context with ectopic lymphoid organization revealed specific shifts in chemotactic profiles and altered regulation of apoptotic processes.
Chaudhury NMA, et al., 2016 (38)	25 pSS 35 HC	UWS Western blot, LC-MS/MS	The concentration of mucins MUC5B and MUC7 were similar between patients and controls, but a comparison of protein Western blotting and glycan staining identified a ↓ in mucin glycosylation in SS, particularly on MUC7. Analysis of O-glycans released from MUC7 by β-elimination revealed an increase in core 1 sulfation, but an even larger reduction in sialylation resulting in a global decline of charged glycans. This was primarily due to the loss of the extended core 2 disialylated structure, with and without fucosylation. A reduction in the extended, fucosylated core 2 disialylated structure on MUC7, residual mucosal wetness, and whole saliva flow rate appeared to have a negative and cumulative effect on the perception of oral dryness.
Aqrawi LA, et al., 2017 (25)	27 pSS 32 HC	SWS, EV, tears LC-MS	SWS: ↑ of neutrophil gelatinase-associated lipocalin (LCN2, innate immunity), calmodulin (CALM, cell signalling) and calmodulin-5 (CALM-5, wound repair), granulins (GRN, wound repair) and epididymal secretory protein-1 (ESP1, cholesterol homeostasis within the endosome and/or lysosome) in pSS. SWS EV: ↑ adipocyte plasma membrane-associated protein (APMAP, adipocyte differentiation), guanine nucleotide-binding protein subunit alpha-13 (GNA-13, cell signalling), WD repeat-containing protein-1 (WDR1, involved in the disassembly of actin filaments), tyrosine-protein phosphatase non-receptor type substrate-1 (SIRPA, regulates NK cells and dendritic cell inhibition) and lymphocyte-specific protein 1 (LSP1, activation of innate immune system) in pSS.
Hall SC, et al., 2017 (40)	15 pSS 15 non-pSS sicca 14 HC	USW, PS iTRAQ, Lectin affinity capture-MS	The iTRAQ analyses revealed up- and down-regulation of numerous proteins that could be involved in the disease process (e.g., histones) or attempts to mitigate the ensuing damage (e.g., bactericidal/permeability increasing fold containing family (BPIF) members). An immunoblot approach confirmed the pSS-associated ↑ of β2-microglobulin (in PS) and ↓ of carbonic anhydrase VI (in WS) and BPIFB2 (in PS). Beyond the proteome, the N-glycosites of pSS and HC samples were profiled. They were enriched for glycopeptides using lectins Aleuria aurantia and wheat germ agglutinin, which recognize fucose and sialic acid/N-acetyl glucosamine, respectively. MS analyses showed that pSS is associated with increased N-glycosylation of numerous salivary glycoproteins in PS and WS.
Tasaki S, et al., 2017 (54)	30 pSS 30 HC	Whole blood transcriptomes, serum proteomes and peripheral immuno-phenotyping SOMAmer-based capture array	Identification of SS gene signatures (SGS) dysregulated in widespread omics layers, including epigenomes, mRNAs and proteins. SGS predominantly involved the interferon signature and ADAMs substrates. Besides, SGS was significantly overlapped with SS-associated genes indicated by a genome-wide association study and expression trait loci analyses. Combining the molecular signatures with immunophenotypic profiles revealed that cytotoxic CD8 T cells were associated with SGS. Activation of SGS in cytotoxic CD8 T cells isolated from patients with pSS was observed.
Bodewes ILA, et al., 2019 (57)	63 pSS (including 22 with fatigue and 23 without fatigue 20 HC	Serum SOMAscan, ELISA	pSS vs. HC: 58 proteins were ↑ and 46 were ↓. IFN-pos. and IFN-neg. pSS patients: ↑ IgG levels, higher frequency of anti-SSA and -SSB and ↓ levels of C3 complement in IFN-pos. pSS patients. 22 fatigued vs. 23 non-fatigued pSS patients: 14 serum proteins were ↑ including SNAP-25, ENO1, UCHL1 and 2 serum proteins were ↓ in fatigued. IL36a and several complement factors were upregulated in fatigued pSS patients compared to non-fatigued.
Aqrawi LA, et al., 2019 (21)	10 pSS 15 non-pSS, sicca 10 HC	SWS, tears LC-MS	SWS from pSS vs. non-pSS sicca: ↑ of *peptidyl-prolyl cis-trans isomerase FKB1A* (T-cell regulation, upregulation of NF-kappa-B signaling), *CD44 antigen* (FOXP3 expression and regulatory T-cell suppresion), *β-2 microglobulin* (B2MG, innate immunity). SWS from pSS vs. HC: ↑ *Secreted Ly-6/uPAR-related protein 1* (Ach-receptor activity, cell migration and proliferation), *B2MG, Clusterin* (Innate immunity, modulates NF-kappa-B activity and TNF production). SWS-EV from pSS vs. non-pSS sicca: *CD44*, *Major vault protein* (IFN-mediated signaling, MAP kinase activity, neutrophil degranulation), *Neutrophil gelatinase-associated lipocalin* (Innate immunity, tumor-associated antigen, cell adhesion). SWS-EV from pSS vs. HC: *Ficolin-1* (Innate immunity), *CD44*, *Annexin A4* (NF-kappa-B, apoptosis, IL-8 secretion).

(Continued)

TABLE 1 Continued

Author (year)	No. of subjects	Materials and methods	Findings
Qiao L, et al., 2019 (58)	26 pSS with NMOSD 34 pSS without NMOSM 30 NMOSD	Serum 2-DGE, MALDI-TOF/MS, ELISA	Nine proteins were significantly differently expressed between pSS with NMOSD and pSS without NMOSD). Serum levels of clusterin and complement factor H (CFH) were further verified by ELISA. Serum clusterin was higher in NMOSD with pSS than without (298.33 ± 184.52 vs. 173.49 ± 63.03 ng/ml, $p < 0.01$), while the levels of CFH were lower in pSS patients with NMOSD than without.
Cecchettini A, et al., 2019 (43)	20 pSS 20 HC	UWS Nano-HPLC-SWATH-MS	PSS patients were stratified in three subgroups according to focus score in MSG tissue and unstimulated salivary flow. 203 proteins were differentially expressed in pSS patients compared to HC with evident differences in the expression of normal constituents of the human salivary proteome (i.e. prolactin-inducible protein, proline-rich proteins, and cystatins) and several mediators of inflammatory processes. 63 proteins were shared and specifically modulated in the three subsets of pSS patients converging on several inflammatory pathways. Among them S100A protein appeared of particular interest merging on IL-12 signaling and being significantly influenced by either salivary flow impairment or intensity of immune cell infiltration in the tissue.
Sembler-Møller, et al., 2020 (22)	24 pSS 16 non-pSS sicca	SWS, plasma, MSGB LC-MS	1013 proteins were detected in SWS, 219 proteins in plasma and 3166 in MSGT. SWS: 40 proteins differed significantly between the two groups, 34 of which were ↑ in the pSS group. In pSS, proteins involved in immunoinflammatory processes were ↑, whereas proteins related to salivary secretion were ↓. The combination of neutrophil elastase, calreticulin and TRIM-29 revealed the best performance in distinguishing pSS from non-pSS with an AUC of 0.97.
Huang S, et al., 2020 (60)	8 pSS 10 HC	PBMC Immobilized metal affinity chromatography (IMAC)	787 proteins were identified as differentially expressed proteins, and 175 phosphosites on 123 proteins were identified as differentially phosphorylated proteins. Using module and hub protein analyses, 16 modules for the proteins were identified, 2 clusters for the phosphoproteins and selected the top 10 hub proteins (UBA52, MAPK1, HSPA8, ACTB, ACLY, APP, ACTN1, ACTN4, VWF, and TGFB1). Finally, 22 motifs were identified using motif analysis of the phosphosites and found 17 newly identified motifs, while 6 motifs were experimentally verified for known protein kinases.
Tian Q, et al., 2020 (61)	133 pSS 108 HC	PBMC ELISA, Immunofluorescence staining, tranfection assay, and IFN-alfa treatment.	The ↑ of PARP-9 and CXCL10 as well as their co-localization was confirmed in pSS. PARP-9 levels in LSGs ↑ with ↑ focus scores in patients with pSS. PARP-9 and DTX3L were present in the infiltrating mononuclear cells from salivary glands in female NOD/LtJ mouse models. Ingenuity Pathway Analysis networks of differentially expressed proteins demonstrated that PARP-9, STAT1, and IFN-induced protein with tetratricopeptide repeats 1 (IFIT-1) participated in the IFN-related pathway. Furthermore, PARP-9 could ↑ the expression of IFIT1 and CXCL10 in B cells. Moreover, PARP-9 and CXCL10 could be induced by IFNα in B cells.
Schmidt A, et al., 2020 (62)	45 pSS, 30 controls	Plasma Hybrid immunoaffinity targeted LC-MS	The aim was to quantify plasma levels of the chemokine CXCL10, which has been associated with many immunological disorders including pSS. The hybrid approach enabled sensitive, specific, and simultaneous quantification of total, full-length (active) CXCL10 1–77 and DPP4-truncated (inactive) CXCL10 3–77 in human plasma down to the low pg/mL level, reaching ELISA sensitivities. The ratio of CXCL10 1–77 to truncated CXCL10 3–77 was ↑ in patients with pSS and provided the highest correlation with pSS disease activity.

Arrow up: upregulated.
Arrow down: downregulated.

parotid saliva and saliva from the submandibular/sublingual glands, respectively (23). Thus, stimulated whole saliva appears to be more suitable for detection of biomarkers than glandular specific secretions. In whole saliva, 25 proteins were upregulated while 16 proteins were downregulated in patients with pSS patients compared to healthy controls, all reflecting salivary gland damage and oral inflammation in pSS (23). Furthermore, 10 peptides were upregulated and six were downregulated in pSS, while 27 salivary mRNA transcripts were upregulated (≥3-fold) in pSS. Among the 27 genes that were highly overexpressed in pSS, 13 were validated by RT-quantitative PCR, substantiating upregulation of particularly IFN-inducible protein G1P2 in pSS patients. In addition, genes related to lymphocyte infiltration and antigen presentation were found overexpressed (23).

A number of studies report upregulation of β2-microglobulin in parotid saliva (23, 30, 40), unstimulated whole saliva (28, 44), stimulated whole saliva (21–23, 32) and sublingual/submandibular saliva (23) in patients with pSS versus non-pSS patients and/or healthy controls. This supports earlier findings based on different techniques, e.g. sandwich enzyme immunoassay (64). A study found that the combination of upregulated β2-microglobulin, cathepsin D and α-enolase yielded a receiver-operating characteristic (ROC) value of 0.99 in distinguishing patients with pSS from healthy subjects (65). However, this finding has not been further validated. β-2 microglobulin is a non-glycosylated protein, and constitutes the light-chain component of major histocompatibility (MHC) class I molecules. Interestingly, salivary levels of β2-microglobulin have been found associated with the extent of lymphocytic infiltration of the salivary glands in patients with pSS (40, 66) as well as with the presence of anti-SSA/Ro serum antibodies (28).

Alpha-enolase, also known as enolase 1 (ENO1), has also been found upregulated in patients with pSS compared to healthy controls and to patients with non-SS sicca in unstimulated whole saliva (28, 41). Of note, the levels of α-enolase are elevated in serum from pSS patients with fatigue compared to the levels in serum from non-fatigued pSS patients and healthy control subjects (57). Alpha-enolase is a glycolytic enzyme that is expressed in most tissues and

has been identified as an autoantigen in Hashimoto encephalopathy (67) and cancer (68). It has been suggested that α-enolase is an autoantigen in pSS, as patients with pSS had higher levels of anti-citrullinated α-enolase IgG antibodies in serum than healthy controls and patients with RA (69). However, the presence of IgA and IgG antibodies against citrullinated and native α-enolase was not associated with any clinical manifestations (69).

A number of other salivary proteins have been found upregulated in pSS, including neutrophil gelatinase-associated lipocalin (NGAL/lipocalin-2) (21, 31), calgranulin A (S100A8) (35), calgranulin B (S100A9) (28), psoriasin (S100A7) (28, 35), epidermal fatty acid binding protein (E-FABP) (21, 23, 28), ACTB protein (actin) and b-Actin fragment (23, 31) as well as immunoglobulin kappa light chain (23, 28, 30, 35). Neutrophil gelatinase-associated lipocalin (NGAL), a glycoprotein belonging to the lipocalin family, is expressed in several normal tissues, where it provides protection against bacterial infection and modulates oxidative stress through anti-apoptotic effects. Levels of NGAL increase in response to inflammation, infection, intoxication, ischemia, acute kidney injury and neoplastic transformation (70). Interestingly, levels of acinar NGAL have been found elevated in minor salivary glands from patients with pSS compared to glands from non-SS patients (71). Calgranulin B (S100A9) and psoriasin (S100A7) are calcium-binding proteins involved in regulation of cellular growth. Both calgranulin-B and psoriasin have been found highly upregulated in ductal carcinoma *in situ* of the breast and in psoriasis (72). Cecchettini et al. (43) also demonstrated upregulation of S100A proteins in patients with pSS compared to healthy controls, especially in patients with a high focus score and low salivary flow rates, indicating that these proteins play a central role in the progression of glandular dysfunction. Jazaar et al. (42) found salivary S100A8/A9 associated with MALT lymphoma in pSS (see below 1.4.). Calgranulin A (S100A8) has been found upregulated in unstimulated whole saliva and parotid saliva from patients with pSS (35, 42). However, S100A8 was absent in whole saliva samples from patients with pSS in the study by Hu et al. (17). Sembler-Møller et al. (22) combined the analysis of stimulated whole saliva, plasma and salivary gland tissue. They found that salivary proteome of patients with pSS differed from that of non-pSS patients, but no significant difference in protein expression in plasma and labial salivary gland tissue was found between the groups. Several proteins were upregulated in stimulated whole saliva including neutrophil elastase, calreticulin, tripartite motif-containing protein 29 (TRIM29), clusterin and vitronectin. The combination of neutrophil elastase, calreticulin and TRIM-29 had the best performance in distinguishing pSS from non-pSS with an AUC of 0.97 (22).

Aqrawi et al. (25) identified additional upregulated proteins including calmodulin (CALM), calmodulin-like protein 5 (CALML5), granulins (GRN) and epididymal secretory protein-1 (ESP1) in whole saliva from patients with pSS. CALM and CALML5 are both calcium-binding proteins that play a role intracellular signalling and differentiation of keratinocytes, respectively. GRN are involved in wound repair and tissue remodelling, and ESP1 is involved in cholesterol homeostasis within the endosome and/or lysosome.

The most frequently identified downregulated proteins include prolactin-inducible protein (PIP) (21, 28, 34), carbon anhydrase VI (CA6) (23, 28, 30, 31, 40); salivary α-amylases (26, 28), most of the cystatins and a number of other secretory proteins (23, 28, 30, 31). PIP is a secretory protein, which is present in glycosylated and non-glycosylated forms in human saliva. Gross cystic disease fluid protein-15 (GCDFP-15)/PIP, which binds to aquaporin 5, a water channel critical to saliva formation, has been found downregulated in pSS, and the GCDFP-15/PIP expression correlated with both the salivary flow rate and focus score of minor salivary gland biopsies (34). Salivary PIP also binds to dental enamel (hydroxyapatite) and presumably participates in the formation of the enamel pellicle (73). It has been demonstrated that PIP-deficient mice (*Pip* $^{-/-}$ mice) develop impaired T-helper type 1 response and cell-mediated immunity (74). The role of PIP in the pathogenesis of SS requires further investigation.

CA6 is a zinc-containing metalloenzyme secreted in the salivary glands. CA6 catalyzes the conversion of salivary bicarbonate and hydrogen ions to carbon dioxide and water. The process is essential for the maintenance of salivary pH homeostasis and prevention of demineralization of the dental enamel (75). Reduced CA6 expression could imply impairment of the salivary bicarbonate buffer capacity and may explain the occurrence of increased caries activity in patients with SS.

Cystatins are cysteine protease inhibitors, which provide protecting against proteases by regulating uncontrolled proteolysis and tissue damages (76). The family of cystatins includes cystatin S, cystatin SN, cystatin C, and cystatin D. Cystatins may differ with respect to phosphorylation and/or glycosylation. Giusti et al. (31) found reduction of cystatin SN precursor in patients with pSS compared to control subjects, whereas the other cystatins were scarcely represented or totally absent. Ryu et al. (30) found an increase in salivary levels of cystatin C (about 1.3-fold) compared to the levels in saliva from controls. The diverging results may reflect variation in the levels of cystatins in the different types of saliva, i.e. whole saliva versus parotid saliva. Cystatin C levels have been reported increased in whole saliva of patients with periodontitis, and this may also contribute to explain the conflicting results. The reported decrease in salivary α-amylases (23, 28, 30, 31) may be a result of fragmentation caused by protease endogenous truncation or to the acinar cell damage.

Hall et al. (40) confirmed upregulation of β2-microglobulin in parotid saliva and downregulation of CA6 in whole saliva based on isobaric mass tagging (iTRAQ) and lectin affinity capture mass spectrometry (MS)-based approach, but also detected downregulation of parotid saliva BPIFB2 (bactericidal/permeability increasing fold containing family B2), and increased N-glycosylation of numerous salivary glycoproteins in both parotid and whole saliva from patients with pSS compared to control subjects (40).

Finally, Table 1 includes studies that have reported upregulated or downregulated MALDI peaks (m/z) (peptides or fragments

derived from proteolytic activity in parotid or whole saliva from patients with pSS compared to healthy controls) (33).

3.2.2 Proteomic analysis of salivary gland tissue

In a study by Hjelmervik et al. (45), using LC-ESI-MS/MS and 2-D PAGE, six proteins were exclusively detected in labial salivary gland tissue from patients with pSS, including α-defensin-1 and calmodulin. Alpha-defensin-1 plays a central role in virus defence and upregulates the type I IFN response genes (77) and had previously been suggested as a salivary biomarker for oral inflammation in pSS (26). Calmodulin regulates inflammatory processes, and elevated levels of calmodulin-binding proteins in the salivary glands from pSS patients have also been reported (78).

3.2.3 Proteomic analysis of plasma, serum or PBMC

While Sembler-Møller et al. found no difference in the protein expression profile in plasma between patients with pSS and non-pSS sicca controls, other studies on serum, plasma and PBMC found multiple proteins to be upregulated and downregulated in patients with pSS compared to controls, which may reflect different control group designs (22). Bodewes et al. (57) identified a set of proteins that could not only discriminate pSS from healthy controls, but also distinguish fatigued-pSS patients from non-fatigued pSS patients. IFN-positive pSS patients had higher levels of IgG and anti-SSA and -SSB and lower levels of C3 complement than IFN-negative pSS patients. Several serum proteins, including neuroactive synaptosomal-associated protein 25 (SNAP-25), α-enolase, ubiquitin carboxyl-terminal hydrolase isozyme L1 (UCHL1) and IL36a as well as several complement factors were upregulated in fatigued pSS patients compared to non-fatigued pSS (57).

Another study by Qiao et al. (58) found upregulation of clusterin and complement factor H in pSS patients with neuromyelitis optica spectrum disorder (NMOSD) compared to pSS patients without this disorder. These findings suggest that serum clusterin and factor H could be potential biomarkers for pSS patients with NMOSD and play a role in the pathogenesis of the disease, but further verification is needed.

Nishikawa et al. (52) identified five proteins as disease activity-associated biomarkers, including CXCL13, TNF-R2, CD48, B-cell activating factor (BAFF), and PD-L2. CXCL13 significantly correlated to the lymphadenopathy, glandular, and pulmonary domains of the EULAR Sjögren's syndrome disease activity index (ESSDAI). CXCL13, TNF-R2 and CD48 correlated positively with the biological domains of the ESSDAI, while TNF-R2 exhibited the most negative correlation with uptake in the submandibular gland.

In a study on PBMC (60), 787 proteins were identified as differentially expressed, and 175 phosphosites on 123 proteins were identified as differentially phosphorylated proteins. The study identified 16 modules for the proteins, two clusters for the phosphoproteins and selected the top 10 hub proteins (UBA52, MAPK1, HSPA8, ACTB, ACLY, APP, ACTN1, ACTN4, VWF, and TGFB1). Finally, 22 motifs were identified using motif analysis of the phosphosites, and the authors found 17 novel motifs, while 6 motifs were experimentally verified for known protein kinases. The differentially expressed proteins enabled discrimination of patients with pSS from healthy controls and were suggested as candidate biomarkers in the diagnosis of pSS.

3.3 Comparative proteomic analysis of saliva, salivary gland tissue and/or blood from patients with pSS and other inflammatory connective tissue diseases

Table 2 shows the proteomic analysis of saliva, salivary gland tissue and/or blood from patients with pSS and other inflammatory connective tissue diseases. An experimental study with peroral pilocarpine treatment on patients with pSS, sSS and healthy controls showed that the levels of almost all of the 60% salivary proteins, which was not present or present at low levels prior to treatment in pSS, reached similar levels in unstimulated whole saliva in all groups 30-60 minutes after treatment with pilocarpine. Patients with pSS also had β-defensin-2 in their saliva and higher levels of α-defensin-1 than patients with sSS and healthy controls, indicating that α-defensin-1 and β-defensin-2 may be used as biomarkers of oral inflammation in patients with pSS (26).

Baldini et al. (28) identified 15 differently expressed proteins in patients with pSS compared to healthy controls, non-pSS sicca, patients with RA-sSS and SSc-sSS. S100A9, β-2 microglobulin, epidermal fatty acid binding protein (E-FABP), psoriasin (S100A7), immunoglobulin k light chain (IGKC) and α-enolase were upregulated in patients with pSS compared to healthy controls, whereas AMY1A, carbonic anhydrase VI (CA6), glyceraldehydes-3-phosphate dehydrogenase (G3PDH), cystatin SN precursor protein (CST1), prolactin-inducible protein precursor (PIP), short palate, lung and nasal epithelium carcinoma associated protein 2 (SPLUNC-2) were downregulated in patients with pSS. PIP, SPLUNC-2 G3PDH, AMY1A, CA6 were upregulated in patients with pSS compared to non-pSS, sicca patients. Lipocalin was upregulated, while rheumatoid factor D5 light chain was downregulated in patients with pSS compared to patients with RA-sSS. Lastly, a comparison with patients with SSc-sSS revealed an upregulation of cystatin in patients with pSS (28).

One hundred differential m/z peaks associated with pSS were identified by Li Y al (13)., and the m/z (mass-to-charge) peaks at 8,133.85, 11,972.8, 2,220.81, and 4,837.66 were used to establish a diagnostic model for pSS. The proteomic model could distinguish pSS from non-pSS controls (SLE, RA and healthy controls) with a sensitivity of 77.1% and a specificity of 85.5%. The efficacy was confirmed by a blinded validation study.

Two studies detected differently expressed proteins using multiplexed antibody-assay in unstimulated whole saliva and serum (36, 59). Based on a 187-plex-antibody assay, 61 and 55 proteins were differently expressed in unstimulated whole saliva in pSS and RA, respectively, compared to healthy controls (36). A 4-plex and 6-plex biomarker signature was then developed, including IL-4, IL-5 and clusterin, which achieved accurate prediction of an individual group

TABLE 2 Comparative proteomic analysis of saliva, salivary gland tissue and/or blood from patients with pSS patients with RA, SLE, systemic sclerosis, mixed connective tissue disease (MCTD) and poly- and dermatomyositis (1.2).

Author (year)	No. of subjects	Materials and methods	Findings
Peluso G, et al., 2007 (26)	9 pSS 3 RA-sSS 3 SSc-sSS 3 SLE-sSS 9 HC	UWS HPLC-ESI-MS	In 6 of the pSS patients, saliva was collected at 30 minutes, 60 minutes, and 24 hours after taking 5 mg of pilocarpine. Before pilocarpine, 60% of salivary proteins in samples from pSS patients were not identifiable or showed lower levels than those in controls. After 30–60 minutes following pilocarpine treatment, 1/3 of the less represented proteins was found in a similar percentage in pSS and controls. Almost all of the proteins that were detectable at lower levels in pSS compared to controls reached levels similar to those in controls at 30–60 minutes after pilocarpine. The parotid gland proteins had the best response to pilocarpine. PSS patients were characterized by higher α-defensin 1 levels and presence of β-defensin 2. sSS patients showed an intermediate protein profile between that of the pSS patients and HC.
Baldini C, et al., 2011 (28)	59 pSS 40 sSS 61 HC 20 non-pSS, sicca	UWS	15 differently expressed proteins were identified in pSS samples with respect to HC, non-SS sicca, SSc-sSS and RA-sSS. pSS vs. HC: ↑ S100A9, B2M, epidermal fatty acid binding protein (E-FABP), psoriasin (S100A7), immunoglobulin k light chain (IGKC) and α-enolase. ↓ AMY1A, carbonic anhydrase VI (CA6), glyceraldehydes-3-phosphate dehydrogenase (G3PDH), cystatin SN precursor protein (CST1), prolactin-inducible protein precursor (PIP), short palate, lung and nasal epithelium (SPLUNC-2). pSS vs. non-pSS sicca: ↑ PIP, SPLUNC-2 G3PDH, AMY1A, CA6. pSS vs. RA-sSS: ↑ lipocalin. ↓ rheumatoid factor D3 light chain. pSS vs. SSc-sSS: ↓ cystatin.
Li Y, et al., 2014 (50)	60 pSS 50 SLE 50 RA 51 HC	Serum MALDI-TOF-MS	100 differential M/Z peaks associated with pSS were identified (18 were ↑ in pSS). The m/z peaks at 8,133.85, 11,972.8, 2,220.81, and 4,837.66 were used to establish a diagnostic model for pSS which could distinguish pSS from non-pSS controls with a sensitivity of 77.1 % and a specificity of 85.5 %. Its efficacy was confirmed in a blinded testing set with a sensitivity and specificity of 95.5% and 88%, respectively.
Delaleu N, et al., 2015 (36)	48 pSS 12 RA 12 HC	UWS 187-plex capture antibody-based assay	Based on a 187-plex antibody-based assay, 61 and 55 proteins were differentially expressed in pSS and RA, compared to HC. All proteins were upregulated in pSS patients, except FGF-4. Based on 4-plex and 6-plex biomarker signatures, which both included IL-4, IL-5 and clusterin, achieved accurate prediction of an individual's group membership for at least 94% of cases.
Bosello S, et al., 2016 (39)	9 pSS 7 SLE 7 RA 7 sSS/SSc 7 sSS/SLE 7 sSS/RA 7 SSc 10 HC	UWS, MSGB HPLC-ESI-MS (UWS), immunostaining (MSGB)	↑ levels of Tβ4 in pSS compared to other subgroups. Tβ10 detectable in 66,7% of pSS subjects and 42,9% of sSS/SSc patients. Tβ4 sulfoxide detectable in 44,4% of pSS patients and 42,9% of sSS/SSc patients. Tβ4 and Tβ10 not detectable in non-ss associated patients and HC. All patients had immunoreactivity for Tβ10. Tβ4 immunoreactivity was absent in pSS and sSS/RA-patients, but present in sSS/SSc and sSS/SLE-patients. In pSS, salivary Tβ expression was generally overexpressed.
Ohlsson M et al, 2021 (59)	73 pSS (AECG) 39 SLE 46 RA 82 ANCA-SV 77 HC	Serum 393-plex antibody microarray	All 393 antibodies could discriminate between IRD's from HC with an AUC of 0.94. Based on a panel consisting of the 40 best-performing antibodies IRD could be discriminated from HC with an AUC of 0.93. The IRD could also be discriminated from each other with AUC levels ranging from 0.79 to 0.96. 77 analytes, targeted by 114 antibodies were differentially expressed in IRD compared to HC: 326 antibodies targeting 160 analytes for SV, 207 antibodies targeting 127 analytes for SS, 127 antibodies targeting 85 analytes for SLE and 114 antibodies targeting 81 analytes for RA. ↑ immunoregulatory analytes included apolipoprotein, A1, IL-6, IL-12, TNF-alfa, IL-16, osteopontin. Antibodies targeting C3, IL-4, VEGF, SPDLY-1 etc. were ↓. Among the top 25 antibodies, most of the analytes were ↑ in SLE, RA and SS (15, 21 and 25, respectively). The majority of analytes (n = 23) were ↓ in ANCA-SV.
Thiagarajan D et al, 2020 (63)	324 pSS 374 SLE 354 RA 77 MCTD 65 PAPs 118 UCTD, 331 SSc 515 HC	Serum, PBMC ELISA, LC-MS	Significantly lower IgM anti-PC but not anti-MDA was seen in MCTD compared to HC. No significant difference in levels of anti-PC nor anti-MDA was identified between disease groups, but low levels of IgM were more prevalent in MCTD, SLE, SjS, SSc and UCTD, more for anti-PC than anti-MDA.

Arrow up: upregulated.
Arrow down: downregulated.

in at least 94% of the cases (36). Ohlsson et al., 2020 (59) used a 393-plex antibody microarray to test the discriminatory performance in distinguishing between different inflammatory rheumatic diseases (i.e., pSS, SLE, RA and antineutrophil cytoplasmic antibody-associated systemic vasculitis (ANCA-SV) from healthy controls in serum. An analysis including all 393 antibodies could discriminate the patient groups from the healthy controls (HC vs. SLE+RA+SS +SV) with an AUC of 0.94. Serum samples from patients with pSS could be distinguished from the other patient samples (SS vs. SLE +RA+SV) with an AUC of 0.80. A total of 207 antibodies targeting 127 analytes were found to be differentially expressed in patients with pSS compared to healthy controls.

Bosello S. et al. (39) investigated the salivary levels of Tβ4, Tβ10, and Tβ4 sulfoxide in patients with pSS, SLE, RA, SSc, sicca

syndrome + SSc (ss/SSc), sicca syndrome + SLE (ss/SLE), sicca syndrome + RA (ss/RA) and healthy controls. Tβ10 and Tβ4 sulfoxide were not detectable in healthy controls and patients without sicca syndrome. Patients with pSS had higher levels of Tβ4 than the other patient groups. Tβ10 and Tβ4 sulfoxide were detectable in 66.7% and 44.4% of the patients with pSS, respectively. Overall, the patients with pSS displayed highest expression of salivary Tβ, whereas Tβ4 immunoreactivity in minor salivary glands was completely absent in patients with pSS.

3.4 Autoantibodies in patients with SS

Ten studies eligible for inclusion focused on proteomic analysis of serum or salivary autoantibodies in patients with SS (27, 29, 32, 46–51, 55, 56) (Table 3). Anti-SSA and -SSB antibodies are clinically important antinuclear antibodies in patients with SS. However, these antibodies may not be present in all patients with SS, and they may also be found in other inflammatory rheumatic diseases, including SLE, polymyositis and SSc, as well as in patients with

TABLE 3 Proteomic analysis of saliva and/or serum specifically related to autoantibodies in patients with SS and control subjects (1.3).

Author (year)	No. of subjects	Materials and methods	Findings and conclusion
Ottosson L, et al., 2006 (27)	10 pSS	Serum MALDI-TOF-MS	Two structured parts of Ro52 were identified, corresponding to the RING-B-box and the coiled-coil regions. The two subregions were independently structured. Analysis indicated Zn^{2+}-dependent stabilization against proteolysis and functional Zn^{2+}-binding sites in both the RING and the B-box. Oligomerization of the coiled-coil was investigated showing weak homodimer affinity, in parity with other coiled-coil domains involved in regulatory interactions. The findings form a basis for further Ro52 functional studies on the proteome level.
Van den Bergh K, et al., 2009 (46)	93 pSS 6 sSS 147 SLE, RA, scleroderma, polymysitis, MCTD and dermatomyositis	Serum Immunofluorescence, SDS-PAGE, WB, MALDI-TOF/TOF	Recombinant rat heterogeneous nuclear ribonucleoprotein H1 (hnRNP H1) reacted with 48% of sera from pSS patients and 5.2% of 153 sera from patients with other connective tissue diseases. Five of 11 pSS patients with no anti-SSA or -SSB antibodies had anti-hnRNP H1 antibodies. hnRNP H1 was suggested as novel, potential and additional diagnostic marker in pSS.
Hu S, et al., 2011 (32)	48 pSS 47 SLE 47 HC	Whole saliva PhotoArray, ELISA	Identification of 24 potential autoantibody biomarkers that could discriminate patients with pSS from both patients with SLE and healthy subjects. Four saliva autoantibody biomarkers, anti-transglutaminase, anti-histone, anti-SSA, and anti-SSB, were further tested in independent groups of pSS and SLE patients and healthy control subjects and all were successfully validated with ELISA.
Lindop R, et al., 2011 (47)	7 pSS	Serum High-resolution Orbitrap mass spectrometry (MS), 2-DE, ELISA	Proteomic analysis revealed a Ro60-peg-specific IgG1κ-restricted monoclonal autoantibody that was present in the sera of all patients and specified by a V(H)3–23 heavy chain paired with a V(κ)3–20 light chain. The public anti–Ro 60–peg clonotype was specified further by common mutations in the heavy-chain CDR1 and light-chain complementarity-determining regions. Titers and relative affinities of clonotypic IgG did not vary over the course of the disease. The expression of a Ro 60-reactive public B cell clonotype in a subset of patients with pSS as a long-lived, class-switched circulating autoantibody implies a common breach of B cell tolerance checkpoints in these patients.
Arentz G, et al., 2012 (48)	24 pSS 14 HC SLE Polymyositis SSc	Serum 2-DGE, MS	*De novo* sequencing was used to determine the clonality and V region structures of human autoantibodies directed against Ro52 (TRIM21). Anti-Ro52 autoantibodies from patients with pSS, SLE, SSc or polymyositis were restricted to two IgG1 kappa clonotypes that migrated as a single species on isoelectric focusing; shared a common light chain (VK3-20) paired with one of two closely-related heavy chains (VH3-7, VH3-23); and were public in unrelated patients. Targeted mass spectrometry using these uniquely mutated V rion peptides as surrogates detected anti-Ro52 autoantibodies in sera with high sensitivity (87.5%) and specificity (92.9%).
Thurgood LA, et al., 2013 (49)	7 pSS, anti-SSA- and -SSB pos. 2 pSS, anti-SSA pos. and anti-SSB neg. (controls) 1 asymptomic, anti-SSA and -SSB pos. (control) 4 HC	Serum High-resolution Orbitrap mass spectrometry (MS), 2-DE, ELISA	A majority of patients with linked anti-Ro60/Ro52/La responses target an NH2-terminal epitope designated LaA, which is expressed on Ro/La ribonucleoprotein complexes and the surface membrane of apoptotic cells. Autoantibody responses comprised two heavily mutated IgG1 kappa-restricted monoclonal species that were shared (public) across unrelated patients; one clonotype was specified by an IGHV3-30 heavy chain paired with IGKV3-15 light chain, and the second by an IGHV3- 43/IGKV3-20 pairing. Shared amino acid replacement mutations were also seen within heavy and light chain complementarity-determining regions, consistent with a common breach of B cell tolerance followed by antigen-driven clonal selection.
Ohyama K, et al., 2015 (51)	14 pSS 14 SLE 11 HC 7 SSc 7 AAV 7 TA 9 MCTD 8 DM	Serum Nano-LC-MS/MS	468 distinct IC-associated antigens were identified, 62 were disease-specific antigens, and least three disease-specific antigens for each of the 7 autoimmune diseases. Coiled-coil domain-containing protein 158 and spectrin were identified as potential autoantigens important to SSc and SS pathogenesis, respectively; notable titin and spectrin autoantibodies were reportedly found in SSc and SS patients, respectively. The sensitivity of each disease-specific antigen was less than 33%. Immune complexome analysis may be generally applicable to the study of the relationship between ICs and autoimmune diseases.

(Continued)

TABLE 3 Continued

Author (year)	No. of subjects	Materials and methods	Findings and conclusion
Liao CC et al, 2016 (53)	18 pSS 25 RA-sSS, 18 RA 25 HC	Serum Con A affinity chromatography, 1D SDS-PAGE, in-gel digestion, and protein identification by LC-MS/M	In summary, Con A-bound ITIH3 in serum was identified as a robust diagnostic biomarker enabling discriminating RA-sSS from both HC and from pSS and RA alone. The performance of antibody isotypes against citrullinated peptides was generally better than their non-citrullinated/native counterparts, in discriminating between pSS, RA and RA-sSS and, healthy controls.
Wang JJ, et al., 2016 (55)	8 pSS 3 SLE anti-Ro60 pos. 4 HC 2 asymptomatic anti-Ro60 pos.	Serum High-resolution mass spectrometry (MS)	Monospecific anti-Ro60 Igs comprised dominant public and minor private sets of IgG1 kappa and lambda restricted heavy and light chains. Specific IgV amino acid substitutions stratified anti-Ro60 from anti-Ro60/La responses, providing a molecular fingerprint of Ro60/La determinant spreading and suggesting that different forms of Ro60 antigen drive these responses. Sequencing of linked anti-Ro52 proteomes from individual patients and comparison with their anti-Ro60 partners revealed sharing of a dominant IGHV3–23/IGKV3–20 paired clonotype but with divergent IgV mutational signatures. In summary, anti-Ro60 IgV peptide mapping provides insights into Ro/La autoantibody diversification and reveals serum-based molecular markers of humoral Ro60 autoimmunity.
Wang JJ, et al., 2018 (29)	15 RF-positive pSS 5 RF-negative pSS (controls) 30 HC 13 RF-pos + anti-Ro/LA pos. asymptomatic donor	Serum, PBMC Novo mass spectrometric sequencing, IGH repertoire sequencing	RF-specific heavy-chain third complementarity-determining region (CDR3) peptides were identified by searching RF heavy-chain peptide sequences against the corresponding IGH RNA sequence libraries. Heavy-chain CDR3 peptides were used as biomarkers to track serum RF clonotypes using quantitative multiple reaction monitoring. Serum RFs were clonally restricted and composed of shared sets of IgM heavy-chain variable region (Ig VH) 1-69, 3-15, 3-7, and 3-74 subfamilies. Cryoprecipitable RFs from patients with mixed cryoglobulinemia were distinguishable from non-precipitating RFs by a higher frequency of amino acid substitutions and identification of stereotypic heavy-chain CDR3 transcripts. Potentially pathogenic RF clonotypes were detected in serum by multiple reaction monitoring years before patients presented with mixed cryoglobulinemia. Levels of Ig VH4–34 IgM-RF decreased following immunosuppression and remission of mixed cryoglobulinemia.
Burbelo PD, et al., 2019 (56)	20 SS 20 HC 20 ICIS 11 APECED without sicca 9 APECED with sicca	Unstimulated whole saliva, serum	High percentage of autoantibody seropositivity was detected against Ro52, Ro60, and La in SS, whereas few ICIS patients were seropositive. A few APECED patients had autoantibodies to Ro52 and La, but only Ro60 autoantibodies were weakly associated with a small subset of APECED patients with sicca. Additional testing of the salivary panel failed to detect autoantibodies against any of the salivary-enriched proteins in the SS and ICIS patients. However, APECED patients selectively demonstrated seropositivity against BPI fold containing family A member 1 (BPIFA1), BPI fold containing family A member 2 (BPIFA2)/parotid salivary protein (PSP), and lactoperoxidase, 3 salivary-enriched proteins. Moreover, high levels of serum autoantibodies against BPIFA1 and BPIFA2/PSP occurred in 30% and 67% of the APECED patients with sicca, respectively, and were associated with an earlier age onset of oral dryness. These findings highlight the complexity of humoral responses in different sicca diseases and provide new insights and biomarkers for APECED-associated sicca.

primary biliary cirrhosis (PBC) and hepatitis C viral infection (79). Anti-SSA/Ro autoantibodies are the most frequently identified antinuclear antibodies directed against Ro antigens, consisting of two different proteins, Ro60 and Ro52. The Ro 60 kDa autoantigen is an RNA-binding protein, associated with one of several human Y RNAs (small non-coding RNAs, required for DNA replication). Ro52/TRIM21 is an IFN-inducible protein, which is also induced by viral infection (80). Anti-SSB/La also recognizes the Ro-ribonucleoprotein. Anti-Ro52 and anti-Ro60 autoantibodies are closely linked but also display different clinical associations (81). Thus, anti-SSA/Ro52/TRIM21 antibodies show a wider spectrum of disease-associations than anti-SSA/Ro60 antibodies (82). Both Ro antigens have been found expressed in the surface of ductal epithelial salivary gland cells during apoptosis indicating that the initiation of anti-SSA/Ro60 and anti-Ro52/TRIM21 responses play a role of in the pathogenesis of SS (83). In addition, anti-SSA/Ro60- and anti-SSA/Ro52/TRIM21-specific B cells compatible with plasmablasts or plasma cells have been detected in salivary glands of patients with pSS (84). Autoantibodies may be present years before the clinical symptoms of SS, and anti-SSA and anti-SSB antibodies are therefore central biomarker targets that are useful in the diagnosis of SS (85).

Patients having circulating serum autoantibodies often present more symptoms and clinical disease manifestations than patients without presence of circulating antibodies (14). It has been shown that anti-SSA/-SSB negative patients with SS have a lower prevalence of lymphoproliferative lesions and lower risk of developing lymphoma than those who are SSA and/or SSB autoantibody positive (86). Proteomic analyses of serum from patients with pSS have revealed expression of public clonotypic autoantibodies against Ro52/TRIM21 and Ro60 antigens as well as public clonotypic autoantibodies directed against an immunodominant epitope on La (47–49). The findings of shared amino acid replacement mutations within heavy and light chain complementarity-determining regions imply a common breach of B-cell tolerance checkpoints that is followed by an antigen-driven clonal selection (48, 49). Accordingly, the findings support that the humoral immune responses against protein-RNA complexes are mediated by public sets of autoreactive B-cell clonotypes leading to systemic autoimmunity. Moreover, anti-Ro52 serum autoantibodies from patients with pSS, SLE, systemic sclerosis and polymyositis were restricted to two IgG1/kappa clonotypes, and targeted mass spectrometry detected anti-SSA/Ro52 serum autoantibodies with high sensitivity and specificity compared with conventional ELISA-

technique (48). Further analysis using high-resolution mass spectrometry to sequence precipitating anti-Ro60 proteomes revealed that specific immunoglobulin variable-region peptide signatures stratified anti-Ro60 from anti-Ro60/La responses, indicating that different forms of Ro60 antigen drive the humoral Ro60 immune responses (55).

An earlier study including an immunologic analysis of the stable protein regions in sera from patients with SS showed that immunodominant epitopes predominantly are localized in the structurally stable parts of Ro52 (27). Apparently, the findings have not been substantiated by further functional studies at the proteome level.

A more recent study reported a high percentage of autoantibodies against Ro52, Ro60, and La in SS, whereas only a few patients with immune checkpoint inhibitor-induced sicca (ICIS) presented with these autoantibodies. Further testing of the salivary panel did not reveal autoantibodies against any of the salivary-enriched proteins in patients with SS and ICIS (56).

Another recent study identified antibodies against heterogeneous nuclear ribonucleoprotein H1 (hnRNP H1) in serum from about 43% patients with SS (2 primary and 5 secondary) and in about 8% patients with various autoimmune connective tissues diseases, all being ANA-positive (titer >1:160). Interestingly, 45% (5/11) of the anti-SSA/anti-SSB sero-negative patients had anti-hnRNP H1 antibodies. Thus, anti-hnRNP H1 antibody represents a potential novel diagnostic marker that can be helpful in discriminating patients with pSS from patients with SLE (potentially with sSS) (46).

Hu et al. (32) identified 24 potential salivary autoantibody biomarkers that can discriminate patients with pSS from both patients with SLE and healthy subjects. Four of them, including anti-transglutaminase, anti-histone, anti-SSA and anti-SSB antibodies, were successfully validated by means of ELISA, and on independent groups of patients with pSS, SLE, and healthy control subjects (32).

A study on molecular profiling and clonal tracking of secreted rheumatoid factors (RF) in pSS found that cryoprecipitable RF clonotypes linked to vasculitis in pSS display different molecular profiles than non-precipitating RFs. Interestingly, potentially pathogenic RF clonotypes were detected in serum by multiple reaction monitoring years before patients presented with mixed cryoglobulinemia. Furthermore, levels of Ig VH4-34 IgM-RF diminished after immunosuppression and remission of cryoglobulinemia (29).

Liao et al. (53) found serum autoantibodies against the citrullinated-inter-alpha-trypsin inhibitor heavy chain (ITIH3)$^{542-556}$ peptide in serum in patients with pSS, RA and RA-sSS. IHIT3 is one of five chains that comprises the family of inter-alpha-trypsin inhibitors (ITI), which have the ability to bind to hyaluronic acid (HA) to interact with inflammatory cells (87). Thus, the ITIH3-HA complex is potentially involved in inflammatory diseases such as RA and pSS (88). Previous studies have reported PTM (post-translational modification)-modified proteins in patients with pSS such as citrullinated Ro60 and histone 1 (89). Furthermore, salivary antibodies against cyclic citrullinated peptide (anti-CCP), a proxy for anti-citrullinated protein antibodies (ACPA), have been identified in patients with pSS (90), suggesting that citrullinated proteins can be a utilized as diagnostic biomarkers. Liao et al. (53) found that Concanavalin A (Con A)-bound ITIH3 in serum was a robust diagnostic biomarker enabling discriminating RA-sSS from both healthy controls and from pSS and RA alone. The performance of antibodies against citrullinated peptides was generally better than antibodies against their non-citrullinated/native counterparts in discriminating between pSS, RA and RA-sSS and healthy controls. In addition, we have previously found that anti-SSA alone can differentiate pSS from non-pSS with an AUC of 0.9, while combining the presence of anti-SSA positivity with the upregulation of TRIM29 protein marker raised the AUC to 0.995 with both sensitivity and specificity between 91%-100% (91).

3.5 Proteomic analysis of saliva and salivary gland tissue in SS patients with and without non-Hodgkin MALT lymphoma

Patients with SS, and particularly with pSS, have an increased risk of developing lymphoproliferative malignancy. About 5-10% of the patients develop non-Hodgkin lymphoma (NHL), most commonly the mucosa-associated lymphoid tissue (MALT) B-cell lymphoma type (92–94). Risk factors include swelling of the parotid gland, vasculitis, hypergammaglobulinemia, CD4+ T lymphocytopenia, low CD4+/CD8+ T-cell ratio, low complement protein levels, cryoglobulinemia and high focus score and ectopic germinal center formation in the salivary gland tissue (92, 94). The mechanisms underlying malignant transformation of a lymphoproliferative process remain elusive.

Three studies on proteomic analysis of saliva and salivary gland tissue were eligible for inclusion in this review (41, 42, 44) (Table 4). Hu et al. (44) aimed at clarifying differences in gene expression and proteomic profile in parotid gland tissue from patients with pSS, patients with pSS and MALT lymphoma and non-pSS control subjects (patients with oral or oro-pharyngeal squamous cell carcinoma). Six highly associated hub genes (i.e., genes involved in proteasome degradation, apoptosis, signal peptides, complement activation, cell growth and death and integrin-mediated cell adhesion, and major histocompatibility (MHC) genes) distinguished patients with pSS from non-pSS control subjects. Eight hub genes (i.e., genes involved in translation, ribosome, protease degradation, signal peptides (MHC) class I, G13 signaling pathway, complement activation, and integrin-mediated cell adhesion) distinguished pSS patients with MALT from pSS patients. A total of 115 proteins were upregulated in patients with pSS and pSS/MALT lymphoma. Twenty-five proteins were upregulated in both pSS groups compared to non-pSS control patients, 20 proteins were upregulated in pSS compared to pSS/MALT and non-pSS control patients, and 70 proteins were upregulated in pSS/MALT compared to pSS and non-pSS control patients. The identified disease hub genes represent promising targets for therapeutic intervention, diagnosis, and prognosis (44).

Cui et al. (41) found α-enolase, cofilin-1, annexin A2 and Rho GDP-dissociation inhibitor 2 (RGI2) overexpressed in parotid gland tissue from patients with pSS and in patients pSS and

TABLE 4 Proteomic analysis of saliva and salivary gland tissue in SS patients with and without non-Hodgkin MALT lymphoma.

Author (year)	No. of subjects	Materials and methods	Findings
Hu S. et al., 2009 (44)	9 pSS 6 pSS/MALT 8 non-pSS controls	Parotid gland tissue 2-DGE, Weighted gene co-expression network analysis (WGCNA)	Six highly associated hub genes (involved in proteasome degradation, apoptosis, signal peptides (MHC) class I, complement activation, cell growth and death, and integrin-mediated cell adhesion) distinguished pSS from non-pSS control subjects. Eight hub genes (involved in translation, ribosome, protease degradation, signal peptides (MHC) class I, G13 signaling pathway, complement activation, and integrin-mediated cell adhesion) distinguished pSS/MALT from pSS.
Cui L. et al., 2017 (41)	6 pSS 6 pSS/MALT 6 HC	SWS 2-DGE/MS, ELISA	↑ α-enolase, cofilin-1, annexin A2 and Rho GDP-dissociation inhibitor 2 (RGI2) in pSS and pSS/MALT. ↑ α-enolase, cofilin-1 and RGI2 in pSS/MALT compared to pSS. The combination of the latter 3 antibodies yielded AUC 0.94 (86% sensitivity, 93% specificity in pSS vs HC) and AUC 0.86 (75% sensitivity, 94% specificity in pSS vs pSS/MALT)
Jazzar AA. et al., 2018 (42)	14 pSS/MALT (SS-M) 18 pSS high-risk of MALT (SS-HR) 19 pSS low-risk of MALT 19 pSS non-risk 14 SNOX, 18 HC	UWS parotid saliva LC-MS/MS ELISA	↑ levels of S100A8(calgranulin A) and S100A9 (calgranulin B) in parotid saliva of SS-HR and SS-M patients compared to HC. ↑ levels of S100A8/A9 in UWS in SS subgroups compared to HC and SNOX. The median concentration in SS-M were higher than in HC, SNOX and non-risk pSS patients. S100A8 and -A9 were 20-fold higher in UWS than parotid saliva.

MALT (41). Moreover, the levels of anti-α-enolase, anti-coffilin-1, and anti-RGI2 antibodies were higher in patients with pSS/MALT than in patients with pSS and healthy subjects, and significantly higher in pSS patients than in healthy subjects (41). The combination of the three antibodies yielded an AUC of 0.94 with an 86% sensitivity and 93% specificity in distinguishing patients with pSS from healthy controls, an AUC of 0.99 with a 95% sensitivity and 94% specificity in distinguishing patients with pSS and MALT lymphoma from healthy controls, and an AUC of 0.86 with a 75% sensitivity and 94% specificity in distinguishing patients with pSS and MALT from patients with pSS (41) (Table 4). The combination of these autoantibodies may be helpful in the diagnosis of pSS and prediction of development into MALT lymphoma.

Another study investigated the potential of S100A8 (Calgranulin A) and S100A9 (Calgranulin B) as biomarkers to discriminate patients with pSS from healthy subjects and patients with pSS from patients with pSS and MALT lymphoma (42). The levels of S100A8 and S100A9 were upregulated in parotid saliva from patients with pSS compared to healthy controls. In addition, the levels of S100A8 and S100A9 were upregulated in unstimulated whole saliva of patients with pSS, pSS/MALT compared to healthy controls and disease controls (patients with non-specified sialadenitis). Furthermore, the levels were higher in pSS patients with MALT lymphoma and pSS patients with high lymphoma risk than in pSS patients with low risk of lymphoma, healthy subjects and disease controls. Interestingly, S100A8 and S100A9 levels were 20-fold higher in unstimulated whole saliva than in parotid saliva. These findings suggest that S100A8 and S100A9 can assist in distinguishing pSS patients from healthy subjects and pSS patients with MALT lymphoma from pSS without lymphoma (42) (Table 4). S100A8 and S100A9 are proinflammatory proteins that play a central role in the acute and chronic inflammation. They have been found associated with autoimmune diseases and upregulated in various human cancers (117, 118).

3.6 MiRNA analysis of blood, PBMC, saliva and salivary gland tissue

MicroRNAs (miRNAs) are short non-coding RNA molecules, which main function is to regulate gene expression posttranscriptionally by messenger (mRNA) degradation or translational repression (119). Previous findings indicate aberrant miRNA expression in PBMC (96, 98, 99, 102, 104, 109, 120) and salivary gland tissue of patients with pSS (95, 97, 121). However, the number of publications within the field of miRNA expression profiling is increasing, revealing novel biomarkers of interest.

All studies except one used a cross-sectional design, which was a longitudinal study (108) (Table 5). In 16 studies, the miRNA analysis was performed on plasma, serum or peripheral mononuclear blood cells (PMBC). Six studies included miRNA analysis on salivary gland tissue. We have previously performed combined miRNA analyses on whole saliva, plasma and minor salivary gland tissue (114), and Gourzi et al. (101) combined miRNA analyses on PBMC, minor salivary gland tissue and salivary gland epithelial cells.

As with the proteomics studies, the findings in the 23 studies were very heterogeneous in terms of number and type of differentially expressed miRNAs. Nevertheless, several studies

TABLE 5 miRNA analysis of plasma, serum, PBMC, saliva and salivary gland tissue.

Author (year)	No. of subjects	Material and methods	Findings
Alevizos I, et al., 2011 (95)	16 pSS 5 HC 1 non-pSS, sicca 1 myositis 1 peripheral neuropathy	MSGT RT-qPCR	MiRNA expression patterns in minor salivary gland tissue accurately distinguished pSS patients from healthy controls. Validation of miR-768-3p and miR-574 in an independent cohort revealed increased expression of miR-768-3p, and decreased expression of miR-574 with an increasing focus score. Comparison of miRNAs from patients with preserved or low salivary flow identified a set of differentially expressed miRNA, most of which were increased in in the group with decreased salivary gland function, suggesting that the targets of miRNA may have a protective effect on epithelial cells.
Zilahi E, et al., 2012 (96)	21 pSS 10 HC	PBMC qRT-PCR	Increased expression of miR-146a and miR-146b and the gene of TRAF6 in patients with pSS compared to healthy controls. Decreased expression of IRAK1 gene suggests transcriptional repression of IRAK1 in PBMC of pSS patients, whereas the other NF-κB pathway-regulating gene, TRAF6, is overexpressed.
Tandon M, et al., 2012 (97)	6 pSS 3 HC	MSGT qPCR	Six previously unidentified miRNA sequences (hsa-miR-4524b-3p, hsa-miR-4524b-5p, hsa-miR-5571-3p, hsa-miR-5571-5p, hsamiR-5100, and hsa-miR-5572) found in patient samples and in several cell lines. Validation of hsa-miR-5100 showed decreased expression in pSS patients with low salivary flow rates.
Peng L, et al., 2014 (98)	33 pSS 10 HC	PBMC Microassay, qRT-PCR	202 miRNA were upregulated and 180 were downregulated in pSS patients compared to healthy controls. MiR-181a differed most profoundly. No difference in miRNA-181a expression between patients with different disease phenotypes.
Shi H, et al., 2014 (99)	27 pSS 22 HC	PBMC RT-PCR	Higher expression levels of miR-146a in patients with pSS than in healthy controls, and levels correlated with the VAS scores for parotid swelling and dry eyes). Low miR-155 expression level in the patients with pSS, levels correlated with the VAS score for dry eyes.
Chen JQ, et al., 2015 (100)	23 pSS 10 HC	PBMC RT-PCR	MiR-155 is regarded as a central modulator of T-cell responses. This study evaluated the expression rate of miR-155 and its functional linked gene (SOCS1). MiR-155 and SOCS1 gene was both overexpressed in the PBMC of patients with pSS. However, there was no significant correlation between expression values of SOCS1 and miR-155 in the pSS patients.
Gourzi VC, et al., 2015 (101)	29 pSS 24 non-pSS, sicca	PBMC, MSG tissue, SGEC RT-PCR	Higher levels of miR16 in minor salivary gland tissue of miR200b-3p in salivary gland epithelial cells and miR483-5p in PBMCs from pSS patients than in non-pSS, sicca controls. Levels of let7b, miR16, miR181a, miR223 and miR483-5p correlated with Ro52/TRIM21-mRNA. MiR181a and miR200b-3p correlated negatively with Ro52/TRIM21 and Ro60/TROVE2 mRNAs in salivary epithelial cells, respectively, whereas let7b, miR200b-5p and miR223 correlated with La/SSB-mRNA. In PBMCs, let7b, miR16, miR181a and miR483-5p correlated with Ro52/TRIM21, whereas let7b, miR16 and miR181a correlated with La/SSB-mRNA expression. Lower levels of miR200b-5p in pSS patients with MALT-lymphoma than in those without.
Willams AEG, et al., 2016 (102)	21 pSS 9 sSS 17 SLE 18 RA 17 HC	PBMC CD4+ qRT-PCR	Higher levels of miRNAs monocytes from patients with SS than in healthy controls. MiR-34b-3p was differentially expressed between SS patients and healthy controls and RA. Higher levels of miR4701-5p and miR-3162.3p in SS patients. QRT-PCR supported co-regulation of miR-34b-3p, miR-4701-5p, miR-609, miR-300, miR-3162-3p, and miR-877-3p in SS monocytes (43%) in comparison with SLE (5.8%) and RA (5.6%). MiRNA-target pathway predictions identified SS-associated miRNAs appear to preferentially target the TGFβ signaling pathway as opposed to the IL-12 and Toll-like receptor/NFkB-pathways.
Yan T, et al., 2017 (103)	57 pSS - group 1: FS=1 - group 2: FS=2 - group 3: FS=3 13 HC	MSGT qRT-PCR	The differences between HC and the 3 pSS subgroups were statistically significant for positive findings of salivary flow rate, Schirmer test and laboratory indices. In LMSG tissues: expression level of miR-18a was ↑ in patients of the 3 pSS subgroups compared to HC, while expression level of miR-92a was ↓. MiR-18a was progressively ↑ along the advanced histological stages of the 3 pSS subgroups, while the miR-92a was progressively ↓. There was no notable difference in the expression levels of miR-17, miR-19a, miR-19b, and miR-20a.
Chen JQ, et al., 2017 (104)	8 pSS 8 SLE 7 HC	Peripheral blood Illumina next-generation sequencing	135 miRNA and 26 miRNAs showed altered expression in SLE and pSS, respectively, compared to HC. The 25 miRNAs including miR-146a, miR-16 and miR-21, which were over-expressed in pSS patients, were also found to be elevated in SLE group. miR-150-5p was ↓ in pSS. Levels of several miRNAs over-expressed in SLE, were not changed in pSS, such as miR-148a-3p, miR-152, miR-155, miR-223, miR-224, miR-326 and miR-342. Expression levels of miR-223-5p, miR-150-5p, miR-155-5p and miR-342-3p, which miRNAs are potentially linked to B cell functions, showed associations with the B cell proportions within PBMC.
Jiang Z, et al., 2017 (105)	60 pSS 53 RA 23 HC 45 SSc 49 DM 11 PM	PBMC qRT-PCR	The miR-200c level in the SSc group was significantly ↑ than in the DM/PM, pSS, and RA groups, and the levels in the DM/PM and pSS groups were significantly ↑ than in the RA group. The level of miR-200c in the CTD+ILD group was significantly ↑ than in the CTD–ILD group, and the level in the severe ILD group was significantly ↑ than in the mild ILD group. FVC and FEV1 were significantly different among the different CTD groups, and among the different CTD+ILD groups. There was a negative correlation between the level of miR-200c and FVC and FEV1.

(Continued)

TABLE 5 Continued

Author (year)	No. of subjects	Material and methods	Findings
Lopes AP, et al., 2018 (106)	37 pSS 17 HC 21 non-pSS, sicca	Serum RT-qPCR	10 sncRNAs were differentially expressed between the groups in the array. In the validation cohort, the ↑ expression of U6-snRNA and miR-661 in the iSS group as compared to HC was confirmed, but none of the differentially expressed sncRNA from the discovery cohort were validated in the validation cohort. However, within this group several miRNAs correlated with laboratory parameters. Unsupervised clustering distinguished three clusters of pSS patients. Patients in one cluster showed ↑ serum IgG, prevalence of anti-SSB, IFN-score, and ↓ leukocyte counts compared to the two other clusters. Patients with pSS, being anti-SSA/-SBB positive, showed ↓ expression of several sncRNAs when compared to antibody-negative patients with pSS.
Kapsogeorgou EK, et al., 2018 (107)	79 pSS - 27 low-risk who did not develop lymphoma during follow-up. - 17 high risk diagnosed with NHL during follow up, 35 SS-associated lymphoma. 8 non-pSS sialadenitis - 4 associated with sarcoidosis - 4 associated with HCV infection.	MSGT qPCR	The MSG levels of miR200b-5p were significantly ↓in pSS patients, who will develop or have NHL, and strongly discriminated ($p<0.0001$) them from those without lymphoma or non-SS sialadenitis. Furthermore, they were reduced long before clinical onset of lymphoma, did not significantly change on transition to lymphoma and, importantly, were proved strong independent predictors of patients, who will develop NHL ($p<0.0001$). MiR200b-5p levels correlated negatively with ESSDAI and biopsy focus score, and positively with serum C4 levels.
Jiang CR, et al., 2018 (108)	70 pSS 60 HC	PBMC qRT-PCR	The expressions of miR-146a and miR-4484 in the pSS group were significantly ↑ compared to HC. After treatment, the expressions of miR-146a and miR-4484 were significantly ↓ compared with those before treatment ($p<0.05$). Combined detection of miR-146a and miR-4484 was superior to single index detection in the diagnosis and prognosis of pSS ($p<0.05$). The 3-years follow-up showed that the incidences of renal injury and pulmonary interstitial lesion in patients with low miR-146a and miR-4484 expressions were significantly lower than those with high expressions ($p<0.05$). No significant differences in the survival rate between the two groups ($p>0.05$).
Wang-Renault SF, et al., 2018 (109)	Discovery cohort: 17 pSS, 15 HC Replication cohort: 27 pSS 12 HC	Purified B- and T lymphocytes RT-qPCR	In CD4+ T-cells, hsa-let-7d-3p, hsa-miR-155-5 p, hsa-miR-222-3 p, hsa-miR-30c-5p, hsa-miR-146a-5p, hsa-miR-378a-3p and hsa-miR-28-5 p were significantly differentially expressed in both cohorts. In B cells, hsa-miR-378a-3p, hsa-miR-222-3 p, hsa-miR-26a-5p, hsa-miR-30b-5p and hsa-miR-19b-3p were significantly differentially expressed. Potential target mRNAs were enriched in disease relevant pathways. There was an inverse correlation between expression of BAFF and hsa-miR-30b-5p in B cells from pSS patients. Functional experiments showed increased expression of BAFF after inhibiting hsa-miR-30b-5p.
Wang J, et al., 2019 (110)	20 pSS 20 HC	PBMC qRT-PCR, Western Blot, ELISA	Expression of miR-let-7d-3p was dramatically regulated in CD4+ T cells from pSS-ptt. Expression of miR-let-7d-3p was negatively correlated with the expression of IL-17 in pSS patients on both mRNA and protein levels. Besides, the AKT1/mTOR signaling pathway was found critical for miR-let-7d-3p-mediated IL-17 expression. AKT1 was proved to be the direct target of miR-let-7d-3p; miR-let-7d-3p targeted AKT1 to bridge the regulation of IL-17. It was also verified that AKT1 co-expression could rescue IL-17 downregulation caused by miR-let-7d-3p.
Hillen MR, et al., 2019 (111)	30 pSS 16 HC	Peripheral blood OpenArray Q-PCR-based technique	20 miRNAs were differentially expressed at a lower level in pSS pDCs compared with HC pDCs. Differential expression of 10 miRNAs was confirmed in the replication cohort (miR-29a and miR-29c showed the most robust fold-change difference between pSS and HC). The dysregulated miRNAs were involved in phosphoinositide 3-kinase-Ak strain transforming and mammalian target of rapamycin signaling, as well as regulation of cell death. In addition, a set of novel protein targets of miR-29a and miR-29c were identified, including five targets that were regulated by both miRs (FSTL1, CASP7, CD276, SEPINH1, F11R).
Gallo A, et al., 2019 (112)	5 pSS (high salivary	MSGT In silico	126 out of 754 miRNA were significantly deregulated in pSS vs. HC, with a trend that was inversely proportional with the impairment of salivary flow rates. In silico approach pinpointed several upregulated miRNA in patients with pSS

(Continued)

TABLE 5 Continued

Author (year)	No. of subjects	Material and methods	Findings
	flow) 6 pSS (low salivary flow) 5 non-pSS, sicca	analysis, Human glycosylation-RT2 Profiler PCR array.	target important genes in the mucin O-glycosylation. This was confirmed by RT-qPCR highlighting downregulation of some glycosyltransferase and glycosidase genes in pSS samples compared to HC, such as GALNT1, responsible for mucin-7 glycosylation.
Talotta R, et al., 2019 (113)	28 pSS 23 HC	UWS, plasma miRNA RT-qPCR	No significant difference in salivary miRNA expression between patients and HC. Patients with SS had higher expression of salivary miR146a than HC. Salivary miR146b was significantly more expressed in the ptt. with worse ESSPRI scores (p=0.02), whereas salivary miR17 and 146b and plasma miR17 expression was ↓ in the patients with higher ultrasound scores (respectively p=0.01, p=0.01 and p=0.04). Salivary miR18a expression was significantly ↑ in the patients who were anti-La/SSB positive (p=0.04). Neither salivary nor plasma miRNAs correlated with disease duration or concomitant therapies.
Sembler-Møller M, et al., 2020 (114)	24 pSS 16 non-pSS, sicca	WS, plasma, MSGT miRNA RT-qPCR	In saliva 14 miRNAs were significantly differentially expressed between pSS and non-pSS; 11 of these were downregulated incl. the miR-17 family in pSS. In MSGT of pSS-ptt. miR-29a-3p was significantly upregulated. Plasma miRNAs did not differ between the two groups. The combination of miR-17-5p and let-7i-5p in saliva yielded an AUC of 97% (CI 92%-100%). Several miRNAs correlated significantly with one another and with salivary flow rates and histopathology.
Yang Y, et al., 2020 (115)	8 pSS X? HC	MSGT RT-qPCR, western blot, Annexin-V-FITC, TUNEL	TRIM21-targeting miRNAs were identified, miR-1207-5p and miR-4695-3p. Transfection of miR-1207-5p or miR-4695-3p mimics lower expression of TRIM21 and the levels of pro-apoptotic genes BAX, CASP-9 and CASP-8, leading to antiapoptotic phenotypes in HSG cells. Consistent with the antiapoptotic activity, transfection of microRNA inhibitors ↑ the expression of TRIM21 and led to a pro-apoptotic phenotype. Thus, proposing that miR-1207-5p and miR-4695-3p are antiapoptotic microRNAs functioning through apoptosis pathway. Assays performed with MSGT revealed ↓ of miR-1207-5p and miR-4695-3p + ↑ of TRIM21 and pro-apoptotic CASP-8 gene in pSS patients.
Gong B, et al., 2021 (116)	13 pSS 13 HC	PBMC RT-qPCR	The numbers of aberrant miRNAs in pSS naïve (vs. healthy naïve), pSS activation (vs. pSS naïve), MSC treatment and pre–IFN–γ MSC treatment (vs. pSS activation) groups were 42, 55, 27 and 32, respectively. Gene enrichment analysis revealed 259 pathways associated with CD4+ T cell stimulation, and 240 pathways associated with MSC treatment. Increased miRNA–7150 and miRNA–5096 and ↓ miRNA–125b–5p and miRNA–22–3p levels in activated CD4+ T cells from patients with pSS were reversed by MSC treatment. Notably, the proliferation of CD4+ T cells and CD4+ IFN–γ+ cells, expression levels of miRNA–125b–5p and miRNA–155 in CD4+ T cells and supernatant IFN–γ secretion were associated with disease activity. MiRNA may play a vital role in MSC treatment for activated CD4+ T cells.

Arrow up: upregulated.
Arrow down: downregulated.

identified similar miRNAs to be differentially expressed such as miR-146, miR-155 and miR-188.

A study by Zilahi et al. (96) found both miR-146a and miR-146b to be significantly overexpressed in patients with pSS compared to healthy controls inPBMC. Two additional studies (99, 108) supported these findings displaying a higher expression of miRNA-146a in patients with than in healthy controls in PBMC. Wang-Reanult et al. (109) found miR-146a to be differentially expressed in CD4+ T cells. Moreover, miR-146a has been found upregulated in saliva in patients with pSS and in addition, miR-146b levels correlated with ESSPRI scores, while being downregulated in patients with high salivary gland ultrasound scores (113).

MiR-155 is a central modulator of T-cell responses, and SOCS1 is its functional linked gene (100). Shi H et al. (99) reported a lower expression of miR-155 in patients with pSS. Furthermore, miR-155 correlated with VAS score for dry eyes. On the other hand, Chen et al. (100) reported higher expression of both miR-155 and SOCS1 gene in PBMC in patients with pSS. In another study, miR-155 was higher expressed in patients with SLE, but unchanged in patients with pSS (104). In a recent study, the expression levels of miR-155 and miR-125b-5p in CD4+ T cells were found associated with disease activity (116). These findings may provide insight in the pathogenesis and disease course of SS and suggest a novel target for treatment.

We identified a downregulation of several miR-17 family members (i.e. miR-17-5p, miR-106a, miR-106b, and miR-20b-5p) in patients with pSS compared to non-pSS subjects (114), which confirms the results of previous studies (109, 119, 121). The miR-17-family takes part in the miR-17-92 cluster, previously shown to be related to carcinogenesis and autoimmunity (122). In addition, we previously found upregulation of let-7i-5p in patients with pSS that was inversely correlated with salivary flow rates and positively correlated with higher focus score, suggesting that let-7i-5p canbe used as a marker for disease activity/advanced disease state (114).

Gourzi et al. (101) determined the levels of miR-181a among other miRNAs in minor salivary gland tissue and epithelial cells and PBMC in patients with pSS and non-pSS, sicca. The levels of miR-181a, let7b, miR-16 and miR-483-5p in minor salivary gland tissue correlated with Ro52/TRIM21-mRNA. On the contrary, riR181a and miR-200b-3p correlated negatively with Ro52/TRIM21 and Ro60/TROVE2-mRNA in salivary gland epithelial cells, respectively. Let7b, miR-200b-5p and miR-233 correlated with La/SSB-mRNA. In PMBCs, miR181a, miR-16 and let7b correlated with both Ro/52-TRIM21- and La/SSB-mRNA

expression (101). It has previously been shown that miR-200b-5p correlate inversely with ESSDAI and focus score in labial salivary gland biopsies, and positively with serum C4 levels (107). Furthermore, Kaspsogeorgou et al. (107) found lower expression of miR-200b-5p in pSS patients with NHL or with a high risk of developing NHL compared to patients with pSS without lymphoma and patients with non-pSS sialadenitis. In fact, the levels of miR200b-5p were lower long before clinical onset of lymphoma and were proved to be strong independent predictor of patients who will develop Non-Hodgkin's lymphoma (NHL). These findings suggest that levels of miR-200b-5p in minor salivary gland tissue may represent a predictive biomarker for development of SS-associated NHL.

Lopes et al. (106) investigated serum levels of 758 small non-coding RNAs (snRNA) including miRNAs in patients with pSS, non-pSS sicca and healthy controls. Three and nine sncRNAs were differentially expressed in the pSS-group and non-pSS sicca-group, respectively, compared to healthy controls. Two of the sncRNAs, including, U6-snRNA and miR-29c-3p, were differently expressed in both patient groups. Interestingly, the abundance of several of the differentially expressed snRNAs correlated with laboratory parameters and disease activity (i.e., low C3/C4, decreased leukocyte count, high focus score and anti-SSA/Ro and/or anti-SSB/La).

Furthermore, the specific pattern of snRNA expression could identify different disease phenotypes within the pSS group. Hierarchical clustering was performed to subgroup the pSS patients into 3 clusters based on their expression of the nine sncRNAs. One group (cluster 3) presented with an increased disease activity, including increased IgG levels, autoantibody positivity and IFN-score in their serum, decreased leukocyte count and furthermore, an overall decreased in the expression of all nine sncRNAs compared to the two other groups. It was concluded that no snRNAs could discriminate pSS from non-pSS sicca. However, the snRNA levels may reflect the disease activity and can be used to identify pSS patients with increased B cell hyperactivity. Hillen et al. (111) supported the findings of differentially expressed miR-29c as they reported miR-29a and miR-29c to be significantly downregulated in plasmacytoid dentritic cells (pDC) from patients with pSS compared to healthy controls.

Gallo et al. (112) found a higher expression of miR-18b, miR-20a, miR-106 and miR-146b in minor salivary gland tissue from patients with pSS than in those of healthy controls. These miRNAs correlated inversely with salivary flow rates. MiR-635 and miR-372 were downregulated and correlated positively with salivary flow rates. The most significant pathways that could be targeted by the 100 most regulated miRNA (>2 fold change) in minor salivary gland biopsies from the patients with pSS included the KEGG and mucin type O-glycan biosynthesis pathways. It is well-known that mucins are important for the rheological properties in saliva (123, 124). Interestingly, a glycosylation profiling analysis on salivary samples from pSS and healthy controls revealed deregulation of some glycosyltransferases and glycosidases suggesting that an alteration of miRNA-target genes in the mucin type O-glycan biosynthesis may influence the glycosylation of salivary mucins and salivary functions in pSS (112).

Two TRIM21-targeting miRNAs, miR-1207-5p and miR-4695-3p, have previously been identified (115), and their role in the development of pSS has been investigated using human submandibular gland cells. Transfection of miRNA mimics into human submandibular gland cells revealed downregulation of mRNA to 53% and 42% for miR-1207-5p and miR-4695-3p, respectively. The expression of TRIM21 was also downregulated to 18% and 33% for miR-1207-5p and miR-4695-3p, respectively. Additionally, upregulation of TRIM21 was seen after transfection of miRNA inhibitor. Findings indicate that miR-1207-5p and miR-4695-3p are anti-apoptotic in human submandibular glands cells and regulate the expression of TRIM21 and multiple pro-apoptotic genes in salivary glands (115). In pSS, an upregulated expression of TRIM21 due to decreased miR-1207-5p and miR-4695-3p may lead to upregulation of the CASP-8 and ultimately facilitates the minor salivary glands cells to undergo apoptosis (115).

Peng et al. (98) found 180 miRNAs upregulated and 202 miRNAs were downregulated in PBMC from patients with pSS. Eleven of these (miRNA-let-7b, miRNA-142-3p, MiRNA-142-5p, miRNA-146a, miRNA-148b, miRNA-155, miRNA-18b, miRNA-181a, miRNA-223, miRNA-23a and miRNA-574-3p) are involved immune regulatory mechanisms. MiR-181a was the most significant differentially expressed miRNA in patients with pSS compared to healthy controls. MiRNA-181a only correlated with ANA, suggesting that PBMC miRNA-181a is a potential biomarker to distinguish pSS from healthy controls, but cannot be used to discriminate between different disease phenotypes.

4 Conclusion

Overall, the proteomic and miRNA studies revealed considerable variations with regard to candidate biomarker proteins and miRNAs, most likely due to variation in collection method, sample size, processing and analytical methods, but also reflecting the complexity of SS and patient heterogeneity. Furthermore, the high rate of salivary posttranslational modifications such as glycosylation, phosphorylation, sulfation, transglutaminase and proteolytic cleavages adds structural and functional diversity to the proteome, which may challenge interpretation of the data. It should also be noted that while serum-derived proteins in saliva are mainly involved in cell cycle, signal transduction etc., salivary proteins and peptides are involved in antibacterial activity, lubrication, digestion, oral homeostasis and more likely express local changes and thus better reflect changes/diseases in the oral cavity.

Nevertheless, interesting novel knowledge has emerged and several studies support the findings of differential expression of certain proteins such as upregulation of cystatin A, β2M, α-enolase,

actin, E-FABP, N-GAL, Ig-κ light-chain and C3 as well as downregulation of PRPs, CA6, α-amylase, histatins, PIP, cystatin S and cystatin SN. Another novel finding was the discriminatory performance of an anti-SSA/Ro combined with TRIM29, which showed a higher sensitivity than anti-SSA/Ro positivity alone. However, further validation with larger multicenter studies is needed to confirm their potential role as biomarkers in SS.

Data availability statement

The original contributions presented in the study are included in the article/supplementary material. Further inquiries can be directed to the corresponding author.

Author contributions

SK and AP: Contributed with conception of the work, data acquisition, prepared the figures and tables, and drafted the manuscript. SK, AP, MS-M, and CN critically reviewed and edited the final version of the manuscript. All authors contributed to the article and approved the submitted version.

Conflict of interest

The authors declare that the research was conducted in the absence of any commercial or financial relationships that could be construed as a potential conflict of interest.

Publisher's note

References

1. Fox RI. Sjögren's syndrome. *Lancet* (2005) 366(9482):321–31. doi: 10.1016/S0140-6736(05)66990-5

2. Brito-Zerón P, Baldini C, Bootsma H, Bowman SJ, Jonsson R, Mariette X, et al. Sjögren syndrome. *Nat Rev Dis Primers.* (2016) 2:16047. doi: 10.1038/nrdp.2016.47

3. Ramos-Casals M, Brito-Zerón P, Kostov B, Sisó-Almirall A, Bosch X, Buss D, et al. Google-Driven search for big data in autoimmune geoepidemiology: analysis of 394,827 patients with systemic autoimmune diseases. *Autoimmun Rev* (2015) 14 (8):670–9. doi: 10.1016/j.autrev.2015.03.008

4. Shimizu T, Nakamura H, Kawakami A. Role of the innate immunity signaling pathway in the pathogenesis of sjögren's syndrome. *Int J Mol Sci* (2021) 22(6):3090. doi: 10.3390/ijms22063090

5. Verstappen GM, Kroese FGM, Bootsma H. T Cells in primary sjögren's syndrome: targets for early intervention. *Rheumatol (Oxford)* (2019) 60(7):3088–98.60(7):3088–3098.. doi: 10.1093/rheumatology/kez004

6. Verstappen GM, Pringle S, Bootsma H, Kroese FGM. Epithelial–immune cell interplay in primary sjögren syndrome salivary gland pathogenesis. *Nat Rev Rheumatol* (2021) 17(6):333–48. doi: 10.1038/s41584-021-00605-2

7. Chivasso C, Sarrand J, Perret J, Delporte C, Soyfoo MS. The involvement of innate and adaptive immunity in the initiation and perpetuation of sjögren's syndrome. *Int J Mol Sci* (2021) 22(2):658. doi: 10.3390/ijms22020658

8. Bowman SJ. Primary sjögren's syndrome. *Lupus* (2018) 27(1_suppl):32–5. doi: 10.1177/0961203318801673

9. Goules AV, Kapsogeorgou EK, Tzioufas AG. Insight into pathogenesis of sjögren's syndrome: dissection on autoimmune infiltrates and epithelial cells. *Clin Immunol* (2017) 182:30–40. doi: 10.1016/j.clim.2017.03.007

10. Rivière E, Pascaud J, Tchitchek N, Boudaoud S, Paoletti A, Ly B, et al. Salivary gland epithelial cells from patients with sjögren's syndrome induce b-lymphocyte survival and activation. *Ann Rheum Dis* (2020) 79(11):1468–77. doi: 10.1136/annrheumdis-2019-216588

11. Gottenberg J-E, Busson M, Loiseau P, Cohen-Solal J, Lepage V, Charron D, et al. In primary sjögren's syndrome, HLA class II is associated exclusively with autoantibody production and spreading of the autoimmune response: association of HLA and primary SS. *Arthritis Rheumatol* (2003) 48(8):2240–5. doi: 10.1002/art.11103

12. Lessard CJ, Li H, Adrianto I, Ice JA, Rasmussen A, Grundahl KM, et al. Variants at multiple loci implicated in both innate and adaptive immune responses are associated with sjögren's syndrome. *Nat Genet* (2013) 45(11):1284–92. doi: 10.1038/ng.2792

13. Li Y, Zhang K, Chen H, Sun F, Xu J, Wu Z, et al. A genome-wide association study in han Chinese identifies a susceptibility locus for primary sjögren's syndrome at 7q11. *23. Nat Genet* (2013) 45(11):1361–5. doi: 10.1038/ng.2779

14. Thorlacius GE, Hultin-Rosenberg L, Sandling JK, Bianchi M, Imgenberg-Kreuz J, Pucholt P, et al. Genetic and clinical basis for two distinct subtypes of primary sjögren's syndrome. *Rheumatol (Oxford).* (2021) 60(2):837–48. doi: 10.1093/rheumatology/keaa367

15. Shiboski CH, Shiboski SC, Seror R, Criswell LA, Labetoulle M, Lietman TM, et al. 2016 American College of rheumatology/European league against rheumatism classification criteria for primary sjögren's syndrome: a consensus and data-driven methodology involving three international patient cohorts: Acr/Eular classification criteria for primary SS. *Arthritis Rheumatol* (2017) 69(1):35–45. doi: 10.1002/art.39859

16. Vitali C, Bombardieri S, Jonsson R, Moutsopoulos HM, Alexander EL, Carsons SE, et al. Classification criteria for sjögren's syndrome: a revised version of the European criteria proposed by the American-European consensus group. *Ann Rheum Dis* (2002) 61(6):554–8. doi: 10.1136/ard.61.6.554

17. Hu S, Loo JA, Wong DT. Human saliva proteome analysis. *Ann N Y Acad Sci* (2007) 1098(1):323–9. doi: 10.1196/annals.1384.015

18. Baldini C, Giusti L, Bazzichi L, Lucacchini A, Bombardieri S. Proteomic analysis of the saliva: a clue for understanding primary from secondary sjögren's syndrome? *Autoimmun Rev* (2008) 7(3):185–91. doi: 10.1016/j.autrev.2007.11.002

19. Fleissig Y, Deutsch O, Reichenberg E, Redlich M, Zaks B, Palmon A, et al. Different proteomic protein patterns in saliva of sjögren's syndrome patients. *Oral Dis* (2009) 15(1):61–8. doi: 10.1111/j.1601-0825.2008.01465.x

20. Katsiougiannis S, Wong DTW. The proteomics of saliva in sjögren's syndrome. *Rheum Dis Clin North Am* (2016) 42(3):449–56. doi: 10.1016/j.rdc.2016.03.004

21. Aqrawi LA, Galtung HK, Guerreiro EM, Øvstebø R, Thiede B, Utheim TP, et al. Proteomic and histopathological characterisation of sicca subjects and primary sjögren's syndrome patients reveals promising tear, saliva and extracellular vesicle disease biomarkers. *Arthritis Res Ther* (2019) 21(1):181. doi: 10.1186/s13075-019-1961-4

22. Sembler-Møller ML, Belstrøm D, Locht H, Pedersen AML. Proteomics of saliva, plasma, and salivary gland tissue in sjögren's syndrome and non-sjögren patients identify novel biomarker candidates. *J Proteomics.* (2020) 225(103877):103877. doi: 10.1016/j.jprot.2020.103877

23. Hu S, Wang J, Meijer J, Ieong S, Xie Y, Yu T, et al. Salivary proteomic and genomic biomarkers for primary sjögren's syndrome. *Arthritis Rheumatol* (2007) 56 (11):3588–600. doi: 10.1002/art.22954

24. Jasim H, Olausson P, Hedenberg-Magnusson B, Ernberg M, Ghafouri B. The proteomic profile of whole and glandular saliva in healthy pain-free subjects. *Sci Rep* (2016) 6(1):39073. doi: 10.1038/srep39073

25. Aqrawi LA, Galtung HK, Vestad B, Øvstebø R, Thiede B, Rusthen S, et al. Identification of potential saliva and tear biomarkers in primary sjögren's syndrome, utilising the extraction of extracellular vesicles and proteomics analysis. *Arthritis Res Ther* (2017) 19(1):14. doi: 10.1186/s13075-017-1228-x

26. Peluso G, De Santis M, Inzitari R, Fanali C, Cabras T, Messana I, et al. Proteomic study of salivary peptides and proteins in patients with sjögren's syndrome before and after pilocarpine treatment. *Arthritis Rheumatol* (2007) 56(7):2216–22. doi: 10.1002/art.22738

27. Ottosson L, Hennig J, Espinosa A, Brauner S, Wahren-Herlenius M, Sunnerhagen M. Structural, functional and immunologic characterization of folded subdomains in the Ro52 protein targeted in sjögren's syndrome. *Mol Immunol* (2006) 43(6):588–98. doi: 10.1016/j.molimm.2005.04.013

28. Baldini C, Giusti L, Ciregia F, Da Valle Y, Giacomelli C, Donadio E, et al. Proteomic analysis of saliva: a unique tool to distinguish primary sjögren's syndrome from secondary sjögren's syndrome and other sicca syndromes. *Arthritis Res Ther* (2011) 13(6):R194. doi: 10.1186/ar3523

29. Wang JJ, Reed JH, Colella AD, Russell AJ, Murray-Brown W, Chataway TK, et al. Molecular profiling and clonal tracking of secreted rheumatoid factors in primary sjögren's syndrome. *Arthritis Rheumatol* (2018) 70(10):1617–25. doi: 10.1002/art.40539

30. Ryu OH, Atkinson JC, Hoehn GT, Illei GG, Hart TC. Identification of parotid salivary biomarkers in sjögren's syndrome by surface-enhanced laser desorption/ionization time-of-flight mass spectrometry and two-dimensional difference gel electrophoresis. *Rheumatol (Oxford).* (2006) 45(9):1077–86. doi: 10.1093/rheumatology/kei212

31. Giusti L, Baldini C, Bazzichi L, Ciregia F, Tonazzini I, Mascia G, et al. Proteome analysis of whole saliva: a new tool for rheumatic diseases – the example of sjögren's syndrome. *Proteomics* (2007) 7(10):1634–43. doi: 10.1002/pmic.200600783

32. Hu S, Vissink A, Arellano M, Roozendaal C, Zhou H, Kallenberg CGM, et al. Identification of autoantibody biomarkers for primary sjögren's syndrome using protein microarrays. *Proteomics* (2011) 11(8):1499–507. doi: 10.1002/pmic.201000206

33. Wei P, Kuo WP, Chen F, Hua H. Diagnostic model of saliva peptide finger print analysis of primary sjögren's syndrome patients by using weak cation exchange magnetic beads. *Biosci Rep* (2013) 33(4):567–73. doi: 10.1042/BSR20130022

34. Gallo A. Gross cystic disease fluid protein-15(GCDFP-15)/prolactin-inducible protein (PIP) as functional salivary biomarker for primary sjögren's syndrome. *J Genet Syndr Gene Ther* (2013) 04(04):10.4172/2157-7412. doi: 10.4172/2157-7412.1000140

35. Deutsch O, Krief G, Konttinen YT, Zaks B, Wong DT, Aframian DJ, et al. Identification of sjögren's syndrome oral fluid biomarker candidates following high-abundance protein depletion. *Rheumatol (Oxford).* (2015) 54(5):884–90. doi: 10.1093/rheumatology/keu405

36. Delaleu N, Mydel P, Kwee I, Brun JG, Jonsson MV, Jonsson R. High fidelity between saliva proteomics and the biologic state of salivary glands defines biomarker signatures for primary sjögren's syndrome: salivary proteomics closely mirrors the biologic state of salivary glands. *Arthritis Rheumatol* (2015) 67(4):1084–95. doi: 10.1002/art.39015

37. Delaleu N, Mydel P, Brun JG, Jonsson MV, Alimonti A, Jonsson R. Sjögren's syndrome patients with ectopic germinal centers present with a distinct salivary proteome. *Rheumatol (Oxford).* (2016) 55(6):1127–37. doi: 10.1093/rheumatology/kew013

38. Chaudhury NMA, Proctor GB, Karlsson NG, Carpenter GH, Flowers SA. Reduced mucin-7 (Muc7) sialylation and altered saliva rheology in sjögren's syndrome associated oral dryness. *Mol Cell Proteomics.* (2016) 15(3):1048–59. doi: 10.1074/mcp.M115.052993

39. Bosello S, Peluso G, Iavarone F, Tolusso B, Messana I, Faa G, et al. Thymosin β4 and β10 in sjögren's syndrome: saliva proteomics and minor salivary glands expression. *Arthritis Res Ther* (2016) 18(1):229. doi: 10.1186/s13075-016-1134-7

40. Hall SC, Hassis ME, Williams KE, Albertolle ME, Prakobphol A, Dykstra AB, et al. Alterations in the salivary proteome and n-glycome of sjögren's syndrome patients. *J Proteome Res* (2017) 16(4):1693–705. doi: 10.1021/acs.jproteome.6b01051

41. Cui L, Elzakra N, Xu S, Xiao GG, Yang Y, Hu S. Investigation of three potential autoantibodies in sjogren's syndrome and associated MALT lymphoma. *Oncotarget* (2017) 8(18):30039–49. doi: 10.18632/oncotarget.15613

42. Jazzar AA, Shirlaw PJ, Carpenter GH, Challacombe SJ, Proctor GB. Salivary S100A8/A9 in sjögren's syndrome accompanied by lymphoma. *J Oral Pathol Med* (2018) 47(9):900–6. doi: 10.1111/jop.12763

43. Cecchettini A, Finamore F, Ucciferri N, Donati V, Mattii L, Polizzi E, et al. Phenotyping multiple subsets in sjögren's syndrome: a salivary proteomic SWATH-MS approach towards precision medicine. *Clin Proteomics.* (2019) 16(1):26. doi: 10.1186/s12014-019-9245-1

44. Hu S, Zhou M, Jiang J, Wang J, Elashoff D, Gorr S, et al. Systems biology analysis of sjögren's syndrome and mucosa-associated lymphoid tissue lymphoma in parotid glands. *Arthritis Rheumatol* (2009) 60(1):81–92. doi: 10.1002/art.24150

45. Hjelmervik TOR, Jonsson R, Bolstad AI. The minor salivary gland proteome in sjögren's syndrome. *Oral Dis* (2009) 15(5):342–53. doi: 10.1111/j.1601-0825.2009.01531.x

46. Van den Bergh K, Hooijkaas H, Blockmans D, Westhovens R, Op De Beéck K, Verschueren P, et al. Heterogeneous nuclear ribonucleoprotein h1, a novel nuclear autoantigen. *Clin Chem* (2009) 55(5):946–54. doi: 10.1373/clinchem.2008.115626

47. Lindop R, Arentz G, Chataway TK, Thurgood LA, Jackson MW, Reed JH, et al. Molecular signature of a public clonotypic autoantibody in primary sjögren's syndrome: a "forbidden" clone in systemic autoimmunity. *Arthritis Rheumatol* (2011) 63(11):3477–86. doi: 10.1002/art.30566

48. Arentz G, Thurgood LA, Lindop R, Chataway TK, Gordon TP. Secreted human Ro52 autoantibody proteomes express a restricted set of public clonotypes. *J Autoimmun* (2012) 39(4):466–70. doi: 10.1016/j.jaut.2012.07.003

49. Thurgood LA, Arentz G, Lindop R, Jackson MW, Whyte AF, Colella AD, et al. An immunodominant La/SSB autoantibody proteome derives from public clonotypes: public La/SSB autoantibody clonotypes. *Clin Exp Immunol* (2013) 174(2):237–44. doi: 10.1111/cei.12171

50. Li Y, Sun X, Zhang X, Yang Y, Jia R, Liu X, et al. Establishment of a novel diagnostic model for sjögren's syndrome by proteomic fingerprinting. *Clin Rheumatol* (2014) 33(12):1745–50. doi: 10.1007/s10067-014-2762-4

51. Ohyama K, Baba M, Tamai M, Aibara N, Ichinose K, Kishikawa N, et al. Proteomic profiling of antigens in circulating immune complexes associated with each of seven autoimmune diseases. *Clin Biochem* (2015) 48(3):181–5. doi: 10.1016/j.clinbiochem.2014.11.008

52. Nishikawa A, Suzuki K, Kassai Y, Gotou Y, Takiguchi M, Miyazaki T, et al. Identification of definitive serum biomarkers associated with disease activity in primary sjögren's syndrome. *Arthritis Res Ther* (2016) 18(1):106. doi: 10.1186/s13075-016-1006-1

53. Liao C-C, Chou P-L, Cheng C-W, Chang Y-S, Chi W-M, Tsai K-L, et al. Comparative analysis of novel autoantibody isotypes against citrullinated-inter-alpha-trypsin inhibitor heavy chain 3 (ITIH3)542–556 peptide in serum from Taiwanese females with rheumatoid arthritis, primary sjögren's syndrome and secondary sjögren's syndrome in rheumatoid arthritis. *J Proteomics.* (2016) 141:1–11. doi: 10.1016/j.jprot.2016.03.031

54. Tasaki S, Suzuki K, Nishikawa A, Kassai Y, Takiguchi M, Kurisu R, et al. Multiomic disease signatures converge to cytotoxic CD8 T cells in primary sjögren's syndrome. *Ann Rheum Dis* (2017) 76(8):1458–66. doi: 10.1136/annrheumdis-2016-210788

55. Wang JJ, Al Kindi MA, Colella AD, Dykes L, Jackson MW, Chataway TK, et al. IgV peptide mapping of native Ro60 autoantibody proteomes in primary sjögren's syndrome reveals molecular markers of Ro/La diversification. *Clin Immunol* (2016) 173:57–63. doi: 10.1016/j.clim.2016.09.001

56. Burbelo PD, Ferré EMN, Chaturvedi A, Chiorini JA, Alevizos I, Lionakis MS, et al. Profiling autoantibodies against salivary proteins in sicca conditions. *J Dent Res* (2019) 98(7):772–8. doi: 10.1177/0022034519850564

57. Bodewes ILA, van der Spek PJ, Leon LG, Wijkhuijs AJM, van Helden-Meeuwsen CG, Tas L, et al. Fatigue in sjögren's syndrome: a search for biomarkers and treatment targets. *Front Immunol* (2019) 10:312. doi: 10.3389/fimmu.2019.00312

58. Qiao L, Deng C, Wang Q, Zhang W, Fei Y, Xu Y, et al. Serum clusterin and complement factor h may be biomarkers differentiate primary sjögren's syndrome with and without neuromyelitis optica spectrum disorder. *Front Immunol* (2019) 10:2527. doi: 10.3389/fimmu.2019.02527

59. Ohlsson M, Hellmark T, Bengtsson AA, Theander E, Turesson C, Klint C, et al. Proteomic data analysis for differential profiling of the autoimmune diseases SLE, RA, SS, and ANCA-associated vasculitis. *J Proteome Res* (2021) 20(2):1252–60. doi: 10.1021/acs.jproteome.0c00657

60. Huang S, Zheng F, Liu L, Meng S, Cai W, Zhang C, et al. Integrated proteome and phosphoproteome analyses of peripheral blood mononuclear cells in primary sjögren syndrome patients. *Aging (Albany NY).* (2020) 13(1):1071–95. doi: 10.18632/aging.202233

61. Tian Q, Zhao H, Ling H, Sun L, Xiao C, Yin G, et al. Poly(ADP -ribose) polymerase enhances infiltration of mononuclear cells in primary sjögren's syndrome through interferon-induced protein with tetratricopeptide repeats 1–mediated up-regulation of CXCL 10. *Arthritis Rheumatol* (2020) 72(6):1003–12. doi: 10.1002/art.41195

62. Schmidt A, Farine H, Keller MP, Sebastian A, Kozera L, Welford RWD, et al. Immunoaffinity targeted mass spectrometry analysis of human plasma samples reveals an imbalance of active and inactive CXCL10 in primary sjögren's syndrome disease patients. *J Proteome Res* (2020) 19(10):4196–209. doi: 10.1021/acs.jproteome.0c00494

63. Thiagarajan D, Oparina N, Lundström S, Zubarev R, Sun J. PRECISESADS clinical consortium, et al. IgM antibodies against malondialdehyde and phosphorylcholine in different systemic rheumatic diseases. *Sci Rep* (2020) 10(1):11010. doi: 10.1038/s41598-020-66981-z

64. Mogi M, Kage T, Chino T, Yoshitake K, Harada M. Increased beta 2-microglobulin in both parotid and submandibular/sublingual saliva from patients with sjögren's syndrome. *Arch Oral Biol* (1994) 39(10):913–5. doi: 10.1016/0003-9969(94)90024-8

65. Hu S, Gao K, Pollard R, Arellano-Garcia M, Zhou H, Zhang L, et al. Preclinical validation of salivary biomarkers for primary sjögren's syndrome. *Arthritis Care Res (Hoboken).* (2010) 62(11):1633–8. doi: 10.1002/acr.20289

66. Michalski JP, Daniels TE, Talal N, Grey HM. Beta2Microglobulin and lymphocytic infiltration in sjögren's syndrome. *N Engl J Med* (1975) 293(24):1228–31. doi: 10.1056/NEJM197512112932404

67. Yoneda M, Fujii A, Ito A, Yokoyama H, Nakagawa H, Kuriyama M. High prevalence of serum autoantibodies against the amino terminal of alpha-enolase in hashimoto's encephalopathy. *J Neuroimmunol* (2007) 185(1–2):195–200. doi: 10.1016/j.jneuroim.2007.01.018

68. He P, Naka T, Serada S, Fujimoto M, Tanaka T, Hashimoto S, et al. Proteomics-based identification of alpha-enolase as a tumor antigen in non-small lung cancer. *Cancer Sci* (2007) 98(8):1234–40. doi: 10.1111/j.1349-7006.2007.00509.x

69. Olivares-Martínez E, Hernández-Ramírez DF, Núñez-Álvarez CA, Llorente L, Hernandez-Molina G. α-enolase is an antigenic target in primary sjögren's syndrome. *Clin Exp Rheumatol* (2019) 37 Suppl 118(3):29–35.

70. Singer E, Markó L, Paragas N, Barasch J, Dragun D, Müller DN, et al. Neutrophil gelatinase-associated lipocalin: pathophysiology and clinical applications. *Acta Physiol (Oxf).* (2013) 207(4):663–72. doi: 10.1111/apha.12054

71. Aqrawi LA, Jensen JL, Fromreide S, Galtung HK, Skarstein K. Expression of NGAL-specific cells and mRNA levels correlate with inflammation in the salivary gland, and its overexpression in the saliva, of patients with primary sjögren's syndrome. *Autoimmunity* (2020) 53(6):333–43. doi: 10.1080/08916934.2020.1795140

72. Carlsson H, Yhr M, Petersson S, Collins N, Polyak K, Enerbäck C. Psoriasin (S100A7) and calgranulin-b (S100A9) induction is dependent on reactive oxygen species and is downregulated by bcl-2 and antioxidants. *Cancer Biol Ther* (2005) 4 (9):998–1005. doi: 10.4161/cbt.4.9.1969

73. Dorkhan M, Svensäter G, Davies JR. Salivary pellicles on titanium and their effect on metabolic activity in streptococcus oralis. *BMC Oral Health* (2013) 13(1):32. doi: 10.1186/1472-6831-13-32

74. Edechi CA, Nasr MR, Karim A, Blanchard AA, Ellison CA, Qui H, et al. The prolactin inducible protein/gross cystic disease fluid protein-15 deficient mice develop anomalies in lymphoid organs. *Immunobiology* (2019) 224(6):811–6. doi: 10.1016/j.imbio.2019.08.005

75. Bardow A, Moe D, Nyvad B, Nauntofte B. The buffer capacity and buffer systems of human whole saliva measured without loss of CO2. *Arch Oral Biol* (2000) 45(1):1–12. doi: 10.1016/s0003-9969(99)00119-3

76. Baron A, DeCarlo A, Featherstone J. Functional aspects of the human salivary cystatins in the oral environment. *Oral Dis* (1999) 5(3):234–40. doi: 10.1111/j.1601-0825.1999.tb00307.x

77. Falco A, Mas V, Tafalla C, Perez L, Coll JM, Estepa A. Dual antiviral activity of human alpha-defensin-1 against viral haemorrhagic septicaemia rhabdovirus (VHSV): inactivation of virus particles and induction of a type I interferon-related response. *Antiviral Res* (2007) 76(2):111–23. doi: 10.1016/j.antiviral.2007.06.006

78. Deming FP, Al-Hashimi I, Haghighat N, Hallmon WW, Kerns DG, Abraham C, et al. Comparison of salivary calmodulin binding proteins in sjögren's syndrome and healthy individuals: calmodulin binding proteins in sjögren's syndrome. *J Oral Pathol Med* (2007) 36(3):132–5. doi: 10.1111/j.1600-0714.2006.00494.x

79. Franceschini F, Cavazzana I. Anti-Ro/SSA and La/SSB antibodies. *Autoimmunity* (2005) 38(1):55–63. doi: 10.1080/08916930400022954

80. Strandberg L, Ambrosi A, Espinosa A, Ottosson L, Eloranta M-L, Zhou W, et al. Interferon-alpha induces up-regulation and nuclear translocation of the Ro52 autoantigen as detected by a panel of novel Ro52-specific monoclonal antibodies. *J Clin Immunol* (2008) 28(3):220–31. doi: 10.1007/s10875-007-9157-0

81. Schulte-Pelkum J, Fritzler M, Mahler M. Latest update on the Ro/SS-a autoantibody system. *Autoimmun Rev* (2009) 8(7):632–7. doi: 10.1016/j.autrev.2009.02.010

82. Menéndez A, Gómez J, Escanlar E, Caminal-Montero L, Mozo L. Clinical associations of anti-SSA/Ro60 and anti-Ro52/TRIM21 antibodies: diagnostic utility of their separate detection. *Autoimmunity* (2013) 46(1):32–9. doi: 10.3109/08916934.2012.732131

83. Ohlsson M, Jonsson R, Brokstad KA. Subcellular redistribution and surface exposure of the Ro52, Ro60 and La48 autoantigens during apoptosis in human ductal epithelial cells: a possible mechanism in the pathogenesis of sjögren's syndrome: SS autoantigens and apoptosis. *Scand J Immunol* (2002) 56(5):456–69. doi: 10.1046/j.1365-3083.2002.01072_79.x

84. Aqrawi LA, Skarstein K, Øijordsbakken G, Brokstad KA. Ro52- and Ro60-specific b cell pattern in the salivary glands of patients with primary sjögren's syndrome: SSA-specific b cells in SG of pSS patients. *Clin Exp Immunol* (2013) 172 (2):228–37. doi: 10.1111/cei.12058

85. Theander E, Jonsson R, Sjöström B, Brokstad K, Olsson P, Henriksson G. Prediction of sjögren's syndrome years before diagnosis and identification of patients with early onset and severe disease course by autoantibody profiling: prediagnostic autoantibody profiling in primary SS. *Arthritis Rheumatol* (2015) 67(9):2427–36. doi: 10.1002/art.39214

86. Quartuccio L, Baldini C, Bartoloni E, Priori R, Carubbi F, Corazza L, et al. Anti-SSA/SSB-negative sjögren's syndrome shows a lower prevalence of lymphoproliferative manifestations, and a lower risk of lymphoma evolution. *Autoimmun Rev* (2015) 14 (11):1019–22. doi: 10.1016/j.autrev.2015.07.002

87. Ebana Y, Ozaki K, Inoue K, Sato H, Iida A, Lwin H, et al. A functional SNP in ITIH3 is associated with susceptibility to myocardial infarction. *J Hum Genet* (2007) 52 (3):220–9. doi: 10.1007/s10038-006-0102-5

88. Zhuo L, Hascall VC, Kimata K. Inter-alpha-trypsin inhibitor, a covalent protein-glycosaminoglycan-protein complex. *J Biol Chem* (2004) 279(37):38079–82. doi: 10.1074/jbc.R300039200

89. Terzoglou AG, Routsias JG, Moutsopoulos HM, Tzioufas AG. Post-translational modifications of the major linear epitope 169-190aa of Ro60 kDa autoantigen alter the autoantibody binding. *Clin Exp Immunol* (2006) 146(1):60–5. doi: 10.1111/j.1365-2249.2006.03192.x

90. Herrera-Esparza R, Rodríguez-Rodríguez M, Pérez-Pérez ME, Badillo-Soto MA, Torres-Del-Muro F, Bollain-Y-Goytia JJ, et al. Posttranslational protein modification in the salivary glands of sjögren's syndrome patients. *Autoimmune Dis* (2013) 2013:548064. doi: 10.1155/2013/548064

91. Sembler-Møller ML, Belstrøm D, Locht H, Pedersen AML. Combined serum anti-SSA/Ro and salivary TRIM29 reveals promising high diagnostic accuracy in patients with primary sjögren's syndrome. *PloS One* (2021) 16(10):e0258428. doi: 10.1371/journal.pone.0258428

92. Theander E. Lymphoma and other malignancies in primary sjogren's syndrome: a cohort study on cancer incidence and lymphoma predictors. *Ann Rheum Dis* (2006) 65(6):796–803. doi: 10.1136/ard.2005.041186

93. Liang Y, Yang Z, Qin B, Zhong R. Primary sjögren's syndrome and malignancy risk: a systematic review and meta-analysis. *Ann Rheum Dis* (2014) 73(6):1151–6. doi: 10.1136/annrheumdis-2013-203305

94. Kapsogeorgou EK, Voulgarelis M, Tzioufas AG. Predictive markers of lymphomagenesis in sjögren's syndrome: from clinical data to molecular stratification. *J Autoimmun* (2019) 104(102316):102316. doi: 10.1016/j.jaut.2019.102316

95. Alevizos I, Alexander S, Turner RJ, Illei GG. MicroRNA expression profiles as biomarkers of minor salivary gland inflammation and dysfunction in sjögren's syndrome. *Arthritis Rheumatol* (2011) 63(2):535–44. doi: 10.1002/art.30131

96. Zilahi E, Tarr T, Papp G, Griger Z, Sipka S, Zeher M. Increased microRNA-146a/b, TRAF6 gene and decreased IRAK1 gene expressions in the peripheral mononuclear cells of patients with sjögren's syndrome. *Immunol Lett* (2012) 141 (2):165–8. doi: 10.1016/j.imlet.2011.09.006

97. Tandon M, Gallo A, Jang S-I, Illei GG, Alevizos I. Deep sequencing of short RNAs reveals novel microRNAs in minor salivary glands of patients with sjögren's syndrome: novel miRNA discovery in sjögren's syndrome. *Oral Dis* (2012) 18(2):127–31. doi: 10.1111/j.1601-0825.2011.01849.x

98. Peng L, Ma W, Yi F, Yang Y-J, Lin W, Chen H, et al. MicroRNA profiling in Chinese patients with primary sjögren syndrome reveals elevated miRNA-181a in peripheral blood mononuclear cells. *J Rheumatol* (2014) 41(11):2208–13. doi: 10.3899/jrheum.131154

99. Shi H, Zheng L-Y, Zhang P, Yu C-Q. miR-146a and miR-155 expression in PBMCs from patients with sjögren's syndrome. *J Oral Pathol Med* (2014) 43(10):792–7. doi: 10.1111/jop.12187

100. Chen J-Q, Zilahi E, Papp G, Sipka S, Zeher M. Simultaneously increased expression of microRNA-155 and suppressor of cytokine signaling 1 (SOCS1) gene in the peripheral blood mononuclear cells of patients with primary sjögren's syndrome. *Int J Rheum Dis* (2017) 20(5):609–13. doi: 10.1111/1756-185x.12804

101. Gourzi VC, Kapsogeorgou EK, Kyriakidis NC, Tzioufas AG. Study of microRNAs (miRNAs) that are predicted to target the autoantigens Ro/SSA and La/SSB in primary sjögren's syndrome: MiRNAs targeting Ro/SSA and La/SSB autoantigens in sjögren's syndrome. *Clin Exp Immunol* (2015) 182(1):14–22. doi: 10.1111/cei.12664

102. Williams AEG, Choi K, Chan AL, Lee YJ, Reeves WH, Bubb MR, et al. Sjögren's syndrome-associated microRNAs in CD14(+) monocytes unveils targeted TGFβ signaling. *Arthritis Res Ther* (2016) 18(1):95. doi: 10.1186/s13075-016-0987-0

103. Yan T, Shen J, Chen J, Zhao M, Guo H, Wang Y. Differential expression of miR-17-92 cluster among varying histological stages of minor salivary gland in patients with primary sjögren's syndrome. *Clin Exp Rheumatol* (2019) 37 Suppl 118(3):49–54.

104. Chen JQ, Papp G, Póliska S, Szabó K, Tarr T, Bálint BL, et al. MicroRNA expression profiles identify disease-specific alterations in systemic lupus erythematosus and primary sjögren's syndrome. *PloS One* (2017) 12(3):e0174585. doi: 10.1371/journal.pone.0174585

105. Jiang Z, Tao J-H, Zuo T, Li X-M, Wang G-S, Fang X, et al. The correlation between miR-200c and the severity of interstitial lung disease associated with different connective tissue diseases. *Scand J Rheumatol* (2017) 46(2):122–9. doi: 10.3109/03009742.2016.1167950

106. Lopes AP, Hillen MR, Chouri E, Blokland SLM, Bekker CPJ, Kruize AA, et al. Circulating small non-coding RNAs reflect IFN status and b cell hyperactivity in patients with primary sjögren's syndrome. *PloS One* (2018) 13(2):e0193157. doi: 10.1371/journal.pone.0193157

107. Kapsogeorgou EK, Papageorgiou A, Protogerou AD, Voulgarelis M, Tzioufas AG. Low miR200b-5p levels in minor salivary glands: a novel molecular marker predicting lymphoma development in patients with sjögren's syndrome. *Ann Rheum Dis* (2018) 77(8):1200–7. doi: 10.1136/annrheumdis-2017-212639

108. Jiang C-R, Li H-L. The value of MiR-146a and MiR-4484 expressions in the diagnosis of anti-SSA antibody positive sjogren syndrome and the correlations with prognosis. *Eur Rev Med Pharmacol Sci* (2018) 22(15):4800–5. doi: 10.26355/eurrev_201808_15614

109. Wang-Renault S-F, Boudaoud S, Nocturne G, Roche E, Sigrist N, Daviaud C, et al. Deregulation of microRNA expression in purified T and b lymphocytes from patients with primary sjögren's syndrome. *Ann Rheum Dis* (2018) 77(1):133–40. doi: 10.1136/annrheumdis-2017-211417

110. Wang J, Wang X, Wang L, Sun C, Xie C, Li Z. MiR-let-7d-3p regulates IL-17 expression through targeting AKT1/mTOR signaling in CD4+ T cells. *In Vitro Cell Dev Biol Anim.* (2020) 56(1):67–74. doi: 10.1007/s11626-019-00409-5

111. Hillen MR, Chouri E, Wang M, Blokland SLM, Hartgring SAY, Concepcion AN, et al. Dysregulated miRNome of plasmacytoid dendritic cells from patients with sjögren's syndrome is associated with processes at the centre of their function. *Rheumatol (Oxford).* (2019) 58(12):2305–14. doi: 10.1093/rheumatology/kez195

112. Gallo A, Vella S, Tuzzolino F, Cuscino N, Cecchettini A, Ferro F, et al. MicroRNA-mediated regulation of mucin-type O-glycosylation pathway: a putative mechanism of salivary gland dysfunction in sjögren syndrome. *J Rheumatol* (2019) 46 (11):1485–94. doi: 10.3899/jrheum.180549

113. Talotta R, Mercurio V, Bongiovanni S, Vittori C, Boccassini L, Rigamonti F, et al. Evaluation of salivary and plasma microRNA expression in patients with sjögren's syndrome, and correlations with clinical and ultrasonographic outcomes. *Clin Exp Rheumatol* (2019) 37 Suppl 118(3):70–7.

114. Sembler-Møller ML, Belstrøm D, Locht H, Pedersen AML. Distinct microRNA expression profiles in saliva and salivary gland tissue differentiate patients with primary sjögren's syndrome from non-sjögren's sicca patients. *J Oral Pathol Med* (2020) 49 (10):1044–52. doi: 10.1111/jop.13099

115. Yang Y, Hou Y, Li J, Zhang F, Du Q. Characterization of antiapoptoticmicroRNAsin primary sjögren's syndrome. *Cell Biochem Funct* (2020) 38(8):1111–8. doi: 10.1002/cbf.3569

116. Gong B, Zheng L, Lu Z, Huang J, Pu J, Pan S, et al. Mesenchymal stem cells negatively regulate CD4+ T cell activation in patients with primary sjögren syndrome through the miRNA–125b and miRNA–155 TCR pathway. *Mol Med Rep* (2021) 23 (1):1. doi: 10.3892/mmr.2020.1168

117. Salama I, Malone PS, Mihaimeed F, Jones JL. A review of the S100 proteins in cancer. *Eur J Surg Oncol* (2008) 34(4):357–64. doi: 10.1016/j.ejso.2007.04.009

118. Bresnick AR, Weber DJ, Zimmer DB. S100 proteins in cancer. *Nat Rev Cancer.* (2015) 15(2):96–109. doi: 10.1038/nrc3893

119. Alevizos I, Illei GG. MicroRNAs in sjögren's syndrome as a prototypic autoimmune disease. *Autoimmun Rev* (2010) 9(9):618–21. doi: 10.1016/j.autrev.2010.05.009

120. Pauley KM, Stewart CM, Gauna AE, Dupre LC, Kuklani R, Chan AL, et al. Altered miR-146a expression in sjögren's syndrome and its functional role in innate immunity: innate immunity. *Eur J Immunol* (2011) 41(7):2029–39. doi: 10.1002/eji.201040757

121. Wang Y, Zhang G, Zhang L, Zhao M, Huang H. Decreased microRNA-181a and -16 expression levels in the labial salivary glands of sjögren syndrome patients. *Exp Ther Med* (2018) 15(1):426–32. doi: 10.3892/etm.2017.5407

122. Mogilyansky E, Rigoutsos I. The miR-17/92 cluster: a comprehensive update on its genomics, genetics, functions and increasingly important and numerous roles in health and disease. *Cell Death Differ* (2013) 20(12):1603–14. doi: 10.1038/cdd.2013.125

123. Veerman EC, Valentijn-Benz M, Amerongen N. Viscosity of human salivary mucins: effect of pH and ionic-strength and role of sialic-acid. *J Biol Buccale.* (1989) 17 (4):297–306.

124. Chaudhury NMA, Shirlaw P, Pramanik R, Carpenter GH, Proctor GB. Changes in saliva rheological properties and mucin glycosylation in dry mouth. *J Dent Res* (2015) 94(12):1660–7. doi: 10.1177/0022034515609070

frontiers | Frontiers in Medicine

TYPE Review
PUBLISHED 23 June 2023
DOI 10.3389/fmed.2023.1183535

OPEN ACCESS

EDITED BY
Jill M. Kramer,
University at Buffalo, United States

REVIEWED BY
Celine C. Berthier,
University of Michigan, United States
Rhea Bhargava,
Tulane University, United States

*CORRESPONDENCE
Hege Lynum Pedersen
✉ hege.lynum.pedersen@uit.no

†These authors have contributed equally to this work

RECEIVED 10 March 2023
ACCEPTED 01 June 2023
PUBLISHED 23 June 2023

CITATION
Fenton KA and Pedersen HL (2023) Advanced methods and novel biomarkers in autoimmune diseases - a review of the recent years progress in systemic lupus erythematosus.
Front. Med. 10:1183535.
doi: 10.3389/fmed.2023.1183535

Advanced methods and novel biomarkers in autoimmune diseases - a review of the recent years progress in systemic lupus erythematosus

Kristin Andreassen Fenton[1,2†] and Hege Lynum Pedersen[1,2*†]

[1]UiT The Arctic University of Norway, Tromsø, Norway, [2]Centre of Clinical Research and Education, University Hospital of North Norway, Tromsø, Norway

There are several autoimmune and rheumatic diseases affecting different organs of the human body. Multiple sclerosis (MS) mainly affects brain, rheumatoid arthritis (RA) mainly affects joints, Type 1 diabetes (T1D) mainly affects pancreas, Sjogren's syndrome (SS) mainly affects salivary glands, while systemic lupus erythematosus (SLE) affects almost every organ of the body. Autoimmune diseases are characterized by production of autoantibodies, activation of immune cells, increased expression of pro-inflammatory cytokines, and activation of type I interferons. Despite improvements in treatments and diagnostic tools, the time it takes for the patients to be diagnosed is too long, and the main treatment for these diseases is still non-specific anti-inflammatory drugs. Thus, there is an urgent need for better biomarkers, as well as tailored, personalized treatment. This review focus on SLE and the organs affected in this disease. We have used the results from various rheumatic and autoimmune diseases and the organs involved with an aim to identify advanced methods and possible biomarkers to be utilized in the diagnosis of SLE, disease monitoring, and response to treatment.

KEYWORDS

SLE, systemic lupus erythematosus, transcriptomics (RNA-Seq), PET/MRI, imaging - computed tomography, organ specific, urine biomarker, biomarker

Introduction

Systemic chronic inflammation (SCI) is the presence of a slow low-grade inflammation lasting for longer periods from several months to years (1). It is caused by the constant activation and infiltration of immune cells into the affected organs. SCI may advance into autoimmune diseases with the characteristic development of autoantigen-specific lymphocytes and autoantibodies that may progress into clinical disease manifestations (2). However, because the preclinical phase often is silent, it is difficult to predict the progression from harmless inflammation to activation of autoantigen-specific T and B cells leading to production of autoantibodies and activation of effector cells, the hallmarks of autoimmune diseases. There is still a lack of detailed clinical and molecular knowledge that can lead to a better understanding of the pathogenesis behind such diseases, and there is a need for suitable predictive biomarkers that can identify patients that are at risk to develop autoimmune diseases (2).

Systemic lupus erythematosus (SLE) is a chronic inflammatory autoimmune disease disposed to inflammation in nearly all organs. The production of autoantibodies (specifically

anti-double stranded (ds) DNA) and the formation of immune complexes is a hallmark of SLE (3), but there is still a lack of clinically useful diagnostic markers and markers that can predict organ involvement.

Biomarkers are as the word imply, biological markers. There are different kinds of biomarkers such as diagnostic, mechanistic, clinical, therapeutic. These markers can identify gene variants, gene or protein expression, disease monitoring, and therapeutic response. Common for all, is that they objectively predict biological characteristics that is difficult to observe. Perhaps the biggest advantage of implementing good, clinical biomarkers could be the implementation of precision medicine. In a review article by Giacomelli et al. (4) regarding biomarkers in autoimmune rheumatic diseases, they concluded that biomarkers and personalized medicine (e.g., precision medicine that target treatment to individual patients based on precise and specific information of the patients disease) would be future central points in management of patients affected by rheumatic and autoimmune diseases.

Transcriptomics is the study of expression profiling of levels of mRNA in an organism at a given time. RNA sequencing (RNAseq) allows the characterization of different states of cells or tissue by expression patterns. Utilizing these methods, the molecular mechanisms underlying a phenotype and identifying differential expressed biomarkers in diseases compared to healthy individuals, can be investigated. The use of transcriptomics in autoimmune diseases have increased our knowledge of the pathophysiology of such diseases. In particular, the immune cells, signaling pathways, and the genes involved have been in focus (5). Monocytes and macrophages, including tissue specific resident macrophages, are key cells commonly expressed across different inflammatory and autoimmune diseases. However, the biggest challenge still lies in linking the results from RNA-seq into clinical application.

One of the newest techniques in transcriptomic analyses, single cell RNA sequencing (scRNAseq), was developed in 2009 by Tang et al. and has been one of the most used transcriptomic methods the last decade (6). In autoimmune diseases, the use of scRNAseq has opened for the identification of cell and molecular biomarkers that may predict disease progression, disease outcome, and individualized therapy (7). The use of scRNAseq in autoimmune inflammatory rheumatic disease has recently been reviewed and highlight the current challenges to overcome before we can utilize novel findings in new advanced diagnostic tools (8). The single cell multiomics data complexity require interdisciplinary collaborations, the high cost of reagents and equipment prevents the profiling of large patients cohorts, and in the end, few user-friendly, easy accessible interface linking the results with the whole research field makes the transition into the clinics difficult (8).

Molecular imaging allows for the detection of cellular and molecular changes within living species. It can characterize and measure biological processes *in vivo* and allows for visualization of the whole body down to cellular resolution level (9). Positron emission tomography (PET) together with computed tomography (CT) (PET/CT) or magnetic resonance imaging (MRI) (PET/MRI) take advantage of tracers with radioactive isotopes that can measure metabolic activity in cells and organs. Carbohydrate metabolism [glucose, ^{18}F fluorodeoxyglucose (FDG) and mannose receptor (^{18}F-fluoro-D-mannose; ^{18}F-FDM)], chemokine receptors (C-X-C Motif Chemokine Receptor 4 (CXCR4), ^{68}Ga-pentixafor), somatostatin receptors (^{68}Ga-labeled DOTA-peptides), cell adhesion molecules (CAMs, ^{18}F-galacto-RGD, ^{68}Ga-PRGD2, and ^{18}F-fluciclatide), fibroblast Activation Protein-α (FAP, ^{68}Ga-FAPI), folate receptor (FR, ^{18}F-fluoro-PEG-folate), and mitochondrial translocator protein (TSPO, ^{11}C-PK11195 or ^{18}F-flutriciclamide) are some of the targets of tracers developed to detect inflammation in different diseases (10).

Given the fast development of new, sophisticated techniques generating vast amount of data in combination with machine learning and artificial intelligence (AI), there are tremendous opportunities ahead of us. The results should lead to new advancements in disease diagnosis, monitoring and response to therapy. Despite good research on animal models, there is a knowledge gap when it comes to new biomarkers, methods, and treatment regarding SLE. Previous work has mostly focused on cutaneous SLE and lupus nephritis (LN), but since SLE is a systemic disease, we wanted to review what is known about SLE and organs such as joint, liver, pancreas, brain, salivary gland (SG), and lung to look for organ specific markers of inflammation. Here, we give an overview of research involving SLE and organ specific research on biomarkers, transcriptomics/scRNAseq, and molecular imaging.

Inclusion and exclusion criteria

While SLE is defined as an autoantibody and immune complex disease, most of its organ manifestations are inflammatory. That is why we in this review have focused on the inflammatory milieu in the different organs included in our investigation. Thus, we used inflammation and human as a prerequisite in most of our PubMed searches. We included research on other autoimmune diseases to compare the findings in SLE, especially where there is a lack of research on SLE. To limit the results and focus on human research we excluded paper containing virus, animal, and cancer research (Supplementary Table S1). We have also focused on the articles published the last 5–10 years.

Inflammation in different organs of autoimmune and rheumatic diseases

Doing a PubMed search on inflammation, different diseases, and organ, revealed that a vast amount of research has been performed on joint compared to other organs like brain, skin, kidney, SG, lung, and pancreas, respectively (Figure 1; Supplementary Table S1). Organ affection in SLE include all the above-mentioned organs, in addition to circulating immune cells in peripheral blood. Other autoimmune and rheumatic diseases are more organ specific, like multiple sclerosis (MS) and brain, and Type 1 Diabetes (T1D) and pancreas, while others like Rheumatic arthritis (RA) and Sjogren's syndrome (SS) can be both organ specific and systemic. The search confirmed the typical organ manifestation of the different diseases as most of the papers in rheumatoid arthritis (RA) were found in joint, in MS the brain had more publications, SG in Sjogren's syndrome (SS), pancreas in Type 1 diabetes (T1D), and the kidney in SLE patient (Figure 1). The results revealed that, despite being a systemic disease affecting multiple organs, most of the published articles on SLE involved kidney, skin, and joint, and fewer papers on the other organs, especially SG, and pancreas (Supplementary Table S1; Figure 1).

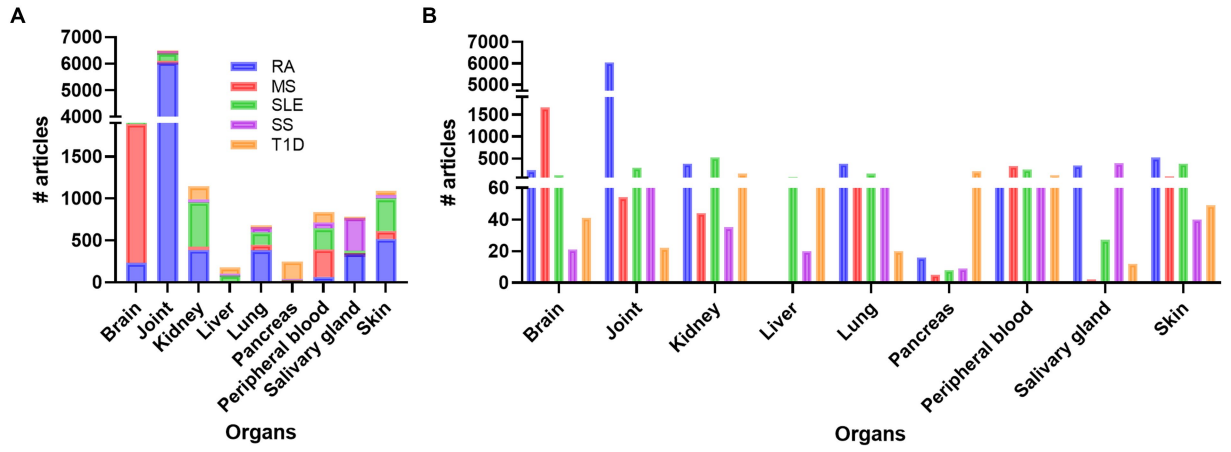

FIGURE 1
Overview of the number of publications on disease, inflammation, and organ involvement **(A)**. In **(B)** the individual results of each disease related to organs and number of publications are shown. RA, rheumatoid arthritis; MS, multiple sclerosis; SLE, systemic lupus erythematosus; SS, Sjogren's syndrome; T1D: type 1 diabetes.

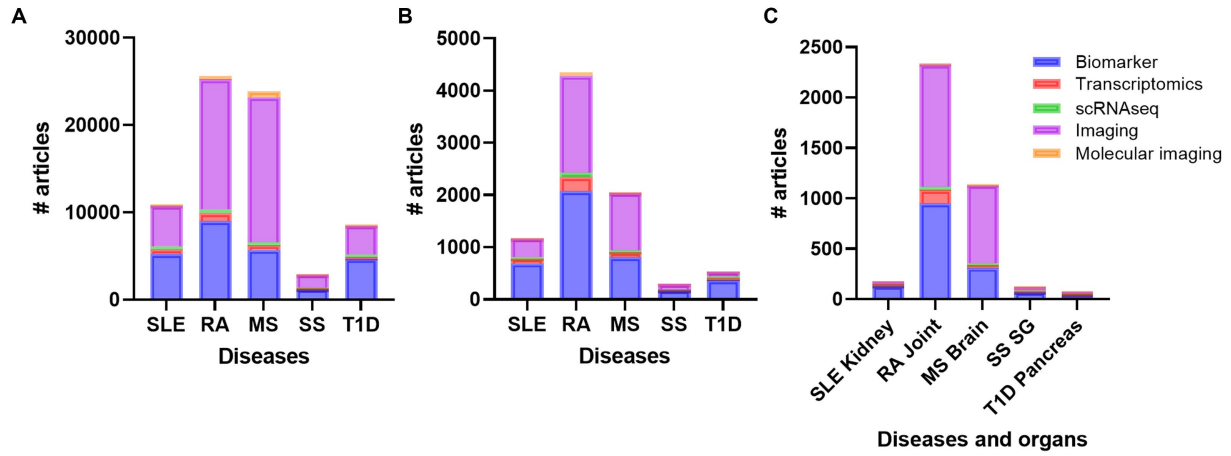

FIGURE 2
Overview of the number of publications on diseases **(A)** diseases and inflammation **(B)** and diseases, inflammation and organs **(C)** with the topics biomarker, transcriptomics, single cell sequencing, imaging, and molecular imaging. RA, rheumatoid arthritis; MS, multiple sclerosis; SLE, systemic lupus erythematosus; SS, Sjogren´s syndrome; T1D: type 1 diabetes; SG, salivary gland.

Disease and organ specific biomarkers and advanced methods

To get an overview of different organ specific biomarkers in the field of autoimmune and rheumatic diseases, we did several defined PubMed searches on the diseases SLE, RA, MS, SS, and T1D. These searches revealed that there are more studies performed on MS and RA compared to SLE, SS, and T1D on every search we did, respectively (Figure 2A). We did searches on advanced methods such as transcriptomics, single-cell sequencing, imaging, molecular imaging, and biomarkers (Supplementary Table S2; Figure 2A). When we included inflammation, the number of papers decreased, but the overall results showed the same trend (Supplementary Table S3; Figure 2B). These results were also supported when we added the different organs to the search terms (Supplementary Table S4; Figure 2C). Biomarker and imaging got the most hits, and after including specific organs, the findings even increased the disparities in number of works done between RA and MS compared to the other diseases (Figure 2C).

Biomarkers in SLE

Autoantibodies have been widely used as biomarkers for rheumatic [reviewed in (11)] and autoimmune diseases [reviewed in (12)] such as SLE [reviewed in (13)]. Anti-nuclear antibody (ANA), anti-dsDNA, anti-Sm, antiphospholipid, and low C3 and/or low C4 are used in clinical practice today as diagnostic biomarkers of SLE

[reviewed in (14)]. Although there are several publications available on novel biomarkers for use in diagnosis [(15) and references therein], and monitoring [reviewed in (14, 16)] of SLE, few of them are in use in clinical practice. The heterogeneity of SLE makes it difficult to diagnose and monitor the disease progression. Performing a PubMed search on inflammation, SLE and biomarker, gave 689 results, of which 488 articles were published the last ten years (Supplementary Table S3; Figure 2B). Of these, 91 publications were reviews, compared to 121 in total.

Since a primary goal for developing new biomarkers is to identify non-invasive markers most of the works utilized blood or urine from patients with SLE. Searching PubMed for human SLE, peripheral blood and biomarker, excluding virus and cancer, gave 71 results, including five review papers, while the same search with urine instead of blood revealed 66 results, including eight review papers. Several studies have taken advantage of proteomics in the identification of new biomarkers. Adding proteomics to our PubMed searches revealed 31 original articles and 8 reviews, and only 6 articles when inflammation was included. The last five years revealed few experimentally work on serological and urinary biomarkers for the detection of inflammatory human SLE (Table 1), nearly all of them detecting active LN. Most of the identified biomarkers included in this table are part of molecular pathways involved in the pathogenesis of SLE. However, some of the markers such as albumin, ceruloplasmin, transferrin, lipocalin-type prostaglandin D2 synthase (LPGDS), and different collagen types are most likely a response to or caused by the inflammatory process. A recent review by Fasano et al. covers different tissue, serological, urinary, and cellular biomarkers related to molecular pathways in SLE (48). Since late 1980s, work has been published on double-negative T cells. These cells are implicated in inflammation, immune disorders, cancer, and kidney as reviewed in (49, 50). These cells have been observed in SLE, RA, and SS where they are described to have a worsening role, and in T1D where they are described to be protective [(51) and references therein]. In SLE, double-negative T cells have been suggested as potential serum biomarkers for SLE patients, possibly with kidney involvement (52). Exosomes are spherical lipid bilayer vesicles consisting of lipids, proteins, nucleic acids, and other bioactive compounds. Exosomes have been implied to be involved in immune responses and regulating the development of autoimmune disease through the transfer of signaling molecules as reviewed in (53). Studies have investigated exosomes and its components, both in serum and urine, and suggested them as potential biomarkers in SLE (54, 55), reviewed in (56, 57).

Plasma cytokines are also potential biomarkers in patients with SLE. Multiplex studies performed by Idborg et al. (22), showed that TNF-α and p-albumin worked as potential biomarkers to differentiate between SLE patients and controls, as well as indicators of disease activity. In addition, they showed that for SLE patients with joint involvement/active arthritis, IP-10, IL-1α, IL-6, TNF-α, and ESR were significantly increased compared with patients without these manifestations. They also investigated whether organ specific, active disease was associated to selected cytokines. P-albumin and TNF-α showed the highest association to kidney involvement, while IL-16, anti-dsDNA and IL-10 were elevated in active nephritis. Previously, Pentraxin 3 (PTX3) has been suggested as a biomarker of tubulointerstitial damage. Indeed, in a large, multicenter cross-sectional study, ELISA showed that higher PTX3 levels were found both in serum and urine of active phase LN patients (58). Peripheral blood mononuclear cells (PBMC) are also an easily accessible source of potential biomarkers. In a recent study by Fu et al. cyclic GMP-AMP synthase (cGAS) and interferon-I-inducible protein 16 (IFI16) were found to correlate with SLE disease activity (23). An interferon (IFN) signature with an increased expression of type I IFN-regulated genes, are well-known in patients with SLE. Jiang and colleagues (59) utilized bioinformatics and machine learning to identify biomarkers for use in SLE diagnosis. They identified ten potential diagnostic biomarkers and found one, IFI44, a type I IFN signature gene, that had the best potential of being an optimal diagnostic biomarker for SLE. However, the process of validating these findings experimentally and clinically remains to be done.

SLE organ specific biomarkers

Monitoring disease activity and organ damage in SLE is challenging due to the lack of dependable biomarkers and disease heterogeneity. Both permanent organ damage and ongoing systemic and organ-specific inflammation can be hard to differentiate. Thus, organ-specific biomarkers would be precious for systemic diseases such as SLE. A search on SLE and organs and biomarkers demonstrated that most of the research has been performed on kidney, and peripheral blood, followed by skin, joint, brain, lung, and liver, while very few articles on biomarkers in SGs and and pancreas exist (Supplementary Table S5; Figure 3A). Here we searched PubMed for articles comprising SLE, inflammation and different organs such as kidney, skin, joint, lung, brain, liver, pancreas, and SG looking for SLE biomarkers specific for the different organs (Figure 3B). From this search, we did not find any experimental papers on joint, liver, and pancreas.

SLE biomarkers in skin, lungs, brain, and salivary glands

Xie et al. identified L-alpha-aminobutyric acid, dehydroascorbic acid, glycine, and L-tyrosine as serum metabolites with diagnostic potential for SLE patients with skin lesions (24). Cutaneous lupus erythematosus has been found to be associated with an increase of invariant natural killer T (iNKT) cells expressing CCR4 at the site of active dermal cutaneous lesions, with a subsequent deficiency in circulating iNKT cells (60). One study also showed serum DNase I activity and apoptotic index evaluated by immunohistochemistry to be possible biomarkers of cutaneous lupus erythematosus (61). Nitric oxide (NO) in exhaled air has been shown to be significantly increased and correlated with disease activity and might be used as a marker for lung involvement in patients with SLE (62). In one study from Tumurkhuu et al. (25), SLE subjects showed highly significant increases in blood *NAMPT* mRNA expression and eNAMPT protein levels compared to healthy controls. In mice, this is shown to be associated with increased alveolar hemorrhage and lung inflammation. Going through publications on brain and SLE, we excluded publications on SLE and pregnancy. However, one publication on childhood-onset systemic lupus erythematosus (cSLE) showed that serum levels of S100A8/9, S100B, NGAL, aNR2-AB and aP-AB and combinations of those, could detect neurocognitive deficits in cSLE (sensitivity: 100%; specificity 76%) in exploratory analysis

TABLE 1 Summary of the proposed serological and urinary markers in inflammatory, human SLE revealed in this review.

Biomarker	Detects	References
Serological		
VCAM1	Predict nephritic flare, active non-renal lupus, and CKD	(17)
ICAM-1	Nephritic flare, LN remission	(17)
Syndecan-1	Predict nephritic flare, active LN, active non-renal lupus and patients with non-lupus CKD, renal interstitial inflammation	(18)
Hyaluronan, Thrombomodulin	Active LN,LN patients in remission and non-lupus CKD, renal chronicity	(18)
PRO-C6, Collagen Type III and IV	Kidney fibrosis	(19)
IL-35	Renal involvement	(20)
MALT1	Severity and inflammation in LN	(21)
TNF-α, p-albumin	Differentiate between SLE patients and controls, and indicators of disease activity	(22)
IP-10, IL-1α, IL-6, TNF-α, and ESR	Joint involvement/active arthritis	(22)
IL-16, anti-dsDNA and IL-10	Active LN	(22)
cGAS, IFI16	Correlate with SLE disease activity	(23)
L-alpha-aminobutyric acid, dehydroascorbic acid, glycine, and L-tyrosine	Skin manifestation	(24)
NAMPT, eNAMPT	Increased alveolar hemorrhage and lung inflammation	(25)
IL-26	Active disease	(26)
S100A8/A9 + S100A12	Response to treatment of rituximab	(27)
CD5L	Monitoring of SLE and therapeutic efficacy	(28)
TNFSF13B (BAFF) and *OAS1*	Diagnostic marker SLE and metabolic syndrome	(29)
EGF, Lipocalin-2/NGAL, uPA, IL-18	Biomarkers of renal pathology	(30)
IgA2 anti-dsDNA ab	Active renal disease	(31)
Urinary		
CD163	Active LN, higher CKD stage	(32, 33)
IL-16	Proliferative LN	(33, 34)
MCP-1 (CCL2)	Active LN, non-response, LN flare, loss of kidney function	(35, 36)
EGF	Biomarker of CKD progression in patients with glomerular disease (in adults and children)	(37, 38)
Serpin-A3	Active LN, proliferative LN, response to therapy in proliferative LN	(39)
Leukocytes	Active LN, response to treatment	(40)
Ig binding protein 1	Active LN	(41)
C3M	Kidney fibrosis	(19)
TWEAK	Active LN	(42)
Semaphorin3A	Renal involvement in SLE	(43)
suPAR	LN activity	(44)
S100	Active LN	(27)
Transferrin, AGP-1, MCP-1, sVCAM-1	Higher in SLE patients	(45)
Transferrin, LPGDS, ceruloplasmin, MCP-1 + sVCAM-1	Active LN	(45)
LPGDS, transferrin, AGP-1, ceruloplasmin, MCP-1 + sVCAM-1	Response to rituximab treatment	(45)
Angiostatin, CXCL4, VCAM-1	Biomarkers of LN	(46)
Exosomal miR-146a	LN and SLE flares	(47)

Results from the last 5 years. LN: lupus nephritis; CKD: chronic kidney disease; SLE: systemic lupus erythematosus.

(63). Another work showed that Progranulin (PGRN) was moderately increased in cerebrospinal fluid (CSF) of SLE patients (64). Many SLE patients are diagnosed with secondary Sjogren's syndrome. In one study, two of 34 patients were diagnosed with SLE and secondary SS. The authors showed that with higher pathologic grade, the presence of Sjogren's-syndrome-related antigen A (SSA) or a higher

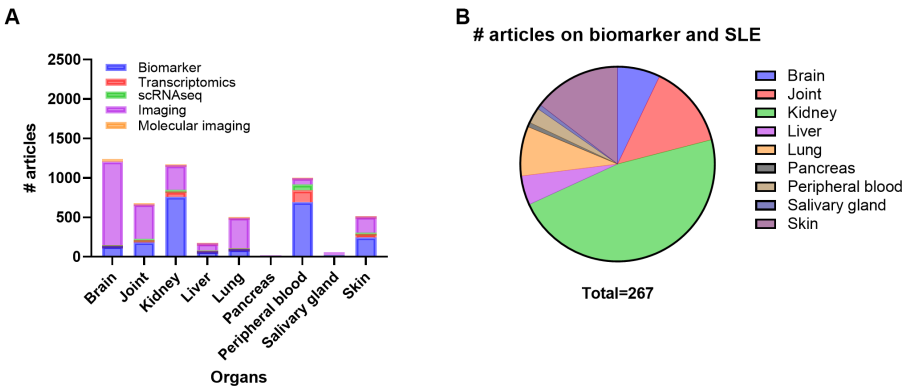

FIGURE 3
Overview of the number of publications on systemic lupus erythematosus (SLE), organ involvement and biomarker, transcriptomics, scRNAseq, imaging, and molecular imaging **(A)** and number of publications on biomarker in SLE with inflammation and organ involvement **(B)**. scRNAseq, single cell RNA sequencing.

titer of ANA were significantly associated with the overexpression of TRAIL, MMP-3, or ICAM-1 in the SG mononuclear cells in patients with SS (65).

Kidney specific biomarkers in SLE

Kidney is definitively the organ that has been most extensively researched in SLE. LN is also one of the most serious manifestations of SLE. A retrospective study by Mao et al. where they did proteomics on kidney biopsies, revealed renal mTORC1 activation as a possible biomarker for disease activity and prediction of clinical prognosis in LN patients (66). Another study showed urinary C3M, and serum derived PRO-C6, Collagen Type III and VI, to correlate with kidney fibrosis in SLE patients (19). Studies on serum Interleukin-35 (IL-35), and mucosa-associated lymphoid tissue lymphoma translocation protein 1 (MALT1) propose low IL-35, and high MALT1, respectively, to be potential biomarkers for renal involvement in SLE patients (20, 21). Biomarkers that can be indicative of response to treatment are useful. Indeed, Shipa et al. did a study where they identified serum IgA2 anti-dsDNA antibody concentrations that could predict a clinical response to belimumab after rituximab treatment (31). The presence of anti-ribosomal P antibody (anti-P) was in a study with 79 patients shown to be associated with better histological findings. In addition, at a median follow-up time of 47 months, anti-P-positive patients shown better renal outcomes than those without anti-P (58). A study by Sun et al. showed that urine tumor necrosis factor-related weak inducer of apoptosis (TWEAK) may be utilized as a biomarker of LN activity (42). The same was shown in a study on urinary DNase I, showing that its expression and activity declined with disease progression (67). A marker of podocyte injury was investigated by Bouachi et al. (68). Here they found that CMIP induction in LN appears constrained to non-proliferative glomerulopathies and may define a specific pattern of injury to these cells (68).

Due to the heterogeneity of SLE, there exist few biomarkers with the potential to capture the complexity of disease monitoring. Therefore, we need a combination of biomarkers and/or organ-specific biomarkers to follow disease progression. This review reveals that kidney, skin, and joint, respectively, have traditionally received the most attention in SLE because they are the most affected organs with frequent complications, but little progress has been achieved on organ-specific diagnostic or therapeutic markers.

SLE transcriptomics

Transcriptomic data analyses offer a unique insight into processes involved in different autoimmune disease. Since 2005, transcriptional analyses on human SLE and inflammation have been published in 85 research papers and 10 review papers (Supplementary Table S3). As for biomarkers, most of the transcriptomic research has been performed on peripheral blood followed by kidney, skin and joint (Supplementary Table S6; Figure 4A). PBMC analyses have revealed increased differences in the composition of immune cells (B, T, and myeloid cells), type 1 IFN signature, chemokines, and different transcriptional levels of cytosolic RNA and DNA sensors (69–76). Especially, it seems to be a correlation between reduced circular levels of naïve T cells and increased T cells in the different organs affected. A dysregulation of T regulatory cells vs. T helper cells (Th1, Th2 and Th17) is known to be important for the pathogenesis of SLE, and the involvement of Th1, Th2 and Th17 in SLE has recently been thoroughly reviewed (77). Transcriptomic analyses of circulating immune cells found upregulation of Th17 related genes *CXCL1, ICAM1, IL10, IL5, IL8, ISG20, JAK2*, and down regulation of *CD28, CD40LG, S1PR1, IL17RE, IL23R, RORC* genes (78).

The IFN signature in SLE can divide the patients into two groups: SLE1 with low levels IFN induced gene expression and SLE2 with high levels of IFN induced gene expression (79). In SLE2 patients a subset of cytotoxic $CD4^+$ T cells has been identified (72). Buang et al. found a downregulation of mitochondria-derived genes and metabolic pathways T cells of IFN high SLE patients (80). A transcriptome-wide association study (TWAS) was performed using a model on blood B cells, T cells, monocytes, NK cells and PBMC. Here they identified *BANK1, IRF5, BLK, NCOA2, WDFY4, SLC15A4 and RASGRP1* as differential expressed genes and potential biomarkers (81).

In the kidney, the early articles on transcriptomic data identified specific cellular expression of glomerular cells and

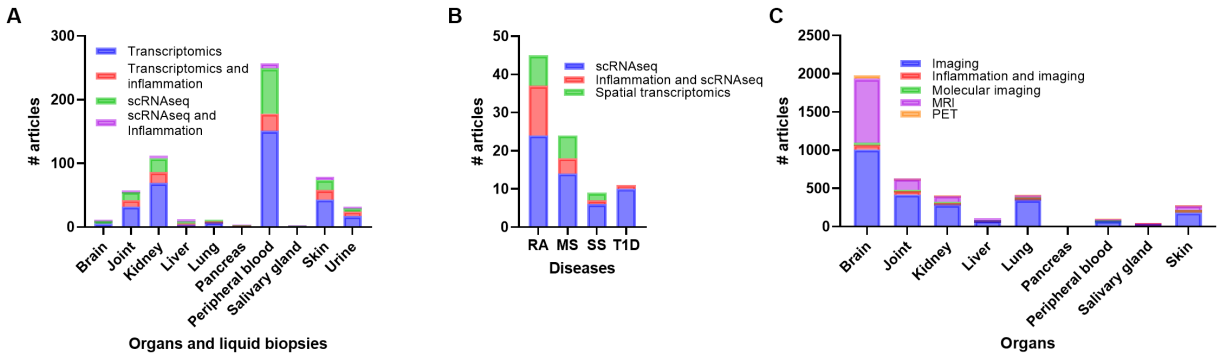

FIGURE 4
Overview of number of publications on transcriptomics, transcriptomics + inflammation, scRNAseq, and scRNAseq + inflammation in systemic lupus erythematosus (SLE) **(A)**, number of publications on scRNAseq, scRNAseq + inflammation, and spatial transcriptomics in rheumatoid arthritis (RA), multiple sclerosis (MS), Sjogren's syndrome (SS) and Type 1 diabetes (T1D) **(B)**, and number of publications on imaging, imaging + inflammation, molecular imaging, magnetic resonance imaging (MRI) and positron emmission tomography (PET) in SLE **(C)**. scRNAseq, single cell RNA sequencing.

selected inflammatory markers of infiltrating cells using qPCR analyses (82, 83). The newly published research includes transcriptional profiling of kidney tubular cells and immune cell infiltration in patients with LN (84–89). The main findings identify, like in peripheral blood samples, inflammatory markers such as type I IFNs, IL-18, TNF, immune cells including myeloid cells, T cells, natural killer cells and B cells, plasma cells and chemokines and chemokine receptors. Especially chemokine receptors *CXCR4* and *CX3CR1* expression by kidney immune cells seems to be candidates for use as biomarkers (85). In the skin of SLE and cutaneous lupus erythematosus (CLE) a hypersensitive response to IFNs was observed in keratinocytes (90).

Biopsies are only taken from patients with suspected kidney disease, but many SLE patients may have changes within the kidney long before they develop clinical detectable inflammation. Several studies have analyzed the transcriptomic profile of cells and cellular casts in urine from patients with SLE and LN (33, 83, 85, 91). Urinary transcriptomics reviled both a podocyte cell specific signature and an enrichment of immune cell types reflecting the inflammation of the kidney (83). Arazi et al. compared immune cells from urine samples with the kidney samples and found that the main fraction of urine cell was phagocytic CD16+ macrophages followed by M2-line $CD16^{+}$ macrophages, $CD56^{dim}$ $CD16^{+}$ NK cells, inflammatory CD16+ macrophages, tissue resident macrophages, and conventional DCs (85). A study analyzing both proteomics on urine samples and transcriptomics on kidney biopsies found increased urine levels of IL-16, CD163 and TGFB1 and an increased expression of *IL16* in most of the infiltrating immune cells, *CD163* in a subset of myeloid cells, and *TGFB1* was mostly expressed by NK cells (33). In a recent article addressing the proteomics in paired urine and biopsy from SLE and LN patients, they identified over 112 urine analytes and especially found proteins involved in granulocyte-associated and macrophage-associated pathways, including CD163 (92).

SLE single cell sequencing (scRNAseq)

ScRNAseq has mostly been performed on peripheral blood, with fewer studies on kidney, skin, and joint samples from SLE patients (Figure 4A). ScRNAseq performed on kidney (84, 85), skin (84, 93), and PBMC (94) revealed common factors including different immune cell types and type I IFN signature. The chemokines and chemokine receptors expression were linked to tubular cells (kidney) or keratinocytes (skin) and immune cells (84). Guo et al. identified a reduction of $CXCR5^{+}$ T cells in SLE patients and found an exhausted regulatory $CD4^{+}$ T cell subset in PBMC from SLE patients induced by type 1 IFN signaling (95).

In the skin, the same types of T cells including $CD4^{+}$ and $CD8^{+}$ memory T cells, Tregs, cytotoxic T cells, Th cells, and others were found to express increased levels of IFN-genes, but appeared less activated and cytotoxic and did not show an exhausted phenotype as T/NK cells from the kidney of LN patients (87). Zheng et al. analyzed cells from different cutaneous lesions of SLE patients and found both similar and differences in cell compositions of skin biopsies from patient with discoid lupus erythematosus (DLE) and SLE (96). Similarities included the proportion of macrophages and dendritic cells in both epidermis and dermis, while differences in T, NK and B cells were prominent in dermis as DLE patients had more T, NK, and B cells. DLE skin biopsies showed a more organized accumulation of immune cells (96).

Li et al. (97) performed both proteomics and scRNAseq on PBMC from SLE patients. They identified, by using machine learning, combinations of biomarkers that could diagnose SLE and the cellular source of these proteins was determined using scRNAseq (97). The six-protein combination included IFN inducible genes (IFIT3, MX1, TOMM40, STAT1, STAT2, and OAS3) and the nine- protein combinations included mitochondrial enzymes, adhesion molecule, kinases and other proteins (PHACTR2, GOT2, L-selectin, CMC4, MAP2K1, CMPK2, ECPAS, SRA1, and STAT2) (97). Genes in the six-protein combinations were shown to be mostly upregulated in memory B cells, while the nine-protein combination genes were upregulated in CD14 monocyte clusters. Tang et al. performed scRNAseq on PBMC from SLE patients to analyze the expression of acetyl transferases that can regulate cyclic GMP-AMP synthase (cGAS) a cytoplasmic DNA sensor (75). They identified an upregulation of histone acetyltransferase *KAT2A* in SLE patients and showed that the pathway was increased in specific subtypes of myeloid dendritic

cells (DC), monocytes, T and B cells observed in SLE patients with a high SLEDAI score (75).

Itotagawa et al. used existing scRNAseq data to identify the BAFF producing cells in the kidney of SLE patients and linking the urinary BAFF levels to LN (98). The usage of available scRNAseq data together with advanced proteomics and the development of AI pipelines offers a deeper understanding of the complexity of disease progression. Wang et al. used a combination of machine learning algorithm and scRNAseq analysis to find possible biomarkers and identified both protein and gene expression of TNFSF13B and OAS1 (29). As mentioned under the section on biomarkers, a study using scRNAseq data from SLE patients (99) identified IFI44 as possible biomarker for SLE (59). However, linking these findings to the existing clinical parameters and developing new and better disease biomarkers is a challenge.

Transcriptomics and scRNAseq in other autoimmune diseases

Transcriptomics and scRNAseq data from other autoimmune diseases may fill in the lack of data in SLE. A PubMed search on RA, MS, SS, T1D and scRNAseq and scRNAseq + inflammation, including only original articles with new scRNAseq data gave 24 and 13 results on RA, 14 and 4 results on MS, 6 and 1 results on SS and 10 and 1 results on T1D, respectively (Figure 4B). In RA, $CD4^+$ T cell clones in peripheral blood and synovial tissue were shown to be under constant activation and had a senescent phenotype (100). Some studies have analyzed and compared the gene expression profiles between autoimmune diseases. Tuller et al. analyzed gene expression profiles of PBMC from MS, SLE, juvenile (J)RA, crohn's disease (CD), ulcerative colitis (UC) and T1D patients compared to healthy controls (101). A common trend was observed for the chemokines *CXCL1-3, 5, 6,* and *IL8* in addition to differentially expressed genes involved in cell proliferation, inflammatory response, general signaling cascades, and apoptosis. The authors suggest that despite the similarities, the results indicate an activation through different sub-signaling pathways (101). In another study, distinct DC clusters characterized by up-regulation of *TAP1*, *IRF7*, and *IFNAR1*, were identified in systemic autoimmune diseases and *PTPN6*, *TGFB*, and *TYROBP* were shown to be downregulated in DCs in T1D (73). Liao et al. used existing scRNA data on fibroblasts from RA and osteoarthritis from synovial tissue (102). They identified CCL2 and MMP13 as possible diagnostic and therapeutic markers. Another study focusing on transcription factors revealed five regulators BATF, POU2AF1, STAT1, LEF1 and IRF4 specific for RA fibroblast-like synoviocytes (103).

Stephenson et al. used a low-cost microfluidic instrumentation to perform scRNAseq analyses and identified synovial fibroblast (SF) subtypes in addition to well-known immune cell clusters (104). The fibroblast subtype (*THY1(CD90)*$^+$*HLA-DRA*^{hi}) was verified and linked to *L1B*$^+$ pro-inflammatory monocytes, *ITGAX*$^+$*TBX21*$^+$ autoimmune-associated B cells and *PDCD1*$^+$ T peripheral helper (Tph) and T follicular helper (Tfh) (105). In synovial macrophages isolated from RA patients, the expression of signaling lymphocytic activation molecule F7 (SLAMF7) was identified as a marker for super activated macrophages (106), and upregulation of CD86 and CD206 was observed in cells from the synovium lining layer (107). Yamada et al. analyzed synovial scRNAseq data identifying a subset of pre-dendritic cells possibly predicting resistant to treatment (108). Another study analyzing the $CD4^+$ T cell subsets in RA identified two Tph states (*CXCL13* high and low) and a cytotoxic $CD4^+$ T cell subset where all expressed GPR56 (*ADGRG1*) (109). Moon et al. used scRNAseq and TCR sequencing on $CD8^+$ T cells from blood and found seven distinct clusters of $CD8^+$ T cells (Naïve, Memory, *TCRgd*$^+$, *GZMK*$^+$, *GZMB*$^+$ *GNLY*$^+$, *GZMB*$^+$ *KIR*$^+$ *and CCR6*$^+$ *CD161*$^+$) where cluster *GZMB*$^+$ *KIR*$^+$, *TCRgd*$^+$, and memory were increased, and cluster *CCR6*$^+$ *CD161*$^+$ were decreased in RA patients compared to healthy controls (110). Two groups have studied different classes of monocytes and macrophages isolated from blood of RA patients to analyze response to treatment and the function of macrophages, respectively (111, 112). Several studies have used existing and/or own scRNAseq data to identify RA mechanisms or disease markers. An article by Orange et al. showed increased expansion of preinflammatory mesenchymal cells (113), while Micheroli et al. identified four distinct SF clusters (114). Yang et al. studied scRNAseq datasets for SFs revealing *Fibronectin-1* as an important gene in relation to RA disease progression (115). A recent review discusses the development of residential memory T cells in synovial tissue in RA patients and indicate a role for these cells in the transition from acute to chronic inflammation (116).

ScRNAseq on cells from CSF and blood in MS patients demonstrate a strong immune cell profile like the signatures seen in other autoimmune diseases. Especially B cells are increased in CSF in addition to $CD4^+$ and $CD8^+$ T cells (117). Several studies have also analyzed microglial cells using scRNAseq [reviewed in (118)]. In SS scRNAseq analyses on PBMC, monocytes were the abundant cell type and the expression of transcription factor *CEBPD* and tumor necrosis factor (ligand) superfamily, member 10 *TNFSF10* (TRAIL) in $CD14^+$ monocytes were increased (119, 120). Hou et al. showed an increased percentage of Tregs while $CD8^+$ T cells, mucosal associated invariant T cells (MAIT) and double positive $CD4^+$ $CD8^+$ T cells were reduced in SS compared to healthy donors (121). However, a recent publication from Xu et al. showed increased expression of $CD8^+$ T cells in patients with SS (122). These granzyme K^+ ($GZMK^+$) $CXCR6^+$ $CD8^+$ T cells from blood were similar to a distinct group of tissue-resident memory T cells. The same study showed an increased expression of circulatory IL-15, possibly promoting this specific differentiation of the $CD8^+$ T cells (122). Hong et al. identified an increased cytotoxic $CD4^+$ T cell population in addition to increased *IL1b* in macrophages, *TCL1A* in B cells, and like in SLE an increased expression of IFN responsive genes in most of the immune cells analyzed (123).

A recent review paper gives an overview of the existing sequencing platforms and especially on how scRNAseq has been used in over 41 autoimmune diseases (7). The results from scRNAseq identifies both common and disease specific subtypes of cells triggered by common and different signaling pathways. Here they conclude that the identification of specific disease-causing cells using scRNAseq in combination with other methods is a prerequisite for developing more effective targeting treatments with less side effects (7). Ma et al. used scRNAseq data from SLE patients (124), and compared it to RNA bulk sequencing on PBMC from SLE, RA and MS patients and healthy donors by using machine learning to develop a method to identify characteristic of SLE and to distinguish SLE patients from healthy donors (125). Their mathematical model could also identify patients with RA and MS and proves that the usage of existing scRNAseq and

the development of machine learning models could be used to develop efficient tools for diagnosis of chronic autoimmune diseases.

Spatial transcriptomics

Spatial transcriptomics is a new technique applying scRNAseq on tissue samples allowing visualization and quantitative analyses of spatial gene expression patterns in individual tissue sections at near single-cell resolution (126). We found 8 papers on spatial transcriptomics and RA, 6 on MS and 2 on SS (Figure 4B). However, many of these were review papers. Most of the research involving spatial transcriptomics has been published on synovial tissue from RA patients (127–129) and brain tissue from MS patients (130, 131). So far, no spatial transcriptomics analyses have been published on tissue from SLE or LN patients. However, research have been published on normal kidneys (132), transplanted kidneys (133), and some review papers have given an overview of the use of spatial transcriptomics and analyzing kidney diseases (134–138). Spatial transcriptomics on normal tissue may offer a new understanding of tissue cells and residential immune cells. Madissoon et al. used multi-omics single cell/nuclei and spatial transcriptomics to define the tissue architecture of lungs and airways (139). The results reviled a new specific niche for immune cells in the lungs and may be used further in analyzing molecular and cellular changes during different lung diseases.

Several review papers have addressed the advantage of spatial transcriptomics in different autoimmune diseases (116, 136, 138, 140). The development of disease pathology Atlases based on bulk RNAseq, scRNAseq, and spatial transcriptomics, machine learning models, and the use of AI to combine clinical and multiomics data, will be crucial in the future research on chronic autoimmune diseases including SLE. Especially, to identify clinically relevant patterns in the abundance of information available.

SLE and organ imaging

Imaging, inflammation and SLE reviled 357 papers and 26 of them included kidney (Supplementary Table S7). Papers involving imaging and brain (81), joint (70) and skin (62) were prominent with lung (57) at the same level as kidney (Figure 4C). The imaging methods used included mostly histological or immunohistology assessment of biopsies. Gallium-67 scintigraphy was previously performed on LN patients before and after biopsy to predict response to therapy (141). Recently, a new study analyzed over 250 biopsies from LN patients that underwent renal gallium scans before or after biopsy (142). They found an association of renal gallium uptake and active inflammation measured by hypercellularity, neutrophil infiltration and changes in the activity index.

Research on SLE and molecular imaging consist of 20 articles where 3 are review papers. Including inflammation in the search reduced the papers to 4 (2 reviews). The reviews cover the use of non-invasive imaging of LN and neuropsychiatric SLE and especially the use of PET (143, 144). A more specific search on inflammation, SLE and MRI found 139 papers involving MRI on brain (74), joint (52), skin (10), kidney (6), SG (1) (Supplementary Table S8; Figure 4C). Most of the MRI has been conducted on brain and the association of inflammation and functional and structural brain changes in neuropsychiatric SLE (143, 145). A broader search on SLE, MRI and kidney reviled several research papers on the use of multiparametric MRI including blood oxygen level-dependent (BOLD) imaging by T2* mapping, magnetic resonance elastography (MRE) by tomoelastography, diffusion tensor imaging (DTI) and diffusion-weighted imaging (DWI) for detecting nephropathy in LN patients (145–151). Here BOLD, DTI, and DWI imaging may determine the disease severity, effect of treatment, and outcome of the disease (151).

PET/CT and PET/MRI has been used to image brain (144, 152), kidney (153), and lung (152) of SLE patients [reviewed in (143, 154)]. Most of the research used ^{18}FFDG, but in brain 2 studies used TSPO targeted PET/MRI to image hippocampal neuroinflammation and were able to detect signal alterations [reviewed in (155)]. However, Nwaubani et al. reviled a lack of research to examine hippocampal subfield separatley, and suggests new methods with higher resolution acquisition or post-processing teckniques (155). Despite some preclinical studies using PET/CT or PET/MRI in kidneys, none has been performed on SLE or LN patients. However, Carlucci et al. performed PET/CT with 18F-FDG to quantify vascular inflammation and significant increased aortic inflammation in SLE patients compared to healthy controls (156).

The lung involvement in SLE has recently been reviewed by Shin et al. revealing several imaging methods (157). Chest X-ray (CXR), CT, technetium-99 m hexamethylprophylene amine oxime perfusion scan, and ^{18}FFDG PET are used to diagnose pleuropulmonary involvement in SLE. The involvement includes lupus pleuritis, pleural effusion, acute lupus pneumonitis, shrinking lung syndrome, interstitial lung disease, diffuse alveolar hemorrhage (DAH), pulmonary arterial hypertension, and pulmonary embolism (157).

This review reviled many imaging methods that have been performed on SLE patients with brain and lung involvement. However, despite being a systemic disease, only few imaging methods tested have focused on the detection of systemic inflammation in SLE. One of the reasons is the lack of specific markers for systemic inflammation. Another issue is the filtration of tracers by the kidney, making imaging of this organ difficult. The development of new specific long-lived isotopes (89Zr, 68Cu) (158, 159) conjugated to different immunobiologicals (ligands, antibodies, Fabs) may generate tracers that can detect changes within the kidney and detect early inflammatory events (160). *In vivo* imaging using PET/MRI with specific tracers to detect tissue damage or immune cell involvement may be used as a diagnostic tool to detect inflammatory kidney diseases at an early stage, as a non-invasive method to follow disease progression, and to more specific, tailored/personalized treatment. A tracer that detects systemic inflammation will be beneficial for other autoimmune diseases.

Conclusion

Publications comprising advanced methods and biomarkers that can be used for various diseases, but with a focus on SLE, have been reviewed. Is it possible to find common methods and biomarkers across different diseases, and is it possible to find organ specific biomarkers to monitor organ inflammation? A similar approach has been used in the Taxonomy, Treatment, Targets and Remission (3TR) study where they aim to investigate the mechanisms of response and

non-response to treatment in chronic autoimmune diseases (MS, SLE and RA), inflammatory bowel diseases (Ulcerative Colitis and Crohn's Disease), and respiratory diseases (Asthma and Chronic Obstructive Pulmonary Disease).[1] Since SLE is a systemic disease, it could fit as a model disease to use in such studies. A recent review from the 3TR study on LN gives an overview of biomarkers that is suitable for diagnostics, determine disease activity and organ damage, determine the response to therapy, and biomarkers to be used to determine the prognosis (161).

As heterogenous as SLE is, one ideal biomarker or method does probably not exist for disease diagnosis and monitoring. Instead, we ought to look for biomarkers and methods that have specificity and sensitivity for distinct organ involvement. We suggest that utilizing results from other autoimmune diseases with different organ manifestations would be of interest in SLE. Probably organ-specific biomarkers can be exploited across different diseases. Indeed, Johnson et al. showed that there are selected biomarkers that are more valid for diabetic kidney disease compared to LN, but none of them could distinguish between these two diseases (30). Zhang and Lee used a combined strategy utilizing multi-omics data analysis and computational methods and identified specific variable (V) and joining (J) genes in both T cell receptor and B cell receptor in SLE and RA groups (162). In addition, looking for a combination of biomarkers, composite biomarkers, and combined strategies with biomarkers, new methods and clinical measurements is perhaps the best strategy ahead. Using transcriptomics combined with principal component analyses (PCA)/AI to search for inflammatory markers in blood and urine can substitute for invasive kidney biopsy and allows physicians to monitor treatment and disease progression. Liquid biomarkers enable non-invasive, real-time detection of circulating markers in blood or urine. By its nature, urinary biomarkers are by far the best alternative when it comes to noninvasive biomarkers. Especially for the monitoring of kidney affection, urine is probably the best source for easy follow-ups. However, multiomics studies generate a lot of data, but there are still few, specific studies on autoimmune diseases. Also, there is a need to combine, compare, and extract the results before verifying their importance in the clinic. These issues must be addressed before we can develop tailored treatment strategies for SLE patients, as addressed in a review by Fasano et al. (48).

The use of non-invasive molecular imaging methods with specific markers will provide a more comprehensive picture of organ inflammation and enable serial assessments as patients are treated. The development of multimodality MRI scanners opens for high-resolution functional and molecular imaging research. Molecular imaging biomarkers will improve treatment to individual patients, and the capacity to evaluate the usefulness of new treatments in LN and other autoimmune diseases. Chronic inflammatory diseases like SLE are both debilitating and hard to diagnose. Future studies combining precise biomarkers, bioinformatical profiles and non-invasive imaging may lead to the development of procedures used for precise and early diagnosis, targeted treatment, as well as treatment and disease monitoring. This will increase the quality of life and life-expectancy for the patients.

1 https://www.3tr-imi.eu/

Author contributions

All authors listed have made a substantial, direct, and intellectual contribution to the work and approved it for publication.

Funding

This research was funded in whole or in part by Northern Norway Regional Health Authority (HNF1343-17 and HNF1427-18), and UiT the Arctic University of Tromsø. For the purpose of Open Access, the author has applied a CC BY public copyright licence to any Author Accepted Manuscript (AAM) version arising from this submission.

Conflict of interest

The authors declare that the research was conducted in the absence of any commercial or financial relationships that could be construed as a potential conflict of interest.

Publisher's note

Supplementary material

The Supplementary material for this article can be found online at: https://www.frontiersin.org/articles/10.3389/fmed.2023.1183535/full#supplementary-material

References

1. Furman D, Campisi J, Verdin E, Carrera-Bastos P, Targ S, Franceschi C, et al. Chronic inflammation in the etiology of disease across the life span. *Nat Med*. (2019) 25:1822–32. doi: 10.1038/s41591-019-0675-0

2. Bieber K, Hundt JE, Yu X, Ehlers M, Petersen F, Karsten CM, et al. Autoimmune pre-disease. *Autoimmun Rev*. (2023) 22:103236. doi: 10.1016/j.autrev.2022.103236

3. Rekvig OP. The anti-DNA antibodies: their specificities for unique DNA structures and their unresolved clinical impact-a system criticism and a hypothesis. *Front Immunol*. (2021) 12:808008. doi: 10.3389/fimmu.2021.808008

4. Giacomelli R, Afeltra A, Alunno A, Bartoloni-Bocci E, Berardicurti O, Bombardieri M, et al. Guidelines for biomarkers in autoimmune rheumatic diseases - evidence based analysis. *Autoimmun Rev*. (2019) 18:93–106. doi: 10.1016/j.autrev.2018.08.003

5. Nagafuchi Y, Yanaoka H, Fujio K. Lessons from transcriptome analysis of autoimmune diseases. *Front Immunol*. (2022) 13:857269. doi: 10.3389/fimmu.2022.857269

6. Tang F, Barbacioru C, Wang Y, Nordman E, Lee C, Xu N, et al. mRNA-Seq whole-transcriptome analysis of a single cell. *Nat Methods*. (2009) 6:377–82. doi: 10.1038/nmeth.1315

7. Zeng L, Yang K, Zhang T, Zhu X, Hao W, Chen H, et al. Research progress of single-cell transcriptome sequencing in autoimmune diseases and autoinflammatory disease: a review. *J Autoimmun*. (2022) 133:102919. doi: 10.1016/j.jaut.2022.102919

8. Kuret T, Sodin-Semrl S, Leskosek B, Ferk P. Single cell RNA sequencing in autoimmune inflammatory rheumatic diseases: current applications, challenges and a step toward precision medicine. *Front Med (Lausanne)*. (2021) 8:822804. doi: 10.3389/fmed.2021.827095

9. Penate Medina T, Kolb JP, Huttmann G, Huber R, Penate Medina O, Ha L, et al. Imaging inflammation - from whole body imaging to cellular resolution. *Front Immunol*. (2021) 12:692222. doi: 10.3389/fimmu.2021.692222

10. Iking J, Staniszewska M, Kessler L, Klose JM, Luckerath K, Fendler WP, et al. Imaging inflammation with positron emission tomography. *Biomedicine*. (2021) 9:212. doi: 10.3390/biomedicines9020212

11. Kang EH, Ha YJ, Lee YJ. Autoantibody biomarkers in rheumatic diseases. *Int J Mol Sci*. (2020) 21:1382. doi: 10.3390/ijms21041382

12. Burbelo PD, Iadarola MJ, Keller JM, Warner BM. Autoantibodies targeting intracellular and extracellular proteins in autoimmunity. *Front Immunol*. (2021) 12:548469. doi: 10.3389/fimmu.2021.548469

13. Gomez-Banuelos E, Fava A, Andrade F. An update on autoantibodies in systemic lupus erythematosus. *Curr Opin Rheumatol*. (2023) 35:61–7. doi: 10.1097/BOR.0000000000000922

14. Yu H, Nagafuchi Y, Fujio K. Clinical and immunological biomarkers for systemic lupus erythematosus. *Biomol Ther*. (2021) 11:928. doi: 10.3390/biom11070928

15. Tan G, Baby B, Zhou Y, Wu T. Emerging molecular markers towards potential diagnostic panels for lupus. *Front Immunol*. (2021) 12:808839. doi: 10.3389/fimmu.2021.808839

16. Capecchi R, Puxeddu I, Pratesi F, Migliorini P. New biomarkers in SLE: from bench to bedside. *Rheumatology (Oxford)*. (2020) 59:v12–8. doi: 10.1093/rheumatology/keaa484

17. Yu KY, Yung SS, Chau MK, Tang CS, Yap DY, Tang AH, et al. Clinico-pathological associations of serum VCAM-1 and ICAM-1 levels in patients with lupus nephritis. *Lupus*. (2021) 30:1039–50. doi: 10.1177/09612033211004727

18. Yu KYC, Yung S, Chau MKM, Tang CSO, Yap DYH, Tang AHN, et al. Serum syndecan-1, hyaluronan and thrombomodulin levels in patients with lupus nephritis. *Rheumatology*. (2021) 60:737–50. doi: 10.1093/rheumatology/keaa370

19. Genovese F, Akhgar A, Lim SS, Farris AB, Battle M, Cobb J, et al. Collagen type III and VI Remodeling biomarkers are associated with kidney fibrosis in lupus nephritis. *Kidney360*. (2021) 2:1473–81. doi: 10.34067/KID.0001132021

20. He D, Liu M, Liu B. Interleukin-35 as a new biomarker of renal involvement in lupus nephritis patients. *Tohoku J Exp Med*. (2018) 244:263–70. doi: 10.1620/tjem.244.263

21. Wang M, Huang L, Peng LP, Yang YM, Mao J, Zhu N, et al. MALT1 serves as a biomarker for estimating disease risk of lupus nephritis: a prospective case-control study. *Ann Transl Med*. (2022) 10:3442. doi: 10.21037/atm-22-3442

22. Idborg H, Eketjall S, Pettersson S, Gustafsson JT, Zickert A, Kvarnstrom M, et al. TNF-alpha and plasma albumin as biomarkers of disease activity in systemic lupus erythematosus. Lupus. *Sci Med*. (2018) 5:260. doi: 10.1136/lupus-2018-000260

23. Fu Q, He QY, Dong Q, Xie JY, Geng YY, Han H, et al. The role of cyclic GMP-AMP synthase and interferon-I-inducible protein 16 as candidatebiomarkers of systemic lupus erythematosus. *Clin Chim Acta*. (2022) 524:69–77. doi: 10.1016/j.cca.2021.11.003

24. Xie YY, Liu BY, Wu ZW. Identification of serum biomarkers and pathways of systemic lupus erythematosus with skin involvement through GC/MS-based metabolomics analysis. *Clin Cosmet Investig Dermatol*. (2022) 15:77–86. doi: 10.2147/CCID.S345372

25. Tumurkhuu G, Csanova NG, Kempf CL, Laguna DE, Camp SM, Dagvadorj J, et al. eNAMPT/TLR4 inflammatory cascade activation is a key contributor to SLE lung vasculitis and alveolar hemorrhage. *J Transl Autoimmun*. (2023) 6:100181. doi: 10.1016/j.jtauto.2022.100181

26. Brilland B, Bach-Bunner M, Gomes CN, Larochette V, Foucher E, Plaisance M, et al. Serum Interleukin-26 is a new biomarker for disease activity assessment in systemic lupus erythematosus. *Front Immunol*. (2021) 12:663192. doi: 10.3389/fimmu.2021.663192

27. Davies JC, Midgley A, Carlsson E, Donohue S, Bruce IN, Beresford MW, et al. Urine and serum S100A8/A9 and S100A12 associate with active lupus nephritis and may predict response to rituximab treatment. *RMD Open*. (2020) 6:1257. doi: 10.1136/rmdopen-2020-001257

28. Lai X, Xiang Y, Zou L, Li Y, Zhang L. Elevation of serum CD5L concentration is correlated with disease activity in patients with systemic lupus erythematosus. *Int Immunopharmacol*. (2018) 63:311–6. doi: 10.1016/j.intimp.2018.07.022

29. Wang Y, Huang Z, Xiao Y, Wan W, Yang X. The shared biomarkers and pathways of systemic lupus erythematosus and metabolic syndrome analyzed by bioinformatics combining machine learning algorithm and single-cell sequencing analysis. *Front Immunol*. (2022) 13:1015882. doi: 10.3389/fimmu.2022.1015882

30. Johnson NH, Keane RW, de Rivero Vaccari JP. Renal and inflammatory proteins as biomarkers of diabetic kidney disease and lupus nephritis. *Oxidative Med Cell Longev*. (2022) 2022:5631099. doi: 10.1155/2022/5631099

31. Shipa M, Santos LR, Nguyen DX, Embleton-Thirsk A, Parvaz M, Heptinstall LL, et al. Identification of biomarkers to stratify response to B-cell-targeted therapies in systemic lupus erythematosus: an exploratory analysis of a randomised controlled trial. *Lancet Rheumatol*. (2023) 5:e24–35. doi: 10.1016/S2665-9913(22)00332-0

32. Huang YJ, Lin CH, Yang HY, Luo SF, Kuo CF. Urine soluble CD163 is a promising biomarker for the diagnosis and evaluation of lupus nephritis. *Front Immunol*. (2022) 13:606. doi: 10.3389/fimmu.2022.1058606

33. Fava A, Rao DA, Mohan C, Zhang T, Rosenberg A, Fenaroli P, et al. Urine proteomics and renal single-cell transcriptomics implicate Interleukin-16 in lupus nephritis. *Arthritis Rheumatol*. (2022) 74:829–39. doi: 10.1002/art.42023

34. Hayry A, Faustini F, Zickert A, Larsson A, Niewold TB, Svenungsson E, et al. Interleukin (IL) 16: a candidate urinary biomarker for proliferative lupus nephritis. Lupus. *Sci Med*. (2022) 9:744. doi: 10.1136/lupus-2022-000744

35. Perez-Arias AA, Mendez-Perez RA, Cruz C, Zavala-Miranda MF, Romero-Diaz J, Marquez-Macedo SE, et al. The first-year course of urine MCP-1 and its association with response to treatment and long-term kidney prognosis in lupus nephritis. *Clin Rheumatol*. (2023) 42:83–92. doi: 10.1007/s10067-022-06373-y

36. Gupta R, Yadav A, Aggarwal A. Longitudinal assessment of monocyte chemoattractant protein-1 in lupus nephritis as a biomarker of disease activity. *Clin Rheumatol*. (2016) 35:2707–14. doi: 10.1007/s10067-016-3404-9

37. Ju W, Nair V, Smith S, Zhu L, Shedden K, Song PXK, et al. Tissue transcriptome-driven identification of epidermal growth factor as a chronic kidney disease biomarker. *Sci Transl Med*. (2015) 7:316ra193. doi: 10.1126/scitranslmed.aac7071

38. Azukaitis K, Ju W, Kirchner M, Nair V, Smith M, Fang Z, et al. Low levels of urinary epidermal growth factor predict chronic kidney disease progression in children. *Kidney Int*. (2019) 96:214–21. doi: 10.1016/j.kint.2019.01.035

39. Martinez-Rojas MA, Sanchez-Navarro A, Mejia-Vilet JM, Perez-Villalva R, Uribe N, Bobadilla NA. Urinary serpin-A3 is an early predictor of clinical response to therapy in patients with proliferative lupus nephritis. *Am J Physiol Renal Fluid Electrol Physiol*. (2022) 323:F425–34. doi: 10.1152/ajprenal.00099.2022

40. Bertolo M, Baumgart S, Durek P, Peddinghaus A, Mei H, Rose T, et al. Deep phenotyping of urinary leukocytes by mass cytometry reveals a leukocyte signature for early and non-invasive prediction of response to treatment in active lupus nephritis. *Front Immunol*. (2020) 11:256. doi: 10.3389/fimmu.2020.00256

41. Lee EJ, Kwon OC, Ghang B, Lim DH, Kim DH, Hong S, et al. Immunoglobulin binding protein 1 as a potential urine biomarker in patients with lupus nephritis. *Int J Mol Sci*. (2019) 20:2606. doi: 10.3390/ijms20102606

42. Sun F, Teng J, Yu P, Li W, Chang J, Xu H. Involvement of TWEAK and the NF-kappaB signaling pathway in lupus nephritis. *Exp Ther Med*. (2018) 15:2611–9. doi: 10.3892/etm.2018.5711

43. Doron R, Merav L, Nasrin E, Adi SD, Elias T, Gleb S, et al. Low urine secretion of Semaphorin3A in lupus patients with proteinuria. *Inflammation*. (2022) 45:603–9. doi: 10.1007/s10753-021-01570-4

44. Burcsar S, Toldi G, Kovacs L, Szalay B, Vasarhelyi B, Balog A. Urine soluble urokinase plasminogen activator receptor as a potential biomarker of lupus nephritis activity. *Biomarkers*. (2021) 26:443–9. doi: 10.1080/1354750X.2021.1910343

45. Davies JC, Carlsson E, Midgley A, Smith EMD, Bruce IN, Beresford MW, et al. A panel of urinary proteins predicts active lupus nephritis and response to rituximab treatment. *Rheumatology (Oxford)*. (2021) 60:3747–59. doi: 10.1093/rheumatology/keaa851

46. Mok CC, Soliman S, Ho LY, Mohamed FA, Mohamed FI, Mohan C. Urinary angiostatin, CXCL4 and VCAM-1 as biomarkers of lupus nephritis. *Arthritis Res Ther*. (2018) 20:6. doi: 10.1186/s13075-017-1498-3

47. Perez-Hernandez J, Martinez-Arroyo O, Ortega A, Galera M, Solis-Salguero MA, Chaves FJ, et al. Urinary exosomal miR-146a as a marker of albuminuria, activity changes and disease flares in lupus nephritis. *J Nephrol*. (2021) 34:1157–67. doi: 10.1007/s40620-020-00832-y

48. Fasano S, Milone A, Nicoletti GF, Isenberg DA, Ciccia F. Precision medicine in systemic lupus erythematosus. *Nat Rev Rheumatol*. (2023) 19:331–42. doi: 10.1038/s41584-023-00948-y

49. Newman-Rivera AM, Kurzhagen JT, Rabb H. TCR??+CD4-/CD8-?Double negative? T cells in health and disease-implications for the kidney. *Kidney Int*. (2022) 102:25–37. doi: 10.1016/j.kint.2022.02.035

50. Wu Z, Zheng Y, Sheng J, Han Y, Yang Y, Pan H, et al. CD3(+)CD4(−)CD8(−) (double-negative) T cells in inflammation, Immune Disorders and Cancer. *Front Immunol*. (2022) 13:816005. doi: 10.3389/fimmu.2022.1008047

51. Velikkakam T, Gollob KJ, Dutra WO. Double-negative T cells: setting the stage for disease control or progression. *Immunology*. (2022) 165:371–85. doi: 10.1111/imm.13441

52. Alexander JJ, Jacob A, Chang A, Quigg RJ, Jarvis JN. Double negative T cells, a potential biomarker for systemic lupus erythematosus. *Precis Clin Med*. (2020) 3:34–43. doi: 10.1093/pcmedi/pbaa001

53. Fang Y, Ni J, Wang YS, Zhao Y, Jiang LQ, Chen C, et al. Exosomes as biomarkers and therapeutic delivery for autoimmune diseases: opportunities and challenges. *Autoimmun Rev*. (2023) 22:3260. doi: 10.1016/j.autrev.2022.103260

54. Perez-Hernandez J, Forner MJ, Pinto C, Chaves FJ, Cortes R, Redon J. Increased urinary Exosomal MicroRNAs in patients with systemic lupus erythematosus. *PLoS One*. (2015) 10:e0138618. doi: 10.1371/journal.pone.0138618

55. Lee JY, Park JK, Lee EY, Lee EB, Song YW. Circulating exosomes from patients with systemic lupus erythematosus induce an proinflammatory immune response. *Arthritis Res Ther*. (2016) 18:264. doi: 10.1186/s13075-016-1159-y

56. Wang W, Yue C, Gao S, Li S, Zhou J, Chen J, et al. Promising roles of Exosomal microRNAs in systemic lupus erythematosus. *Front Immunol*. (2021) 12:757096. doi: 10.3389/fimmu.2021.757096

57. Wu H, Chen S, Li A, Shen K, Wang S, Wang S, et al. LncRNA expression profiles in systemic lupus erythematosus and rheumatoid arthritis: emerging biomarkers and therapeutic targets. *Front Immunol*. (2021) 12:792884. doi: 10.3389/fimmu.2021.792884

58. Pang Y, Tan Y, Li YZ, Zhang JC, Guo YB, Guo ZL, et al. Pentraxin 3 is closely associated with tubulointerstitial injury in lupus nephritis a large Multicenter cross-sectional study. *Medicine*. (2016) 95:2520. doi: 10.1097/MD.0000000000002520

59. Jiang Z, Shao M, Dai X, Pan Z, Liu D. Identification of diagnostic biomarkers in systemic lupus erythematosus based on bioinformatics analysis and machine learning. *Front Genet*. (2022) 13:865559. doi: 10.3389/fgene.2022.1061550

60. Hofmann SC, Bosma A, Bruckner-Tuderman L, Vukmanovic-Stejic M, Jury EC, Isenberg DA, et al. Invariant natural killer T cells are enriched at the site of cutaneous inflammation in lupus erythematosus. *J Dermatol Sci*. (2013) 71:22–8. doi: 10.1016/j.jdermsci.2013.04.012

61. Skiljevic D, Bonaci-Nikolic B, Brasanac D, Nikolic M. Apoptosis of keratinocytes and serum DNase I activity in patients with cutaneous lupus erythematosus: relationship with clinical and immunoserological parameters. *J Eur Acad Dermatol*. (2017) 31:523–9. doi: 10.1111/jdv.13943

62. Rolla G, Brussino L, Bertero MT, Colagrande P, Converso M, Bucca C, et al. Increased nitric oxide in exhaled air of patients with systemic lupus erythematosus. *J Rheumatol*. (1997) 24:1066–71.

63. Brunner AM, Wander SA, Neuberg D, Sadrzadeh H, Ballen KK, Amrein PC, et al. Diagnostic features and 2-hydroxyglutarate (2-HG) levels among acute myeloid Leukemia (AML) patients with and without isocitrate dehydrogenase (IDH) mutations. *Blood*. (2014) 124:1045. doi: 10.1182/blood.V124.21.1045.1045

64. Li YQ, Wang DY, Li Y, Zhu JL, Zhao JL, Deng YC, et al. A highly sensitive Sandwich ELISA to detect CSF progranulin: a potential biomarker for CNS disorders. *J Neuropath Exp Neur*. (2019) 78:406–15. doi: 10.1093/jnen/nlz022

65. Chen WS, Lin KC, Chen CH, Liao HT, Wang HP, Li WY, et al. Autoantibody and biopsy grading are associated with expression of ICAM-1, MMP-3, and TRAIL in salivary gland mononuclear cells of Chinese patients with Sjogren's syndrome. *J Rheumatol*. (2009) 36:989–96. doi: 10.3899/jrheum.080733

66. Mao ZM, Tan Y, Tao J, Li LL, Wang H, Yu F, et al. Renal mTORC1 activation is associated with disease activity and prognosis in lupus nephritis. *Rheumatology*. (2022) 61:3830–40. doi: 10.1093/rheumatology/keac037

67. Pedersen HL, Horvei KD, Thiyagarajan D, Norby GE, Seredkina N, Moroni G, et al. Lupus nephritis: low urinary DNase I levels reflect loss of renal DNase I and may be utilized as a biomarker of disease progression. *J Pathol Clin Res*. (2018) 4:193–203. doi: 10.1002/cjp2.99

68. Bouachi K, Moktefi A, Zhang SY, Oniszczuk J, Sendeyo K, Remy P, et al. Expression of CMIP in podocytes is restricted to specific classes of lupus nephritis. *PLoS One*. (2018) 13:7066. doi: 10.1371/journal.pone.0207066

69. Becker AM, Dao KH, Han BK, Kornu R, Lakhanpal S, Mobley AB, et al. SLE peripheral blood B cell, T cell and myeloid cell transcriptomes display unique profiles and each subset contributes to the interferon signature. *PLoS One*. (2013) 8:e67003. doi: 10.1371/journal.pone.0067003

70. Wardowska A, Komorniczak M, Skoniecka A, Bullo-Piontecka B, Lisowska KA, Debska-Slizien MA, et al. Alterations in peripheral blood B cells in systemic lupus erythematosus patients with renal insufficiency. *Int Immunopharmacol*. (2020) 83:106451. doi: 10.1016/j.intimp.2020.106451

71. Nehar-Belaid D, Hong S, Marches R, Chen G, Bolisetty M, Baisch J, et al. Mapping systemic lupus erythematosus heterogeneity at the single-cell level. *Nat Immunol*. (2020) 21:1094–106. doi: 10.1038/s41590-020-0743-0

72. Trzupek D, Lee M, Hamey F, Wicker LS, Todd JA, Ferreira RC. Single-cell multi-omics analysis reveals IFN-driven alterations in T lymphocytes and natural killer cells in systemic lupus erythematosus. *Wellcome Open Res*. (2021) 6:149. doi: 10.12688/wellcomeopenres.16883.1

73. Ashton MP, Eugster A, Dietz S, Loebel D, Lindner A, Kuehn D, et al. Association of Dendritic Cell Signatures with Autoimmune Inflammation Revealed by single-cell profiling. *Arthritis Rheumatol*. (2019) 71:817–28. doi: 10.1002/art.40793

74. Zhang R, Li Y, Pan B, Li Y, Liu A, Li X. Increased expression of hub gene CXCL10 in peripheral blood mononuclear cells of patients with systemic lupus erythematosus. *Exp Ther Med*. (2019) 18:4067–75. doi: 10.3892/etm.2019.8013

75. Tang Y, Li X, Wei Y, Sun Y, Yang Y, Zhang X, et al. A preliminary study of KAT2A on cGAS-related immunity in inflammation amplification of systemic lupus erythematosus. *Cell Death Dis*. (2021) 12:1036. doi: 10.1038/s41419-021-04323-1

76. Perez RK, Gordon MG, Subramaniam M, Kim MC, Hartoularos GC, Targ S, et al. Single-cell RNA-seq reveals cell type-specific molecular and genetic associations to lupus. *Science*. (2022) 376:eabf1970. doi: 10.1126/science.abf1970

77. Li H, Boulougoura A, Endo Y, Tsokos GC. Abnormalities of T cells in systemic lupus erythematosus: new insights in pathogenesis and therapeutic strategies. *J Autoimmun*. (2022) 132:102870. doi: 10.1016/j.jaut.2022.102870

78. Pan HF, Leng RX, Feng CC, Li XP, Chen GM, Li BZ, et al. Expression profiles of Th17 pathway related genes in human systemic lupus erythematosus. *Mol Biol Rep*. (2013) 40:391–9. doi: 10.1007/s11033-012-2073-2

79. Ronnblom L, Leonard D. Interferon pathway in SLE: one key to unlocking the mystery of the disease. *Lupus Sci Med*. (2019) 6:e000270. doi: 10.1136/lupus-2018-000270

80. Buang N, Tapeng L, Gray V, Sardini A, Whilding C, Lightstone L, et al. Type I interferons affect the metabolic fitness of CD8(+) T cells from patients with systemic lupus erythematosus. *Nat Commun*. (2021) 12:1980. doi: 10.1038/s41467-021-22312-y

81. Yin X, Kim K, Suetsugu H, Bang SY, Wen L, Koido M, et al. Biological insights into systemic lupus erythematosus through an immune cell-specific transcriptome-wide association study. *Ann Rheum Dis*. (2022) 81:1273–80. doi: 10.1136/annrheumdis-2022-222345

82. Tangtanatakul P, Thammasate B, Jacquet A, Reantragoon R, Pisitkun T, Avihingsanon Y, et al. Transcriptomic profiling in human mesangial cells using patient-derived lupus autoantibodies identified miR-10a as a potential regulator of IL8. *Sci Rep*. (2017) 7:14517. doi: 10.1038/s41598-017-15160-8

83. dos Santos M, Bringhenti RN, Rodrigues PG, do Nascimento JF, Pereira SV, Zancan R, et al. Podocyte-associated mRNA profiles in kidney tissue and in urine of patients with active lupus nephritis. *Int J Clin Exp Pathol*. (2015) 8:4600–13.

84. Der E, Suryawanshi H, Morozov P, Kustagi M, Goilav B, Ranabothu S, et al. Tubular cell and keratinocyte single-cell transcriptomics applied to lupus nephritis reveal type I IFN and fibrosis relevant pathways. *Nat Immunol*. (2019) 20:915–27. doi: 10.1038/s41590-019-0386-1

85. Arazi A, Rao DA, Berthier CC, Davidson A, Liu Y, Hoover PJ, et al. The immune cell landscape in kidneys of patients with lupus nephritis. *Nat Immunol*. (2019) 20:902–14. doi: 10.1038/s41590-019-0398-x

86. Gilmore AC, Wilson HR, Cairns TD, Botto M, Lightstone L, Bruce IN, et al. Immune gene expression and functional networks in distinct lupus nephritis classes. *Lupus Sci Med*. (2022) 9:615. doi: 10.1136/lupus-2021-000615

87. Dunlap GS, Billi AC, Xing X, Ma F, Maz MP, Tsoi LC, et al. Single-cell transcriptomics reveals distinct effector profiles of infiltrating T cells in lupus skin and kidney. JCI. *Insight*. (2022) 7:341. doi: 10.1172/jci.insight.156341

88. Crickx E, Tamirou F, Huscenot T, Costedoat-Chalumeau N, Rabant M, Karras A, et al. Molecular signatures of kidney antibody-secreting cells in lupus patients with active nephritis upon immunosuppressive therapy. *Arthritis Rheumatol*. (2021) 73:1461–6. doi: 10.1002/art.41703

89. Parikh SV, Malvar A, Song H, Shapiro J, Mejia-Vilet JM, Ayoub I, et al. Molecular profiling of kidney compartments from serial biopsies differentiate treatment responders from non-responders in lupus nephritis. *Kidney Int*. (2022) 102:845–65. doi: 10.1016/j.kint.2022.05.033

90. Tsoi LC, Hile GA, Berthier CC, Sarkar MK, Reed TJ, Liu J, et al. Hypersensitive IFN responses in lupus keratinocytes reveal key mechanistic determinants in cutaneous lupus. *J Immunol*. (2019) 202:2121–30. doi: 10.4049/jimmunol.1800650

91. Szeto CC, Kwan BC, Tam LS. Urinary mRNA in systemic lupus erythematosus. *Adv Clin Chem*. (2013) 62:197–219. doi: 10.1016/B978-0-12-800096-0.00005-6

92. Akhgar A, Sinibaldi D, Zeng L, Farris AB 3rd, Cobb J, Battle M, et al. Urinary markers differentially associate with kidney inflammatory activity and chronicity measures in patients with lupus nephritis. *Lupus Sci Med*. (2023) 10:747. doi: 10.1136/lupus-2022-000747

93. Billi AC, Ma F, Plazyo O, Gharaee-Kermani M, Wasikowski R, Hile GA, et al. Nonlesional lupus skin contributes to inflammatory education of myeloid cells and primes for cutaneous inflammation. *Sci Transl Med*. (2022) 14:eabn2263. doi: 10.1126/scitranslmed.abn2263

94. Maier-Moore JS, Koelsch KA, Smith K, Lessard CJ, Radfar L, Lewis D, et al. Antibody-secreting cell specificity in labial salivary glands reflects the clinical presentation and serology in patients with Sjogren's syndrome. *Arthritis Rheumatol*. (2014) 66:3445–56. doi: 10.1002/art.38872

95. Guo C, Liu Q, Zong D, Zhang W, Zuo Z, Yu Q, et al. Single-cell transcriptome profiling and chromatin accessibility reveal an exhausted regulatory CD4+ T cell subset in systemic lupus erythematosus. *Cell Rep*. (2022) 41:111606. doi: 10.1016/j.celrep.2022.111606

96. Zheng M, Hu Z, Mei X, Ouyang L, Song Y, Zhou W, et al. Single-cell sequencing shows cellular heterogeneity of cutaneous lesions in lupus erythematosus. *Nat Commun*. (2022) 13:7489. doi: 10.1038/s41467-022-35209-1

97. Li Y, Ma C, Liao S, Qi S, Meng S, Cai W, et al. Combined proteomics and single cell RNA-sequencing analysis to identify biomarkers of disease diagnosis and disease exacerbation for systemic lupus erythematosus. *Front Immunol*. (2022) 13:969509. doi: 10.3389/fimmu.2022.1072573

98. Itotagawa E, Tomofuji Y, Kato Y, Konaka H, Tsujimoto K, Park J, et al. SLE stratification based on BAFF and IFN-I bioactivity for biologics and implications of BAFF produced by glomeruli in lupus nephritis. *Rheumatology (Oxford)*. (2022) 62:1988–97. doi: 10.1093/rheumatology/keac528

99. Banchereau R, Hong S, Cantarel B, Baldwin N, Baisch J, Edens M, et al. Personalized Immunomonitoring uncovers molecular networks that stratify lupus patients. *Cells*. (2016) 165:551–65. doi: 10.1016/j.cell.2016.03.008

100. Ishigaki K, Shoda H, Kochi Y, Yasui T, Kadono Y, Tanaka S, et al. Quantitative and qualitative characterization of expanded CD4+ T cell clones in rheumatoid arthritis patients. *Sci Rep*. (2015) 5:12937. doi: 10.1038/srep12937

101. Tuller T, Atar S, Ruppin E, Gurevich M, Achiron A. Common and specific signatures of gene expression and protein-protein interactions in autoimmune diseases. *Genes Immun*. (2013) 14:67–82. doi: 10.1038/gene.2012.55

102. Liao L, Liang K, Lan L, Wang J, Guo J. Marker genes change of synovial fibroblasts in rheumatoid arthritis patients. *Biomed Res Int*. (2021) 2021:5544264. doi: 10.1155/2021/5544264

103. Zerrouk N, Miagoux Q, Dispot A, Elati M, Niarakis A. Identification of putative master regulators in rheumatoid arthritis synovial fibroblasts using gene expression data and network inference. *Sci Rep*. (2020) 10:16236. doi: 10.1038/s41598-020-73147-4

104. Stephenson W, Donlin LT, Butler A, Rozo C, Bracken B, Rashidfarrokhi A, et al. Single-cell RNA-seq of rheumatoid arthritis synovial tissue using low-cost microfluidic instrumentation. *Nat Commun*. (2018) 9:791. doi: 10.1038/s41467-017-02659-x

105. Zhang F, Wei K, Slowikowski K, Fonseka CY, Rao DA, Kelly S, et al. Defining inflammatory cell states in rheumatoid arthritis joint synovial tissues by integrating single-cell transcriptomics and mass cytometry. *Nat Immunol*. (2019) 20:928–42. doi: 10.1038/s41590-019-0378-1

106. Simmons DP, Nguyen HN, Gomez-Rivas E, Jeong Y, Jonsson AH, Chen AF, et al. SLAMF7 engagement superactivates macrophages in acute and chronic inflammation. *Sci Immunol*. (2022) 7:eabf2846. doi: 10.1126/sciimmunol.abf2846

107. Li X, Sun H, Li H, Li D, Cai Z, Xu J, et al. A single-cell RNA-sequencing analysis of distinct subsets of synovial macrophages in rheumatoid arthritis. *DNA Cell Biol*. (2023) 42:212–22. doi: 10.1089/dna.2022.0509

108. Yamada S, Nagafuchi Y, Wang M, Ota M, Hatano H, Takeshima Y, et al. Immunomics analysis of rheumatoid arthritis identified precursor dendritic cells as a key cell subset of treatment resistance. *Ann Rheum Dis*. (2023) 82:809–19. doi: 10.1136/ard-2022-223645

109. Argyriou A, Wadsworth MH, Lendvai A, Christensen SM, Hensvold AH, Gerstner C, et al. Single cell sequencing identifies clonally expanded synovial CD4(+) T(PH) cells expressing GPR56 in rheumatoid arthritis. *Nat Commun*. (2022) 13:4046. doi: 10.1038/s41467-022-31519-6

110. Moon JS, Younis S, Ramadoss NS, Iyer R, Sheth K, Sharpe O, et al. Cytotoxic CD8(+) T cells target citrullinated antigens in rheumatoid arthritis. *Nat Commun*. (2023) 14:319. doi: 10.1038/s41467-022-35264-8

111. Wampler Muskardin TL, Fan W, Jin Z, Jensen MA, Dorschner JM, Ghodke-Puranik Y, et al. Distinct single cell gene expression in peripheral blood monocytes correlates with tumor necrosis factor inhibitor treatment response groups defined by type I interferon in rheumatoid arthritis. *Front Immunol*. (2020) 11:1384. doi: 10.3389/fimmu.2020.01384

112. Murthy S, Karkossa I, Schmidt C, Hoffmann A, Hagemann T, Rothe K, et al. Danger signal extracellular calcium initiates differentiation of monocytes into SPP1/osteopontin-producing macrophages. *Cell Death Dis*. (2022) 13:53. doi: 10.1038/s41419-022-04507-3

113. Orange DE, Yao V, Sawicka K, Fak J, Frank MO, Parveen S, et al. RNA identification of PRIME cells predicting rheumatoid arthritis flares. *N Engl J Med*. (2020) 383:218–28. doi: 10.1056/NEJMoa2004114

114. Micheroli R, Elhai M, Edalat S, Frank-Bertoncelj M, Burki K, Ciurea A, et al. Role of synovial fibroblast subsets across synovial pathotypes in rheumatoid arthritis: a deconvolution analysis. *RMD Open*. (2022) 8:e001949. doi: 10.1136/rmdopen-2021-001949

115. Yang J, Zhang Y, Liang J, Yang X, Liu L, Zhao H. Fibronectin-1 is a dominant mechanism for rheumatoid arthritis via the mediation of synovial fibroblasts activity. *Front Cell Dev Biol*. (2022) 10:1010114. doi: 10.3389/fcell.2022.1010114

116. Gao A, Zhao W, Wu R, Su R, Jin R, Luo J, et al. Tissue-resident memory T cells: the key frontier in local synovitis memory of rheumatoid arthritis. *J Autoimmun*. (2022) 133:102950. doi: 10.1016/j.jaut.2022.102950

117. Ramesh A, Schubert RD, Greenfield AL, Dandekar R, Loudermilk R, Sabatino JJ Jr, et al. A pathogenic and clonally expanded B cell transcriptome in active multiple sclerosis. *Proc Natl Acad Sci U S A*. (2020) 117:22932–43. doi: 10.1073/pnas.2008523117

118. van der Poel M, Ulas T, Mizee MR, Hsiao CC, Miedema SSM, Adelia , et al. Transcriptional profiling of human microglia reveals grey-white matter heterogeneity and multiple sclerosis-associated changes. *Nat Commun*. (2019) 10:1139. doi: 10.1038/s41467-019-08976-7

119. Liu J, Gao H, Li C, Zhu F, Wang M, Xu Y, et al. Expression and regulatory characteristics of peripheral blood immune cells in primary Sjogren's syndrome patients using single-cell transcriptomic. *iScience*. (2022) 25:105509. doi: 10.1016/j.isci.2022.105509

120. He Y, Chen R, Zhang M, Wang B, Liao Z, Shi G, et al. Abnormal changes of monocyte subsets in patients with Sjogren's syndrome. *Front Immunol*. (2022) 13:864920. doi: 10.3389/fimmu.2022.1093990

121. Hou X, Hong X, Ou M, Meng S, Wang T, Liao S, et al. Analysis of gene expression and TCR/B cell receptor profiling of immune cells in primary Sjogren's syndrome by single-cell sequencing. *J Immunol*. (2022) 209:238–49. doi: 10.4049/jimmunol.2100803

122. Xu T, Zhu HX, You X, Ma JF, Li X, Luo PY, et al. Single-cell profiling reveals pathogenic role and differentiation trajectory of granzyme K+CD8+ T cells in primary Sjogren's syndrome. *JCI Insight*. (2023) 8:490. doi: 10.1172/jci.insight.167490

123. Hong X, Meng S, Tang D, Wang T, Ding L, Yu H, et al. Single-cell RNA sequencing reveals the expansion of cytotoxic CD4(+) T lymphocytes and a landscape of immune cells in primary Sjogren's syndrome. *Front Immunol*. (2020) 11:594658. doi: 10.3389/fimmu.2020.594658

124. Mandric I, Schwarz T, Majumdar A, Hou K, Briscoe L, Perez R, et al. Optimized design of single-cell RNA sequencing experiments for cell-type-specific eQTL analysis. *Nat Commun*. (2020) 11:5504. doi: 10.1038/s41467-020-19365-w

125. Ma Y, Chen J, Wang T, Zhang L, Xu X, Qiu Y, et al. Accurate machine learning model to diagnose chronic autoimmune diseases utilizing information from B cells and monocytes. *Front Immunol*. (2022) 13:870531. doi: 10.3389/fimmu.2022.1044462

126. Stahl PL, Salmen F, Vickovic S, Lundmark A, Navarro JF, Magnusson J, et al. Visualization and analysis of gene expression in tissue sections by spatial transcriptomics. *Science*. (2016) 353:78–82. doi: 10.1126/science.aaf2403

127. Carlberg K, Korotkova M, Larsson L, Catrina AI, Stahl PL, Malmstrom V. Exploring inflammatory signatures in arthritic joint biopsies with spatial transcriptomics. *Sci Rep*. (2019) 9:18975. doi: 10.1038/s41598-019-55441-y

128. Hardt U, Carlberg K, Af Klint E, Sahlstrom P, Larsson L, van Vollenhoven A, et al. Integrated single cell and spatial transcriptomics reveal autoreactive differentiated B cells in joints of early rheumatoid arthritis. *Sci Rep*. (2022) 12:11876. doi: 10.1038/s41598-022-15293-5

129. Vickovic S, Schapiro D, Carlberg K, Lotstedt B, Larsson L, Hildebrandt F, et al. Three-dimensional spatial transcriptomics uncovers cell type localizations in the human rheumatoid arthritis synovium. *Commun Biol*. (2022) 5:129. doi: 10.1038/s42003-022-03050-3

130. Kaufmann M, Evans H, Schaupp AL, Engler JB, Kaur G, Willing A, et al. Identifying CNS-colonizing T cells as potential therapeutic targets to prevent progression of multiple sclerosis. *Med (N Y)*. (2021) 2:296–312 e8. doi: 10.1016/j.medj.2021.01.006

131. Misrielal C, Alsema AM, Wijering MHC, Miedema A, Mauthe M, Reggiori F, et al. Transcriptomic changes in autophagy-related genes are inversely correlated with inflammation and are associated with multiple sclerosis lesion pathology. *Brain Behav Immun Health*. (2022) 25:100510. doi: 10.1016/j.bbih.2022.100510

132. Wu H, Liu F, Shangguan Y, Yang Y, Shi W, Hu W, et al. Integrating spatial transcriptomics with single-cell transcriptomics reveals a spatiotemporal gene landscape of the human developing kidney. *Cell Biosci*. (2022) 12:80. doi: 10.1186/s13578-022-00801-x

133. Salem F, Perin L, Sedrakyan S, Angeletti A, Ghiggeri GM, Coccia MC, et al. The spatially resolved transcriptional profile of acute T cell-mediated rejection in a kidney allograft. *Kidney Int*. (2022) 101:131–6. doi: 10.1016/j.kint.2021.09.004

134. Bell RMB, Denby L. Myeloid heterogeneity in kidney disease as revealed through single-cell RNA sequencing. *Kidney360*. (2021) 2:1844–51. doi: 10.34067/KID.0003682021

135. Cheung MD, Agarwal A, George JF. Where are they now: spatial and molecular diversity of tissue-resident macrophages in the kidney. *Semin Nephrol*. (2022) 42:151276. doi: 10.1016/j.semnephrol.2022.10.002

136. Fritz D, Inamo J, Zhang F. Single-cell computational machine learning approaches to immune-mediated inflammatory disease: new tools uncover novel fibroblast and macrophage interactions driving pathogenesis. *Front Immunol*. (2022) 13:1076700. doi: 10.3389/fimmu.2022.1076700

137. Noel T, Wang QS, Greka A, Marshall JL. Principles of spatial transcriptomics analysis: a practical walk-through in kidney tissue. *Front Physiol*. (2021) 12:809346. doi: 10.3389/fphys.2021.809346

138. Zheng Z, Chang L, Li J, Wu Y, Chen G, Zou L. Insights gained and future outlook from scRNAseq studies in autoimmune rheumatic diseases. *Front Immunol*. (2022) 13:849050. doi: 10.3389/fimmu.2022.1095657

139. Madissoon E, Oliver AJ, Kleshchevnikov V, Wilbrey-Clark A, Polanski K, Richoz N, et al. A spatially resolved atlas of the human lung characterizes a gland-associated immune niche. *Nat Genet*. (2023) 55:66–77. doi: 10.1038/s41588-022-01243-4

140. Chiricosta L, Blando S, D'Angiolini S, Gugliandolo A, Mazzon E. A comprehensive exploration of the transcriptomic landscape in multiple sclerosis: a systematic review. *Int J Mol Sci*. (2023) 24:1448. doi: 10.3390/ijms24021448

141. Lin WY, Lan JL, Wang SJ. Gallium-67 scintigraphy to predict response to therapy in active lupus nephritis. *J Nucl Med*. (1998) 39:2137–41.

142. Hsieh TY, Lin YC, Hung WT, Chen YM, Wen MC, Chen HH, et al. Change of renal gallium uptake correlated with change of inflammation activity in renal pathology in lupus nephritis patients. *J Clin Med*. (2021) 10:4654. doi: 10.3390/jcm10204654

143. Thurman JM, Serkova NJ. Non-invasive imaging to monitor lupus nephritis and neuropsychiatric systemic lupus erythematosus. *F1000Res*. (2015) 4:153. doi: 10.12688/f1000research.6587.2

144. Mauro D, Barbagallo G, D'Angelo S, Sannino P, Naty S, Bruno C, et al. Role of positron emission tomography for central nervous system involvement in systemic autoimmune diseases: status and perspectives. *Curr Med Chem*. (2018) 25:3096–104. doi: 10.2174/0929867324666170523144402

145. Rapacchi S, Smith RX, Wang Y, Yan L, Sigalov V, Krasileva KE, et al. Towards the identification of multi-parametric quantitative MRI biomarkers in lupus nephritis. *Magn Reson Imaging*. (2015) 33:1066–74. doi: 10.1016/j.mri.2015.06.019

146. Zheng Z, Wang Y, Yan T, Jia J, Li D, Wei L, et al. Detection of renal hypoxia configuration in patients with lupus nephritis: a primary study using blood oxygen level-dependent MR imaging. *Abdom Radiol (NY)*. (2021) 46:2032–44. doi: 10.1007/s00261-020-02794-y

147. Shi H, Jia J, Li D, Wei L, Shang W, Zheng Z. Blood oxygen level dependent magnetic resonance imaging for detecting pathological patterns in lupus nephritis patients: a preliminary study using a decision tree model. *BMC Nephrol*. (2018) 19:33. doi: 10.1186/s12882-017-0787-z

148. Zheng Z, Yan T, Jia J, Li D, Wei L, Shang W, et al. Assessment of renal pathological changes in lupus nephritis using diffusion weighted imaging: a multiple correspondence analysis. *Kidney Blood Press Res*. (2018) 43:847–59. doi: 10.1159/000490333

149. Shi H, Yan T, Li D, Jia J, Shang W, Wei L, et al. Detection of renal hypoxia in lupus nephritis using blood oxygen level-dependent MR imaging: a multiple correspondence analysis. *Kidney Blood Press Res*. (2017) 42:123–35. doi: 10.1159/000472720

150. Li X, Xu X, Zhang Q, Ren H, Zhang W, Liu Y, et al. Diffusion weighted imaging and blood oxygen level-dependent MR imaging of kidneys in patients with lupus nephritis. *J Transl Med*. (2014) 12:295. doi: 10.1186/s12967-014-0295-x

151. Chen YX, Zhou W, Ye YQ, Zeng L, Wu XF, Ke B, et al. Clinical study on the use of advanced magnetic resonance imaging in lupus nephritis. *BMC Med Imaging*. (2022) 22:210. doi: 10.1186/s12880-022-00928-w

152. Wang L, Xiong C, Li M, Zeng X, Wang Q, Fang W, et al. Assessment of lung glucose uptake in patients with systemic lupus erythematosus pulmonary arterial hypertension: a quantitative FDG-PET imaging study. *Ann Nucl Med*. (2020) 34:407–14. doi: 10.1007/s12149-020-01461-y

153. Makis W, Ciarallo A, Gonzalez-Verdecia M, Probst S. Systemic lupus erythematosus associated pitfalls on (18)F-FDG PET/CT: reactive follicular hyperplasia, Kikuchi-Fujimoto disease, inflammation and lymphoid hyperplasia of the spleen mimicking lymphoma. *Nucl Med Mol Imaging*. (2018) 52:74–9. doi: 10.1007/s13139-017-0471-z

154. Curiel R, Akin EA, Beaulieu G, DePalma L, Hashefi M. PET/CT imaging in systemic lupus erythematosus. *Ann N Y Acad Sci*. (2011) 1228:71–80. doi: 10.1111/j.1749-6632.2011.06076.x

155. Nwaubani P, Cercignani M, Colasanti A. In vivo quantitative imaging of hippocampal inflammation in autoimmune neuroinflammatory conditions: a systematic review. *Clin Exp Immunol*. (2022) 210:24–38. doi: 10.1093/cei/uxac058

156. Carlucci PM, Purmalek MM, Dey AK, Temesgen-Oyelakin Y, Sakhardande S, Joshi AA, et al. Neutrophil subsets and their gene signature associate with vascular inflammation and coronary atherosclerosis in lupus. *JCI Insight*. (2018) 3:276. doi: 10.1172/jci.insight.99276

157. Shin JI, Lee KH, Park S, Yang JW, Kim HJ, Song K, et al. Systemic lupus erythematosus and lung involvement: a comprehensive review. *J Clin Med*. (2022) 11:6714. doi: 10.3390/jcm11226714

158. De Feo MS, Pontico M, Frantellizzi V, Corica F, De Cristofaro F, De Vincentis G. Zr-89-PET imaging in humans: a systematic review. *Clin Transl Imaging*. (2022) 10:23–36. doi: 10.1007/s40336-021-00462-9

159. Clausen AS, Christensen C, Christensen E, Cold S, Kristensen LK, Hansen AE, et al. Development of a cu-64-labeled CD4(+) T cell targeting PET tracer: evaluation of CD4 specificity and its potential use in collagen-induced arthritis. *EJNMMI Res*. (2022) 12:934. doi: 10.1186/s13550-022-00934-7

160. van der Krogt JMA, van Binsbergen WH, van der Laken CJ, Tas SW. Novel positron emission tomography tracers for imaging of rheumatoid arthritis. *Autoimmun Rev*. (2021) 20:102764. doi: 10.1016/j.autrev.2021.102764

161. Palazzo L, Lindblom J, Mohan C, Parodis I. Current insights on biomarkers in lupus nephritis: a systematic review of the literature. *J Clin Med*. (2022) 11:759. doi: 10.3390/jcm11195759

162. Zhang Y, Lee TY. Revealing the immune heterogeneity between systemic lupus erythematosus and rheumatoid arthritis based on multi-omics data analysis. *Int J Mol Sci*. (2022) 23:5166. doi: 10.3390/ijms23095166

frontiers | Frontiers in Immunology

TYPE Original Research
PUBLISHED 12 July 2023
DOI 10.3389/fimmu.2023.1084299

OPEN ACCESS

EDITED BY
Yudong Liu,
Chinese Academy of Medical Sciences, China

REVIEWED BY
Fei Han,
Zhejiang University, China
Vladimir Tesar,
Charles University, Czechia

*CORRESPONDENCE
Yong Zhong
zhongyong121@163.com
Yigang Pei
xypyg0731@163.com
Wenzheng Li
wenzheng727@163.com

†These authors have contributed equally to this work and share first authorship

RECEIVED 30 October 2022
ACCEPTED 19 June 2023
PUBLISHED 12 July 2023

CITATION
Chen J, Meng T, Xu J, Ooi JD, Eggenhuizen PJ, Liu W, Li F, Wu X, Sun J, Zhang H, Zhou Y-O, Luo H, Xiao X, Pei Y, Li W and Zhong Y (2023) Development of a radiomics nomogram to predict the treatment resistance of Chinese MPO-AAV patients with lung involvement: a two-center study. *Front. Immunol.* 14:1084299. doi: 10.3389/fimmu.2023.1084299

Development of a radiomics nomogram to predict the treatment resistance of Chinese MPO-AAV patients with lung involvement: a two-center study

Juan Chen[1,2†], Ting Meng[3†], Jia Xu[3], Joshua D. Ooi[3,4], Peter J. Eggenhuizen[4], Wenguang Liu[1,2], Fang Li[1,2], Xueqin Wu[5], Jian Sun[5], Hao Zhang[5], Ya-Ou Zhou[6], Hui Luo[6], Xiangcheng Xiao[3], Yigang Pei[1,2*], Wenzheng Li[1,2*] and Yong Zhong[3,7*]

[1]Department of Radiology, Xiangya Hospital, Central South University, Changsha, Hunan, China, [2]National Clinical Research Center for Geriatric Disorders, Xiangya Hospital, Central South University, Changsha, Hunan, China, [3]Department of Nephrology, Xiangya Hospital, Central South University, Changsha, Hunan, China, [4]Centre for Inflammatory Diseases, Monash University, Clayton, VIC, Australia, [5]Department of Nephrology, The third Xiangya Hospital, Central South University, Changsha, Hunan, China, [6]Department of Rheumatology and Immunology, Xiangya Hospital, Central South University, Changsha, China, [7]Key Laboratory of Biological Nanotechnology of National Health Commission, Xiangya Hospital, Central South University, Changsha, Hunan, China

Background: Previous studies from our group and other investigators have shown that lung involvement is one of the independent predictors for treatment resistance in patients with myeloperoxidase (MPO)–anti-neutrophil cytoplasmic antibody (ANCA)-associated vasculitis (MPO-AAV). However, it is unclear which image features of lung involvement can predict the therapeutic response in MPO-AAV patients, which is vital in decision-making for these patients. Our aim was to develop and validate a radiomics nomogram to predict treatment resistance of Chinese MPO-AAV patients based on low-dose multiple slices computed tomography (MSCT) of the involved lung with cohorts from two centers.

Methods: A total of 151 MPO-AAV patients with lung involvement (MPO-AAV-LI) from two centers were enrolled. Two different models (Model 1: radiomics signature; Model 2: radiomics nomogram) were built based on the clinical and MSCT data to predict the treatment resistance of MPO-AAV with lung involvement in training and test cohorts. The performance of the models was assessed using the area under the curve (AUC). The better model was further validated. A nomogram was constructed and evaluated by DCA and calibration curves, which further tested in all enrolled data and compared with the other model.

Results: Model 2 had a higher predicting ability than Model 1 both in training (AUC: 0.948 vs. 0.824; p = 0.039) and test cohorts (AUC: 0.913 vs. 0.898; p = 0.043). As a better model, Model 2 obtained an excellent predictive performance (AUC: 0.929; 95% CI: 0.827–1.000) in the validation cohort. The DCA curve

demonstrated that Model 2 was clinically feasible. The calibration curves of Model 2 closely aligned with the true treatment resistance rate in the training (p = 0.28) and test sets (p = 0.70). In addition, the predictive performance of Model 2 (AUC: 0.929; 95% CI: 0.875–0.964) was superior to Model 1 (AUC: 0.862; 95% CI: 0.796–0.913) and serum creatinine (AUC: 0.867; 95% CI: 0.802–0.917) in all patients (all p< 0.05).

Conclusion: The radiomics nomogram (Model 2) is a useful, non-invasive tool for predicting the treatment resistance of MPO-AAV patients with lung involvement, which might aid in individualizing treatment decisions.

KEYWORDS

ANCA-associated vasculitis, myeloperoxidase, lung involvement, treatment resistance, radiomics nomogram

Introduction

Antineutrophil cytoplasmic antibody (ANCA)-associated vasculitis (AAV) is a serious autoimmune disease with multisystem involvement (1), which has a preference for affecting the kidney and lung (2) and is life threatening without treatment (3). AAV is commonly associated with the presence of ANCA against proteinase 3 (PR3) and myeloperoxidase (MPO) (1). MPO-AAV is the dominant form of AAV in China (4) with more than 90% MPO-AAV patients exhibiting kidney involvement and over 60% with pulmonary involvement. Initial renal function and pulmonary involvement are independent predictors of all-cause mortality in AAV (5, 6).

Currently, the outcome of AAV patients has dramatically improved with the introduction of steroids together with cyclophosphamide (CTX) or rituximab for induction therapy. However, 10%–30% of AAV patients remain resistant to this treatment (7). An increase in glucocorticoid dose and switching from cyclophosphamide to rituximab could be considered in AAV patients with treatment resistance (2). However, 96.9% of patients who were resistant to therapy progressed to end-stage renal disease (ESRD), and 50% of them died (8). Thus, the prediction of treatment resistance is crucial to personalize therapy for those AAV patients before therapy commencement, especially for MPO-AAV patients in China.

At present, there are some studies to forecast treatment resistance. Previous studies suggested that being female, black ethnicity, older age, and having elevated serum creatinine levels may be independent predictors of treatment resistance in patients with AAV (7–9). In addition, our previous study has shown that lung involvement is one of the independent predictors of treatment resistance in Chinese patients with MPO-AAV (8). Lung involvement in MPO-AAV was considered likely in the presence of hemoptysis, pulmonary hemorrhage, respiratory failure, and radiographic proof of infiltrates, nodules, or cavities without evidence of infection (10). However, it remains unclear which specific image features of lung involvement can predict a response to treatment in MPO-AAV patients, which is vital in decision-making for these patients.

Radiomics is a newly emerging form of imaging analysis that automatically extracts potentially unrecognizable information from medical images (11). Some reports suggest that radiomics could predict the therapeutic response and prognosis of interstitial lung disease (12, 13). Feng et al. (12) found that radiomics had a good predictive performance for interstitial lung disease treated by glucocorticoids. Yang et al. (13) proposed that radiomics could predict the response of antifibrotic treatment to idiopathic pulmonary fibrosis. These studies suggest that radiomics might be an effective tool to potentially predict the treatment resistance for MPO-AAV patients.

However, to the best of our knowledge, the use of radiomics analysis to forecast the treatment resistance for MPO-AAV patients with lung involvement has not been reported. Therefore, in this retrospective study, our aim is to develop a radiomics nomogram to predict the treatment resistance of MPO-AAV patients with lung involvement in a two-center study of Chinese patients.

Methods

Patient enrollments

This retrospective study was conducted by the Hunan Vasculitis Study Group (HuVas) in China. The study protocol followed the provisions of the Declaration of Helsinki and was approved by the Ethics Committee of each participating institution. Informed consent was obtained from all individual participants or their legally acceptable representatives.

We searched the database of two institutions to retrieve the radiological and clinical data of patients with confirmed MPO-AAV between August 2011 and September 2021. Consecutive patients with confirmed MPO-AAV were identified and enrolled as the following inclusion criteria: (1) a positive test for MPO-ANCA with the criteria of Chapel Hill Consensus Conferences Nomenclature of

Vasculitis proposed in 2012 (14); (2) detailed clinical data; (3) multiple slices computed tomography (MSCT) imaging performed within 1 month before treatment; (4) sufficient image quality to allow accurate interpretation of radiological features; and (5) lung involvement on MSCT. Exclusion criteria were as follows: (1) eosinophilic granulomatosis with polyangiitis (EGPA), secondary vasculitis, or any other systemic autoimmune disease; (2) patients who died within 4 weeks after the beginning of induction therapy; (3) patients without a low-dose MSCT scan before treatment; (4) suboptimal image quality making the evaluation of imaging characteristics difficult; and (5) CT changes caused by other reason [such as pulmonary infection [clinical signs including fever, cough, and purulent secretions, with the presence of interstitial infiltrates, masses, cavitations, and abscesses in CT (15)], heart failure [cardiomegaly, ground glass opacification, different stages of pulmonary edema, pleural effusion, and increased peripheral vascular diameter in CT (16)], and connective tissue disease associated interstitial pneumonia (CTD-ILD)]. A total of 151 patients out of the 563 subjects were enrolled. The development cohort consisted of 124 patients who were diagnosed at institution 1 (The Xiangya Hospital of Central South University, Changsha, China). The validation cohort consisted of 27 patients who were diagnosed and treated at institution 2 (The Third Xiangya Hospital of Central South University, Changsha, China). Patient enrollment details are listed in Figure 1.

MPO-AAV and therapy resistance

Birmingham Vasculitis Activity Score (BVAS) was used to measure disease activity (17). Organ system involvement was considered only if the manifestations were due to AAV (17). Particularly, lung involvement was considered likely in the presence of hemoptysis, pulmonary hemorrhage, respiratory failure, or radiographic proof of infiltrates, nodules, or cavities without evidence of infection (9, 18, 19). The estimated glomerular filtration rate (eGFR) was determined as described previously (20).

Serum ANCA was detected by both antigen-specific ELISA (Inova Diagnostics, San Diego, USA) and indirect immunofluorescence (IIF) (Euroimmun, Lübeck, Germany).

Treatment resistance was defined as unchanged or increased disease activity in patients with acute AAV after 4 weeks of treatment with standard therapy or a reduction of <50% in the disease activity score after 6 weeks of treatment or chronic, persistent disease defined as the presence of at least one major item or three minor items on the BVAS list after 12 weeks of treatment (21).

Treatment process and therapy resistance

MPO-AAV patients received therapy, as previously described (22). In brief, oral glucocorticoids (prednisolone, starting at a dosage of 1 mg/kg daily for 4–6 weeks, tapered over 3–6 months to 12.5–15 mg/day) and cyclophosphamide (CTX) were administered intravenously at 0.5–0.75 g/m^2 every month. For those over 65 years old or those with severe renal insufficiency, a 25% dose reduction of CTX was used, and CTX was temporarily stopped for those who developed leukocytopenia or thrombocytopenia. Some patients with rapidly progressive glomerulonephritis or pulmonary hemorrhage received an intravenous methylprednisolone pulse before the standard

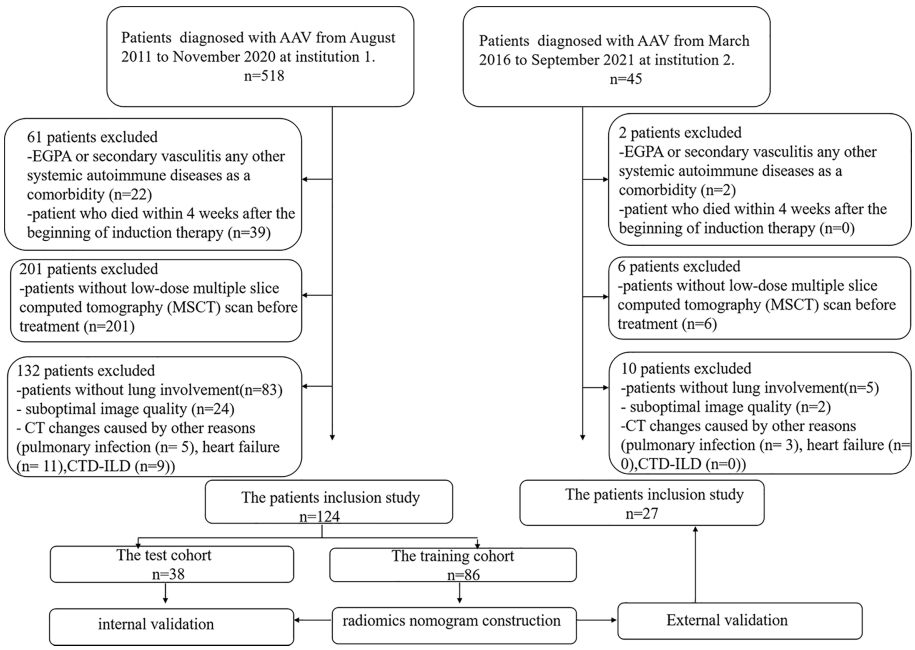

FIGURE 1
Workflow of patient enrollment.

induction therapy and/or plasma exchange. Patients were followed up via phone and medical records to determine their status.

The collection of clinical data

All patient demographic data and laboratory parameters were collected retrospectively from the electronic medical record system, including age (years), gender, white blood cells (10^9/L), hemoglobin (g/L), platelet (10^9/L), serum albumin (g/L), serum globulin (g/L), serum creatinine (μmol/L), erythrocyte sedimentation rate (ESR) (mm/h), C-reactive protein (CRP) (mg/L), C3 (mg/L), C4 (mg/L), IgA (mg/L), IgG (g/L), IgM (mg/L), alanine aminotransferase (ALT) (U/L), aspartate aminotransferase (AST) (U/L), total bilirubin (TBIL) (μmol/L), direct bilirubin (DBIL) (μmol/L), blood urea nitrogen (BUN) (mmol/L), neutrophil (10^9/L), lymphocyte (10^9/L), and eosinophil (10^9/L) (Table 1). These laboratory data were obtained within 4 weeks before treatment.

Evaluation of lung involvement on MSCT

The MSCT images with lung involvement were collected for those MPO-AAV patients from the picture archiving and communication system (PACS). The image acquisition parameters are shown in detail in Appendix E1 and Supplementary Table S1. Two radiologists, reader 1 and reader 2, with 5 and 15 years of thoracic radiology experience, respectively, reviewed all MSCT images and assigned the following qualitative features for each patient: (a) alveolar hemorrhage (AH), the appearance of diffuse pulmonary infiltrates with bilateral opacities, ground-glass, and crazy-paving pattern (2) (Figure 2A); (b) interstitial lung diseases

TABLE 1 The clinical characteristics between treatment-resistant and treatment-responsive group.

	Treatment-resistant (n=55)	Treatment-responsive (n=96)	*p*
Age (years)	61 ± 12	61 ± 11	0.771
White blood cells (10^9/L)	9.02 ± 4.30	10.26 ± 4.16	0.083
Hemoglobin (g/L)	77.36 ± 18.30	86.60 ± 19.81	0.005
Platelet (10^9/L)	238.42 ± 101.08	298.19 ± 109.50	0.001
Serum albumin (g/L)	32.10(28.30–37.30)	31.45(26.75–36.33)	0.574
Serum globulin (g/L)	30.67 ± 7.77	33.07 ± 8.13	0.078
Serum creatinine (μmol/L)	643.28 ± 295.19	258.71 ± 242.61	<0.001
ESR (mm/h)	66.73 ± 36.59	71.36 ± 40.30	0.484
CRP (mg/L)	18.40(7.25–68.20)	38.14(5.77–95.85)	0.188
C3 (mg/L)	693.40 ± 261.76	802.48 ± 342.59	0.030
C4 (mg/L)	214.33 ± 105.50	218.97 ± 105.86	0.796
IgA (mg/L)	2413.93 ± 1435.34	2635.28 ± 1572.43	0.392
IgG (g/L)	14.04 ± 5.96	15.61 ± 5.54	0.104
IgM (mg/L)	860.00 ± 456.19	1054.42 ± 630.60	0.047
ALT (U/L)	9.90(5.40–14.30)	14.90(8.90–24.13)	0.001
AST (U/L)	16.00(12.60–25.90)	18.60(14.90–31.88)	0.046
TBIL (μmol/L)	5.30(4.20–7.00)	6.60(4.70–8.70)	0.024
DBIL (μmol/L)	2.50(1.90–3.80)	2.90(1.90–4.08)	0.393
BUN (mmol/L)	21.04 ± 10.54	11.62 ± 8.53	0.001
Neutrophil (10^9/L)	7.10 ± 3.92	8.10 ± 4.85	0.197
Lymphocyte (10^9/L)	1.00(0.60–1.40)	1.10(0.70–1.60)	0.519
Eosinophil (10^9/L)	0.12(0.03–0.20)	0.10(0.00–0.30)	0.451
Total Prednisolone, g Median(Q1,Q3)	4.69(3.60,5.00)	4.96(4.95,6.30)	<0.001
Total CTX, g Median(Q1,Q3)	2.40(1.80,3.60)	4.80(3.60,4.80)	<0.001
MP, n (%)	14 (25.5%)	12 (12.5%)	0.043
PE, n (%)	25 (45.5%)	22 (22.9%)	0.004

ESR, erythrocyte sedimentation rate; CRP, C-reactive protein; ALT, alanine aminotransferase; AST, aspartate aminotransferase; TBIL, total bilirubin; DBIL, direct bilirubin; BUN, blood urea nitrogen; CTX, cyclophosphamide; MP, methylprednisone pulse; PE, plasma exchange.

(ILD) including ground glass (Figure 2B), reticular opacities (Figure 2C), interlobular septal thickening (Figure 2D), parenchymal consolidations (Figure 2E) and honeycombing (Figure 2F) (23); (c) pulmonary granuloma, manifested as a nodule, mass, or cavity and ranged from a few millimeters to more than 10 cm in diameter (24) (Figure 2G); and (d) pleural effusion (Figure 2H). The two radiologists were blinded to the clinical and pathological information for evaluating lung involvement of MPO-AAV patients. Any disagreement was resolved through consultation.

Independent predictors acquisition

Univariate analysis was used to compare the differences in clinical factors and qualitative MSCT features between treatment-resistant and treatment-responsive groups. A p-value< 0.05 indicates a significant difference. The significant factors were entered into a multivariate analysis to select the independent predictors. Odds ratio (OR) and 95% confidence intervals (CIs) for each independent predictor were computed.

Building of Model 1 (radiomics signature)

Region of interest segmentation

3D segmentation of the primary lung lesions was performed by two readers (reader 1 and reader 2, with 5 and 15 years of experience in thoracic imaging, respectively) for the regions of interest (ROIs) that were manually or semi-automatically delineated on the MSCT images based on the threshold method and edge-based method by using 3D-slicer software (version 4.8.1; http://www.slicer.org) (2).

For those lesions with unclear borders, such as alveolar hemorrhage and interstitial lung disease, the threshold method

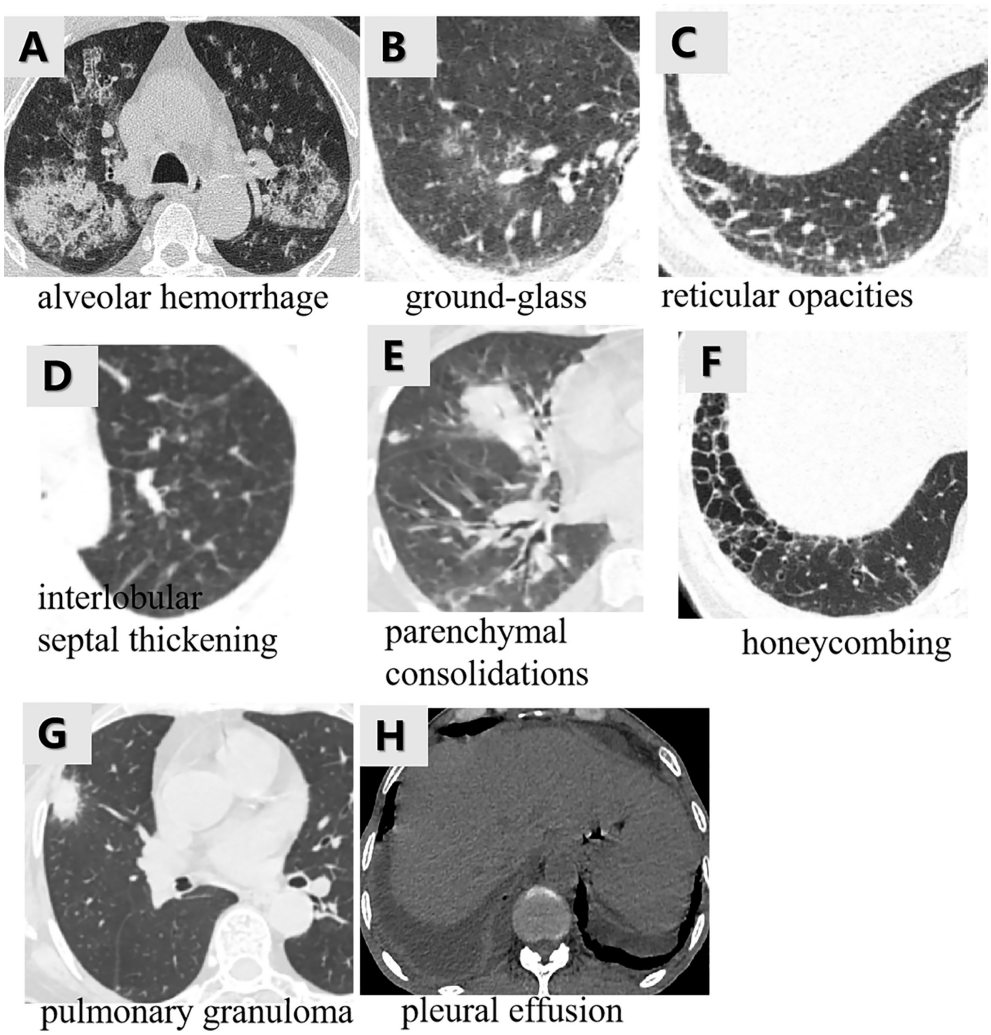

FIGURE 2
The various imaging features of MPO-AAV patients with lung involvement in MSCT. Alveolar hemorrhage was the appearance of diffuse pulmonary infiltrates with bilateral opacities, ground-glass, and crazy-paving pattern **(A)**; interstitial lung disease including the five imaging features **(B–F)**; pulmonary granuloma surrounded with halo sign, manifested as a nodule, mass, or cavity and ranged from a few millimeters to more than 10 cm in diameter **(G)**; bilateral pleural effusion **(H)**.

was applied to sketch them with the Hounsfield unit (HU) values (−700 to −150 HU). Manual corrections were carried out when the automatically registered borders did not correspond to the actual lesion's margin (25, 26). The criteria of manual modification were as follows: 1) for those lesions that were not covered completely in ROI, including patch and nodules, manual delineation was applied; 2) for those lung lesions that were not included in the ROI automatically, manual delineation was applied; 3) the main and leaf bronchi were not contained in the ROI, such as when the segmental and inferior bronchi were connected to pixels that were distinguishable by the naked eye, meaning that they would not be sketched into the ROI. The small scattered bronchus of the lungs was contained in the ROI; 4) the hilar vessels were carefully excluded (27).

For the distinct boundary-pulmonary granuloma, ROI was manually contoured along the boundary of the lesion in every slice (28). The vascular or bronchial structure were included within the segmentation when they were surrounded by the lesion and excluded when they were close to the lesion's edge (29). The lesion in the last slices was not included to avoid volume averaging with adjacent structures. Initially, both readers independently segmented 30 randomly selected patients (including 18 treatment-resistant and 12 treatment-responsive subjects). After that, a reader (*BLINDED*) repeated the same segmentation a week later to obtain intra- and inter-rater intra-class correlation coefficients (ICC) as described by (30). Texture features with ICC > 0.75 were considered to have a good agreement. Reader 1 continued with the remaining image segmentation.

Radiomic feature extraction

The ROIs and original images were transferred into the radiomics platform AK software 3.3.0 (Analysis kit, GE Healthcare, China) for image preprocessing. All MSCT images and segmented ROIs were resampled to 1.0×1.0×1.0 mm^3 voxel size to standardize the voxel spacing. A Gaussian filter of 0.5 mm bandwidth was used to filter noise from the images. Radiomics features including shape (n=14), first-order (n=18), second-order [glcm(n=24), glrlm (n=16), glszm (n=16), ngtdm (n=5), gldm (n=14)] and higher-order (wavelet transform) (n=744) features, which were confirmed to reflect heterogeneity of lesions and potentially reflected changes in image structure, were extracted from MSCT images (31). Wavelet transform (sigma = 2.0, 3.0) filters (n=8) were selected to transform features. A total of 851 features were extracted for each patient (Supplementary Table S2).

To select robust radiomics features, the features with outliers (under the first quartile or above the third quartile of the feature distribution) and missing values were replaced by the feature's median value in the dataset. Finally, all features were standardized using zero-mean normalization to remove pixels that fall outside a specified range of gray levels.

Construction of Model 1

The development cohort (patients from institution 1) was randomly split into training and test cohorts at a ratio of 7:3. First, the radiomics features with ICC > 0.75 from the MSCT images in the training cohort were selected to train the predictive model. Subsequently, the variance threshold method was used to remove variance with a value<0.8. Thereafter, the features were entered into the multivariate logistic regression to select the robust features. The radiomics score (Rad-score) for each patient was calculated based on the robust features with a calculation formula (Appendix E2). Model 1 (radiomics signature) was thus built based on Rad-score and further tested in the test cohort. Odds ratio (OR) and 95% confidence intervals (CIs) for the Rad-score were evaluated.

Construction of Model 2

A combined radiomics model (Model 2) was built by the independent clinical predictors combined with the Rad-score, whose predictive performance was analyzed in the training and test cohorts (institution 1). A better model was chosen with the maximum area under the curve (AUC) between Model 1 and Model 2. The workflow of model construction is shown in Figure 3.

The clinical utility of the better model

The better model was further validated in the validation cohort (institution 2). A decision curve analysis (DCA) was used to estimate the clinical utility of the better models by calculating the net benefits for a range of threshold probabilities (percentage risk threshold of detecting the subtype). For each decision curve, the net clinical benefit was computed using the formula (32):

$$\text{Net benefit} = \frac{True\ \ positives}{N} - \frac{False\ \ positives}{N} \times \frac{p_t}{1-p_t}$$

where p_t is the threshold probability for detecting a positive patient.

The decision curve plots net clinical benefit (y-axis) against threshold probability (x-axis). The clinical utility of the curve is indicated by the highest net clinical benefit at the lowest threshold probability.

A nomogram for the better clinically applicable model was also constructed based on the AUC performance and clinical utility at the lower threshold probability. The process of graphical presentation of the nomogram is described in Appendix E3.

The predictive performance of the better model was also compared with the other model and the previous independent predictors in all enrolled patients (institutions 1 and 2), respectively.

Statistical analysis

All data were analyzed using the statistical software SPSS (version 22, IBM SPSS Inc., Chicago) and R statistical software (Version 3.4.1, http://www.Rproject.org). Baseline characteristics were presented as means and standard deviations (SDs) or median with interquartile range for continuous variables and

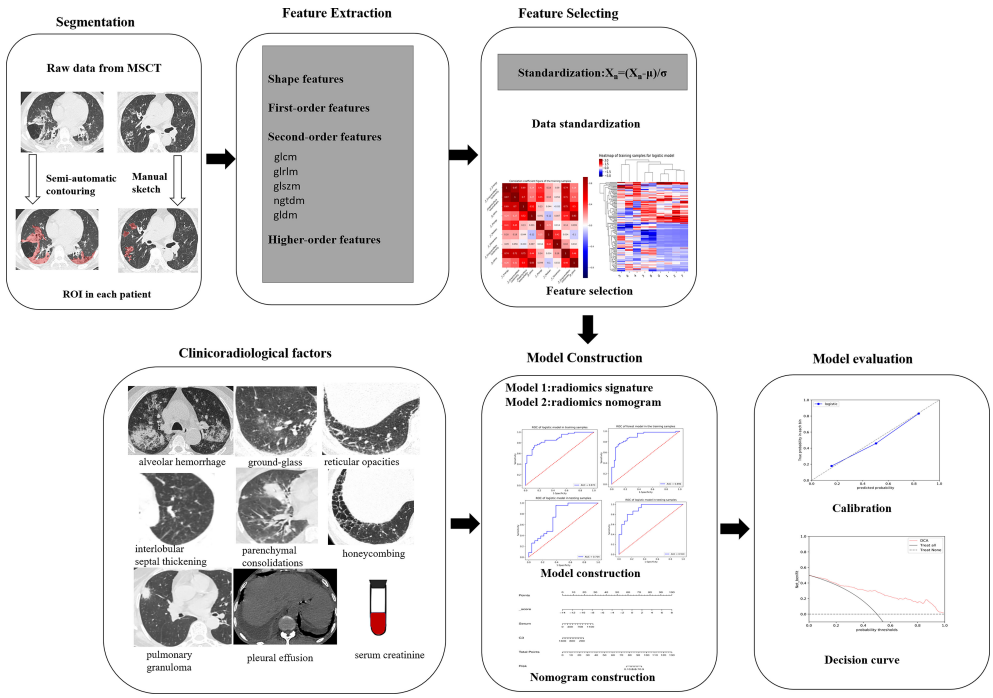

FIGURE 3
Workflow of the radiomics signature building and model construction.

percentages for categorical variables. It was considered statistically significant when the *p*-value was < 0.05. Univariate analyses were used to compare differences between the treatment-resistant and treatment-responsive groups regarding clinical–radiological characteristics using chi-squared or Fisher's exact tests for categorical variables and Mann–Whitney U test for continuous variables. The diagnostic performance of the models in differentiating treatment-resistant patients from treatment-responsive patients was assessed by the AUC (with 95% CI), accuracy (ACC), sensitivity (SEN), and specificity (SPE), in training, test, and validation cohorts. A model is considered to have excellent, good, or poor performance when it has an AUC of 0.85–1.0, 0.7–0.85, or<0.7, respectively (33). The curves of the models were compared using the Delong test. Decision curve analysis (DCA) compared the net benefits under different threshold probabilities given by the better model. Calibration curves of the better model were drawn to evaluate the consistency between the predicted results and the real results.

Results

Basic clinical–radiological characteristics

A total of 151 patients (mean age 60 ± 11 years; 70 men and 81 women) were enrolled, including 55 patients (mean age 60 ± 12 years; 26 men and 29 women) with treatment resistance and 96 subjects (mean age 61 ± 11 years; 44 men and 52 women) showing a response to treatment. They were divided into a training cohort (86 patients of mean age 60 ± 13 years; 38 men and 48 women; 33 patients with treatment resistance and 53 subjects with treatment response), a test cohort (38 patients of mean age 61 ± 14 years; 21 men and 17 women; 15 patients with treatment resistance and 23 patients with treatment response), and validation cohort (27 patients of median age, 63 ± 8 years; 16 men and 11 women; 7 treatment-resistant and 20 treatment-responsive), respectively (Figure 1). For clinical data, the levels of serum platelets, creatinine, C3, IgM, ALT, AST, TBIL, and BUN were higher in the treatment resistance group than in the treatment response cohort (p<0.05) (Table 1). For example, the value of serum creatinine in the treatment resistance cohort was much higher compared to the treatment response group (p< 0.001). The total CTX dose was 2.40 g (1.80,3.60) in treatment-resistant group and 4.80 g (3.60,4.80) in treatment-responsive group. The cumulative dose of CTX were significant lower in treatment-resistant group than in treatment-responsive group (p<0.001) (Table 1). Since 21 of the 55 patients in the treatment-resistant group were on dialysis at onset and remain dialysis-dependent after 3 months of induction therapy. According to KDIGO Guideline (34, 35), the immunosuppressive medication therapy was discontinued in these dialysis-dependent patients. For radiological features, interlobular septal thickening, honeycombing, and pleural effusion were significantly different in the treatment-resistant group compared with the treatment-responsive set (p<0.05) (Table 2). Finally, the serum creatinine (OR: 1.004; 95% CI: 1.002–1.006, p < 0.001) remained as an independent predictor of treatment resistance with multivariate analysis (Table 3).

Performance of Model 1 (radiomics signature)

A total of 355 features with ICC > 0.75 were selected from 851 texture features. Features with variance > 0.8 were screened for further analysis. After multivariate logistic analysis, nine optimal features (original_shapeSurfaceVolumeRatio, wavelet-LLH_firstorder_Energy, wavelet-HLH_firstorder_Range, wavelet-HHH_firstorder_Median, wavelet-HLH_firstorder_Skewness, wavelet-HHL _glszm_GrayLevelNonUniformity, wavelet-LHL_glcm_Idmn, wavelet-LLL_glszm_GrayLevelNonUniformity, and wavelet-HLL_glcm_Idmn) were shown to be distinctly associated with the treatment-resistant cohort (Supplementary Table S3). Rad-scores based on the above nine features are presented in (Appendix E4, Supplementary Figure S1) and used to build Model 1. Model 1 presented an excellent predictive performance in the training cohort (AUC: 0.824; 95% CI: 0.757–0.883; ACC: 0.717; SEN: 0.585; SPE: 0.849) and test cohort (AUC: 0.898; 95% CI: 0.816-0.962; ACC: 0.804; SEN: 0.826; SPE: 0.783) (Table 4, Figure 4). The OR value was 2.995, and 95% CI was 1.877–4.780 for the Rad-score with multivariate analysis ($p < 0.01$).

Performance of Model 2 (radiomics nomogram)

Model 2 showed an excellent predictive performance in the training (AUC: 0.948; 95% CI: 0.908–0.979; ACC: 0.849; SEN: 0.939; SPE: 0.792) and test cohort (AUC: 0.913; 95% CI: 0.835–0.975; ACC: 0.816; SEN: 0.867; SPE: 0.783), which was better than

TABLE 2 The imaging features of patients between treatment-resistant and treatment-responsive group.

	Treatment-resistant (n=55) n (%)	Treatment-responsive (n=96) n (%)	*p*-value
Alveolar hemorrhage			0.098
Y	14(25.5)	14(14.6)	
N	41(74.5)	82(85.4)	
Interstitial pneumonia			0.001
Y	7(12.7)	37(38.5)	
N	48(87.3)	59(61.5)	
Ground-glass			0.077
Y	34(61.8)	45(46.9)	
N	21(38.2)	51(53.1)	
Reticular opacities			0.050
Y	2(3.6)	13(13.5)	
N	53(96.4)	83(86.5)	
Interlobular septal thickening			0.034
Y	14(25.5)	41(42.7)	
N	41(74.5)	55(57.3)	
Parenchymal consolidations			0.176
Y	10(18.2)	10(10.4)	
N	45(81.8)	86(89.6)	
Honeycombing			0.012
Y	5(9.1)	25(26.0)	
N	50(90.9)	71(74.0)	
Pulmonary granuloma			0.120
Y	3(5.5)	13(13.5)	
N	52(94.5)	83(86.5)	
Pleural effusion			0.002
Y	19(34.5)	13(13.5)	
N	36(65.5)	83(86.5)	

TABLE 3 Multivariable predictors of treatment resistance.

Predictors	*p*	OR (95%CI)
Serum creatinine	0.000	1.004(1.002–1.006)
Rad-score	0.000	2.995(1.877–4.780)

OR, odds ratio; CI, confidence interval.

Model 1 in the training (p = 0.039) and validation set (p = 0.043), respectively (Table 4, Figure 5). Furthermore, Model 2 (better model) also obtained an outstanding predictive efficiency (AUC: 0.929; 95% CI: 0.827–1.000; ACC: 0.889; SEN: 0.714, SPE: 0.950) in the validation cohort (Table 4, Figure 5). The DCA curve of Model 2 showed that if the threshold probability of a patient was >5%, using Model 2 to predict treatment resistance of MPO-ANCA patients with lung involvement added more benefit than either the treat-none scheme or the treat-all-patients scheme in the three cohorts (Figure 5). A nomogram was constructed for Model 2, as it was easier to implement in routine clinical practice (Figure 6A). Its predicted probabilities closely aligned with the true treatment resistance rates in both training (p = 0.28) and test (p = 0.70) cohorts (Figures 6B, C).

In all patients, the predictive efficiency of Model 2 (AUC: 0.929; 95% CI: 0.875–0.964) was superior to that of Model 1 (AUC: 0.862; 95% CI: 0.796–0.913) (p<0.01) and serum creatinine (AUC: 0.867; 95%CI: 0.802–0.917) (p = 0.02), respectively (Figure 7).

Discussion

At present, 10%–30% of AVV patients suffer from treatment resistance after 4 weeks of standard therapy (7, 36). Predicting treatment resistance is significant to monitor strategies and weigh up the relative benefits of different treatment strategies for MPO-AAV patients with lung involvement. Thus, we developed and validated various predictive models based on MSCT and clinical data to predict the treatment resistance for MPO-AAV patients with lung involvement before therapy.

In our study, the elevated serum creatinine level was the independent predictor of treatment resistance for MPO-AAV patients with lung involvement, which was in keeping with the findings of previous studies (7, 37). Li et al. (7) proposed that the poor response to treatment was associated with reduced renal function. The worse the renal function, the higher the level of serum creatinine, which causes a greater incidence of treatment resistance. Patients with a high level of serum creatinine had already sustained chronic, irreversible renal damage and interstitial scarring, which results in resistance to immunosuppressive therapy (9). Our results indicated that serum creatinine level can be a biomarker for predicting the treatment resistance of MPO-AAV patients with lung involvement.

In our study, we observed that interstitial lung disease (interlobular septal thickening, honeycombing) and pleural effusion performed a significant difference between the treatment-resistant group and the treatment-responsive set. The emergence of interstitial lung disease is a favorable factor for treatment response in our study. It is plausible that certain agents, such as rituximab, may have a beneficial effect as seen in CTD-ILD (38). It was observed that pleural effusion was more frequent in treatment-resistant patients, which might relate to MPO-ANCA activity (39). However, qualitative radiological features were not an independent predictor of treatment resistance for MPO-AAV patients with lung involvement, which was different to the findings that lung involvement is an independent predictor of treatment resistance in MPO-AAV patients (8). The most plausible explanation for this discrepancy

TABLE 4 ROC curve analysis of Models 1 and 2.

	Training cohort				Test cohort				Validation cohort			
	AUC (95%CI)	SEN	SPE	ACC	AUC (95%CI)	SEN	SPE	ACC	AUC (95%CI)	SEN	SPE	ACC
Model 1	0.824 (0.757–0.883)	0.585	0.859	0.717	0.898 (0.816–0.962)	0.826	0.783	0.804	–	–	–	–
Model 2	0.948 (0.908–0.979)	0.939	0.792	0.849	0.913 (0.835–0.975)	0.867	0.783	0.816	0.929 (0.827–1.000)	0.714	0.950	0.889

ROC, receiver operating characteristic; CI, confidence interval; SEN, sensitivity; SPE, specificity; ACC, accuracy.

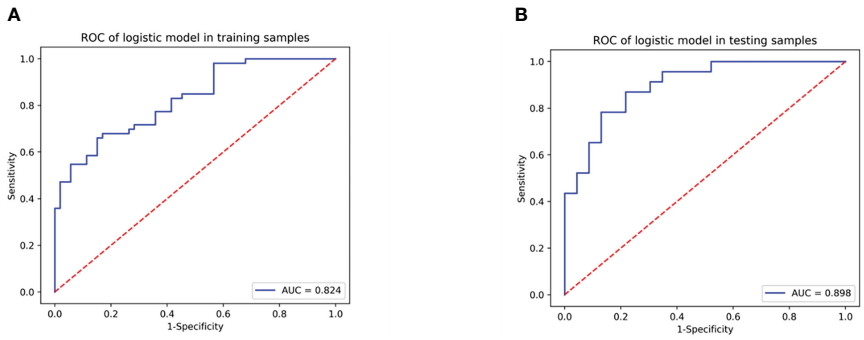

FIGURE 4
The predicting efficiency of Model 1 in the training cohort **(A)** and test cohort **(B)**.

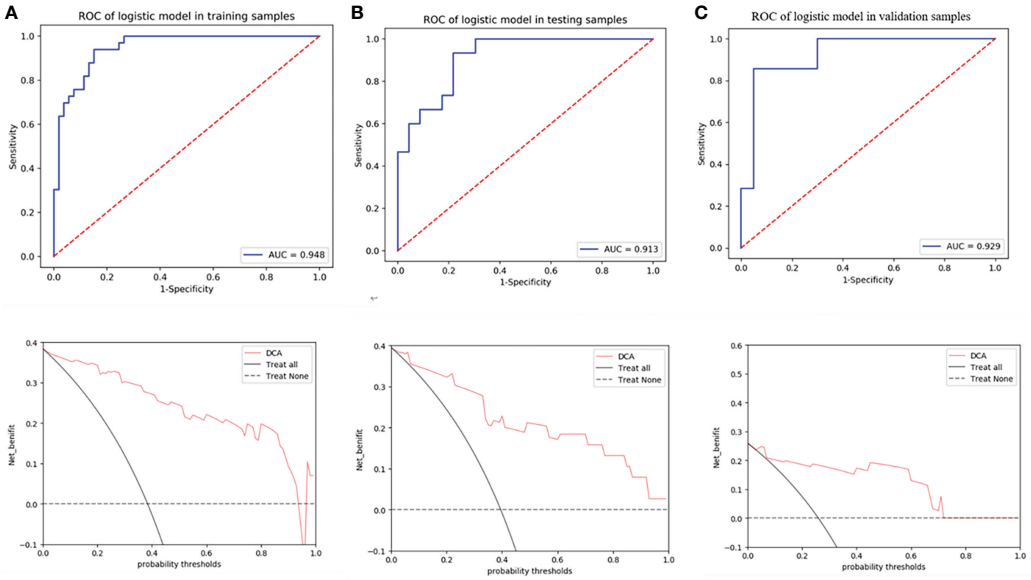

FIGURE 5
ROC curves of radiomics nomogram and decision curve analysis to detect the presence of treatment resistance in the training **(A)**, test **(B)**, and validation **(C)** cohorts, respectively.

might be that lung involvement includes various radiological features, including alveolar hemorrhage and interstitial lung disease. The lung involvement can be an independent factor of MPO-AAV patients, but their specific imaging features might not be. In addition, the enrollment of patients included some MPO-AAV patients without lung involvement in our previous report (8), which was different from the present study and led to selection bias.

Nine vital radiomics features (original_shapeSurfaceVolumeRatio, wavelet-LLH_firstorder_Energy, wavelet-HLH_firstorder_Range, wavelet-HHH_firstorder_Median, wavelet-HLH_firstorder_Skewness, wavelet-HHL _glszm_GrayLevelNonUniformity, wavelet-LHL_glcm_Idmn, wavelet-LLL_glszm_GrayLevelNonUniformity, and wavelet-HLL_glcm_Idmn) were associated with treatment resistance for those MPO-AAV patients with lung involvement,

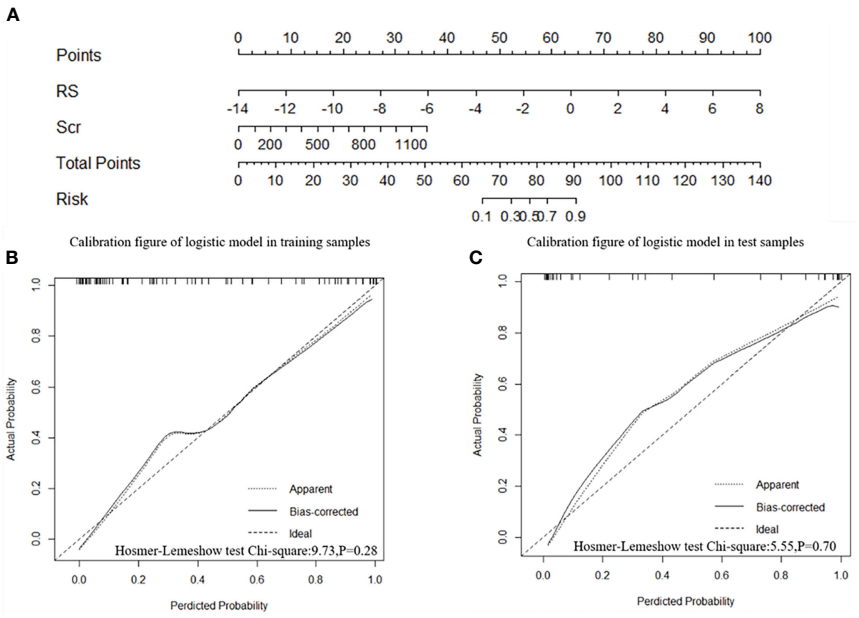

FIGURE 6
Radiomics nomogram and calibration curves. **(A)** The radiomics nomogram was developed in the training cohort with the Rad-score and serum creatinine. The calibration curve of the radiomics nomogram for treatment resistance in the training cohort **(B)** and test cohort **(C)**, respectively.

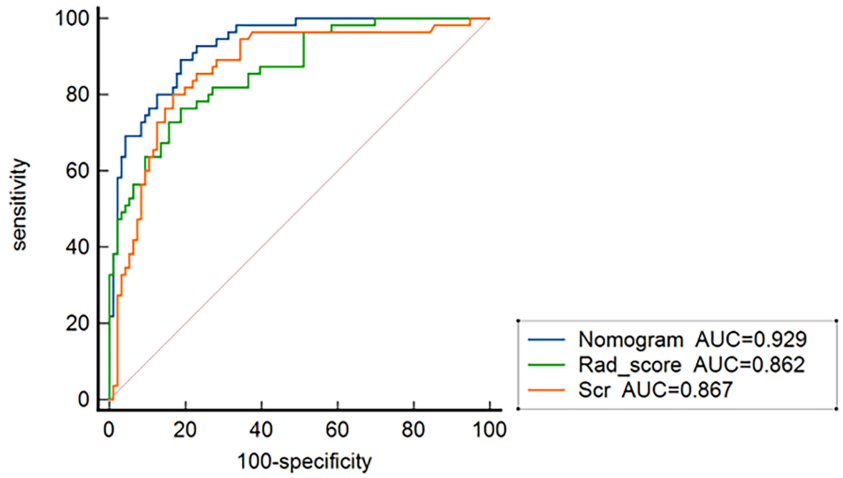

FIGURE 7
ROC curves for nomogram, the radiomics signature, and serum creatinine for predicting treatment resistance in all 151 patients.

including one shape feature (shapeSurfaceVolumeRatio) (SVR), eight wavelet features {four features from first-order features (Energy, Range, Median, Skewness) and four features from textural features [Gray-Level Size Zone Matrix (GLSZM), Gray-Level Co-occurrence Matrix (GLCM)]}. A greater SVR indicates more spiculated and irregular lesions (40), which indicated a poor response to treatment. Energy refers to the magnitude of voxel values in the image, which could predict the earlier treatment response (41). In our study, it relates to the treatment resistance of patients with 12 weeks standard treatment. Lesion volume and maximum diameter had the highest predictive performance in response to treatment with Gefitinib for non-small-cell lung carcinoma patients (41), which indicated that the range and median of the lesion can predict treatment resistance for those MPO-AAV patients with lung involvement. Higher skewness occurs when a lesion contains regions of different intensities, implying greater lesion heterogeneity in the treatment-resistant group. Hötker et al. (42) found that the skewness could identify nephroblastoma patients at risk of poor response to treatment early. Our results implied that skewness could forecast the treatment resistance for the MPO-AAV patients with lung involvement early.

GLCM analyzed the spatial distribution of image texture features through different spatial positions and angles with 0°, 45°, 90°, and 135° as the angles generally used (43). The GLCM features can clearly predict the degree of lung injury (none/mild/severe) after stereotactic body radiotherapy at three various time points (3, 6, and 9 months) (44), which is in accordance with the finding that it can forecast the treatment resistance in our study. GLSZM quantifies gray-level zones in an image, and GLN (GrayLevelNonUniformity) from GLSZM measures the variability of gray-level intensity values in the image (45), which indicates the heterogeneity in the lung involvement lesion and reflects the resistance to treatment for those MPO-AAV patients.Model 2 has a higher predictive performance than Model 1 in both training and test cohorts. It is in keeping with several previous studies. Ligero et al. (46) reported that the radiomics clinical model improved the predictive performance to immune checkpoint inhibitors in advanced solid tumors compared with only radiomics model (AUC: 0.74 vs. 0.70; $p< 0.001$]. Another study found that the radiomics nomogram established by integrating the radiomics signature with clinical data outperformed the clinical nomogram alone in predicting induction chemotherapy response of nasopharyngeal carcinoma patients. (C-index in validation cohort: 0.863 vs. 0.549; $p< 0.01$) (47). This study has demonstrated the combined model (Model 2) benefit MPO-AAV patients with lung involvement by adding a prediction of treatment resistance.

As a better model, Model 2 was beneficial in detecting treatment resistance at a lower threshold probability of 5%, which is a lower threshold than the reported prevalence in predicting therapeutic effect according to the clinical utility analysis (48). This indicates its value in assisting clinicians in improving pretherapeutic decision-making. In addition, the predictive performance of Model 2 is superior to Model 1 and serum creatinine in all patients, respectively. This has further confirmed that the radiomics nomogram is a reliable and feasible model for predicting the treatment resistance of MPO-AAV patients with lung involvement, which is suitable to use in routine clinical practice and provides an important quantitative indicator and reference for the management of MPO-AAV patients.

This study has several limitations. First, the texture features were extracted from each MPO-AAV patient with lung involvement but not from four different kinds of lesions (alveolar hemorrhage, interstitial lung disease, pulmonary granuloma, and pleural effusion) due to them being difficult to distinguish from the sum of various lesions in fused lesions. Second, the lung involvement may be caused by other diseases rather than MPO-AAV because they were not confirmed by the percutaneous pulmonary biopsy, although patients with other lung disease such as tuberculosis and connective tissue disease-associated interstitial pneumonia were excluded. Finally, the included population was relatively small despite there being 563 MPO-AAV patients in our study. A larger sample size is necessary to further investigate the potential radiomics features to predict the treatment response of MPO-AAV patients.

In conclusion, our results indicate the feasibility of radiomics analysis in predicting treatment resistance in MPO-AAV patients

with lung involvement. The radiomics nomogram constructed from a Rad-score combined with serum creatinine level is a useful, non-invasive tool for predicting the treatment resistance of MPO-AAV patients with lung involvement, which is helpful for clinicians in pretherapeutic decision-making for these MPO-AAV patients.

Data availability statement

The original contributions presented in the study are included in the article/Supplementary Material. Further inquiries can be directed to the corresponding authors.

Ethics statement

The study was approved by the Medical Ethics Committee of the Xiangya Hospital of Central South University (approval number 202108374) and the third Xiangya Hospital of Central South University for Human Studies (approval number 202109215). The patients/participants provided their written informed consent to participate in this study. Written informed consent was obtained from the individual(s), and minor(s)' legal guardian/next of kin, for the publication of any potentially identifiable images or data included in this article.

Author contributions

YP, WZL, and YZ conceived and designed the research. JC and TM wrote the paper. JO and PE revised the paper. JX, WGL, FL, XW, JS, HZ, and Y-OZ collected the clinical and radiological parameters of patients. JC, TM, HL, and XX analyzed data. All authors approved the final version of the manuscript.

Funding

This work was funded by the National Key R&D Program of China (2020YFC2005000 to XX), the Key Research and Development Program of Hunan province (2020WK2008 to YZ), the Science and Technology Innovation Program of Hunan Province (2020RC5002 to JO), the Natural Science Foundation of Hunan Province (2021JJ31130 to YZ), the Project of Health Commission of Hunan Province (A202303050036 to YZ), "Yiluqihang Shenmingyuanyang" Medical Development and Scientific Research Fund Project on Kidney Diseases (SMYY20220301001 to YZ), the National Natural Science Foundation of China (82071895 to WZL), and China Postdoctoral Science Foundation (2019M652807 to YP).

Acknowledgments

Parts of the present study have been accepted as ePoster presentation for ASN Kidney Week 2022, which will be organized from 3 to 6 November 2022.

Conflict of interest

The authors declare that the research was conducted in the absence of any commercial or financial relationships that could be construed as a potential conflict of interest.

Publisher's note

Supplementary material

The Supplementary Material for this article can be found online at: https://www.frontiersin.org/articles/10.3389/fimmu.2023.1084299/full#supplementary-material

References

1. Shobha V, Fathima S, Prakash R. Granulomatosis with polyangiitis: clinical course and outcome of 60 patients from a single center in South India. *Clin Exp Med* (2018) 18(3):347–53. doi: 10.1007/s10238-018-0492-7

2. Kitching AR, Anders HJ, Basu N, Brouwer E, Gordon J, Jayne DR, et al. ANCA-associated vasculitis. *Nat Rev Dis Primers* (2020) 6(1):71. doi: 10.1038/s41572-020-0204-y

3. Booth AD, Almond MK, Burns A, Ellis P, Gaskin G, Neild GH, et al. Outcome of ANCA-associated renal vasculitis: a 5-year retrospective study. *Am J Kidney Dis* (2003) 41(4):776–84. doi: 10.1016/S0272-6386(03)00025-8

4. Li ZY, Ma TT, Chen M, Zhao MH. The prevalence and management of anti-neutrophil cytoplasmic antibody-associated vasculitis in China. *Kidney Dis (Basel)* (2016) 1(4):216–23. doi: 10.1159/000441912

5. Lai QY, Ma TT, Li ZY, Chang DY, Zhao MH, Chen M. Predictors for mortality in patients with antineutrophil cytoplasmic autoantibody-associated vasculitis: a study of 398 Chinese patients. *J Rheumatol* (2014) 41(9):1849–55. doi: 10.3899/jrheum.131426

6. Wu T, Zhong Y, Zhou Y, Chen J, Yang Y, Tang R, et al. Clinical characteristics and prognosis in 269 patients with antineutrophil cytoplasimc antibody associated vasculitis. *Zhong Nan Da Xue Xue Bao Yi Xue Ban* (2020) 45(8):916–22. doi: 10.11817/j.issn.1672-7347.2020.190436

7. Li ZY, Chang DY, Zhao MH, Chen M. Predictors of treatment resistance and relapse in antineutrophil cytoplasmic antibody-associated vasculitis: a study of 439 cases in a single Chinese center. *Arthritis Rheumatol* (2014) 66(7):1920–6. doi: 10.1002/art.38621

8. Huang L, Shen C, Zhong Y, Ooi JD, Zhou YO, Chen JB, et al. Risk factors for treatment resistance and relapse of Chinese patients with MPO-ANCA-associated vasculitis. *Clin Exp Med* (2020) 20(2):199–206. doi: 10.1007/s10238-020-00614-7

9. Hogan SL, Falk RJ, Chin H, Cai J, Jennette CE, Jennette JC, et al. Predictors of relapse and treatment resistance in antineutrophil cytoplasmic antibody-associated small-vessel vasculitis. *Ann Intern Med* (2005) 143(9):621–31. doi: 10.7326/0003-4819-143-9-200511010-00005

10. Robson JC, Grayson PC, Ponte C, Suppiah R, Craven A, Judge A, et al. 2022 American college of Rheumatology/European alliance of associations for rheumatology classification criteria for granulomatosis with polyangiitis. *Ann Rheum Dis* (2022) 81 (3):315–20. doi: 10.1136/annrheumdis-2021-221795

11. Incoronato M, Aiello M, Infante T, Cavaliere C, Grimaldi AM, Mirabelli P, et al. Radiogenomic analysis of oncological data: a technical survey. *Int J Mol Sci* (2017) 18 (4):805. doi: 10.3390/ijms18040805

12. Feng DY, Zhou YQ, Xing YF, Li CF, Lv Q, Dong J, et al. Selection of glucocorticoid-sensitive patients in interstitial lung disease secondary to connective tissue diseases population by radiomics. *Ther Clin Risk Manag* (2018) 14:1975–86. doi: 10.2147/TCRM.S181043

13. Yang CC, Chen CY, Kuo YT, Ko CC, Wu WJ, Liang CH, et al. Radiomics for the prediction of response to antifibrotic treatment in patients with idiopathic pulmonary fibrosis: a pilot study. *Diagnostics (Basel)* (2022) 12(4):1002. doi: 10.3390/diagnostics12041002

14. Jennette JC, Falk RJ, Bacon PA, Basu N, Cid MC, Ferrario F, et al. 2012 revised international chapel hill consensus conference nomenclature of vasculitides. *Arthritis Rheum* (2013) 65(1):1–11. doi: 10.1002/art.37715

15. Ruiz M, Arosio C, Salman P, Bauer TT, Torres A. Diagnosis of pneumonia and monitoring of infection eradication. *Drugs* (2000) 60(6):1289–302. doi: 10.2165/00003495-200060060-00004

16. Marano R, Pirro F, Silvestri V, Merlino B, Savino G, Rutigliano C, et al. Comprehensive CT cardiothoracic imaging: a new challenge for chest imaging. *Chest* (2015) 147(2):538–51. doi: 10.1378/chest.14-1403

17. Mukhtyar C, Lee R, Brown D, Carruthers D, Dasgupta B, Dubey S, et al. Modification and validation of the Birmingham vasculitis activity score (version 3). *Ann Rheum Dis* (2009) 68(12):1827–32. doi: 10.1136/ard.2008.101279

18. Hogan SL, Nachman PH, Wilkman AS, Jennette JC, Falk RJ. Prognostic markers in patients with antineutrophil cytoplasmic autoantibody-associated microscopic polyangiitis and glomerulonephritis. *J Am Soc Nephrol* (1996) 7(1):23–32. doi: 10.1681/ASN.V7123

19. Nachman PH, Hogan SL, Jennette JC, Falk RJ. Treatment response and relapse in antineutrophil cytoplasmic autoantibody-associated microscopic polyangiitis and glomerulonephritis. *J Am Soc Nephrol* (1996) 7(1):33–9. doi: 10.1681/ASN.V7133

20. Ma YC, Zuo L, Chen JH, Luo Q, Yu XQ, Li Y, et al. Modified glomerular filtration rate estimating equation for Chinese patients with chronic kidney disease. *J Am Soc Nephrol* (2006) 17(10):2937–44. doi: 10.1681/ASN.2006040368

21. Hellmich B, Flossmann O, Gross WL, Bacon P, Cohen-Tervaert JW, Guillevin L, et al. EULAR recommendations for conducting clinical studies and/or clinical trials in systemic vasculitis: focus on anti-neutrophil cytoplasm antibody-associated vasculitis. *Ann Rheum Dis* (2007) 66(5):605–17. doi: 10.1136/ard.2006.062711

22. Huang L, Zhong Y, Ooi JD, Zhou YO, Zuo X, Luo H, et al. The effect of pulse methylprednisolone induction therapy in Chinese patients with dialysis-dependent MPO-ANCA associated vasculitis. *Int Immunopharmacol* (2019) 76:105883. doi: 10.1016/j.intimp.2019.105883

23. Sacoto G, Boukhlal S, Specks U, Flores-Suarez LF, Cornec D. Lung involvement in ANCA-associated vasculitis. *Presse Med* (2020) 49(3):104039. doi: 10.1016/j.lpm.2020.104039

24. Feragalli B, Mantini C, Sperandeo M, Galluzzo M, Belcaro G, Tartaro A, et al. The lung in systemic vasculitis: radiological patterns and differential diagnosis. *Br J Radiol* (2016) 89(1061):20150992. doi: 10.1259/bjr.20150992

25. Mansoor A, Bagci U, Foster B, Xu Z, Papadakis GZ, Folio LR, et al. Segmentation and image analysis of abnormal lungs at CT: current approaches, challenges, and future trends. *Radiographics* (2015) 35(4):1056–76. doi: 10.1148/rg.2015140232

26. Pang T, Guo S, Zhang X, Zhao L. Automatic lung segmentation based on texture and deep features of HRCT images with interstitial lung disease. *BioMed Res Int* (2019) 2019:2045432. doi: 10.1155/2019/2045432

27. Yanling W, Duo G, Zuojun G, Zhongqiang S, Yankai W, Shan L, et al. Radiomics nomogram analyses for differentiating pneumonia and acute paraquat lung injury. *Sci Rep* (2019) 9(1):15029. doi: 10.1038/s41598-019-50886-7

28. Chen H, Zeng M, Wang X, Su L, Xia Y, Yang Q, et al. A CT-based radiomics nomogram for predicting prognosis of coronavirus disease 2019 (COVID-19) radiomics nomogram predicting COVID-19. *Br J Radiol* (2021) 94(1117):20200634. doi: 10.1259/bjr.20200634

29. Gülbay M, Özbay BO, Mendi BAR, Baştuğ A, Bodur H. A CT radiomics analysis of COVID-19-related ground-glass opacities and consolidation: is it valuable in a differential diagnosis with other atypical pneumonias? *PLoS One* (2021) 16(3): e0246582. doi: 10.1371/journal.pone.0246582

30. Nie P, Yang G, Guo J, Chen J, Li X, Ji Q, et al. A CT-based radiomics nomogram for differentiation of focal nodular hyperplasia from hepatocellular carcinoma in the non-cirrhotic liver. *Cancer Imaging* (2020) 20(1):20. doi: 10.1186/s40644-020-00297-z

31. Thawani R, McLane M, Beig N, Ghose S, Prasanna P, Velcheti V, et al. Radiomics and radiogenomics in lung cancer: a review for the clinician. *Lung Cancer* (2018) 115:34–41. doi: 10.1016/j.lungcan.2017.10.015

32. Vickers AJ, Van Calster B, Steyerberg EW. Net benefit approaches to the evaluation of prediction models, molecular markers, and diagnostic tests. *BMJ* (2016) 352:i6. doi: 10.1136/bmj.i6

33. Mandrekar JN. Receiver operating characteristic curve in diagnostic test assessment. *J Thorac Oncol* (2010) 5(9):1315–6. doi: 10.1097/JTO.0b013e3181ec173d

34. Chapter 13: pauci-immune focal and segmental necrotizing glomerulonephritis. *Kidney Int Suppl (2011)* (2012) 2(2):233–9. doi: 10.1038/kisup.2012.26

35. KDIGO 2021 clinical practice guideline for the management of glomerular diseases. *Kidney Int* (2021) 100(4s):S1–s276. doi: 10.1016/j.kint.2021.05.021

36. Pagnoux C, Hogan SL, Chin H, Jennette JC, Falk RJ, Guillevin L, et al. Predictors of treatment resistance and relapse in antineutrophil cytoplasmic antibody-associated small-vessel vasculitis: comparison of two independent cohorts. *Arthritis Rheum* (2008) 58(9):2908–18. doi: 10.1002/art.23800

37. Cao Y, Tian Z, Li W, Ma L, Yu Y, Ren W. Predictors of treatment resistance and relapse in Chinese patients with antineutrophil cytoplasmic antibody-associated disease. *J Rheumatol* (2014) 41(5):916–22. doi: 10.3899/jrheum.130758

38. Sharp C, McCabe M, Dodds N, Edey A, Mayers L, Adamali H, et al. Rituximab in autoimmune connective tissue disease-associated interstitial lung disease. *Rheumatol (Oxford)* (2016) 55(7):1318–24. doi: 10.1093/rheumatology/kew195

39. Chinese Society of nephrology, *Chinese guidelines for the diagnosis and treatment of anti-neutrophil cytoplasmic antibody-associated glomerulonephritis*. *Chin J Nephrol* (2021) 37(07):603–20. doi: 10.3760/cma.j.cn441217-20210107-00092

40. Lee G, Lee HY, Park H, Schiebler ML, van Beek EJR, Ohno Y, et al. Radiomics and its emerging role in lung cancer research, imaging biomarkers and clinical management: state of the art. *Eur J Radiol* (2017) 86:297–307. doi: 10.1016/j.ejrad.2016.09.005

41. Aerts HJ, Grossmann P, Tan Y, Oxnard GR, Rizvi N, Schwartz LH, et al. Defining a radiomic response phenotype: a pilot study using targeted therapy in NSCLC. *Sci Rep* (2016) 6:33860. doi: 10.1038/srep33860

42. Hötker AM, Mazaheri Y, Lollert A, Schenk JP, Zheng J, Capanu M, et al. Diffusion-weighted MRI and histogram analysis: assessment of response to neoadjuvant chemotherapy in nephroblastoma. *Abdom Radiol (NY)* (2021) 46 (7):3317–25. doi: 10.1007/s00261-021-03032-9

43. Zhao Q, Shi CZ, Luo LP. Role of the texture features of images in the diagnosis of solitary pulmonary nodules in different sizes. *Chin J Cancer Res* (2014) 26(4):451–8. doi: 10.3978/j.issn.1000-9604.2014.08.07

44. Moran A, Daly ME, Yip SSF, Yamamoto T. Radiomics-based assessment of radiation-induced lung injury after stereotactic body radiotherapy. *Clin Lung Cancer* (2017) 18(6):e425–31. doi: 10.1016/j.cllc.2017.05.014

45. van Griethuysen JJM, Fedorov A, Parmar C, Hosny A, Aucoin N, Narayan V, et al. Computational radiomics system to decode the radiographic phenotype. *Cancer Res* (2017) 77(21):e104–7. doi: 10.1158/0008-5472.CAN-17-0339

46. Ligero M, Garcia-Ruiz A, Viaplana C, Villacampa G, Raciti MV, Landa J, et al. A CT-based radiomics signature is associated with response to immune checkpoint inhibitors in advanced solid tumors. *Radiology* (2021) 299(1):109–19. doi: 10.1148/radiol.2021200928

47. Zhao L, Gong J, Xi Y, Xu M, Li C, Kang X, et al. MRI-Based radiomics nomogram may predict the response to induction chemotherapy and survival in locally advanced nasopharyngeal carcinoma. *Eur Radiol* (2020) 30(1):537–46. doi: 10.1007/s00330-019-06211-x

48. Kong C, Zhao Z, Chen W, Lv X, Shu G, Ye M, et al. Prediction of tumor response via a pretreatment MRI radiomics-based nomogram in HCC treated with TACE. *Eur Radiol* (2021) 31(10):7500–11. doi: 10.1007/s00330-021-07910-0

frontiers | Frontiers in Medicine

TYPE Original Research
PUBLISHED 27 July 2023
DOI 10.3389/fmed.2023.1193303

OPEN ACCESS

EDITED BY
Miao Pan,
Children's National Hospital, United States

REVIEWED BY
Elena Sticchi,
University of Florence, Italy
Jyoti Sharma,
Harvard Medical School, United States

*CORRESPONDENCE
Xing Zhang
✉ zhichi616@126.com
Yuqin Wu
✉ wuyuqin@etyy.cn
Chenghao Zhanghuang
✉ zhanghuangchenghao@etyy.cn

†These authors have contributed equally to this work

RECEIVED 24 March 2023
ACCEPTED 10 July 2023
PUBLISHED 27 July 2023

CITATION
Liu X, Chen Y, Yang Y, Su Z, Wang F, Zhanghuang C, Wu Y and Zhang X (2023) Association between *FGA* gene polymorphisms and coronary artery lesion in Kawasaki disease. *Front. Med.* 10:1193303. doi: 10.3389/fmed.2023.1193303

Association between *FGA* gene polymorphisms and coronary artery lesion in Kawasaki disease

Xingzhu Liu[1†], Yanfei Chen[2†], Yanfei Yang[1], Zhongjian Su[2], Feng Wang[3], Chenghao Zhanghuang[4*†], Yuqin Wu[1*†] and Xing Zhang[2*†]

[1]Department of Special Needs Ward, Kunming Children's Hospital, Kunming, Yunnan, China, [2]Department of Cardiology, Kunming Children's Hospital, Kunming, Yunnan, China, [3]Institute of Medical Biology, Chinese Academy of Medical Sciences, Kunming, Yunnan, China, [4]Department of Urology, Yunnan Key Laboratory of Children's Major Disease Research, Kunming Children's Hospital, Yunnan Province Clinical Research Center for Children's Health and Disease, Kunming, Yunnan, China

Objective: To investigate the correlation between *FGA* gene polymorphisms and coronary artery lesion in Kawasaki disease.

Methods: Two hundred and thirty four children with Kawasaki disease (KD group), 200 healthy children (normal group) and 208 children with non-KD fever (fever group) were enrolled. General clinical indicators, the concentration of serum MMPs, TIMP-1, FG-α,fibrinogen level, molecular function (FMPV/ODmax) and *FGA* Thr312Ala polymorphism were detected individually by testing peripheral venous blood after fasting in the morning.

Results: There was no significant difference in average age among the three groups, which were 3.03±1.22years, 3.17±1.30years, and 3.21±1.31years, respectively. Compared with those in the fever group, the levels of white blood cell count (WBC), platelet count (PLT), procalcitonin (PCT), C-reactive protein (CRP), erythrocyte sedimentation rate (ESR), interleukin-6 (IL-6), monocyte chemoattractant protein-1 (MCP-1), and fibrinogen (Fg) levels were significantly increased in the KD group. Red blood cell count (RBC) and hemoglobin (Hb) levels were significantly decreased ($p<0.05$).The concentration of serum MMPs, TIMP-1, and FG-α in the KD and fever groups were significantly higher than those in the normal group ($p<0.05$). The concentration of MMP-2, MMP-3, MMP-9, MMP-13, TIMP-1, and FG-α in the KD group were significantly higher than those in the fever group ($p<0.05$).The KD group was divided into two subgroups,55 patients with combined CAL and 179 patients without combined CAL. The plasma fibrinogen concentration in the combined CAL group was significantly higher than that in the non-combined CAL and normal groups ($p<0.01$). There was no statistically significant difference in FMPV/ODmax among the three groups ($p>0.05$). Compared with normal group, the FGA GG, GA, and AA genotype and G, A allele frequency of the FGA gene polymorphism in the KD group showed no significant difference ($p>0.05$). In the KD group, the most common type in children with CAL was GA, while the most common type in children without CAL was GG.

Conclusion: MMPs and FG-α were significantly upregulated in KD patients. The proportion of *FGA* genotype GA in children with CAL was significantly higher than that in children without CAL, suggesting that *FGA* gene polymorphisms affect coronary artery lesion in children with KD.

KEYWORDS
Kawasaki disease, coronary artery lesion, MMP, *FGA* gene, polymorphism

Introduction

Kawasaki disease (KD) is a common systemic vasculitis disease prone to occur in children aged 6 months to 5 years. The main pathological changes of KD are systemic small–and medium-sized vasculitis, especially coronary arteritis. In severe cases, coronary artery lesion (CAL) and coronary artery aneurysm (CAA) may occur, which may lead to irreversible destruction of the vascular wall (1). Even after standardized treatment (high-dose gamma globulin + high-dose aspirin), 20% of children with KD still present with coronary artery disease, which can progress to ischemic heart disease (2, 3).

Plasma fibrinogen (FG) is an important protein involved in the process of coagulation and hemostasis, and its elevation is an independent risk factor for cardiovascular disease. In a prospective meta-analysis, it was found that every 1 g/L increase in *FGB* (β-148C/T-455G/A genotype)would double the mortality associated with coronary heart disease and stroke (4). FG consists of three polypeptide chains (α, β, γ), and their corresponding coding genes are *FGA*, *FGB*, and *FGG* (5). Previous studies have found that the *FGB* genotype affects FG levels and is a risk factor affecting intimal artery thickness (IMT) (6, 7); however, there are few reports on whether the *FGA* Thr312Ala genotype participates in the pathophysiological process of KD. In this study, we examined the levels of fibrinogen α (FGα) and total fibrinogen level in the peripheral venous blood and *FGA* genotype and analyzed the correlation between *FGA* Thr312Ala genetic polymorphism and coronary artery disease in KD to provide a theoretical basis for exploring a new treatment plan for KD.

Data and methods

Subjects

This study included 234 children with KD, who were admitted to our hospital between January 2020 and October 2022 (KD group), 200 healthy children (normal group), and 208 non-KD children with fever (fever group) as the control group.

Inclusion and exclusion criteria

KD was confirmed according to the 2017 American Heart Association criteria (8). The study was approved by the medical ethics committee of our hospital. Written and signed informed consent was obtained from the parents/guardians of the children. The exclusion criteria included the use of glucocorticoids, immunosuppressants, and gamma globulin in the past 2 weeks; complicated with cardiovascular and respiratory diseases; incomplete clinical data or history of transfer during treatment; and unwillingness to cooperate with treatment.

The diagnostic criteria for coronary artery disease were as follows: Z-score was used as the diagnostic criteria for coronary artery disease. (1) Normal: Z-value <2; (2) Coronary artery dilation: 2 ≤ Z-value <2.5; (3) Small coronary aneurysm: 2.5 ≤ Z-value <5; (4) Medium coronary aneurysm: 5 ≤ Z-value <10, absolute diameter < 8 mm; (5) Giant coronary artery aneurysm: Z-value ≥10, or internal diameter > 8 mm. A Z-value ≥2.0 was considered CAL+.

Research methods and indicators

Specimen collection

Five mL of peripheral venous blood was collected from each participant in the KD, normal, and fever groups after fasting in the morning on day 2 and day 10 after admission. Blood samples were centrifuged at 3000 rpm for 30 min. The supernatant was collected and placed in a PC box at −75°C. Each sample was split into two, one to test for general clinical indicators {MMPs, TIMP-1, FGα expression, and fibrinogen level and molecular function [fibrinogen monomer polymerization velocity (FMPV)/maximum optical density (ODmax)] μL} and the other for determining the *FGA* genotype.

DNA extraction

Take the PureGene DNA extraction kit and follow the instructions in the kit to extract the DNA of blood genosets. The specific steps are as follows: (1) 900uL blood cell lysate was added into Eppendorf tube; (2) Add 300uL of whole blood into the upper tube and mix it upside down. Incubate it at room temperature for about 10 min to make the red blood cells crack. During incubating, mix it upside down at least once; (3) Centrifuge at 12000xg at room temperature for 60s, then absorb and discard most of the supernatant with the suction head; (4) Oscillate the upper tube on the vortex to make the cells suspended in the residual fluid, so as to facilitate the next step of leukocyte lysis: (5) Add 450pL leukocyte lysis fluid into the hand tube and pump it repeatedly with the suction head to make the cell lysis: (6) At room temperature, 150uL of protein precipitating liquid was added into the upper tube, and then the solution was mixed by high speed oscillation with a vortex for 30s-60s; (7) Centrifuged at 4°C 12000xg for 3 min, the precipitated protein was a dense, dark brown substance; (8) Put the supernatant containing DNA into a new Eppendorf tube, and then add 600uL 100% isopropyl alcohol, and gently pour 50 times to make the solution mixed; (9) After centrifugation at 4°C 12000xg for 1 min, white DNA precipitates can be seen; (10) Run to the superclear liquid, on the drying paper short dry suction pipe in the remaining liquid, then add 70% ethanol 450uL, and gently up and down frequency countdown, to wash the DNA precipitation: (11) at 12000xg high heart 2 min, carefully pour away the ethanol; (12) Place the centrifugal tube upside down on the drying paper and dry it in air for 10 min to 15 min; (13) The DNA bath solution wave was added into the upper tube, incubated at 65°C for 1 h, and the Eppendorf tube was flipped to promote DNA dissolution.

Research methods

FMPV/ODmax

10 μL reaction mixture and 50 μL plasma were fully mixed in a 0.5 cm optical path colorimetric cup and immediately placed into the

TABLE 1 Comparison of general clinical indicators.

	Normal group (n = 200)	KD group (n = 234)	Fever group (n = 208)	P
Age(y)	3.03 ± 1.22	3.17 ± 1.30	3.21 ± 1.31	0.227
Gender(male)	89(44.50)	107(45.73)	92(44.23)	0.558
Fever time(d)	0.00 ± 0.00	4.25 ± 1.33	1.93 ± 0.79	<0.001
WBC(10^3/μL)	8.41 ± 2.65	17.22 ± 5.44*	11.53 ± 3.86	<0.001
RBC(10^6/mm3)	4.79 ± 0.64	3.66 ± 0.39*	4.26 ± 0.49	<0.001
Hb(g/dL)	11.83 ± 1.32	9.81 ± 1.19*	11.47 ± 1.26	<0.001
PLT(10^3/μL)	310.66 ± 108.18	411.53 ± 139.22*	344.92 ± 117.84	<0.001
CRP(mg/dL)	10.11 ± 5.92	58.29 ± 29.48*	26.43 ± 13.44	<0.001
PCT(ng/L)	0.43 ± 0.22	1.21 ± 0.88*	0.68 ± 0.26	<0.001
ESR(mm/h)	3.03 ± 1.22	65.97 ± 30.52*	3.03 ± 1.22	<0.001
IL-6(pg/ml)	13.25 ± 6.22	47.03 ± 20.22*	35.44 ± 19.85	<0.001
MCP-1(pg/ml)	104.55 ± 37.22	222.47 ± 67.30*	149.36 ± 48.36	<0.001
Fg(g/L)	3.14 ± 0.68	8.83 ± 1.22*	5.26 ± 0.96	<0.001

WBC, white blood cell count; RBC, red blood cell count; Hb, hemoglobin; PLT, platelet count; CRP, C-reactive protein; PCT, procalcitonin; ESR, erythrocyte sedimentation rate; IL-6, interleukin-6; MCP-1, monocyte chemoattractant protein-1; Fg, fibrinogen.
*The statistically significant (p-values < 0.05)compared with those in the fever group.

spectrophotometer color chamber. The fibrinogen monomer polymerization process was detected at 340 nm, and FMPV and ODmax were determined. Then, the FMPV/ODmax was calculated to reflect the molecular function of fibrinogen.

ELISA

ELISA kits of MMP-2, MMP-3, MMP-9, MMP-13, TIMP-1, and FG-α were used. Samples were added according to the layout of the plate. A total of 50 μL sample (10 μL sample and 40 μL sample diluent; a 5-fold dilution) or 50 μL standard was added per well. Then, 100 μL horseradish peroxidase labeled detection antibody was added to each well, and the plate was sealed with a plate membrane and incubated at 30°C for 60 min. After which, the liquid was discarded, 200 μL detergent was added per well, and the plate was left to stand for 1 min on an absorbent paper. Then, the detergent was discarded, the plate was pat dry on the absorbent paper, and this process was repeated five times. Next, 50 μL of soybean substrate A and B were added to each well and the plate was incubated for 15 min at 30°C in the dark. Lastly, 50 μL of termination solution was added to each well and the absorbance value of each well was measured at a wavelength of 450 nm.

DNA extraction and polymorphism detection: White blood cells were separated from venous blood using the 2% EDTA hypotonic method. DNA was extracted with phenol:chloroform:isoamyl alcohol (25,24:1) and precipitated with ethanol. The target DNA was amplified by polymerase chain reaction (PCR). The upstream primer was 5 '-GGAGTGGAAGGCATTAACAGA-3', and the downstream primer was 5 '- GGGTTTTGGTTTTTCCAGTACTTC-3'. The total reaction volume was 30 μL. The reaction mixture contained DNA 0.3 μg, 0.2 mM dNTPs, 10 pM primers, 1.5 mM $MgCl_2$, and 1 U Taq DNA polymerase. The PCR conditions were as follows: 95°C for 3 min predegeneration, (95°C for 20 s, 63°C for 30 s, 72°C for 1 min) × 28 cycles, and 72°C for 7 min. Then, 10 μL of the PCR product was added to 10 U of endo Rse I, incubated at 37°C overnight, and subjected to electrophoresis with 2% agarose.

Statistical methods

SPSS 22.0 was used for statistical analysis, and the Mann–Whitney U test was used for comparison of differences between groups. One-way analysis of variance (ANOVA) and the Tukey test were used for comparison of multiple groups, followed by the LSD method for comparison between two groups. $p < 0.05$ was considered statistically significant.

Results

Comparison of general clinical indicators: There was no significant difference in average age among the three groups, which were 3.03 ± 1.22 years, 3.17 ± 1.30 years, and 3.21 ± 1.31 years, respectively. Compared with the normal group, the fever time in Kawasaki disease group and fever group was significantly prolonged. The levels of white blood cell count (WBC), red blood cell count (RBC), hemoglobin, platelet, procalcitonin (PCT), C-reactive protein (CRP), erythrocyte sedimentation rate (ESR), interleukin-6 (IL-6), monocyte chemotactic protein-1 (MCP-1) and fibrinogen (Fg) were significantly increased. The level of above indexes in Kawasaki disease group was higher than that in fever group, and the difference was statistically significant ($p < 0.05$; Table 1).

The concentration of serum MMPs, TIMP-1, and FG-α: The concentration of serum MMPs, TIMP-1, and FG-α in the KD and fever groups were significantly higher than those in the normal group ($p < 0.05$). The concentration of MMP-2, MMP-3, MMP-9, MMP-13, TIMP-1, and FG-α in the KD group were significantly higher than those in the fever group ($p < 0.05$; Table 2).

Comparison of fibrinogen and its function: The KD group was further divided into two subgroups; 55 patients with combined CAL and 179 patients without combined CAL. The results showed that the plasma fibrinogen concentration in the combined CAL group was significantly higher than that in the non-combined CAL and normal groups ($p < 0.01$). There was no statistically significant

TABLE 2 The expression levels of serum MMPs, TIMP-1, and FG-α.

	Normal group (ng/mL)	KD group (ng/mL)	Fever group (ng/mL)	*F*	*P*
TIMP-1	105.699 ± 6.525	188.476 ± 14.064*#	136.842 ± 12.573*	68.3	< 0.0001
MMP-2	3.087 ± 0.483	4.494 ± 0.27*#	3.877 ± 0.574*	13	0.0004
MMP-3	38.65 ± 5.596	65.302 ± 4.576*#	49.161 ± 4.684*	46.3	< 0.0001
MMP-9	75.124 ± 6.439	115.262 ± 10.844*#	94.482 ± 3.804*	36.94	< 0.0001
MMP-13	38.576 ± 19.621	91.793 ± 33.871*#	66.84 ± 6.935*	6.964	0.0062
FG-α	754.585 ± 184.877	981.017 ± 347.37*#	835.64 ± 265.378*	4.941	0.037

*The statistically significant (p-values < 0.05)compared with those in the normal group;
#The statistically significant (p-values < 0.05)compared with those in the fever group.

TABLE 3 Comparison of fibrinogen and its function.

Group	*N*	Fibrinogen (g /L)	FMPV/ ODmax
Normal group	200	3.14 ± 0.68	3.54 ± 0.63
KD group	234		
CAL subgroup	55	9.52 ± 1.06*	3.91 ± 0.46
No CAL subgroup	179	6.23 ± 0.83	3.70 ± 0.54
F		9.773	0.779
P		<0.01	>0.05

*The statistically significant (p-values < 0.05)compared with those in the normal group and no CAL subgroup.

difference in FMPV/ODmax among the three groups ($p > 0.05$; Table 3).

FGA gene polymorphism: Compared with normal group, the FGA GG, GA, and AA genotype and G, A allele frequency of the FGA gene polymorphism in the KD group showed no significant difference ($p > 0.05$). In the KD group, the most common genotype in children with CAL was GA, while the most common genotype in children without CAL was GG.There was a statistical difference between the two groups($p < 0.05$; Table 4).

Discussion

KD is characterized by the abnormal activation of the immune system and extensive damage to the endothelial system. In the acute phase of KD, the abnormal activation of the immune system leads to the production of inflammatory mediators (proteases and reactive oxygen species), which is believed to induce pathological changes in the vascular system (9). Children with KD that do not undergo standardized treatment are prone to CALs (10), which can lead to myocardial infarction, coronary artery dilation, and coronary artery aneurysm (CAA). Although clinical treatment of KD has made progress, 20% of children with KD children still progress to CAL. An autopsy study found that the coronary artery was the most severely damaged part of the intima; other parts included the aorta, abdominal aorta, carotid artery, subclavian artery, and pulmonary artery (11). Pathological changes are similar to those of nodular polyarteritis in infants, including thickening of the arterial intima, invasion of granulocytes and monocytes, rupture of the inner elastic fiber layer and medial membrane, necrosis of the vascular wall, and formation of aneurysms (12, 13).

This study found that the serum levels of MMPs in children with KD were significantly increased. It is worth noting that MMPs are markers of inflammation. Therefore, the elevated concentration of matrix metalloproteinases in circulation may be a manifestation of coronary artery inflammation. For example, elevated levels of circulating MMPs have also been observed in other inflammatory diseases (such as pneumonia or septicemia), and these diseases do not cause CAL (14); therefore, it is suggested that significantly elevated levels of MMPs play an important role in the destruction of the coronary artery wall, resulting in aneurysms (15). Several studies have compared the MMP levels in KD with other febrile or inflammatory diseases, including bronchitis, pneumonia, sepsis, gastroenteritis, and encephalitis. Previous studies have consistently shown that although CRP shows similar levels of inflammation, the level of MMPs in KD, especially MMP-9, is much higher than that in other inflammatory diseases (about 4–8 times) (16, 17). In addition, MMP levels in pneumonia are positively correlated with CRP levels, but this correlation is not as clear in KD because MMP levels in patients with CALs are significantly higher than in non-CAL patients (18). In another study, the levels of MMPs and TIMPs in febrile non-KD patients were significantly higher than those in the non-febrile healthy control group;however, there was no significant difference in the MMP/TIMP ratio between febrile patients and the non-febrile control group, showing that the normal MMP/TIMP ratio was maintained in inflammatory diseases that did not cause CAAs (19). Only patients with KD showed an imbalance between MMPs and TIMPs, which tended to increase the activation of MMPs. In addition, the interaction between MMPs, MMPs and TIMPs and MMPs and fibrinogen may affect their activity and regulate the pathophysiological process of arterial wall destruction. Existing evidence shows that genetic factors contribute to the formation of adult aneurysms (20). *MMP-9* gene promoter polymorphism has been found in patients with intracranial aneurysm or myocardial infarction. The variation in this polymorphism leads to variation in transcription levels. It has been reported that the polymorphisms of *MMP-3* promoter and *TIMP-1* gene are related to abdominal aortic aneurysm (21). Therefore, in addition to MMPs and TIMPs, we speculate that genetic factors may be involved in the formation of KD aneurysms.

This study found that blood hypercoagulability continues to exist in children with KD from the acute phase until the next few months or years, and there is a possible correlation with the occurrence of CALs (22). Wu MH · S study findings (23) estimated the overall prevalence of KD (≈1/2940) in a population < 40 years. They,

TABLE 4 *FGA* gene polymorphism and the allele distribution frequency.

Group	*N*	Gene polymorphism (%)			The allele distribution frequency (%)	
		GG	AA	GA	G	A
KD group	234	127 (54.3)	22 (9.4)	85 (36.3)	339 (72.4)	129 (27.6)
Normal group	200	102 (51.0)	20 (10.0)	78 (39.0)	282 (70.5)	118 (29.5)
X^2		1.221	0.885			
P		>0.05	>0.05			
KD group						
CAL subgroup	55	23 (41.8)	6 (10.9)	26 (47.3)	37 (67.3)	18 (32.7)
No CAL subgroup	179	127 (70.9)	30 (16.8)	22 (12.3)	138 (77.1)	41 (22.9)
X^2		8.771	0.886			
P		<0.05	>0.05			

*The statistically significant (*p*-values < 0.05)compared with those in the no CAL subgroup; #The statistically significant (*p*-values < 0.05)compared with those in the CAL subgroup.

particularly the males, carry long-term coronary risks from a young age. Risk stratification for a timely coronary intervention and risk modification are mandatory.Lee JJY · S study (24) evaluated the risk of hypertension, major adverse cardiac events (MACE), and all-cause mortality in patients with KD until young adulthood.KD patients with coronary artery aneurysms have a higher risk of developing cardiovascular disease.Blood hypercoagulability is related to abnormal vascular endothelial function, hemorheology, and blood components (including platelets, coagulation, and fibrinolysis). Both the acute and recovery phases of KD are accompanied by abnormalities in vascular endothelial function. Abnormalities in platelet activation and fibrinolysis continue to exist in the acute phase of KD and can persist for a long time after the disease. The polymorphism of Thr312Ala of fibrinogen Aα chain may be associated with PTE, in which GG genotype significantly increases the risk of PTE, and G allele may be the genetic factor associated with PTE pathogenesis. TIMPs-MMPs complex is widely involved in vascular wall inflammation. Children with immune vascular injury, endothelial cell damage, subendothelial matrix exposure, platelet adhesion, aggregation, activation, and release of various inflammatory mediators, thus activating the coagulation pathway and affecting the inflammatory process (25). Vascular inflammation can promote the occurrence of blood hypercoagulability, and the activation factors produced in the coagulation process can also affect the inflammatory process. Fibrinogen is an important cofactor involved in platelet activation, inducing platelet aggregation, increasing blood viscosity, and promoting thrombosis (26). Abnormal blood flow exists in the coronary arteries of children with KD and CALs, which becomes slow or even stagnant owing to the reduction of shear stress. These findings suggest that the occurrence of CALs in children with KD is related to an increase of fibrinogen (27).

The gene encoding fibrinogen is located on the long arm of chromosome 4, and the three polypeptide chains are encoded by the *FGA*, *FGB*, and *FGG* genes. Gene transcription of fibrinogen is coordinated; any kind of mRNA transcription can promote the transcription of other mRNA, thus increasing the synthesis and secretion of molecular fibrinogen (28). Previous studies have found that multiple sites of the *FGB* gene may be related to fibrinogen expression (3), which are also genetic risk factors related to coronary heart disease. However, the relationship between the *FGA* gene of the polypeptide chain and the occurrence of CALs is still unclear, but it was found that expression levels of *FGA* in children with KD complicated with CALs were significantly higher than in the normal and fever groups. This suggests that it might participate in the development of CALs. Further exploration found that *FGA* can affect the interaction between nuclear protein and IL-6 inflammatory factor components, thus affecting the expression level of fibrinogen (29). The change in *FGA* polymorphism may increase the affinity of nuclear transcription factors with corresponding regulatory sites, thus further enhancing gene transcription and affecting the development of thrombosis tendency (30).

FGA polymorphisms are closely associated with adult coronary artery disease, and CAL is the most serious complication of KD. However, there are few studies on the relationship between *FGA* gene polymorphisms and CAL in KD. This study observed the *FGA* genotype and allele frequency, fibrinogen level, and molecular function changes in children with KD and CAL, children without CAL, and normal children. It was found that the KD with CAL GA genotype was significantly higher than in normal children, and fibrinogen levels were significantly higher than those in the children without CAL and normal groups. Therefore, it was speculated that *FGA* gene polymorphisms might be related to the pathogenesis of KD, and individuals carrying the GA genotype may have an increased risk of CAL by affecting fibrinogen levels; therefore, it is important to detect fibrinogen levels and determine the *FGA* genotype in clinical practice for early prediction of the risk of CAL in children with KD.

Conclusion

In summary, MMPs and FG-α were significantly upregulated in KD patients. The proportion of *FGA* genotype GA in children with CAL was significantly higher than that in children without CAL, suggesting that *FGA* gene polymorphisms affect coronary artery disease in children with KD.

Data availability statement

The raw data supporting the conclusions of this article will be made available by the authors, without undue reservation.

Ethics statement

This study was approved by the ethical committee of Kunming Children's Hospital (2022-03-144-K01). Written informed consent to participate in this study was provided by the participants' legal guardian/next of kin. Written informed consent was obtained from the individual(s), and minor(s)' legal guardian/next of kin, for the publication of any potentially identifiable images or data included in this article.

Author contributions

XL, YC, YW, CZ, and XZ carried out the studies, collected the data, and drafted the manuscript. YY and ZS performed the statistical analysis and participated in its design. CZ, ZS, and FW helped to draft the manuscript. All authors read and approved the final manuscript.

Funding

This study was supported by Kunming "Spring City Plan" High-level talent introduced by the Engineering Young Talents Special Project, Technology Talent "1000" training Project [No. 2022- SW (Reserve)-0014], Yunnan Education Department of Science Research Fund (No. 2023 J0295), Department of Science and Technology of Yunnan Province Kunming Medical University Joint Project (No. 202301AY070001-108), Kunming City Health Science and Technology Talent "1000" training Project [No. 2020- SW (Reserve)-112], Kunming Medical Joint Project of Yunnan Science and Technology Department (No. 202001 AY070001-271), and Open Research Fund of Clinical Research Center for Children's Health and Diseases of Yunnan Province (2022-ETYY-YJ-03). The funding bodies played no role in the study's design and collection, analysis and interpretation of data, and writing the manuscript.

Conflict of interest

The authors declare that the research was conducted in the absence of any commercial or financial relationships that could be construed as a potential conflict of interest.

Publisher's note

All claims expressed in this article are solely those of the authors and do not necessarily represent those of their affiliated organizations, or those of the publisher, the editors and the reviewers. Any product that may be evaluated in this article, or claim that may be made by its manufacturer, is not guaranteed or endorsed by the publisher.

References

1. Kawasaki T, Kosaki F, Okawa S, Shigematsu I, Yanagawa H. A new infantile acute febrile mucocutaneous lymph node syndrome (MLNS) prevailing in Japan. *Pediatrics*. (1974) 54:271–6. doi: 10.1542/peds.54.3.271

2. Buonsenso D, Cristaldi S, Reale A, de Jacobis IT, Granata L, Marchesi A. Very early development and recognition of coronary involvement in a febrile infant with typical signs of Kawasaki disease. *Mediterr J Hematol Infect Dis*. (2018) 10:e2018037. doi: 10.4084/mjhid.2018.037

3. Nakaoka H, Hirono K, Yamamoto S, Takasaki I, Takahashi K, Kinoshita K, et al. MicroRNA-145-5p and microRNA-320a encapsulated in endothelial microparticles contribute to the progression of vasculitis in acute Kawasaki disease. *Sci Rep*. (2018) 8:1016. doi: 10.1038/s41598-018-19310-4

4. Orenstein JM, Shulman ST, Fox LM, Baker SC, Takahashi M, Bhatti TR, et al. Three linked vasculopathic processes characterize Kawasaki disease: a light and transmission electron microscopic study. *PLoS One*. (2012) 7:e38998. doi: 10.1371/journal.pone.0038998

5. Chantasiriwan N, Silvilairat S, Makonkawkeyoon K, Pongprot Y, Sittiwangkul R. Predictors of intravenous immunoglobulin resistance and coronary artery aneurysm in patients with Kawasaki disease. *Paediatr Int Child Health*. (2018) 38:209–12. doi: 10.1080/20469047.2018.1471381

6. Roth GS, Mensah GA, Johnson CO, Addolorato G, Ammirati E, Baddour LM, et al. Global burden of cardiovascular diseases and risk factors, 1990–2019: update from the GBD 2019 study. *J Am Coll Cardiol*. (2020) 76:2982–3021. doi: 10.1016/j.jacc.2020.11.010

7. Vilar R, Fish RJ, Casini A, Neerman-Arbez M. Fibrin(ogen) in human disease: both friend and foe. *Haematologica*. (2020) 105:284–96. doi: 10.3324/haematol.2019.236901

8. Mccrindle BW, Rowley AH, Newburger JW, Burns JC, Bolger AF, Gewitz M, et al. Diagnosis, treatment, and long-term management of Kawasaki disease: a scientific statement for health professionals from the American heart association[j]. *Circulation*. (2017) 135:e927–99. doi: 10.1161/CIR.0000000000000484

9. Chen KY, Messina N, Germano S, Bonnici R, Freyne B, Cheung M, et al. Innate immune responses following Kawasaki disease and toxic shock syndrome. *PLoS One*. (2018) 13:e0191830. doi: 10.1371/journal.pone.0191830

10. Liang CD, Kuo HC, Yang KD, Wang CL, Ko SF. Coronary artery fifistula associated with Kawasaki disease. *Am Heart J*. (2009) 157:584–8. doi: 10.1016/j.ahj.2008.11.020

11. Pinna GS, Kafetzis DA, Tselkas OI, Skevaki CL. Kawasaki disease: an overview. *Curr Opin Infect Dis*. (2008) 21:263–70. doi: 10.1097/QCO.0b013e3282fbf9cd

12. Wu MH, Chen HC, Yeh SJ, Lin MT, Huang SC, Huang SK. Prevalence and the long-term coronary risks of patients with Kawasaki disease in a general population <40 years. *Circ Cardiovasc Qual Outcomes*. (2012) 5:566–70. doi: 10.1161/CIRCOUTCOMES.112.965194

13. Kuo HC, Chao MC, Hsu YW, Lin YC, Huang YH, Yu HR, et al. CD40 gene polymorphisms associated with susceptibility and coronary artery lesions of Kawasaki disease in the Taiwanese population. *ScientifificWorldJournal*. (2012) 2012:520865:1–5. doi: 10.1100/2012/520865

14. Senzaki H, Masutani S, Kobayashi J, Kobayashi T, Nakano H, Nagasaka H, et al. Circulating matrix metalloproteinase and their inhibitors in patients with Kawasaki disease. *Circulation*. (2001) 104:860–3. doi: 10.1161/hc3301.095286

15. Raffffetto JD, Khalil RA. Matrix metalloproteinases and their inhibitors in vascular remodeling and vascular disease. *Biochem Pharmacol*. (2008) 75:346–59. doi: 10.1016/j.bcp.2007.07.004

16. Wang H, Wang T, Yuan Z, Cao Y, Zhou Y, He J, et al. Role of receptor for advanced glycation end products in regulating lung fuid balance in lipopolysaccharideinduced acute lung injury and infection-related acute respiratory distress syndrome. *Shock (Augusta, Ga)*. (2018) 50:472–82. doi: 10.1097/SHK.0000000000001032y

17. Mccrindle BW, Li JS, Minich LL, Colan SD, Atz AM, Takahashi M, et al. Coronary artery involvement in children with Kawasaki disease: risk factors from analysis of serial normalized measurements. *Circulation*. (2007) 116:174–9. doi: 10.1161/CIRCULATIONAHA.107.690875

18. Kuo HC, Li SC, Huang LH, Huang YH. Epigenetic hypomethylation and upregulation of matrix metalloproteinase 9 in Kawasaki disease. *Oncotarget*. (2017) 8:60875–91. doi: 10.18632/oncotarget.19650

19. Levi M, Vad Der Poll T, Buller HR. Bidirectional relation between inflammation and coagulation. *Circulation*. 109:2698–704. doi: 10.1161/01.CIR.0000131660.51520.9A

20. Wang L, Yang Y, Cui Q, Cui Y, Li Q, Che X, et al. Evaluating the added predictive ability of MMP-9 in serum for Kawasaki disease with coronary artery lesions. *J Investig Med*. (2020) 69:13–9. doi: 10.1136/jim-2020-001281

21. Guizani I, Zidi W, Zayani Y, Boudiche S, Hadj-Taieb S, Sanhaji H, et al. Matrix metalloproteinase-3 predicts clinical cardiovascular outcomes in patients with coronary artery disease: a 5 years cohort study. *Mol Biol Rep*. (2019) 46:4699–707. doi: 10.1007/s11033-019-04914-4

22. Senzaki H, Masutani S, Kobayashi J, Kobayashi T, Nakano H, Nagasaka H, et al. Circulating matrix metalloproteinases and their inhibitors in patients with Kawasaki disease. *Circulation*. (2001) 104:860–3. doi: 10.1161/hc3301.095286

23. Wu MH, Chen HC, Yeh SJ, Lin MT, Huang SC, Huang SK. Prevalence and the long-term coronary risks of patients with Kawasaki disease in a general population <40 years: a national database study. *Circ Cardiovasc Qual Outcomes*. (2012) 5:566–70. doi: 10.1161/CIRCOUTCOMES.112.965194

24. Lee JJY, Feldman BM, McCrindle BW, Li P, Yeung RS, Widdifield J. Evaluating the time-varying risk of hypertension, cardiac events, and mortality following Kawasaki disease diagnosis. *Pediatr Res*. (2023) 93:1439–46. doi: 10.1038/s41390-022-02273-8

25. Kattula S, Byrnes JR, Wolberg AS. Fibrinogen and fibrin in hemostasis and thrombosis. *Arter Thromb Vasc Biol*. (2017) 37:13–21. doi: 10.1161/ATVBAHA.117.308564

26. Simurda T, Snahnicanova Z, Loderer D, Sokol J, Stasko J, Lasabova Z, et al. Fibrinogen martin: A novel mutation in FGB (Gln180Stop) causing congenital afifibrinogenemia. *Semin Thromb Hemost*. (2016) 42:455–8. doi: 10.1055/s-0036-1581104

27. Yuan D, Jiang P, Zhu P, Jia S, Zhang C, Liu Y, et al. Prognostic value of fifibrinogen in patients with coronary artery disease and prediabetes or diabetes following percutaneous coronary intervention: 5-year fifindings from a large cohort study. *Cardiovasc Diabetol*. (2021) 20:143. doi: 10.1186/s12933-021-01335-1

28. Kryczka KE, Kruk M, Demkow M, Lubiszewska B. Fibrinogen and a triad of thrombosis, inflflammation, and the reninangiotensin system in premature coronary artery disease in women: a new insight into sex-related differences in the pathogenesis of the disease. *Biomol Ther*. (2021) 11:1036. doi: 10.3390/biom11071036

29. Jiang P, Gao Z, Zhao W, Song Y, Tang XF, Xu JJ, et al. Relationship between fifibrinogen levels and cardiovascular events in patients receiving percutaneous coronary intervention: a large single-center study. *Chin Med J*. (2019) 132:914–21. doi: 10.1097/CM9.0000000000000181

30. Celebi S, Celebi OO, Berkalp B, Amasyali B. The association between the fifibrinogen-to-albumin ratio and coronary artery disease severity in patients with stable coronary artery disease. *Coron Artery Dis*. (2020) 31:512–7. doi: 10.1097/MCA.0000000000000868

31. Gurofsky RC, Sabharwal T, Manlhiot C, Redington AN, Benson LN, Chahal N, et al. Arterial complications associated with cardiac catheterization in pediatric patients with a previous history of Kawasaki disease. *Catheter Cardiovasc Interv*. (2009) 73:809–13. doi: 10.1002/ccd.21892

Frontiers in Medicine

Translating medical research and innovation into improved patient care

A multidisciplinary journal which advances our medical knowledge. It supports the translation of scientific advances into new therapies and diagnostic tools that will improve patient care.

Discover the latest Research Topics

See more →

Frontiers

Avenue du Tribunal-Fédéral 34
1005 Lausanne, Switzerland
frontiersin.org

Contact us

+41 (0)21 510 17 00
frontiersin.org/about/contact